UNIVERSITY OF SOUTHAMPTON

FACULTY OF ENGINEERING AND THE ENVIRONMENT

School of Civil Engineering and the Environment

The role of beam-to-column connection in the prevention of progressive collapse of steel-frame buildings

by

Ji-Lu Liu

Thesis for the degree of Doctor of Philosophy

February_2017

UNIVERSITY OF SOUTHAMPTON

ABSTRACT

FACULTY OF ENGINEERING AND THE ENVIRONMENT

Civil Engineering

Thesis for the degree of Doctor of Philosophy

THE ROLE OF BEAM-TO-COLUMN CONNECTION IN THE PREVENTION OF PROGRESSIVE COLLAPSE OF STEEL-FRAME BUILDINGS

Ji-Lu Liu

The results of an investigation into the characteristics of catenary action and their effects on structures are reported here. There are five aspects presented in this thesis: a literature review on progressive collapse and beam-to-column connections; an exact analysis of catenary action of truss; nonlinear finite element analyses of different post-column removal performance as a function of the original and retrofitted beam-to-column connection geometries; comparison of different behaviours of different beam-to-column connection geometries; and the minimisation of the strengthening plate weight for the retrofitted structures.

This thesis demonstrates that when a column is removed, the bending moment will decrease significantly as the catenary tensile force and the plastic deformation increase in the beams connected to the damaged column. This thesis also shows that when a column is destroyed by a blast, the failure strain will be reached at the simple beam-to-column joint. To enhance the survival capability of the steel framed structures subjected to terrorist blast, retrofitting schemes were proposed for strengthening the joints of tall steel framed structures, ensuring the full development of catenary action. This thesis simulates the post-column removal behaviour of the original and the strengthened structures by means of the ABAQUS finite element package. For this purpose, sophisticated two- and three-dimensional models of catenary action are developed. Through comparing different results of the original and the strengthened structures from a column removal, the advantages of the proposed retrofitting schemes have been demonstrated. This thesis investigates the relative advantages and shortcomings between two different retrofitting schemes and compares the proposed retrofitting schemes with other moment beam-to-column connections used for new construction. For the same resisting capacity of the retrofitted structure, the Vertical Plate Scheme will require much more material than the Flange Plate Scheme. But the Vertical Plate Scheme still has its advantages. The Vertical Plate Scheme does not require the removal of the floor slab and easier to conduct than the Flange Plate Scheme. Finally, it is demonstrated that the sizes of strengthening plates can greatly change the overall behaviour of the retrofitted structures; with the reduction of the strengthening plate sizes, the stress and strain will increase and the structure will experience elastic stage and elasto-plastic sequentially. This thesis minimises the thickness and the length of the strengthening plates by the exact analytic method for simple structures and the finite element method for complicated structures.

Table of Contents

List of Tables

Table 6.5. Maximum Mises equivalent stresses and equivalent plastic strains of connection and whole structure with respect to different thicknesses (*t*) and lengths (*l*) of flange cover plates for Model 6.3

List of Figures

Fig. 8.4. Deformation and Mises stress distribution after loading

DECLARATION OF AUTHORSHIP

I, Ji-Lu Liu .....
declare that this thesis and the work presented in it are my own and has been generated by me as the result of my own original research.

.....

The role of beam-to-column connection in the prevention of progressive collapse of steel-

frame buildings .....

I confirm that:

1. This work was done wholly or mainly while in candidature for a research degree at this University;
2. Where any part of this thesis has previously been submitted for a degree or any other qualification at this University or any other institution, this has been clearly stated;
3. Where I have consulted the published work of others, this is always clearly attributed;
4. Where I have quoted from the work of others, the source is always given. With the exception of such quotations, this thesis is entirely my own work;
5. I have acknowledged all main sources of help;
6. Where the thesis is based on work done by myself jointly with others, I have made clear exactly what was done by others and what I have contributed myself;
7. Parts of this work have been published as:
   - Liu, J. L. (2010a). "Preventing progressive collapse through strengthening beam-to-column connection, part1: theoretical analysis." Journal of Constructional Steel Research, 66. 229–237.
   - Liu, J. L. (2010b). "Preventing progressive collapse through strengthening beam-to-column connection, part2: finite element analysis." Journal of Constructional Steel Research, 66. 238–247.

Signed: .....

Date: 27th February 2017 .....

Acknowledgements

To begin, I would like to sincerely thank Professor Antonis Zervos, my supervisor, for his technical guidance, understanding, and patience during my graduate studies. Most importantly, I want to thank him for his friendship. He was always there to offer his valuable guidance, insight and comments. I was very fortunate to have him as a supervisor and a friend.

Useful advice and commentary was received from many professors and doctors to whom I am very grateful. Special thanks to Professor Marcus Lee, Professor Stuart Moy, Dr. Mike Byfield and Dr. Alan Bloodworth at University of Southampton, and Professor Andrew Tyas at University of Sheffield for their valuable insight and comments during my graduate studies at University of Southampton.

The work conducted would have not been possible without the support I received from many more friends at University of Southampton in UK and at Shantou University in China. Particular thanks go to Dr. Christine Winter and Dr. George Chellapa of University of Southampton.

Thanks go to my parents, Zheng-Hao Liu and Nai-Rong Zhao, in China who supported me through their encouragement.

I would like to dedicate my thesis to my daughter, Dong-Yu Liu. She is the driving force behind my dreams and ambitions. I also want to dedicate my thesis to my father who had always dreamed that one of his children would grow to earn a Ph.D from the world-famous university.

I would like to also gratefully acknowledge the supports of the EPSRC Dorothy Hodgkin Postgraduate Award (DHPA) scheme, the National Science Foundation of China (NSFC) under Grant No. 50478119, the Natural Science Foundation of Guangdong Province (NSFGP) under Grant No. S2011010005192.

Chapter 1: Introduction

Unlike military structures, ordinary civilian buildings have traditionally not been designed to resist blast loads in the past. However, recent terrorist threats to civilian buildings have demonstrated the need to evaluate the vulnerability of important civilian buildings. Few skills are required to manufacture a crude bomb that can cause serious damages and, as a result, bombing has long been the most common terrorist tactic.

It is widely believed that during explosions most casualties and injuries sustained are not caused by the pressure, heat, or fragments resulting from a bomb detonation, but by the local failure of a building and its disproportional progressive collapse later (NRC 2001). Therefore, ensuring resistance to a blast causing deadly local failure and mitigation of progressive collapse are crucial aims.

Many high-rise steel structures have been built in large cities. Due to their importance, these high-rise buildings are easy to become targets of terrorist attacks. With different structural members being destroyed, the results are quite different. Among a variety of steel structural members, columns are more important than floor slabs and beams.

If a floor slab is destroyed, the influence of this failure is limited within the damaged slab itself. If a beam is destroyed, the beam and the floor slabs supported by this damaged beam may collapse. If a column is destroyed, however, the result is even more serious. The column, and the structural members of all storeys above this damaged column, including all columns,

beams, and floor slabs in the affected bays, may collapse. Consequently, destroying columns may be the most cost-effective choice of terrorists.

It is very important to assure that the occupants of the damaged buildings survive. For this purpose, an alternative static equilibrium configuration needs to be reached to avoid final collapse. A key mechanism thought to assist a damaged structure to reach such an alternative equilibrium configuration is catenary action, as shown in Fig. 1.1. When a load-bearing steel column is removed by a blast, the steel beams connected to this column are required to transfer the load borne by the column and to bridge over the damaged area. As a result, catenary action (Byfield 2004, 2006; Byfield and Paramasivam 2007) will be involved. If the catenary action forces are adequate within the beams, the local damage to the column will not have catastrophic consequences.

For the purpose of preventing progressive collapse, continuity between structural elements is crucial. Studies of many building collapses (Ellingwood and Leyendecker 1978; Gross and McGuire 1983) have also shown that failure could have been avoided or at least reduced in scale at a fairly small additional cost, if structural components had been interconnected more effectively. This is also the basis of the "structural integrity" requirements for concrete structure in the ACI 318 (2002) specification.

For structural steelwork, many standards also recognize the need for continuity between structural elements and make similar specifications. The UK was the first country to address the issue of structural progressive collapse. The UK code (BS 5950 2000) proposed the tying of structural members together. However, for most existing steel structures in UK, the

requirement of resisting progressive collapse by catenary action is rather difficult to fulfil due to the weakness of their simple beam-to-column connections (Byfield and Paramasivam 2007; Liu et al. 2005).

In addition, although those approaches have been integrated into most building codes and specifications, they are usually qualitative instead of quantitative. No special consideration is given as to how a structure behaves when one of its critical members fails.

The determination of catenary action represents a highly indeterminate analytical problem with a large tensile force affecting its flexural behaviour. Only for very simple cases such as modelling the beam as a truss, a closed form solution can be obtained. When lateral loads exist, the analysis of the combined effect of tension and bending becomes rather complicated. The finite element method is an ideal tool for tackling such otherwise intractable problems. A number of powerful finite element software packages have become commercially available, e.g., ADINA, MARC, ANSYS, and ABAQUS. They incorporate facilities that enable a wide range of engineering problems to be efficiently modelled and accurately analyzed.

In this thesis, the characteristics of catenary action are investigated. The need for strengthening the joints of simple construction is illustrated. Retrofitting schemes are proposed for strengthening the simple beam-to-column connection, so that catenary action can be developed in the beams. To illustrate the characteristics of catenary action and to demonstrate the feasibility of the proposed retrofitting schemes, nonlinear finite element analyses were carried out using the ABAQUS (2014) package.

The proposed retrofitting schemes are compared to the moment beam-to-column connection used for new steel construction. The details of retrofitting schemes are parametrically studied both when the stresses and strains are equal to, or not much larger than, the corresponding yield values and when the strains are very large in the inelastic stage.

1.1 Aims and objectives

The general aims of this research are to:

- Investigate the role of catenary action in preventing progressive collapse due to column removal;
- Propose retrofitting schemes for improving the ability of existing steel structures to resist progressive collapse.

The objectives through which the aims will be achieved are:

- Collate and critically review current practice to identify its advantages and shortcomings, and possible areas for improvement;
- Investigate the development of catenary action in beams using simple theoretical and more complex numerical models, and determine qualitatively the influence of different types of beam-to-column connections to this development;
- Propose different retrofitting schemes for strengthening simple beam-to-column connections to allow the development of catenary action in the beam;

- Develop numerical models and use them to assess the ability of the proposed retrofitting schemes to prevent progressive collapse;
- Compare the performance of four different beam-to-column connection geometries;
- Conduct a series of exact analyses and numerical parametric investigations to minimise the plate weight of the proposed retrofitting schemes.

1.2 Structure of the report

In Chapter 2 of this thesis, a literature review is presented. Chapter 2 deals with progressive collapse and catenary action, including case studies, codes and standards, papers and reports. Chapter 2 also describes a variety of beam-to-column connections.

In Chapter 3, catenary action is analyzed. The combined effect of catenary tension and bending moment is investigated. To illustrate the need for strengthening the simple beam-to-column connection, the susceptibility of different beam-to-column connections to the effect of catenary action is examined by exact solution of catenary action of truss models. Two schemes for retrofitting the fin plate beam-to-column connection of the existing structures are proposed.

In Chapter 4, finite element models are used to evaluate the structural response after the removal of a column. Due to the resulting doubling of

the span, the structural steel members will exhibit both material and geometrical nonlinear properties, and therefore the finite element method is needed. The adopted finite element types are described. The presented finite element prediction models are validated by comparing the results to ones available in the literature. For the two retrofitting schemes, the post-attack behaviour of the original and the strengthened structures is evaluated by means of finite element analysis.

In Chapter 5, structures reinforced by the Traditional Moment Connection Scheme and the SidePlate Connection Scheme are evaluated, in addition to the proposed Flange Plate and Vertical Plate Schemes. The performances of these four types of connections following column removal are compared. Their advantages and drawbacks are investigated by means of finite element analysis. In addition to the simplified shell models, the much more detailed 3D solid element models are also adopted to investigate the local behaviour of the end plate connections before and after retrofitted by the above mentioned four schemes. The adopted 3D brick element types are described. The models are validated by comparing the results to ones available in the literature. The contacts among the bolts and the steel plates and the geometries and the material properties of the welds are simulated. The 3D solid element models can provide much more information about the local performance of the connectons than the shell element models.

In Chapter 6, structures retrofitted by the proposed Flange Plate and Vertical Plate Schemes are parametrically studied. The thickness and the length of the retrofitting plates are treated as variables. With the reductions

of the thickness and length, the stress and strain will increase. Because the maximum allowed stress, strain, etc., may be different in elastic stage and in elasto-plastic stage, instead of a single criterion, double criteria are used to analytically optimise simple structures and parametrically study complicated structures.

In Chapter 7, summary and conclusions are given. The overall results of investigating the prevention of progressive collapse by catenary action and the improvement of the catenary behaviour of an existing steel structure are described.

Finally, a plan for future work is briefly outlined in chapter 8.

Chapter 2: Literature review of progressive collapse, prevention of collapse through catenary action, and beam-to-column connections

In order to avoid damage caused by blasts, it is very important to prevent terrorists from reaching a potential target. The most cost-effective means of protection is to maintain a standoff distance between any possible explosion and important buildings, because the blast effects of a bomb diminish dramatically with increasing range (Astaneh-Asl et al. 2001a; Bangash et al. 2006; Smith and Hetherington 1994). In addition to the above mentioned common-sense way of keeping dangerous matters away from buildings, there are traditionally three ways to improve the ability of the structure to survive blast loads: enhancing local resistance, increasing redundancy and adopting ductile structures (Ellingwood and Leyendecker 1978; Ellingwood et al. 1982).

Many structural design standards (BS 5950 2000; ACI 318 2002; ASCE 7 2002; GSA 2003; DoD 2002; DoD 2005) have acknowledged the threat posed by abnormal loads and progressive collapse since shortly after the Ronan Point collapse (Griffiths et al. 1968; Pearson and Delatte 2005). After the terrorist attacks against the Alfred P. Murrah Building in Oklahoma City in 1995 (FEMA 1996; Corley et al. 1998; Mlakar et al. 1998; Sozen et al. 1998) and the World Trade Centre in New York in 2001 (FEMA 2002; Bazant and Zhou 2002), much more research has been conducted. The above mentioned approach of redundancy requires that when any one component fails, alternative paths are available for the loads in that

component and a general collapse does not occur. With this methodology, structural continuity is crucial. When key elements carrying gravity loads are destroyed, it is important that the remaining structure can redistribute the loads without collapsing (Dusenberry and Hamburger 2006; Gross and McGuire 1983; Marjanishvili 2004; Nair 2006).

Because the research field of progressive collapse is relatively new (Astaneh-Asl et al. 2001a), the same or similar Case studies and Codes and Standards appeared repeatedly in many available papers and reports. These Case studies and Codes and Standards are included in this chapter as general background due to their importance. In addition, literature in the field of progressive collapse and catenary action, and different types of beam-to-column connections is also reviewed in this chapter.

2.1 Case Studies of progressive collapse

There are many blast events in the world, but only the following cases are most widely referenced in journal papers because they seriously damaged structures or even destroyed whole buildings. These cases are the Ronan Point Tower, the Alfred P. Murrah Federal Building, and the World Trade Centre.

Ronan Point. Not all damages to structures are caused by terrorist bomb attacks, some accidents can also cause serious damage to buildings. The Ronan Point Tower (Griffiths et al. 1968; Pearson and Delatte 2005) is one of these examples.

The 22-storey Ronan Point Apartment Tower was in London. It had a total height of 64m and overall plan dimensions of 24.4m by 18.3m. In the early morning on May 16, 1968, an occupant on the 18th floor of the tower lit a match to brew her morning cup of tea. The resulting gas explosion blew out the walls of her apartment, and initiated a partial collapse of the structure that killed 4 people and injured 17. The partially collapsed structure is shown in Fig. 2.1 (Pearson and Delatte 2005).

The Ronan Point Apartment Tower was constructed using the Larsen–Neilsen system, which was developed in Denmark in 1948. In this type of structural system, walls, floors and stairways are all precast concrete, and installed one-storey high. Each floor is supported by the load-bearing walls directly beneath it. Gravity load transfer occurred only through these load-bearing walls. The wall and floor panels fitted together in slots. The connection is shown in Fig. 2.2. This type of structure consisted of precast panels joined together without a structural frame, and the connections relied, in large part, on friction (Pearson and Delatte 2005).

The force of the explosion knocked out the opposite corner walls of the apartment on the 18th floor. These walls were the sole support for the walls directly above. This created a chain reaction in which floor 19 collapsed, then floor 20, and so on, propagating upward. The four floors fell onto level 18, which initiated a second phase of the collapse. This sudden-impact loading on floor 18 caused it to give way, smashing floor 17 and progressing until it reached the ground. Because the extent of cumulative damage was absolutely out of proportion to the triggering event, the

Ronan Point progressive collapse failure is definitely a very representative case of disproportionate collapse (Pearson and Delatte 2005).

After investigating, it was found out that the collapse of the Ronan Point was due to its lack of structural redundancy and local resistance, incorporating no fail-safe mechanisms, providing no alternative load paths for the upper floors when a lower level gave away, and poor workmanship at the critical connections between the panels (Pearson and Delatte 2005). The improvement of the connections between the wall panels and the floors, with less reliance on friction due to weight to hold everything together, would likely have greatly reduced the scale of the collapse. The adoption of better interconnection of structural members would have been the key for preventing the disproportionate collapse of the Ronan Point building (Nair 2006).

Murrah Building. On Wednesday morning, April 19, 1995, in the street in front of the Alfred P. Murrah federal building in Oklahoma USA (FEMA 1996; Hayes Jr. et al. 2005; Corley et al. 1998; Mlakar et al. 1998; Sozen et al. 1998; Norville et al. 1999), a rented truck containing about 1,800 kg of explosive material exploded. The column nearest to the explosive was abruptly removed by brisance. The massive explosion sheared the entire north side of the building, killing 168 people. Fig. 2.3 shows the street face of the Murrah Building prior to the 1995 attack and Fig. 2.4 shows the partially collapsed structure. The event greatly raised public awareness of blast hazards for public buildings.

The Murrah Building was designed competently in accordance with ACI 318-71 provisions for non-seismic regions. It consisted of cast-in-place

ordinary reinforced concrete framing with conventionally reinforced columns, beams, and one-way slab system. Reinforced concrete shear walls were used to resist lateral wind loads. The gross building plan dimensions were approximately 67 m, east-west, and 30.5 m, north-south. The building contained ten 6.1 m bays spanning east-west and two 10.7 m bays spanning north-south. A key feature of the structural design was a transfer beam at the third floor level on the north side of the structure, which had a total span of 12.2m and supported column spaced at 6.1m on the upper floors (Hayes Jr. et al. 2005; Osteraas 2006).

After bombing, many investigations were carried out. With regard to how construction practices might be improved to prevent a recurrence of the disaster, some of these investigators gave many valuable suggestions. Among the suggestions were that constructing the building using seismic design details would have reduced damage and catastrophic collapse, and that using ductile systems instead of the less ductile 1970s ordinary moment frame, which was adopted in Murrah Building, could reduce the degree of blast and progressive collapse vulnerability (Corley et al. 1998; Mlakar et al. 1998; Sozen et al. 1998). However, it was cautioned that seismic strengthening measures on their own cannot fully replace specific measures to prevent progressive collapse (Hayes Jr. et al. 2005).

World Trade Centre. On September 11, 2001, the twin towers of the World Trade Centre (WTC) in New York City collapsed as a result of terror attack. Disaster was provoked by two hijacked commercial airliners that were deliberately flown into the two 110-storey towers. The Boeing 767-200ER series aircrafts hit the building and created mass fireballs due to

instant ignition of a portion of the fuel on board. The north tower (WTC 1) was struck first at the centre of north face between floors 94 and 98, with an estimated velocity of 210 m/s. The south tower (WTC 2) was impacted second at a velocity of 254m/s between floors 78 and 84. Of the estimated 17400 occupants of the towers on that day, 2749 lost their lives, including 421 emergency responders. The tragic event has opened up a series of technical investigations of mechanisms of the collapse (FEMA 2002; Bazant and Zhou 2002; Newland and Cebon 2002; Zhou and Yu 2004).

The twin towers of the WTC collapsed not because of the horizontal impact force of the airplane. Owing to the building's wind load design against as much as 5,000 t of lateral load, the building had sufficient capacity to survive the initial airplane impact. This was evidenced by the fact that the towers did not collapse until about 103 min after the initial impact in the North Tower case and 56 min in the South Tower case (FEMA 2002).

The reason why a total collapse occurred was the consequence of the prolonged heating of the steel columns to a very high temperature. The jet fuel flowed on floors and down the centre shafts resulted in the simultaneous ignition and growth of fires on several storeys. Just the jet fuel on board cannot last too long. Fire was fed by the building contents and air necessary for fire was supplied through the breached walls and windows. Although the fire-resulted temperature was unlikely to rise above the steel's melting point, the heating lowered the yield strength and caused viscoplastic buckling of the columns of the framed tube along the

perimeter of the tower and of the columns in the building core. The likely scenario of failure is approximately as follows (Bazant and Zhou 2002).

In stage 1 (Fig. 2.5), the conflagration, caused by the aircraft fuel spilled into the structure, causes the steel of the columns to be exposed to sustained temperatures apparently exceeding 800°C. The heating is probably accelerated by a loss of the protective thermal insulation of steel during the initial blast. At such temperatures, structural steel suffers a decrease of yield strength and exhibits significant viscoplastic deformation (i.e., creep—an increase of deformation under sustained load). This leads to creep buckling of columns, which consequently lose their load carrying capacity (stage 2). Once more than half of the columns in the critical floor that is heated most suffer buckling (stage 3), the weight of the upper part of the structure above this floor can no longer be supported, and so the upper part starts falling down onto the lower part below the critical floor, gathering speed until it impacts the lower part. At that moment, the upper part has acquired an enormous kinetic energy and a significant downward velocity. The vertical impact of the mass of the upper part onto the lower part (stage 4) applies enormous vertical dynamic load on the underlying structure, the dynamic factor could be as high as 31, at least an order of magnitude higher than the load-carrying capacity of the lower part, even though it is not heated. This causes failure of an underlying multifloor segment of the tower (stage 4), in which the failure of the connections of the floor-carrying trusses to the columns is either accompanied or quickly followed by buckling of the core columns and overall buckling of the framed tube, with the buckles probably spanning the height of many floors

(stage 5, at right), and the upper part possibly getting wedged inside an emptied lower part of the framed tube (stage 5, at left). The buckling is initially plastic but quickly leads to fracture in the plastic hinges. The part of building lying beneath is then impacted again by an even larger mass falling with a greater velocity, and the series of impacts and failures then proceeds all the way down (stage 5). The plastic energy dissipation by the building column collapse was only a small portion of the total potential energy released. So large kinetic energy was acquired and the collapse was nearly a free-fall (Bazant and Zhou 2002).

In order to prevent the tragic accident of WTC, Newland and Cebon (2002) proposed a scheme, shown in Fig. 2.6, to modify the WTC by installing energy absorbing telescopic columns, which are filled with metal foam. By doing so, the vertical impact force can be greatly reduced, and these buildings can be prevented successfully from progressively collapsing.

Zhou and Yu (2004) also proposed a similar idea by using metal honeycomb structures, shown in Fig. 2.7, instead of metal foams as the energy absorbing means. By introducing a design parameter called collapse stability index that controls design against progressive collapse, it is found that conventional design of a tall building usually leads to an inherently unstable structure in the event of progressive collapse. In order to arrest progressive collapse, metal-based, heavy-duty honeycomb structures are used to dissipate collapse energy. Zhou and Yu discuss the methods of manufacturing these devices as well as cost considerations related to their use in buildings, and argue that the devices absorb

potential energy efficiently and occupy a relatively small amount of floor space.

From the above case studies, it can be seen that redundancy, local resistance and continuity of structure play a crucial role in preventing progressive collapse. The structures should be designed to be ductile and to have alternative load paths. One of the important reasons of the partial collapse of the Ronan Point is that it could not provide alternative load paths due to lack redundancy and the poor interconnections of structural components (Nair 2006; Pearson and Delatte 2005). As a contrast, because the alternative load paths were available, the twin towers of the WTC could successfully stand for 103min and 56 min respectively after the initial impacts which caused serious local damages, although they finally collapsed due to fire (Byfield and Paramasivam 2007). This performance is the reason why most building occupants could evacuate safely (Corely 2004).

2.2 Designing against progressive collapse: Codes and Standards

Since the progressive collapse of the Ronan Point apartment tower in 1968 (Griffiths et al. 1968; Pearson and Delatte 2005), many codes and standards have attempted to address the issue of this type of collapse. Some of them are reviewed in this section.

2.2.1 *BS 5950-1 Structural use of steelwork in building*

The UK was the first country to address structural progressive collapse and draft rules into its codes. The British Standard *Structural use of steelwork in building, Part 1: Code of practice for design —Rolled and welded sections* (BS 5950-1, 2000) has a clause (Clause 2.4.5) on "Structural Integrity" for the purpose of preventing progressive collapse by tying the structure together. It reads thus: "All buildings should be effectively tied together at each principal floor level. Each column should be effectively held in position by means of horizontal ties in two directions, approximately at right angles, at each principal floor level supported by that column. Horizontal ties should similarly be provided at roof level, except where the steelwork only supports cladding that weighs not more than 0.7 kN/m^2 and that carries only imposed roof loads and wind loads. "

As shown in Fig. 2.8, ties lines should be continuous and arranged as close as practicable to the edges of the floor or roof and to each column line. At re-entrant corners the tie members nearest to the edge should be anchored into the steel framework.

Steel members acting as horizontal ties and their end connections should be capable of resisting the following factored tensile loads, which need not be considered as additive to other loads:

— for internal ties: $0.5(1.4g_k + 1.6q_k)s_t L$ but not less than 75 kN;

— for edge ties: $0.25(1.4g_k + 1.6q_k)s_t L$ but not less than 75 kN.

where

g_k is the specified dead load per unit area of the floor or roof;

L is the span;

q_k is the specified imposed floor or roof load per unit area;

s_t is the mean transverse spacing of the ties adjacent to that being checked.

2.2.2 *ASCE 7 Standard on Minimum Design Loads*

The American Society of Civil Engineers *Minimum Design Loads for Buildings and Other Structures* (ASCE 2002) requires that the arrangement of structural elements should be such that safe load transfer is ensured if a primary member is damaged locally. Three design alternatives related to progressive collapse are suggested: the indirect design approach, the alternative path direct design approach, and the specific local resistance direct design approach. The design alternatives are intended to provide ductility, redundancy, and continuity.

(*a*) *Indirect design approach*:

This method considers resistance to progressive collapse by providing strength, continuity and ductility to key structural members.

(*b*) *Alternative path direct design approach*:

This approach recommends explicitly providing resistance to progressive collapse by requiring the structure to redistribute the load after sustaining the loss of primary load-carrying members and to remain stable. The alternative path direct design requires careful assessment of the capacity of the remaining structure after the loss of primary elements.

After an element is notionally removed, the capacity of the remaining structure should be checked using the following load combination:

$$(0.9 \text{ or } 1.2)D + (0.5L \text{ or } 0.2S) + 0.2W$$

D is the dead load and the 0.9 load factor is used when the dead load enhance the overall building stability. The 0.5*L* corresponds to the mean value of maximum live load. *S* and *W* represent the snow and the wind loads, respectively.

(c) *Specific local resistance direct design approach*:

The specific local resistance direct design considers explicitly resistance to progressive collapse by requiring the key members of a structure to withstand a postulated abnormal load. This approach requires that the design intensity of the abnormal loading must be specified for critical load carrying members.

To check the capacity of a structural element due to an extreme load of magnitude A_k, such as blast pressure, the following load combinations are suggested:

$$1.2D + A_k + (0.5L \text{ or } 0.2S)$$

$$(0.9 \text{ or } 1.2)D + A_k + 0.2W$$

where *D*, *L*, *S* and *W* are defined as above.

2.2.3 *GSA Progressive Collapse Guidelines*

The General Services Administration (GSA) *Progressive Collapse Analysis and Design Guidelines for New Federal Office Buildings and Major*

Modernization Projects (GSA 2003) begins with a process for determining whether a building is exempt from progressive collapse considerations. For low- to medium-rise buildings (up to ten storeys above ground), the suggested analysis is linear–elastic–static. Similar to the ASCE 7-02 alternative path method, the analysis involves examining a series of models with a primary load-carrying member removed. Dynamic load factors are used to approximate the inertial forces resulting from the sudden removal of an essential supporting element.

When performing a static analysis, the GSA vertical load combination is

$$2.0(D + 0.25L)$$

where D is the dead load, and L is the live load, and 2.0 is the dynamic amplification factor. Since the probability that the full live load will be present during a possible progressive collapse event is small, 25 percent of the live load is used in the load combination. Also, the factor of 2.0 is a simplified way of accounting for dynamic effects that amplify the response when a column or wall is instantaneously removed from a building.

When performing a dynamic analysis, the load combination is

$$D + 0.25L$$

which is similar to the static analysis, without the amplification factor. Stresses resulting from the above load should not exceed the unfactored ultimate capacity.

After the analysis has been performed, a demand-capacity ratio (*DCR*) is calculated for each of the structural members in the building:

$$DCR = Q_{UD} / Q_{CE}$$

where Q_{UD} is the load effects such as bending moments, shear forces, and axial forces; and Q_{CE} the respective ultimate strength, without a strength reduction factor.

Whether or not a structural member will fail will depend on the magnitude of the *DCR*. In typical structural configurations, structural elements and connections in reinforced concrete buildings that have *DCR* values for bending moment, axial force, shear force, or a combination thereof that exceed 2.0 are considered to be damaged severely or collapsed. If all of the *DCR* values for a component are less than or equal to 1.0, then the component is expected to behave elastically; whereas if one or more of the *DCR* values for a component are greater than 1.0 but lower than 2.0, then the component is expected to behave in-elastically (FEMA 2000a). There is a similar approach for structures that are deemed to be "atypical", wherein the *DCR* is limited to 1.5. Due to the over-strength and strain-hardening of steels, plastic redistribution can occur and therefore *DCR* up to 2.0 for typical structural configurations and 1.5 for atypical structural configurations are allowed (FEMA 2000a). In the case of *DCR* values being more than 2.0 for typical structures or 1.5 for atypical structures, it is unlikely that members and/or connections will have additional capacity for redistributing loads. In steel-framed buildings, the maximum *DCR* values range between 1 and 3, depending on the structural component, as shown in Table 5.1 in the GSA Guidelines (GSA 2003).

2.2.4 DoD Minimum Antiterrorism Standards for Buildings

The Department of Defense (DoD) of The US *Minimum Antiterrorism Standards for Buildings* (UFC 4-010-01) required that all new and existing buildings three storeys or more in height must be designed to avoid progressive collapse. The following statement was included in its Appendix B-2.1 for avoiding progressive collapse: "For all new and existing inhabited buildings of three storeys or more, design the superstructure to sustain local damage with the structural system as a whole remaining stable and not being damaged to an extent disproportionate to the original local damage. Achieve this through an arrangement of the structural elements that provides stability to the entire structural system by transferring loads from any locally damaged region to adjacent regions capable of resisting those loads without collapse. Accomplish this by providing sufficient continuity, redundancy, or energy dissipating capacity (ductility, damping, hardness, etc.), or a combination thereof, in the members and connections of the structure."

2.2.5 DoD Design of Building to Resist Progressive Collapse

The latest DoD requirements for progressive collapse are in Design of Buildings to Resist Progressive Collapse (UFC 4-023-03), which was published in January 2005. This Unified Facilities Criteria (UFC) must be used in accordance with the above mentioned Minimum Antiterrorism Standards for Buildings (UFC 4-010-01). Progressive collapse protection is required for buildings that are three storeys or higher. The methods described are intended to achieve general structural integrity after a load-carrying member is lost. The standard describes two levels of protection against progressive collapse:

1. *Low level of protection (LLOP)*:

The designer provides general structural integrity by incorporating horizontal and vertical ties. In the tie force method, a building is mechanically tied together. The tie forces, which vary with construction type and location in the structure, typically are resisted by the existing structural members and connections that are designed for gravity and lateral loads. The purpose of the horizontal and vertical ties is to enhance continuity and ductility, and to develop alternative load paths in the structure. Ties must be provided internal and peripheral to the building. In addition, edge and corners columns must be tied to a nearby element. The paths of ties must be straight and continuous; no changes in direction are permitted.

2. *Medium and high levels of protection (MLOP and HLOP)*:

The designer provides horizontal and vertical ties, alternative path capacity as described by ASCE-7, and additional prescribed ductility.

If a nonlinear dynamic analysis is used for structural assessment using the alternative path method, this design guide requires the following load combination:

$$(0.9 \text{ or } 1.2)D + (0.5L \text{ or } 0.2S) + 0.2W$$

where D, L, S and W have the same meaning as in section 2.2.2.

If an element fails during a nonlinear dynamic analysis, that element is removed from the model and the load that it carried is then doubled (Clough and Penzien 1993) and applied to the section directly supported

by the failed element. The doubling of the load is intended to account for impact of loads from a failed element onto the section below it.

If a linear or nonlinear static analysis is employed for structural assessment using the alternative path method, the following load combination is applied to bays immediately adjacent to the removed element and at all floors above the removed element:

$$2.0[(0.9 \text{ or } 1.2)D + (0.5L \text{ or } 0.2S)] + 0.2W$$

where *D* is the dead load, *L* the live load, *S* the snow load, and *W* the wind load. The factor of 2.0 in the above equation accounts for dynamic effects.

For the rest of the structure, the following load combination is applied:

$$(0.9 \text{ or } 1.2)D + (0.5L \text{ or } 0.2S) + 0.2W$$

Subsequent to the analyses, acceptability criteria must be satisfied. This consists of satisfying strength design requirements of the applicable material standards and deformation limits (ductility and rotation) for all of the members in the structure.

When an external column or load-bearing wall is removed, the collapsed area of the floor directly above the removed element must be less than the smaller of 750 square feet or 15 percent of the total area of that floor. Also, the floor directly supported by the removed element should not fail, and collapse must not extend beyond the structure tributary to the removed element. The damage limit for interior columns and walls is two times that of exterior ones. Any collapse must not extend into the bays immediately adjacent to the removed element.

Additional ductility requirements—"For MLOP and HLOP structures, design all perimeter ground floor columns and load-bearing walls such that the lateral uniform load which defines the shear capacity is greater than the load associated with the flexural capacity, including compression membrane effects where appropriate (Page 5-9 of DoD 2005)." It can be seen from the above that the main goal of the additional ductility requirements is to ensure that the failure mode for all external columns and walls in the ground floor is flexural and ductile, rather than shear and brittle. The reason is given as the following.

When the failure mode is flexural, plastic hinges occur, the energy induced by blast can be dissipated due to plastic hinge rotation, the columns and the walls can experience a very large deformation before final failure is reached, and therefore the flexural failure mode is ductile. On the contrary, when the failure mode is shear, the dissipation of the blast energy is rather limited, the failure deformation is very small, and therefore the shear failure mode is much less ductile than the flexural one. In order to avoid the brittle shear failure mode, it is required that the shear strength exceeds the flexural strength.

2.2.6 *Discussion of the Codes and Standards reviewed*

In summary, five codes and standards for progressive collapse were reviewed in this section. There are generally three approaches to reducing the susceptibility of structures to progressive collapse: (1) tying force—The structure can be kept together in the event of abnormal loading; (2) alternative load paths—building structures can tolerate the loss of a column without collapse by providing more redundancy; (3) local

resistance—critical components that might be subjected to attack are able to resist such attacks. In addition, the structural members should be effectively interconnected, and the strength and ductility of structural members and connections are crucial.

Different from the latter four codes, the first code BS 5950-1(2000) is only based on the approach of tying force to preserve structural integrity (Liu et al. 2005; and Byfield et al. 2007). Although it is widely believed that compliance with the tying force method creates structures able to form catenaries if column support is removed, Liu et al. (2005) and Byfield et al. (2007) showed that the provision of horizontal tying stipulated in BS 5950-1 (2000) cannot guarantee the prevention of progressive collapse of a structure by catenary action of beams. In the models of Liu et al. (2005), the horizontal and vertical ties in a building were designed according to the British Code BS 5950-1 (2000). For evaluating the effect of the removal of the columns in buildings, nonlinear dynamic finite element analysis was used. Liu et al. (2005) demonstrated that the forces generated in a numerical simulation of a damaged structure exceed the values recommended by the present code BS 5950-1 (2000) for design. Byfield et al. (2007) showed that the provision of horizontal tying stipulated in BS 5950-1 (2000) cannot guarantee the prevention of progressive collapse of a structure by catenary action of beams. When its load-carrying column is destroyed by a blast, the simple steel construction, widely used in the UK, will be damaged by rupture at its beam-to-column connection.

Otherwise, the latter four codes implement the same principle and philosophy: preventing collapse by ensuring alternative load paths exist.

The approach of alternative load paths requires that after a load-carrying column is lost, the loads from the damaged column can be transferred to adjacent structural members without collapse.

For concrete structures, although it is widely believed that the seismic design provision can improve the resistance to blast loads and progressive collapse, there have been few attempts to quantify such improvement. In order to quantify the improvement, Hayes et al. (2005) investigated the effect of strengthening a structure for seismic upgrade on mitigating progressive collapse. By examining the Murrah Federal Building, Hayes et al. concluded that seismic strengthening and special moment frame detailing of a concrete building would reduce the potential for progressive collapse and enhance resistance. The study was specific to seismic strengthening appropriate for a region of very high seismic activity. Hayes et al. (2005) cautioned that seismic strengthening on its own does not replace specific measures to prevent progressive collapse.

2.3 The role of catenary action in preventing progressive collapse

When an extreme loading event occurs, a limited structural damage is generally accepted as inevitable. Because significant abnormal loads such as explosions are highly random in magnitude and incidence, safety and economy should be balanced. Ellingwood et al. (1978, 1982, 1994, 2005, 2006) and Galambos et al. (1982) provided a framework for addressing issues related to low probability/high consequence events. Three

approaches were discussed for the mitigation of progressive collapse: (1) event control, avoiding or protecting against occurrence of an extreme incident that might lead to a progressive collapse; (2) indirect design method, developing resistance to progressive collapse by specifying a minimum level of strength, continuity and ductility; and (3) direct design method, explicitly considering resistance to progressive collapse and ability to absorb damage. The two basic means of direct design are the specific local resistance method, preventing significant local damage in the case where the extreme event occurs, and the alternative path method, preventing progressive collapse and loss of life even if local damage occurs. A performance acceptance criterion that limits the damaged floor area in a horizontal plane to the smaller of 750 ft^2 (70 m^2) or 15% of the floor area was proposed (Ellingwood and Leyendecker 1978).

Because of local failure of a column damaged by an explosion, the structural members surrounding this column may move downward. If the damaged system cannot reach a new static equilibrium configuration by establishing an alternative load path, progressive collapse of the building will be possible. In the above mentioned approach 3, the direct design method, a key mechanism thought to assist a damaged structure to reach this equilibrium configuration by providing an alternative load path is catenary action. In this case, catenary action is usually the last line of defense against progressive collapse for many high-rise steel structures. The present study focuses mainly on investigating the characteristics of catenary action and preventing progressive collapse by improving

catenary action of simple steel constructions. For this purpose, the literature in this field is reviewed in this section.

The catenary, derived from the Latin word for chain, was first introduced by Leibniz in 1691. It is defined as the curved shape of a chain under self weight. A hanging thread of uniform density and given length, stretched between two posts, will assume this shape, as do telephone and electrical power lines. In structural engineering, the term, "catenary action" refers to the ability of beams to resist lateral loads through very large deformation leading to the development of axial tension. The structural system must be ductile enough to allow the new equilibrium configuration to be achieved.

The inherent toughness of earthquake resistant construction, which promotes redistribution of internal forces and makes possible alternative load paths in the event of member loss, has led to the widespread perception that earthquake resistant design and detailing will also enhance collapse resistance. However, the effect of potentially large catenary forces on connection performance has not yet been adequately investigated. Through using computational structural simulation, Khandelwal et al. (2007) investigated catenary action in moment resisting steel frames. A calibrated micromechanical fracture model (Gurson 1977; Tvergaard 1981; Tvergaard and Needleman 1984) is employed for modelling ductile fracture in structural steel. The simulation results demonstrate the ductility of seismically designed moment frame assemblies and their ability to deform in catenary mode. When the beam depth and the ratio of yield to ultimate strength increase, the ductility and the strength

of beam-to-column connection are adversely affected. The beam web-to-column detail plays an influential role in connection response.

Byfield and Paramasivam checked many records of buildings damaged by general-purpose bombs dropped on London during World War II. Inspection of these records has not revealed any instances of catenary action in practice (Byfield 2004, 2006; Byfield and Paramasivam 2007).

Using a simplified hand calculation method, Byfield and Paramasivam (2007) demonstrated that the deflected shape and the joint deformation described in Fig. 2.9 would be produced once a column is damaged. Such deformations are not possible without fracturing the joints and the reinforcement in the slab. The slab is unlikely to possess the ductility required to withstand such a high degree of deflection. They concluded that catenary action will not prevent progressive collapse in steel-framed buildings with simple beam-to-column connections; and insufficient ductility will be the primary reason for the damage. However, the simple connections is widely adopted in UK and preventing the simple structural steelworks from progressive collapse is very important. Based on these facts, the rest of the research in this thesis mainly focuses on the approach for enhancing the performance of simple connection at column removal.

The review by Byfield and Paramasivam (2007) of bomb-damaged buildings indicated that the provision of emergency bracing is the most effective means of redistributing loads away from damaged columns. Panel walling and diaphragm walls played a vital role in bracing severely damaged structures. In the event of 9/11, the World Trade Centre buildings

were able to survive the immediate aftermath of the impacts partly because damaged columns were able to hang from the outrigger trusses installed in the top floors. The conclusion by Byfield and Paramasivam (2007) is that multi-storey buildings with simple connections that might become a target for malicious actions should be provided with emergency bracing in order to redistribute column loads following localized damage, rather than relying upon catenary action as the sole means for ensuring robustness.

Izzuddin et al. (2007, 2008) concluded that the requirements for the avoidance of disproportionate collapse, which are detailed in material-specific design codes, can be broken down into (i) prescriptive 'tying force' provisions which are deemed sufficient for the avoidance of disproportionate collapse, (ii) 'notional member removal' provisions which need only be considered if the tying force requirements could not be satisfied, and (iii) 'key element' provisions applied to members whose notional removal causes damage exceeding prescribed limits (Izzuddin et al. 2007, 2008).

When a multi-storey building is subjected to sudden column loss, the ensuing structural response is dynamic, typically characterized by significant geometric and material nonlinearities. For steel-framed buildings employing simple or partial-strength connections, the sudden loss of a column invariably leads to a considerable concentration of deformations in the connections within the floors above. The failure of these floors is largely determined by the deformation demands on the connections at the maximum dynamic response in relation to their ductility supply (Izzuddin et al. 2007, 2008).

Izzuddin et al. (2007, 2008) proposed a simplified approach for assessing the progressive collapse of multi-storey building structures. By considering whether the connections have sufficient ductility supply to withstand the associated demands, their method offers for the first time a quantitative framework for the consideration of such important issues as ductility, redundancy and energy absorption. Their method can be directly applied in design practice. The following three main stages are utilized:

(i) nonlinear static response of the damaged structure under gravity loading;

(ii) simplified dynamic assessment to establish the maximum dynamic response under sudden column loss; and,

(iii) ductility assessment of the connections.

The method of Izzuddin et al. (2007, 2008) may be applied at the overall structural level (Fig. 2.10) and at various sub-structural levels (Fig. 2.11), according to the required modelling detail and the feasibility of model reduction. At the first level of model reduction, consideration may be given to the affected bay of the multi-storey building only (Fig. 2.11a), with appropriate boundary conditions to represent the interaction with the surrounding structure. Provided the surrounding columns can resist the redistributed load, further model reduction may consider only the floors above the lost column where deformation is concentrated (Fig. 2.11b). If additionally the affected floors are identical in terms of structure and loading, the axial force in the columns immediately above the lost column becomes negligible, and a reduced model consisting of a single floor

system may be considered (Fig. 2.11c). Finally, ignoring the planar effects within the floor slab, individual steel/composite beams may be considered at the lowest level of model reduction (Fig. 2.11d), subject to appropriate proportions of the gravity load. The typical nonlinear response of the structure under varied gravity loading is shown in Fig. 2.12.

Astaneh-Asl et al. (2001a, b) and Tan et al. (2003) reported the results of full-scale testing of specimens to study the use of steel cables placed inside the floor slabs for new construction or added under the slab for existing structures as a measure of retrofit. The authors argued that the proposed method can be effective in many situations. The main role of these cables was to prevent progressive collapse of the floor by using catenary action of these steel cables in the event of removal of a column. When a column was removed and the floor started to collapse, the catenary action of the cable prevented the collapse and transferred the load of the floor to the neighboring columns and the rest of the structure. As a result, although the floors may have relatively large deformations, full progressive collapse is prevented, as shown in Fig. 2.13.

To test the performance of floors reinforced with steel cables, a full size one storey building was designed and constructed to simulate a portion of a typical braced frame steel structure (Astaneh-Asl et al. 2001a, b; Tan et al. 2003). The structure consisted of a steel frame with simple shear connections in both directions supporting a concrete slab floor cast on the steel corrugated decks. The long slotted holes in the shear tab beam-to-column connection were designed to accommodate beam rotations of up to 0.60 radians during the tests. The concrete slab of the floor had only a

negligible amount of reinforcement to prevent shrinkage cracks. However, within about one meter width of the slab, where the steel cables were placed for new construction, larger reinforcing bars were used.

Three different groups of tests were conducted on the specimen. Group I was conducted for the case when steel cables were placed inside the floor slab. In this group, four high strength Grade 270 (f_U=270 ksi) steel strand cables, each 1.25 inches in diameter, were placed on top of the top flange of the steel beams within the concrete floor slab. Group II was for the case when there was no cable used. In Group III, the specimen represented an existing building retrofitted by adding two 0.75 inches in diameter high strength (f_U=220 ksi) zinc-coated helical steel strand cables to the side of the beams under the floor slab.

Prior to tests, comprehensive nonlinear finite element analyses of the specimen of Group I were conducted to predict the behaviour of the floor upon removal of the middle column. The ribbed floor system (steel deck and concrete slab) was modelled with a constant thickness reinforced concrete slab on top of a flat steel plate as shown in Fig. 2.14. In this figure, the nonlinear material behaviour model for the steel deck/concrete slab is also shown, along with material properties used in the deck/slab model. The result of finite element analyses indicated that if the middle column is removed, the floor will start moving downward due to the acceleration of gravity and will stop after dropping about 20.7 inches, as shown in Fig. 2.13, due to the development of catenary tension force in the cables and steel deck floor.

For Group I tests, it was shown that the maximum load that the cable system could tolerate was more than 3 times the design load. For Group II tests, the ratio of maximum load/design load was barely 1.2. For Group III tests, the specimen was able to tolerate about 1.5 times the design load. The test setup for Group III is shown in Fig. 2.15.

Similar to the above mentioned idea of Astaneh-Asl et al., the cable can also be used for earthquake resistance. As shown in Fig. 2.16, the tensile and rotational capacity of post-tensioned steel cables is utilized to provide a "safety net" for the beam once an angle connection to the column fails under earthquake loading (Ricles et al. 2001, 2002). The connection is self-centring without residual deformation, so the steel moment resistant frame will not have a residual drift after an earthquake unless significant residual deformation occurs at the base of the columns. During an earthquake, the beams and columns remain essentially elastic while inelastic deformation of the connection provides energy dissipation. Significant damage to the steel moment resistant frame is only contained to the angles of the connection. This angle can then be replaced and the building repaired quickly and easily. In addition, site-welding is not required.

In addition to preventing structural collapse caused by blast, catenary action was widely researched in the field of structural fire engineering. Because it is a functional requirement that the structure remains stable to allow adequate time for safe evacuation and rescue, quantitative assessment of the fire resistance of a structure is necessary and advanced numerical simulation tools and computational methods are needed.

To analyze structures in fire, most of the existing analysis methods rely on a finite element approach which calculates the nonlinear response that reflects the spread of plasticity throughout the member cross section and the progression of yielding along the length of the member. This method can trace in detail the behaviour of a member by using the material stress–strain relation at elevated temperature (El-Rimawi et al. 1995; Wang et al. 1995; Wang and Kodur 2000; Huang et al. 2000; Yin et al. 2004). In addition to the finite element analysis, Yin and Wang (2005a, b) developed a simplified hand calculation method of catenary action in axially restrained steel beams at elevated temperature. When assessing the performance of steel beams under fire, the main feature of the behaviour of a beam at large deflections is that end axial restraints cannot be ignored, because these end axial restraints can cause the development of catenary action which can become the dominant load carrying mechanism of the beam.

There are two important design implications in exploring catenary action (Yin and Wang 2005a). Firstly, the development of catenary action is not limited by a beam's material strength but by its deflection. A beam with material strength reduced by high temperatures can still resist the lateral load simply by deflecting more, and it can experience very large deflections without collapse due to high temperature. Therefore, the requirement of fire protection to all steel beams can be reduced. Secondly, an axially restrained beam can develop catenary action at temperatures above the limiting temperature calculated for pure flexural bending. Thus, if the beam's temperature cannot be guaranteed to remain below this limiting temperature, the beam will impose a tension on the adjacent

structure due to its catenary action. If the adjacent structure does not have adequate horizontal strength and stiffness to resist this catenary force of the beam falling down, there is a danger of the adjacent structure collapsing (Yin and Wang 2005a). The reason of the collapse of the adjacent structure is not because it is horizontally pushed outward from this beam extended by the high temperature, but because the adjacent structure is horizontally pulled inward by catenary tension due to this beam falling down. Thus, a very large horizontal displacement may be imposed on the adjacent structure. If this horizontal displacement is too large, the adjacent structure may collapse due to the $P-\Delta$ effect.

2.4 Different types of beam-to-column connections

For high-rise or medium-rise steel framed building structures, the connections between beams and columns can be largely classified into three types: simple, semi-rigid, and rigid joints.

The simple connection is detailed to allow the beam end to rotate and only transmit very small bending moment across the joints, but it can resist shear force through the web cleat very well. The simple connection can be idealized as a pin-connected joint for simplicity. It includes fin plate connection, flexible end plate connection, double angle connection, etc (SCI 2002). Joint details such as the fin plate connection shown in Fig. 2.17 are widely used in practice.

The semi-rigid connection is between the rigid joint and the simple joint (Faella et al. 2000; Kishi and Chen 2007). It is designed to transmit the shear force and a proportion of the bending moment across the joint. A type of semi-rigid connection is shown in Fig. 2.18. Without introducing complicated fabrication of the joint, this type of joint allows some joint rotation but can still partially transfer bending moment, which is smaller than that transferred by a rigid joint but larger than that by a simple joint. The mathematical model for evaluating semi-rigid joints is shown in Fig. 2.19. In this model, the rotational stiffness of the joint is modelled as a spring. There are two extreme cases: (1) when the stiffness of the spring is equal to zero, the joint is a pin-connected joint, which can not transfer moment; and (2) when the stiffness of the spring is infinite, the joint becomes a fixed-connected joint, which has no relative rotation. Although the simple connection and the rigid connection between beam and column are usually modelled as pin-connected joint and fixed-connected joint respectively for simplicity, the pure pin-connected joint and the pure fixed-connected joint are rather rare in practice in steel frames and most joints can be classed as semi-rigid (Faella et al. 2000).

In contrast to the simple connection, the rigid connection can transfer not only the beam shear force, but also the bending moment through fully connecting beam flanges, so it is called moment connection as well (SCI 1995). This connection is detailed to ensure a monolithic joint, and beam end moment is transmitted into the column itself and the beam framing into the column on the opposite side. There are a variety of beam-to-

column connections that are commonly used in moment-resistant steel framed structures. They will be reviewed in the following.

The traditional moment connection detail, as shown in Fig. 2.20, was widely used in the US before the 1994 Northridge earthquake for more than 40 years. The web cleat, which is designed to carry the shear, is shop welded to the column and site bolted to the beam with high strength friction grip (HSFG) bolts. Beam flanges are joined to the face of the column flange on the site using a complete joint penetration (CJP) weld. The flange-to-column welds are usually down-hand welds using backing strips. Column stiffeners, also called continuity plates, are usually required. This detail can avoid flange cover plates as it directly connects the beam flange to the column flange.

The traditional beam-to-column steel connection system was usually assumed to be able to form a plastic hinge in the beam, just outside the column flange face. However, when subjected to a strong earthquake, the site-welded flange connection may not perform so well as originally expected. Instead of the expected gradual moderate yielding of the steel elements to dissipate the earthquake energy delivered to the building, sudden brittle fractures were observed. During the Northridge earthquake 1994, cracks that developed at site welds at or near beam bottom flanges were most frequently reported (FEMA 2000a, Bruneau et al. 1998, Houghton et al. 2001). As shown in Fig. 2.21a, fractures typically initiated at the complete joint penetration (CJP) weld between the beam bottom flange and the column flange. Once initiated, these fractures progressed along a number of different paths and compromised the integrity of the steel frame

in different ways, depending on the individual joint conditions (FEMA 2000b; Houghton et al. 2001).

In some cases, the fractures progressed completely through the thickness of the weld, or the metal at fused zone just behind the weld shown in Fig. 2.21b. Other fracture patterns also developed. In some cases, as shown in Fig. 2.21c, the fracture developed into the column flange base metal behind the CJP weld. In these cases, a portion of the column flange remained bonded to the beam flange, but pulled free from the remainder of the column. This fracture pattern has sometimes been termed a "divot" failure (FEMA 2000b; Houghton et al. 2001).

As shown in Fig. 2.21d, a number of fractures progressed completely through the column flange, along a near horizontal plane that aligns approximately with the beam lower flange. In some cases, these fractures extended into the column web and progressed across the panel zone, as demonstrated in Fig. 2.21e. Some instances where columns fractured entirely across the section have also been reported (FEMA 2000b; Houghton et al. 2001).

Once these brittle fractures occurred, the beam-to-column connection experienced a significant loss of flexural rigidity and strength to resist those loads that tend to open the crack. Residual flexural strength and rigidity must be developed through a couple consisting of forces transmitted through the remaining top flange connection and the web bolts. In providing this residual strength and stiffness, however, the bolted web connections can themselves be subject to failures, as shown in Fig. 2.21f (FEMA 2000b; Houghton et al. 2001).

Observed beam-to-column connection fractures occurred prematurely, precluding the beam's ability to deform in a ductile manner. The observed failure phenomena are also true for frames designed in low seismicity zones because this observed brittle behaviour is typical of traditional connection technology. When a column is destroyed by a blast, a very large tension will be induced in the beams due to catenary action. Then tensile stress will increase significantly at the beam flanges in the beam-to-column connection, and so the failure modes shown in Fig. 2.21 are also possible for the scenario of the removal of a column. Hence, steel frame buildings subjected to terrorist attack loads are susceptible to the same failure phenomena as observed after earthquakes.

After the Northridge earthquake, a variety of connection design options were proposed to mitigate the fundamental design and construction flaws that are characteristic of the traditional way of connecting steel frame beams to columns.

One of those design options, the Reduced Beam Section (RBS), or "dogbone" connection, which is shown in Fig. 2.22, uses cuts near the ends of the beam flanges to reduce the flange area over a length of the beam near the ends of the beam span, to force the plastic hinge to occur in this deliberately weakened segment (Khandelwal et al. 2007). By so doing, the plastic hinge can be driven away from the column face and the bending moment can be reduced at the column face. While the "dogbone" strategy may work well for earthquake loading, it might induce failure during a terrorist attack (Rittenhouse et al. 2001, Smilowitz et al. 2001). Because this intentionally weak link has the disadvantage of reducing the

stiffness and strength, plastic deformation and premature failure can concentrate at this weakened cross-section of the beam.

Other methods have also been proposed for reinforcing the connection to prevent brittle fractures. These are the haunch, rib plate, flange plate, end plate, SidePlate, and Extreme Event Beam Link connections. The strengthened section of the beam end can force the plastic hinge to form in the beam away from the column face and dissipate the energy from the earthquake away from the vital beam-to-column connection.

The haunch, shown in Fig. 2.23, is perhaps the most common method. By increasing the depth at the beam-to-column connection, the haunch can greatly increase stiffness and strength at joints. Various types of haunch have been suggested, the most promising of which is the inverted T-section haunch. Similar to the haunch joint, the rib plate has also been used as method for reducing stress on the welded beam-to-column connection. The detail of the rib plate is shown in Fig. 2.24. (Bruneau et al. 1998)

Flange plates have become one of the most common alternatives since the Northridge earthquake. The flange plate connection can be further divided into two types: shop-welded flange and site-welded flange. For the shop-welded flange plate connection as shown in Fig. 2.25, lapped flange plates are shop-welded to the flanges of the column and are then connected to the flanges of the beam by site-bolting. (Bruneau et al. 1998; Hoeckman et al. 2005)

For the site-welded flange plate connection, shown in Fig. 2.26, the lapped flange plates are connected to the flanges of the column by site butt-welding and to the flanges of the beam by site fillet-welding. The top lapped flange plate is narrower than the top flange of the beam and the bottom lapped flange plate is wider than the bottom flange of the beam. This enables down hand welding (welding from above) to be carried out in both cases leading to a stronger weld. If the bottom plate is welded to the column before the beam is offered up to the column, then it can act as a construction seat speeding the erection process. (Bruneau et al. 1998; Hoeckman et al. 2005)

These two types of connections behave differently. As compared with the bolted flanges connection, the fully welded connection exhibits more ductile behaviour (Popov and Pinkney 1969, Bruneau et al. 1998). As for shear connection, for both types, the beam webs are usually connected by site-bolting. These two types of joints have the advantages that brittle fracture caused by site butt-welding can be avoided, and that the bolts are employed to resist a shear force, rather than a tensile force.

For the end plate connection, the end plate, which is first welded to the end of the beam in shop, is bolted to the flange of the column on site. This type of connection is shown in Fig. 2.27. The end plate can either be stopped at the level of the flange of the beam or be extended beyond the flange to accommodate a row of bolts; the extended end plate is the most economic of the two alternatives. The detail without the extended end plate is only able to carry a relatively small proportion of the beam capacity (assuming that excessively thick end plates and large bolts are

not used). Although it can also avoid the brittle fracture of site butt weld, this type of joint has the disadvantage that the bolts are employed to resist tensile force as well as shear force. When the widely used black bolts and galvanised bolts are subjected to rapid rates of blast loadings, the tensile bolts have lower resistance than under static loading or some slower rates of dynamic loading, and may fail by stripping thread and chipping off nuts (Munoz-Garcia et al. 2005).

The SidePlate connection system, a patented post-Northridge connection design, can avoid the fundamental problems that are inherent with the traditional moment connection by using a wholly different connection geometry. As shown in Fig. 2.28, by using two parallel full-depth side plates that constitute a robust and redundant structural link between the two beams, the SidePlate connection geometry provides a defined structural beam-to-beam continuity across a column in a two-sided connection. Using horizontal fillet welds loaded principally in shear along their length to transfer the axial load to adjacent moment frame beams, the two full-depth side plates can act as effective continuity elements to transfer axial load in 'cable-like' catenary action following the violent removal of a building column. Top and bottom beam flange cover plates strengthen the ends of the beams while satisfying a practical need of bridging the difference between the flange width of a beam and the typically wider flange width of a column (Houghton et al. 2001).

The construction of the SidePlate connection system uses all shop fillet-welded fabrication, configured with simple unrestrained fillet welds for increased quality control of all critical connection welds affecting

connection performance. All fillet welds are made in either the flat or horizontal position using column tree construction for maximum quality. Shop fabricated column trees are erected and joined on the site using one of four link beam splice options to complete the moment-resisting frame. Link beam splice options include a fully complete joint penetration (CJP) welded joint, bolted matching end plates, fillet-welded flange plates, and bolted flange plates, or combinations thereof (Houghton et al. 2001).

In Fig. 2.29, some simulation results of the connections between the removed column and the two beams on its opposite sides are given by Houghton et al. (2001) for both the traditional moment connection and the SidePlate moment connection. For the traditional moment connection, it can be seen from Figs. 2.29a-b that the stress and strain levels are very high in the beam flanges in the vicinity of the welds. These high stress and strain levels can potentially lead to fracture initiation from the region of the flange welds. On the contrary, for the SidePlate connection, it can be seen from Figs. 2.29c-e that stress and strain levels are negligibly low and the beam flange forces can pass over the column core by the side plates. This demonstrates that the SidePlate moment connection can provide a beam-to-beam structural link that is independent of the column, and significantly reduce the stress and strain in the beam flanges near the connection. In Fig. 2.29d, in order to show clearly the stress distribution behind the side plates, one side plate is not shown. From Fig. 2.29d, it can be seen that the stresses of the column and the beam ends between two side plates are very small.

In addition to the above mentioned connections, a new patent steel beam-to-column joint detail for newly constructed steel buildings has been

recently proposed. Named "Extreme Event Beam Link Connection" (Hoeckman et al. 2005), this new type of joint detail is shown in Fig. 2.30. To allow the beam link plates to pass through, the vertical slots are required to cut in the column flanges. The beam flange force can be transferred over the column to the beam on the opposite side through the beam link plates. The beam link plates are made of high strength steel to minimize the loss in column section due to the flange slots. Instead of single shear adopted in the bolted flange plate connection shown in Fig. 2.25, the bolts in the connection here are in double shear due to the use of symmetrical beam links around the extended web fin plates, and therefore only half the number of bolts are required as compared to the single shear. The "Extreme Event Beam Link Connection" has many advantages. Because only the connection of tab and beam web is required during erection, the time under crane need be no greater than for the simplest fin plate connection. After erection, the connection strength can be enhanced by connecting beam flanges; and therefore there is no influence on the critical path of the construction programme. Through connecting beam flanges together by beam links, progressive collapse can be resisted by developing catenary action in the beams (Hoeckman et al. 2005).

2.5 Summary

In this chapter, Case Studies of progressive collapse, Codes and Standards for designing against progressive collapse, the role of catenary action in

preventing progressive collapse, and different types of beam-to-column connections were reviewed.

From the above literature review, it can be seen that there are three methods of preventing progressive collapse disproportionate to original local damage: (1) redundancy or alternative load paths; (2) local resistance; and (3) continuity or interconnection (Nair 2006).

When a column is removed, global system collapse may occur if the damaged system is unable to reach a new static equilibrium configuration. One of the key mechanisms thought to be able to assist a damaged structure to reach an alternative equilibrium configuration is catenary action. Providing an alternative load path by catenary action implies the development of adequately large deformations and tensions such that gravity loads are mainly resisted by the vertical components of axial forces that develop in the beams.

Due to linking the beams at the two opposite sides of a damaged column, beam-to-column connections play a crucial role in the development of catenary action of the beams and are more important than the beams themselves. Some steel frames perform poorly and will fail immediately at their beam-to-column connections once a column is removed by a blast. On the contrary, other structural steelworks behave very well, and the progressive collapse of the structure will be prevented by providing an alterative path because catenary action can be fully developed within the beams originally supported by the damaged column as illustrated in Fig. 1.1. The behaviour of framed structural steelworks will vary significantly with different types of connection being adopted.

The beam-to-column connections can largely be divided to three types: simple connection, which can mainly transfer shear force; moment connection, which can transfer shear force and bending moment; and semi-rigid connection, which can transfer shear force and a portion of bending moment.

Investigation of the records of bomb-damaged in World War II has not revealed any instances of catenary action in practice in UK (Byfield and Paramasivam 2007). The reason for the catenary action cannot be developed in beams is because the simple connections used in UK are too weak to do so (Liu, Davison and Tyas 2005; Byfield and Paramasivam 2007). However, almost all of existing structural steelworks in UK are simple steel construction. The number of existing structural steelworks will be much larger than the number of new ones even in the future. The cost of retrofitting existing one is usually much smaller than that of demolishing the old structural steelwork and re-constructing a new one. Solving this problem will be very useful. As a result, the research in this thesis is devoted for solving the problem of preventing progressive of existing simple steel construction in UK by strengthening its weak simple connection. The necessity, the method and the effect of retrofitting existing simple steel construction will be discussed in the next chapter.

Chapter 3: Prevention of collapse by catenary action and the necessity of strengthening the joints

In this chapter, the characteristics of catenary action due to the removal of a column are investigated. The need for strengthening the joints of a simple construction is illustrated. Two retrofitting schemes are proposed for strengthening the fin plate beam-to-column connection of existing buildings. It is shown that through linking beam flanges together, an originally partial-strength simple joint can be converted to a full-strength moment joint.

3.1 Analysis of catenary action

Normally beams are employed to resist bending moment only, and are seldom called up to resist an axial force. However, when the column supporting a beam is destroyed by a severe blast, the beam will sag significantly, as shown in Fig. 3.1. Because of the diaphragm effect of the floor slab, which is almost rigid within the floor plane, movement in the horizontal direction is greatly restrained. The sagging of the beam generates a rather large axial tensile force due to catenary action. In this situation, it is the beam, originally supported by the destroyed column, that will have to mainly resist this large tensile force. By providing an alternative force transfer path around the damaged column, the beam catenary action enables the structure to support gravity loads without collapse.

Because it is activated only after large deformations have occurred, the beam catenary action represents the last line of defence against collapse.

When subjected to both axial and lateral loads, there will be an axial force and a bending moment in a short beam segment. All possible stress distribution diagrams are given in Fig. 3.2. When the force N and the moment M are not so large, the elastic limit of the material will not be exceeded. Corresponding stress distributions are shown in Figs. 3.2a and 3.2b. In Fig. 3.2a, the neutral axis is within the cross-section, but in Fig. 3.2b, it is out of that. Because the whole section is linear elastic, the total maximum stress may be obtained simply as follows

$$\sigma_{\max} = \sigma_N + \sigma_M = \frac{N}{bh} + \frac{6M}{bh^2} < \sigma_y \tag{3.1}$$

where σ_y represents the yield stress, and *b* and *h* represent the width and depth of rectangular cross-section respectively. In the above equation, stresses σ_N and σ_M are due to the axial force N and the bending moment M, respectively.

As shown in Fig. 3.1, when a middle column in a structure is destroyed, for equilibrating vertical loads, an extremely large catenary force N is involved in the initial stage because the steel beams are horizontal and the beam-to-column joints are a simple connection. It is rather easy for the corresponding normal stress to cause the beam segment to yield. Because of this yielding, the stress is no longer proportional to the strain, and the stress distribution is no longer proportional to the distance from the neutral axis. As a result, the nonlinear stress-strain characteristics of the material are involved.

For any fibre in the cross-section, normal stress develops due to both bending moment and axial force. For simplicity, it is assumed that the adopted stress-strain relationship is elastic-perfectly plastic, the lateral loads remain constant, and only the axial tensile load increases. The sum of the bending moment component and the axial force component can not exceed the yield stress, i.e., $\sigma_N + \sigma_M \le \sigma_y$. As the axial force component σ_N increases, the yield stress σ_y may be reached. If σ_N increases further, σ_M will have to decrease since $\sigma_M = \sigma_y - \sigma_N$. With the axial tensile force component σ_N approaching the yield stress σ_y, the bending moment component σ_M will approach zero at that fibre, i.e., $\sigma_M = \sigma_y - \sigma_N \approx \sigma_y - \sigma_y = 0$. As a result, the shape of the stress distribution in the cross section will change.

In this case, some part of the section is in the plastic range and the other part in the elastic range, and the stress distribution is shown in Figs. 3.2c-e, where the bottom of the cross-section has yielded in tension. As the tensile force N increases, plasticity will develop further, and the stress distribution will change. In Fig. 3.2c, the neutral axis is out of the cross-section; in Fig. 3.2d, it is within, and the compressive region is elastic; and in Fig. 3.2e, part of the compressive stress also reaches the yield level. Unlike the evaluations for the elastic cases, the analysis of the above mentioned combined effect of axial tension and bending becomes much more complicated, because the principle of superposition is no longer valid in the elastoplastic range. The evaluation of the combined effect is rather time consuming because some form of iteration is usually required to find the numerical solution that will satisfy the inelastic tension-bending moment

interaction. To overcome this problem, Yin and Wang (2005a, b) have proposed a simplified hand calculation method through an incremental approach for analyzing the catenary action of I-sectional beams due to fire. Their simplified method is also appropriate for the evaluation of the catenary action due to the removal of a column.

If yielding is fully developed, however, the analysis becomes much simpler. When the whole cross-section approaches the ultimate capacity, the elastic zone disappears, and the stress distribution can be assumed to consist of rectangular diagrams, as shown in Fig. 3.2f. There is only one unknown to be obtained, the location h_M of zero strain from the extreme fibre. Using the notation shown in Fig. 3.2f, one may proceed as follows:

$$T_M = C_M = \sigma_y b h_M \tag{3.2}$$

$$T_M + T_N - C_M = N \tag{3.3}$$

where σ_y represents the yield stress. Combining Eq. (3.2) and Eq. (3.3) give

$$N = T_N = \sigma_y b(h - 2h_M) \tag{3.4}$$

from which

$$h_M = \frac{h}{2}\left(1 - \frac{N}{\sigma_y b h}\right) \tag{3.5}$$

By taking moments about the centroid, one can obtain

$$T_M\left(h - h_M\right) - M = 0 \tag{3.6}$$

By substituting the values of T_M and h_M into the above equation, M can then be given by

$$M = \frac{1}{4}\sigma_y bh^2\left[1-\left(\frac{N}{\sigma_y bh}\right)^2\right] \tag{3.7}$$

For the given axial tensile force N and the bending moment M, the above equation can be rewritten as

$$\frac{M}{M_p}+\left(\frac{N}{N_p}\right)^2 = 1 \tag{3.8}$$

where $M_p = \frac{1}{4}\sigma_y bh^2$ is the plastic bending moment capacity in the absence of any axial force, whereas $N_p = \sigma_y bh$ is the plastic axial force capacity in the absence of any bending moment.

As shown in Fig. 3.1, when a centre column is destroyed by a blast, gravity loads are mainly resisted by the vertical components of axial catenary forces that develop in the beams. It is apparent from Eq. (3.8) that the reduction in the bending moment is proportional to the square of the axial force. Because the beams are horizontal, the tensile forces can be extremely large in the initial stage, and it is possible for the tensile forces to cause the whole cross-section of the beam to yield. With N approaching N_p, the stress distribution will approach Fig. 3.2g, thus M will approach zero. Consequently, when the catenary force is extremely large, the bending moment will almost disappear, the shape of vertical displacement diagram will approximate the shape of the original bending moment diagram, and the behaviour of the structure will change from that of a beam to that of a cable.

Of course, yielding will not necessarily fully develop in the entire cross-section and the stress distribution will perhaps be different from Fig. 3.2f, therefore a general closed form solution is not available. However, whether or not the exact result can be obtained, the conclusion remains true that increasing the axial tension will greatly reduce the moment capacity of the cross-section. When N increases stress redistribution will occur, changing from the elastic stage of Figs. 3.2a and 3.2b through Figs. 3.2c-3.2f, and finally to the pure tensile plastic stage shown in Fig. 3.2g. Due to the stress being uniformly distributed in Fig. 3.2g, there is only pure tension and no bending moment.

For simplicity, only the solution for beams with a rectangular section is given above. For beams with an I-shape cross-section, Yin and Wang (2005a, b) have given the following mathematical expressions, which are more complex than Eq. (3.8).

A universal beam under combined axial load *N* and bending moment *M* is shown in Fig. 3.3. The stress-strain relation is assumed to be linear elasticity-perfect plasticity. If the plastic neutral axis is in the web, as shown in Fig. 3.3a, then the plastic interaction of axial load and bending moment can be given as

$$\frac{M}{M_p}+\frac{(1+\alpha)^2}{\alpha[2(1+\beta)+\alpha]}\left(\frac{N}{N_p}\right)^2=1 \qquad (3.9a)$$

where $\alpha=\frac{A_w}{2A_f}$ and $\beta=\frac{t}{h_0}$.

If the plastic neutral axis is in the flange, as shown in Fig. 3.3b, then the plastic interaction of axial load and bending moment can be given approximately as

$$\frac{1-\gamma}{1-\dfrac{(1+\alpha)^2\gamma^2}{\alpha[2(1+\beta)+\alpha]}}\frac{M}{M_p}+\frac{N}{N_p}=1 \tag{3.9b}$$

in which $\gamma=\dfrac{A_w}{2A_f+A_w}$

In the above equations, the I-beam's pure plastic axial capacity without any bending moment is

$$N_p=A\sigma_y=(2A_f+A_w)\sigma_y \tag{3.10a}$$

and the I-beam's pure plastic bending moment capacity without any axial force is

$$M_p=W_p\sigma_y=\left[A_f(h-t)+\frac{1}{4}A_w h_0)\right]\sigma_y \tag{3.10b}$$

When the plastic neutral axis is in the web of the universal beam, it can be demonstrated by Eq. (3.9a) that the reduction in the bending moment is proportional to the square of the axial force, which is similar to Eq. (3.8). When the plastic neutral axis is in the flange, however, it can be seen from Eq. (3.9b) that the reduction in the bending moment is approximately proportional to the axial force, not to its square like Eq. (3.8). However, no matter what expression one follows, for both the rectangular beam and the I-beam, the bending moment will decrease with increasing axial force.

When the two beam ends are restrained in the horizontal direction by a floor slab, catenary tension can be produced along the beam. As illustrated in Fig. 3.4, one can take a left section at any horizontal distance x along a beam from its right support A. Taking moments about the support A and considering counterclockwise as positive, the equation of moment equilibrium is given as

$$\sum M_A = -M_x - M_A - N_x y_x - V_x x + P_1 L_1 + P_2 L_2 = 0 \qquad (3.11)$$

where x is any horizontal distance measured to the left from the beam right support A; M_x, V_x, N_x and y_x are the bending moment, shear force, tension, and deflection respectively, of the cut section at distance x; M_A is the restraint bending moment at the support A; P_1 and P_2 are concentrated loads, L_1 and L_2 are their horizontal distances from the centre of moments A. Yin and Wang (2005a, b) have also given a similar mathematical expression for analyzing axially restrained steel beam at elevated temperature.

Because the concentrated loads and their horizontal distances usually do not significantly change during loading, Eq. (3.11) may be rewritten as the following

$$M_x + M_A + N_x y_x + V_x x = P_1 L_1 + P_2 L_2 \approx const \qquad (3.12)$$

In the above equation, the term $N_x y_x$, which can significantly reduce the bending moment in the span, is contributed by the catenary action. If the deflection is y_x=0 or the tension is N_x=0, there will be no catenary action, and the above equation will change to an expression of bending

and shear. For preventing collapse by catenary action, the term $N_x y_x$ must be adequately large.

With increasing deflection y_x, the tension N_x will generally increase due to the elongation of the beam segment, except for the yield plateau where it remains roughly constant. It can be seen from Eq. (3.12) that the bending moments M_x, M_A, and shear force V_x will reduce with increasing deflection y_x, because the sum of the four terms on the left side of the equation is approximately constant.

In the middle beam segment, if the deflection y_x is large enough, the bending moment M_x and the shear force V_x will approach zero. At the beam end A, however, the bending moment M_A can not be reduced to zero because the rotation is restrained and the curvature is very large, even though the deflection y_x is also very large. With the combination of the horizontal restraints at two beam ends, this deflection can produce a catenary action, which can reduce the bending moment.

The requirement of utilizing catenary action to prevent collapse can only be satisfied if yielding can be developed in the whole length of the beam. However, the resistant capacity of the simple connection is largely designed according to the maximum shear force. Therefore, if not properly strengthened, the joint will fail prematurely under the extremely large catenary tension. Different results for structures with weak ends and strong ends will be discussed in the next section.

3.2 Exact solution of catenary action of truss model

The susceptibility of different beam connections to the effect of catenary action will be examined here, for the purpose of illustrating the need for reinforcing the joints of simple steel construction. When the tension is extremely large, the contribution of the bending moment approaches zero and the structure changes from a beam to a tensile truss. In addition, because of involving both material and geometric nonlinearities, the truss is the only structural type for which exact results can be obtained in the catenary action analysis. As a result, a truss structure can be taken as a model for simplicity. Although the analysis of the truss is relatively simple, the obtained conclusions remain true for other structural types.

Consider a truss member of initial length *L* and area *A* that is stretched to a current length *l* and area *a*. As a result of catenary action, the deformation is very large, so that both geometric and material nonlinearities are involved. Due to large strains, the widely used small engineering strain measure, which is defined as

$$\varepsilon_E = \frac{l - L}{L} \tag{3.13}$$

is inappropriate here. Consequently, the true strain measure (Belytschko et al. 2000) is adopted here, which is basically of an incremental form and given as the following.

$$d\varepsilon = \frac{dl}{l} \tag{3.14}$$

The current strain can be obtained by adding up all the small strain increments that take place when the truss is continuously stretched from its original length *L* to its current length *l*. This integration process leads to the definition of the logarithmic strain ε as

$$\varepsilon = \ln\left(\frac{l}{L}\right) \tag{3.15}$$

In the following two models, the trusses used are similar with the beams shown in Fig. 4.3 of Chapter 4. As shown in Fig. 3.5, the structures, consisting of one long middle segment and two short end segments, are subjected to a vertical load. The influence of different depths and lengths of the truss end segments on the development of catenary action is evaluated. In Model 3.1, the end segments are weaker than the middle segment. The objective of this evaluation is to simulate the response of the original structure with simple steel beam-to-column joints when a supporting column is removed.

Model 3.1. The initial length of the structure is $L = 0.6m$, and the lengths of the weak end and the normal middle segments are $L_e = 0.05L = 0.03m$ and $L_m = L - 2L_e = 0.54m$, respectively. The steel is assumed to be elastic perfectly plastic. The Young's modulus is $E = 2\times10^{11} N/m^2$. The yield stress is $\sigma_y = 4\times10^8 N/m^2$, and the yield strain is $\varepsilon_y = \sigma_y / E = 2\times10^{-3}$. It is assumed that the failure strain is $\varepsilon_{fail} = 0.25$. It is also assumed that the material is incompressible, i.e., the Poisson's ratio $\nu = 0.5$. The width and the depth of the normal middle segment are 0.01m and 0.02m, respectively. For the weak end connection segment, the width is also 0.01m, but the depth is

0.01m, instead of 0.02m, so that the cross-sectional area is only half of that of normal one. They are given respectively by

$$A_m = 0.01 \times 0.02 = 2 \times 10^{-4} m^2, \ A_e = 0.01 \times 0.01 = 1 \times 10^{-4} m^2$$

Because of their smaller area, the weak end segments reach the failure strain before the normal middle segment. At that time, the length is

$$l_e = L_e \exp(\varepsilon_{fail}) = 0.03 \exp(0.25) = 0.03852 m$$

the area is

$$a_e = A_e \frac{L_e}{l_e} = A_e \exp(-\varepsilon_{fail}) = 1 \times 10^{-4} \times \exp(-0.25) = 0.7788 \times 10^{-4} m^2$$

and the axial force is

$$n_e = a_e \sigma_y = 0.7788 \times 10^{-4} \times 4 \times 10^8 = 3.115 \times 10^4 N$$

For the normal middle segment, the axial force is equal to that of the weak end segments

$$n_m = E a_m \varepsilon_m = E A_m \frac{L_m}{l_m} \ln\left(\frac{l_m}{L_m}\right) = n_e$$

Substituting data into the above equation, then

$$2 \times 10^{11} \times 2 \times 10^{-4} \times \frac{0.54}{l_m} \ln\left(\frac{l_m}{0.54}\right) = 3.115 \times 10^4$$

The above equation can be rewritten as the following

$$\frac{0.54}{l_m} \ln\left(\frac{l_m}{0.54}\right) = 0.7788 \times 10^{-3}$$

Solving the equation, one can obtain

$$l_m = 0.5404m$$

and the current strain in the normal middle segment is given by

$$\varepsilon_m = \ln\left(\frac{l_m}{L_m}\right) = \ln\left(\frac{0.540421}{0.54}\right) = 0.7794\times10^{-3} < \varepsilon_y = 2\times10^{-3}$$

Because the middle segment remains elastic and its strain cannot further increase, all plastic deformation occurs in the end segments. When the failure strain is reached at the weak end, the length of whole structure is

$$\begin{aligned} l &= 2l_e + l_m = 2L_e\exp(\varepsilon_{fail}) + l_m \\ &= 2\times0.03\exp(0.25) + 0.540421 = 0.6175m \end{aligned}$$

The corresponding strain for the whole structure

$$\varepsilon = \ln\left(\frac{l}{L}\right) = \ln\left(\frac{0.6175}{0.6}\right) = 0.0287$$

the vertical displacement

$$y = \sqrt{l^2 - L^2} = \sqrt{0.6175^2 - 0.6^2} = 0.1463m$$

and the corresponding failure load shown in Fig. 3.5a is

$$p = \frac{y}{l}n_e = \frac{0.1463}{0.6175}3.115\times10^4 = 7.380\times10^3 N = 7.380kN$$

All of the above applies to the truss. When lateral loads exist, however, there will be a bending moment and a shear force, and therefore the structure becomes a beam. For a realistic beam with fin plate connection, however, the structure can only fail at the connection at the removal of a column. When the connection fails, the middle segment of the beam is

almost rigid when compared with the deformation of the connection segment. As a result, the evaluation of the end segments is more important than that of the middle segment.

The initial normal stress distribution usually varies in the cross-section due to unintentional restraining. When the beam end is elongated adequately, its plastic strain will fully develop and therefore the stress will change to a uniform distribution. Thus, the transition from bending to pure tension state can occur in the fin plate joint if its ductility is sufficient, and the simplified truss-model may still be useful.

In Model 3.2, the end segments are stronger than the middle segment. The aim of this calculation is to simulate the response of the structure with strengthened beam-to-column joints when catenary action is involved.

Model 3.2. All other conditions are the same as those in Model 3.1, except for the depth of the end segments which is different. In Model 3.1, the end segments are weak; but in this model, they are strengthened. Their depth is changed from 0.01m to 0.03m.

$$A_e = 0.01 \times 0.03 = 3 \times 10^{-4} m^2 = 1.5 A_m$$

Because of its smaller area, the normal middle segment reaches the failure strain before the strong end segments. At that time, the current length

$$l_m = L_m \exp(\varepsilon_{fail}) = 0.54 \exp(0.25) = 0.6934 m$$

the area

$$a_m = A_m \exp(-\varepsilon_{fail}) = 2 \times 10^{-4} \exp(-0.25) = 1.5576 \times 10^{-4} m^2$$

and axial force

$$n_m = a_m \sigma_y = 1.5576 \times 10^{-4} \times 4 \times 10^8 = 6.230 \times 10^4 N$$

For the end segments, the axial force is equal to that of the middle segment

$$n_e = E a_e \varepsilon_e = E A_e \frac{L_e}{l_e} \ln\left(\frac{l_e}{L_e}\right) = n_m$$

Substituting data into the above equation, then

$$2 \times 10^{11} \times 3 \times 10^{-4} \times \frac{0.03}{l_e} \ln\left(\frac{l_e}{0.03}\right) = 6.230 \times 10^4$$

The above equation can be rewritten as the following

$$\frac{0.03}{l_e} \ln\left(\frac{l_e}{0.03}\right) = 1.0384 \times 10^{-3}$$

Solving the equation, one can obtain

$$l_e = 0.0300312\text{m}$$

and the current strain in the end segments is given by

$$\varepsilon_e = \ln\left(\frac{l_e}{L_e}\right) = \ln\left(\frac{0.03003}{0.03}\right) = 1.0395 \times 10^{-3} < \varepsilon_y = 2 \times 10^{-3}$$

Because the end segments remain elastic and their strain cannot increase, all plastic deformation occurs in the middle segment. When the failure strain is reached at the middle segment, the length of whole structure is

$$l = 2l_e + l_m = 2l_e + L_m \exp(\varepsilon_{fail})$$
$$= 2 \times 0.0300312 + 0.54 \exp(0.25) = 0.7534m$$

The corresponding strain for the whole structure

$$\varepsilon = \ln\left(\frac{l}{L}\right) = \ln\left(\frac{0.7534}{0.6}\right) = 0.2277$$

the vertical displacement

$$y = \sqrt{l^2 - L^2} = \sqrt{0.7534^2 - 0.6^2} = 0.4556m$$

and the corresponding failure load shown in Fig. 3.5b is

$$p = \frac{y}{l} n_e = \frac{0.4556}{0.7534} 6.2304 \times 10^4 = 3.768 \times 10^4 N = 37.68kN$$

If the structure is a beam instead of a truss, plastic deformation can be driven from the beam ends to the middle segment as a result of retrofitting the connection. Due to catenary action, the bending moment can be greatly reduced in the middle segment. If the vertical displacement is adequately large, the bending moment can also approach zero and only pure tension takes place.

The ratio of the failure load in this model to that in Model 3.1 is $37.68 / 7.380 = 5.106$. As shown in Tables 3.1 and 3.2 and explained in more detail in the following, as the length and the depth of the end segments decrease, the ratio will greatly increase.

From the above two models, it can be seen that different cross-sectional areas of the end segments can greatly change the global behaviour of the structure by redistributing the stress and the strain along the length of the structure. When the area of the end segments is smaller

than that of the middle segment, yielding occurs in the end segments; whereas when the area of the end segments is larger than that of the middle segment, yielding is driven from the end segments to the middle segment and the failure load is increased significantly.

The relative strength and stiffness of the end segments to the middle segment have been identified as the main factors that influence the behaviour of catenary action. To investigate their influence, two parametric studies are conducted to consider the effect of different lengths and depths of the end segments.

Table 3.1.

Influence of length of end segments on global strain, vertical displacement and failure load in models 3.1 and 3.2

Length	Ratio	Strain		Displacement(m)		Load(kN)	
(m)	(%)	Weak	Strong	Weak	Strong	Weak	Strong
0.03	5	0.029	0.228	0.146	0.456	7.356	37.69
0.015	2.5	0.015	0.239	0.105	0.470	5.362	38.40
0.006	1	0.007	0.246	0.069	0.478	3.578	38.81
0.003	0.5	0.004	0.248	0.053	0.481	2.719	38.95
0.0015	0.25	0.002	0.249	0.042	0.482	2.161	39.02
0.0006	0.1	0.002	0.250	0.034	0.483	1.742	39.06
0.0003	0.05	0.001	0.250	0.030	0.483	1.577	39.07

In Table 3.1, the influence of the lengths of the end segments to the effect of catenary action is examined for both the structures with weak ends and strong ends. Seven ratios of the end segment lengths to the whole length, from 5 percent to 0.05 percent, are examined respectively, to capture their influence. When the failure strain $\varepsilon_{fail} = 0.25$ is reached in the structure, the influences of different lengths of end segments on the

strain for the whole structure, the vertical displacement and the failure load are found. It is shown that for the structure with weak ends, the global failure deformation and load will greatly decrease as the length of end segments decreases. For the structure with strong ends, however, that effect is not so obvious. With decreasing ratio, its results become stable and approach those of the truss whose cross-sectional area of end segments is the same as that of the middle segment.

Table 3.2.

Influence of depth and length of end segments on global strain, vertical displacement and failure load in models 3.1 and 3.2

Depth	Length = 0.03m			Length = 0.003m			Length = 0.0003m		
(m)	Strain	Disp. (m)	Load (kN)	Strain	Disp. (m)	Load (kN)	Strain	Disp. (m)	Load (kN)
0.005	0.028	0.145	3.663	0.003	0.049	1.269	0.001	0.024	0.616
0.010	0.029	0.146	7.356	0.004	0.053	2.719	0.001	0.030	1.577
0.015	0.029	0.147	11.15	0.004	0.056	4.333	0.002	0.036	2.787
0.020	0.250	0.483	39.07	0.250	0.483	39.07	0.250	0.483	39.07
0.025	0.228	0.456	37.69	0.248	0.481	38.95	0.250	0.483	39.07
0.030	0.228	0.456	37.69	0.248	0.481	38.95	0.250	0.483	39.07
0.035	0.228	0.456	37.69	0.248	0.481	38.95	0.250	0.483	39.07

In Table 3.2, seven depths and three lengths of the end segments are examined respectively for their influence to the effect of catenary action. When the depth of the end segments is equal to that of the middle segment, i.e., 0.02m, plastic deformation develops equally in both of them and reaches the maximum value. The values of strain and displacement do not greatly change with the variation of the depth for both the structures with weak ends and strong ends, but vary significantly with the difference

of the length for the structure with weak ends. For the structure with weak ends, the failure load significantly decreases as the length and the depth of the end segments decrease, but this effect is not obvious for the structure with strong ends.

When the initial length of the end segments is $L_e = 0.003m$, the force-displacement relationships in the vertical direction up to failure are shown in Fig. 3.6 for the structure with weak ends and the structure with strong ends. Fig. 3.6 is obtained by applying the following procedure.

For the structure with the weak ends, because of their smaller area, the strain of the weak end segments is larger than that of the normal middle segment. For different values of the strain of the weak ends, ε_e = 0.0001, 0.0002, 0.0003, ……, 0.2500, the corresponding displacement and force can be calculated. For a given ε_e, the current length and area of the end segments are

$$l_e = L_e \exp(\varepsilon_e),\ a_e = A_e \frac{L_e}{l_e} = A_e \exp(-\varepsilon_e) \qquad (3.16, 17)$$

If $0 \le \varepsilon_e < \varepsilon_y$, the end segments are elastic, and their tension is

$$n_e = E\varepsilon_e a_e \qquad (3.18a)$$

and if $\varepsilon_y \le \varepsilon_e \le \varepsilon_{fail}$, they are plastic, and their tension is

$$n_e = a_e \sigma_y \qquad (3.18b)$$

For the normal middle segment, axial force is equal to that of the weak end segments, i.e.

$$n_m = Ea_m\varepsilon_m = EA_m \frac{L_m}{l_m}\ln\left(\frac{l_m}{L_m}\right) = n_e \tag{3.19}$$

The above equation can be rewritten as the following

$$\frac{L_m}{l_m}\ln\left(\frac{l_m}{L_m}\right) = \frac{n_e}{EA_m} \tag{3.20}$$

Substituting Eq. (3.18a) or Eq. (3.18b) into the above and solving the equation, one can obtain l_m. The corresponding length, the strain for the whole structure, the vertical displacement, and the vertical load are

$$l = 2l_e + l_m,\ \varepsilon = \ln\left(\frac{l}{L}\right),\ y = \sqrt{l^2 - L^2},\ p = \frac{y}{l}n_e \tag{3.21-24}$$

For the structure with the strong ends, because of their larger area, the strain of the end segments is smaller than that of the normal middle segment. For different values of the strain of the middle segment ε_m = 0.0001, 0.0002, 0.0003, ……, 0.2500, the corresponding displacement and force can be calculated. For a given ε_m, the current length and area of the middle segment are given as

$$l_m = L_m \exp(\varepsilon_m),\ a_m = A_m \exp(-\varepsilon_m) \tag{3.25, 26}$$

If $0 \le \varepsilon_m < \varepsilon_y$, the middle segment is elastic, and its tension is

$$n_m = E\varepsilon_m a_m \tag{3.27a}$$

and if $\varepsilon_y \le \varepsilon_m \le \varepsilon_{fail}$, it is plastic, and its tension is

$$n_m = a_m\sigma_y \tag{3.27b}$$

For the strong end segments, axial tension is equal to that of the normal middle segment, i.e.

$$n_e = Ea_e\varepsilon_e = EA_e\frac{L_e}{l_e}\ln\left(\frac{l_e}{L_e}\right) = n_m \tag{3.28}$$

The above equation can be rewritten as the following

$$\frac{L_e}{l_e}\ln\left(\frac{l_e}{L_e}\right) = \frac{n_m}{EA_e} \tag{3.29}$$

Substituting Eq. (3.27a) or Eq. (3.27b) into the above and solving the equation, one can obtain l_e. The corresponding length, the strain for the whole structure, the vertical displacement, and the vertical load are

$$l = 2l_e + l_m,\ \varepsilon = \ln\left(\frac{l}{L}\right),\ y = \sqrt{l^2 - L^2},\ p = \frac{y}{l}n_m \tag{3.30-33}$$

It is demonstrated by Fig. 3.6 that through strengthening the weak end segments, the failure displacement and load can increase significantly. It can also be seen that for both the structures with weak ends and strong ends, the failure deformation does not change very much with different cross-sectional areas; because the structural failure is not controlled by cross-sectional force or stress, but by strain. After yielding, a very large plastic deformation is still possible, and the final damage occurs only after the failure strain is reached.

For the structure with weak ends, the deformation mainly concentrates in the end segments. As the length of the end segments decreases, the failure load and global deformation reduce significantly. For a real structure, the ratio for the segment length of the beam-to-column connection to that

of the middle segment is rather small. As a result, once a column is removed, if the joints are not appropriately strengthened the structure will fail at a rather small load and global deformation.

Through strengthening the weak ends, one can drive the yielding away from the short end segments to the long middle segment. It is not important how large the absolute cross-sectional area is. As long as the area of the end segments is larger than that of the middle segments, the failure load and global deformation are almost the same for different end segment depths, and they are not as sensitive to different end segment lengths as in the original structure. These characteristics will be utilized in retrofitting existing simple steel constructions, and two retrofitting schemes will be given in the next section.

3.3 Retrofitting schemes

As mentioned before, ductility is very useful for preventing blast-induced damage. It is true that structural steel is one of the most ductile engineering materials. As shown in the previous section, however, material ductility alone is not a guarantee of structural ductile behaviour because steel components can fail in a premature manner, in which only a small part of the structure is damaged and the stress level in the rest of the structure is still very low. In particular, these premature failures raised important concerns regarding the behaviour of the simple joint. Although the mild steel used in the joint is a very ductile material, the overall behaviour of the structure is not ductile because of premature failure of the connection. The

connection failure is not due to less ductility, but due to lower strength, i.e., tensile capacity. Also as demonstrated in the previous section, the overall ductile behaviour can greatly be improved by increasing the cross-sectional area of the weak simple connection to a certain level.

The fin plate beam-to-column connection shown in Fig. 3.7, also known as "shear tab connection" or "single plate framing connection", is a type of simple connection. The fin plate connection is widely used in steel frames for ease of construction. The connection detail at each end of the beam is only required to be able to transmit the maximum shear force to the column. However, this type of steel structure is not ductile and not immune to blast-induced damage although the used steel is ductile material.

When catenary action occurs, axial deformation mostly concentrates in the very short connection segment at the beam end, because it is the weakest part. At failure, the entire joint section yields and reaches maximum elongation, but the stresses and strains in the rest of the segment of the beam are still rather low, and may still be in the elastic state. Consequently, the global axial deformation of the entire beam is rather small, but the local axial tensile force caused by the catenary action is extremely large in the connection part. Because the axial force is resisted only by the beam web connection, the axial tensile resistance is discontinuous along the length of the beam, plastic deformation mainly concentrates at the weaker joint part, and this part is easily ruptured.

To overcome the problem of premature failure, one can mobilize the cross-sectional area of the beam flange to resist this large tensile force, by connecting the beam flanges together. By so doing, the fin plate

connections change to either a moment connection or a semi-rigid connection. In spite of being stronger than the simple connection, the semi-rigid connection is usually weaker than the moment connection and the beam itself, and therefore the moment connection is considered here. Different types of important moment beam-to-column connections available in literature have been reviewed and discussed in Chapter 2 due to their key function in the prevention of the progressive collapse. Among a variety of moment connections, the end plate connection is difficult to use for retrofitting purposes: The vertical loads on the beam are not easy to transfer to the column during the retrofitting process of removing the existing simple connection and replacing it by the end plate connection, and therefore the end plate connection is only appropriate for new steel moment framed structures. Whereas, in addition to being used in constructing a new moment steel frame, the haunch connection, the rib plate connection, the flange plate connection, the "Extreme Event Beam Link Connection" and the SidePlate connection may be utilized in retrofitting an existing simple steel frame as well because the vertical loads applied on the beam can still to be transferred to the columns through the fin plate during the retrofitting process.

Two such retrofitting schemes, the Flange Plate Scheme and the Vertical Plate Scheme, are shown in Figs. 3.8 and 3.9. Their aim is to strengthen the weak connection section of the existing structure, allowing the whole beam to fully yield in tension. The axial deformation can then be evenly distributed and fully developed along the entire length of the beam,

and thereby the tension induced by catenary action is significantly reduced.

The Flange Plate Retrofitting Scheme is not new. It is the same as the site-welded flange plate connection used in new structures shown in Fig. 2.26 (Engelhardt and Sabol 1995; Bruneau et al. 1998). Except that the flange plate connection is principally used in initial constructions and in resisting bending moment whereas the Flange Plate Retrofitting Scheme is utilized in rehabilitating existing fin plate connection and in overcoming the discontinuity of tension capacity at joint, there is no other significant differences between the flange plate connection and the Flange Plate Retrofitting Scheme. For the Flange Plate Retrofitting Scheme, as shown in Fig. 3.8, in addition to welding the beam flange and the stiffener to the column, the lapped flange plate is connected to the flange of the column by butt welding and to the flange of the beam by fillet welding. Thus, one can drive the weakest cross-section away from the beam-to-column joint, and can greatly improve the ductility, the continuity and the redundancy of the structure.

The Vertical Plate Retrofitting Scheme, shown in Fig. 3.9, is a modification of the SidePlate connection (Houghton et al. 2001). As shown in Fig. 2.28, the SidePlate connection is a column tree, fabricated in a shop. On site, it is linked to beams. As compared with the SidePlate connection, there are no top and bottom beam flange cover plates in the Vertical Plate Retrofitting Scheme. In order to strengthen the ends of the beams while satisfying a practical need of bridging the difference between the flange width of a beam and the wider flange width of a column, this

retrofitting scheme links the vertical plates at two sides of a column flange by complete joint penetration (CJP) butt-welds. The vertical plates are fillet-welded to the beam flanges. Through transferring the beam flange forces across the column, one can greatly strengthen the joint, and further increase the tension resistance of the beams.

If the Flange Plate connection and the SidePlate connection are used for retrofitting an existing simple steel construction, a part of the concrete slab near a load-carrying column needs to be removed. This practice is very labour demanding and expensive. In the Vertical Plate Retrofitting Scheme, however, the vertical plates are directly welded to beam flanges and column, the horizontal cover plates used in the Flange Plate connection and the SidePlate connection are not required, and therefore the removal of the concrete slab on the top of beams near the column is not necessary. Because it is more convenient and less expensive to conduct, the Vertical Plate Scheme is more cost-effective than the Flange Plate connection and the SidePlate connection when retrofitting. In addition, the Vertical Plate Retrofitting Scheme does not reduce the shear capacity of the original fin plate connection at the beam ends, and loads applied on the beams can still be transferred to the column during the retrofitting process.

After linking the beam flanges of the shear joint together, a bending moment can be developed in the joint by transmitting the flange axial forces at the beam end. The relative rotation of the beam with respect to the column can be prevented. By so doing, both the above retrofitting

schemes change a partial-strength simple beam-to-column joint to a full-strength moment joint.

After retrofitting, if no blast occurs and the service loads do not change, no internal force redistribution occurs and the added retrofitting parts will carry no load because the entire structure has already deformed to accommodate the loads. Only live load changes can cause force redistribution. For a heavy-weight building, the live loads are much lower than the dead loads and the blast loads, and therefore the proposed schemes do not have negative effects on the original building.

For a light-weight structure, however, the bending moment of the beam end can be transferred to the columns, because the beam-to-column connection is transformed from a fin plate joint to an almost rigid full-strength moment-resisting joint. As a consequence, a change of the live loads will cause force redistribution and the columns have to withstand additional bending moments for which they were not designed. When subjected to the combined action of this additional bending moment and axial compression, it is possible that plastic hinges occur at the top and bottom ends of the columns, particularly when the columns are weak.

When the columns are weak and their cross-sections are small, it is also difficult to prevent the column ends from yielding under the combined action of compressive load and the additional bending. However, the occurrence of plastic hinges at two ends of the column does not mean that the structure must collapse. This damaged column is linked to a concrete core and the other intact columns through the floor slabs whose in-plane stiffness is generally exceedingly large. Therefore, even though

plastic hinges may form at its top and bottom ends, this column is still prevented from becoming a mechanism by the remaining undamaged structural members restraining the horizontal displacements of its top and bottom ends. The effect of this additional bending moment on a weak column is also investigated by finite element analysis in Model 4.4 of Chapter 4.

3.4 Summary

Firstly, an analysis of catenary action was conducted in this chapter. It was shown that when catenary action occurs, the bending moment will significantly decrease as the tensile force in a beams increases. Secondly, the catenary action of a truss element has been evaluated. For such structures, exact results could be obtained. It has been demonstrated that, for fully developed catenary action, the cross-sectional area of the original weak end segments should be increased, and the increased area should ensure that the end segments should be stronger than, or at least as strong as, the middle segment. Finally, the necessity of strengthening simple beam-to-column joints was discussed. The Flange Plate Retrofitting Scheme and the Vertical Plate Retrofitting Scheme were proposed for strengthening the fin plate beam-to-column connection in order to develop catenary action of beams at the removal of a column. In the next chapter, the strengthening effects of these two retrofitting schemes will be investigated by means of finite element analysis, and their advantages will be demonstrated.

Chapter 4: Finite element analysis

The aim of this chapter is to investigate the effects of the Flange Plate and the Vertical Plate retrofitting schemes proposed in Chapter 3. Through strengthening the fin plate beam-to-column joint, the two proposed retrofitting schemes can greatly improve the ability of structures to resist tensile forces caused by catenary action. The commercial multipurpose finite element software package ABAQUS was employed for comparing different results between before and after retrofitting the joints. All models reported herein considered both geometric and material nonlinearities. The effect of material nonlinearity was modelled using ABAQUS' standard metal plasticity material model which is based on an incremental plasticity formulation.

4.1 Finite element model

When a column is removed by a blast, the two beam spans originally supported by this column become one span and the evaluation of the structural response becomes rather complex. Because of the beam span length increasing significantly, the development of membrane force affects the response to a rather large degree, and therefore structural steel members will exhibit nonlinear material properties due to yielding and strain hardening. The resulting large plastic deflection will significantly change the structural geometrical shape and, in turn, the geometrical deformation will

alter the internal forces considerably. As a result, both material and geometric nonlinearities should be included in the catenary action analysis.

Catenary forces will be introduced within the beams due to the removal of a column. With increasing tension, the stress distribution of cross-section changes from elastic, to elastoplastic, to entirely plastic. When the cross-section is either completely elastic or pure plastic, the evaluation is rather simple. When catenary action is involved, however, the cross-section is usually in the elastoplastic range and the analysis becomes much more complicated. Because the catenary behaviour of structures can be influenced by a large number of variables, solution of these elastoplastic cases requires cumbersome calculations, and therefore a numerical solution procedure is preferred. The software package ABAQUS is used herein.

For material constitutive models, there are four widely used types of classical yield conditions. They are Tresca, von Mises, Mohr-Coulomb and Drucker-Prager. For soil, concrete, and other 'frictional' materials, both the Mohr-Coulomb law and the Drucker-Prager law are frequently used. Both the Tresca law and the von Mises law are well verified in metal plasticity (Zienkiewicz and Taylor 2000b), but the Tresca law is unavailable and only the von Mises law can be used in ABAQUS. When simulating the inelasitc behaviour of structural steelwork, two hardening rule can usually be adopted. The kinematic hardening rule can be used for cyclic analysis, and the isotropic hardening behaviour of the structural steel and weld can be assumed for monotonic analysis (Chen and Lin 2013).

Chen and Lin (2013), Kim et al. (2016), Shi et al. (2008), Wu and Feng (2013), employed the von Mises law to simulate the stress and strain relations of structural steel and weld, and utilised particularly a rate-independent plasticity to analyze their inelastic behaviour. Similar to the above mentioned research, the stress and strain relations of structural steel and weld were simulated based on isotropic hardening behaviour, and plasticification of the models was determined using the von Mises yielding criterion with associated flow rule in this PhD thesis.

The ABAQUS element library contains eight element families, enabling a wide range of engineering problems to be modelled efficiently. 2D solid elements and shell elements are chosen to model various structural members herein. A brief description of the element types used in this chapter is given below.

4.1.1 *2D solid elements*

2D solid elements available here are CPS4, CPS4I, CPS4R, CPE4, CPE4I, CPE4R, CPS8, CPS8R, CPE8 and CPE8R. They are iso-parametric elements with two degrees of freedom at each node. The elements CPS4, CPS4I, CPS4R, CPE4, CPE4I and CPE4R have 4 nodes. The elements CPS8, CPS8R, CPE8 and CPE8R have 8 nodes. The CPE4, CPE4I, CPE4R, CPE8 and CPE8R are plane strain elements, while the CPS4, CPS4I, CPS4R, CPS8 and CPS8R are plane stress elements.

Element types CPS4 and CPE4 are fully integrated, linear conforming elements. When an element is subjected to pure bending, the shear stress in the element should be zero. When the linear conforming element is fully

integrated, however, the obtained shear stress in the element under pure bending is nonzero. This numerical problem is called “shear locking”. Therefore, fully integrated, linear element can be used only if loads will no or only very small bending is produced in models, otherwise the obtained results will be too poor (ABAQUS 2014, Zienkiewicz and Taylor 2000a,b). However, the bending is rather large at beam ends in the models of this chapter, and therefore fully integrated, linear conforming elements CPS4 and CPE4 will not be used here.

Element types CPS4R, CPE4R, CPS8R and CPE8R are reduced-integration elements. Reduced-integration elements use one fewer integration point in each direction than the fully integrated elements. Reduced-integration, linear elements CPS4R and CPE4R have just a single integration point located at the element's centroid. When subjected to pure bending, the linear reduced-integration elements will be too flexible. This numerical problem is called “hourglassing”. Only if an adequately fine mesh is used and this problem is overcome, then the linear reduced-integration elements CPS4R, CPE4R can give acceptable results. In addition, the strain and the stress are constant values within the element. In coarse meshes, the accuracy of the linear reduced-integration elements CPS4R, CPE4R are not as good as that of the elements CPS4I and CPE4I. Therefore, element types CPS4R and CPE4R will not be used here.

Elements CPS4I and CPE4I are bilinear quadrilateral with incompatible mode. Different from the conforming element, the displacement of incompatible element is not conforming on the element boundary. In order to overcome the problems of shear locking in fully integrated, first-order

conforming elements, the incompatible element uses the following displacement approximation (Taylor et al. 1976; Zienkiewicz and Taylor 2000a).

$$u = \sum_{i=1}^{4} N_i u_i + a_1(1-\xi^2) + a_2(1-\eta^2)$$

$$v = \sum_{i=1}^{4} N_i v_i + a_3(1-\xi^2) + a_4(1-\eta^2)$$

where $N_i = \frac{1}{4}(1+\xi_i\xi)(1+\eta_i\eta)$ $(i = 1,2,3,4)$ are the usual conforming bilinear shape function and the last two terms are incompatible modes of deformation.

If the element distortions are adequately small, incompatible mode elements can produce results with high accuracy that are comparable to quadratic elements but at significantly lower computational cost. In the models of this chapter, the shape of the adopted elements is rectangular, no element mesh distortion occurs, and therefore Elements CPS4I and CPE4I can be used.

The elements CPS8, CPS8R, CPE8 and CPE8R have 8 nodes, and they are biquadratic quadrilateral. The elements CPS8 and CPE8 are full integration with 9 integration points. The elements CPS8R and CPE8R are reduced integration with 4 integration points. The reduced integration elements CPS8R and CPE8R have lower computational cost as compared to the fully integrated elements CPS8 and CPE8, and are widely used in modelling. When geometries are complex, the large element mesh distortions make the above mentioned incompatible elements CPS4I and CPE4I too stiff, and very poor results may be produced. In such case, the

reduced-integration, quadratic elements CPE8R and CPS8R can be utilised because they much less sensitive to mesh distortion.

The four solid elements CPS4I, CPE4I, CPS8R and CPE8R are used to model a beam with a rectangular cross-section.

4.1.2 *Shell elements*

Element type S4R is a three-dimensional, iso-parametric, doubly curved general shell element. The element has 4 nodes with five degrees of freedom at each node. It employs reduced integration, hourglass control, and finite membrane strain. The S4R shell element is used to model the beam-to-column connection, as well as the web and the flanges of the adopted beams and columns. Except for element type S4R, another 4 node element S4 is also available. Element type S4 is a fully integrated general-purpose, finite-membrane-strain element. Element type S4 does not require hourglass control. S4 has four integration locations per element and S4R has only one integration location per element. S4 is more computationally expensive than S4R. The difference among their computational results is small for the structures in this thesis. As a result, only the results of S4R are given. Kim et al. (2016) also employed S4R to model the steel beam and column.

4.2 Numerical simulations

Given the reliance of the present study on the robustness of the nonlinear finite element modelling strategies employed herein, it is important to verify

the modelling approach. With the aim of validating the modelling of this study, comparison of results between Jetteur et al. (1991) and this study is undertaken firstly, using Model 4.1 described below. It has also been used as a benchmark by Bursi and Jaspart (1997).

Model 4.1. As shown in Fig. 4.1, a beam is considered in plane strain. The geometric and physical properties of the beam used are the same as those adopted by Jetteur et al. (1991). The length and the depth of the beam are 3mm and 1mm, respectively. A vertical displacement of 2mm is imposed at the right end, which can slide vertically. The stress-strain relationship is linear elastic with linear strain hardening. The von Mises model is used. Young's modulus is $E = 200{,}000 N/mm^2$, strain hardening modulus $E_T = 1{,}000 N/mm^2$, Poisson ratio $\nu = 0.3$, and Mises yield equivalent stress $\sigma_y = 400 N/mm^2$.

For validating the model and analysing the mesh size sensitivity, different elements with different meshes should be used. There for two elements CPE4I and CPE8R are used, and two square meshes 0.125mm×0.125mm and 0.25mm×0.25mm are adopted for the element CPE4I, and one 0.25mm×0.25mm is used for the element CPE8R. Parts of the simulation results are given in Fig. 4.2a and Table 4.1. In Fig. 4.2a, only the results of the two meshes: 0.125mm×0.125mm for the element CPE4I and 0.25mm×0.25mm for the element CPE8R, are given for clarity of the figure.

The vertical reaction force produced by the deformation of the beam is evaluated at the right end of the beam. As shown in Fig. 4.2a, the force and displacement relationship is drawn from the results of the nonlinear

finite element analysis of this study. The results of Jetteur et al. (1991) are shown in Fig. 4.2b. These were also obtained using CPE8R element. Comparing Fig. 4.2a and Fig. 4.2b, it can be seen that the agreement between the results of the present study and those of Jetteur et al. is very good.

Table 4.1.

Force and displacement relationship in Model 4.1

Displace.	CPE4I (N)		CPE8R (N)
(mm)	0.125	0.250	0.250
0.5	137.338(1.6380%)	138.962(0.4748%)	139.625
1.0	202.590(1.2026%)	207.343(1.1153%)	205.056
1.5	284.267(0.7574%)	286.401(0.0124%)	286.436
2.0	348.732(0.5175%)	350.927(0.1087%)	350.546

In Table 4.1, the results obtained by the ABAQUS elements CPE4I and CPE8R are compared quantitatively. From Fig. 4.2a and Table 4.1, it can also be seen that the results obtained by the 4-node element CPE4I and the 8-node element CPE8R are very close. Because the structure can be divided regularly by rectangular meshes, there are no element distortions, and therefore the incompatible element CPE4I can provide high accuracy at a low computational cost.

In Model 4.1, the plane strain elements CPE4I and CPE8R were used. In Model 4.2, the plane stress elements CPS4I and CPS8R will be used. The differences between the plane stress problems and the plane strain problems are the adopted E_0 and ν_0. For plane stress problems $E_0 = E$ and $\nu_0 = \nu$, but for plane strain problems, $E_0 = E/(1-\nu^2)$ and $\nu_0 = \nu/(1-\nu)$, where E and ν are the Young's Modulus and the the Poison's ratio respectively.

Although it is not slender and does not have lateral loads in the span, the beam of Model 4.1 does involve catenary action. Through employing software verified in Model 4.1, Model 4.2 will demonstrate the characteristics of catenary action mentioned in the previous chapter: the bending moment will decrease as tension and deformation increase. It will also be seen that the relative strength between the end segments and the middle segment can significantly change the global behaviour of structure.

Model 4.2. A single span beam with rectangular cross-section is adopted in the simulation. As shown in Fig. 4.3, the beam carries two concentrated loads and consists of three segments: one long middle and two short end segments. For the middle segment, the width and the depth of the section are 0.01m and 0.02m, respectively. There are two types of end segments: weak and strong, representing the original and the strengthened joints. The width of the section is 0.01m for both the weak and the strong end segments. The depth is 0.01m for the weak ends, and 0.03m for the strong ends, respectively. The initial length of the whole beam is $L = 0.6m$, and those of the end and the middle segments are $L_e = 0.05L = 0.03m$ and $L_m = L - 2L_e = 0.54m$, respectively. The two concentrated loads are applied at the third points in the span. The original design value of two loads is 900*N*. For both structures with weak ends and with strong ends, the dynamic effect is considered due to the sudden removal of the left support, and the dynamic amplification factor is assumed to be 2.0; as a result, the two loads become 1800*N* each. The material properties are: the Young's modulus $E = 2 \times 10^{11} N/m^2$, the yield strength $\sigma_y = 4 \times 10^8 N/m^2$ and the strain hardening modulus $E_r = 1 \times 10^9 N/m^2$.

For both beams, the simulation consists of two steps. The first step is intended to apply the two concentrated loads on the beam. In this step the boundary conditions at the two beam ends are fixed. The second step is intended to impose vertical displacement at the left end. In this step, the right end boundary condition remains unchanged, but the left one is changed from fixed end to vertical slide, i.e., only the horizontal displacement and the rotation will be restrained at the left end while a progressively increasing vertical displacement is applied.

The beams are similar to the trusses used in Chapter 3. If there were no load in the bay and the joints were pins, the case would become rather simple and a closed-form solution can be obtained, as given in Chapter 3. Because of the lateral loads, however, obtaining a closed-form solution becomes impossible and numerical simulation is necessary.

In Figs. 4.4 and 4.5, the vertical reaction force versus vertical displacement curves for the left end are obtained from the nonlinear finite element analyses of the solid model. Because the catenary deformation of the beam is rather large, both material and geometrical nonlinearities are considered.

To gain insight into the performance of the aforementioned solid element as a function of spatial discretisation, different mesh densities are evaluated herein. For the solid element CPS8R modelling, the beam is discretised with square mesh 0.005m×0.005m. In addition to 8-node quadratic reduced-integration planar element CPS8R, 4-node incompatible planar element CPS4I is also employed here due to its good performance in the case of no element distortion. For the solid element

CPS4I, two square meshes 0.0025m×0.0025m and 0.005m×0.005m are adopted, respectively. However, because the curves of different mesh sizes almost coincide for the same element type, only the curves with finer mesh are shown in Figs. 4.4-6 for clarity. The mesh sizes adopted in the figures are 0.005m×0.005m for CPS8R and 0.0025m×0.0025m for CPS4I, respectively.

For the structure with weak ends, the relationships between the vertical reaction and the vertical displacement at the left end for these elements are plotted in Fig. 4.4. They indicate good agreement between the two solid models. As the vertical displacement increases, the vertical reaction force will decrease. When the vertical displacement reaches a value of roughly 0.02m, the vertical reaction force is roughly equal to zero, and the downward movement can be arrested. For the structure with strong ends, the relationships between the imposed vertical displacement and the vertical reaction at the left end for the two solid element models are shown in Fig. 4.5.

The Mises equivalent stress is defined as $q = \sqrt{\frac{3}{2}(\mathbf{S} : \mathbf{S})}$, where $\mathbf{S}$ is the deviatoric stress tensor, defined as $\mathbf{S} = \boldsymbol{\sigma} - p\mathbf{I}$, where $\boldsymbol{\sigma}$ is the stress, p is the equivalent hydrostatic pressure stress, defined as $p = -\frac{1}{3} trace(\boldsymbol{\sigma})$, and $\mathbf{I}$ is the unit matrix. To investigate the stress distribution, the von Mises stress distribution of the solid element model CPS8R in whole model and in short middle segment of beam with strong ends is shown in Fig. 4.6 for the beginning and the end of the left beam end sliding vertically respectively. The global displacement, deformation, Mises stress and strain distributions of the whole beam can be seen in Figs. 4.6a and 4.6b. It can be demonstrated by Fig. 4.6d that the stress becomes uniformly distributed on

the whole cross-section at the middle of the beam at the end of the left beam end vertically sliding, and therefore only the axial tension components of stress and strain exist and the bending components vanish.

As shown in Fig. 3.1, when a column is removed by a blast, all floors supported by that column will collapse until a new equilibrium position is arrived at through catenary action, preventing general collapse. All storeys above, not just one storey, are drawn towards the damaged column horizontally by the beam's catenary action. The length of the equivalent vertical cantilever structure, which consists of columns and shear walls, is very large. In addition, the horizontal loads introduced by the beam's tensions are huge and far exceed ordinary horizontal loads caused by wind or earthquake. Therefore, the horizontal component of the catenary force cannot be resisted by columns, shear walls or bracing systems. Only the concrete slab can be expected to resist the horizontal component of the catenary force and prevent inward movement because its strength and stiffness are extremely large in plane, although it is relatively flexible out of plane. Because all floors above the damaged column behave in a similar way, a model of a one-storey sub-frame is adequate for investigating this problem and is therefore adopted herein for reducing the computational effort required. Compared with the models used before, this model can consider the influence of the columns on the rotation of the beam ends and give more detailed information on stresses and strains within the beam-to-column connections.

In Model 4.3 presented next, the effect of the Flange Plate Retrofitting Scheme and the Vertical Plate Retrofitting Scheme, proposed in Chapter 3

for strengthening existing structures, is investigated. For the evaluation of the global behaviour of the structure, the actual local geometry of the joints is simplified in order to reduce computational effort. Fig. 4.7 shows the original partial-strength fin plate joint and Figs. 4.8-9 illustrate the full-strength joints retrofitted by the Flange Plate Scheme and the Vertical Plate Scheme. In these simplified shell models, the fin plate is linked to the beam web as though by butt-weld, instead of by bolts as shown in Figs. 3.7-9. This is only very simplified model for analysing the global behaviour of the sub-frame. In order to investigate the local behaviour of the connection, bolts and welds will be modelled in section 5.2 by using the three-dimenional solid element models, which are much more detailed than the shell models adopted herein.

Model 4.3. The sub-frame investigated here consists of two equal bays, each spanning a distance of 9m, and six columns of height 3m. As shown in Fig. 4.10, the lower centre column has been removed, triggering the collapse. The loss of the centre column has effectively modified the frame geometry into a single span of 18m, and the loads must now be carried by the rest of the structure. This loading condition is more severe than the initial condition, and the beam will likely develop plastic deformation. Taking advantage of symmetry, only half of the assemblage is simulated. The beam has a 457x191UB98 cross-section, and the columns 305x305UC283 (Owens and Knowles 1992). The beam and the column are modelled using shell finite elements positioned along the mid-planes of the flange and web components. It is also assumed that the mid-plane of the fin plate is at the same plane as that of the column and the beam webs and the fin plate is

welded to the column and the beam. The length and the depth of the fin plate are 0.05m and 0.36m, respectively. The two concentrated loads are applied at the third points, respectively. The two original design loads are 90kN. For both the original and the strengthened structures, they are changed to 180kN, as a result of accounting for the dynamic effect with an amplification factor of 2.

For the structure retrofitted by the Flange Plate Scheme, the length and the thickness of the strengthening cover plates are 0.5m and 0.025m, respectively, and its width is assumed to be equal to that of the beam flange. To consider the effect of retrofit, different flange thicknesses are assigned at the beam end segments and the beam middle segment. The flange thickness is 0.0446m at the beam ends and 0.0196m in the beam middle segment. The width and the thickness of the column stiffeners are assumed to be the same as those of the strengthened flange at the beam end.

Table 4.2.

Stress and strain values in Fig. 4.11 of Model 4.3

Point	1	2	3	4
Stress(MPa)	235.0	236.0	360.0	490.8
Strain	0.001175	0.01446	0.03653	0.4

For the structure retrofitted by the Vertical Plate Scheme, the length and the thickness of the strengthening plates between the two beam flanges are 0.5m and 0.025m, respectively, and the depth is assumed to be equal to the beam depth. The depth and the thickness of the vertical plates between the two column flanges are assumed to be the same as

those between the two beam flanges at the beam end. The stress-strain constitutive law is shown in Fig. 4.11 and Table 4.2, which is adopted from Faella et al. (2000).

Due to retrofitting, the beam-to-column connection changes from a simple joint to a moment joint, and therefore the strength and the stiffness at the connection part change significantly. For real structures, the simple connection can resist a small amount of bending moment, while the moment connection can have a small relative rotation. However, simplified shell element models are used here to reduce computational effort, and the simple connection and the moment connection are idealized as pin-connected joint and fixed-connected joint respectively. As shown in Figs. 4.12-14, before retrofitting, the beam and the column each have a different slope at their joint, since the pin-connected joint cannot support a moment; whereas after strengthening, the retrofitting schemes cause the fixed-connected joint to rotate the beam and the column by the same angle. Instead of altering the structure itself and changing the pin-connected joint to a fixed-connected joint, an alternative approach is proposed here. As shown in Figs. 4.12-14, by changing the pin-connected joint to fixed-connected joint and imposing specific boundary conditions, the equivalent structure, instead of the real structure, can be evaluated for different steps to simulate the change of the structure. In each step, the differences of the obtained internal forces between the pin-connected structure and the fixed-connected structure are very small because the amount of rotations a_1 shown in Fig. 4.12 is very small for real structures.

For both the original structure and the retrofitted structure, the simulation consists of three steps. For the retrofitted structure, the three simulation steps are shown in Figs. 4.12, 4.13 and 4.14. For consistency with the retrofitted structures, the same boundary conditions are also used in the original structure; however, for the original structure the influence of the column's equivalent rotation on internal forces is not as important as it is for the retrofitted structure due to its weak connection. The first step is intended to simulate zero bending moment at the beam-to-column connection. In this step, loads and specific boundary conditions are applied to the structure. Two concentrated loads of a value of 90kN are applied at the third points in the span. Because the stiffness of the concrete floor slab is very large in plane and relatively rather small out of plane, it is assumed for simplicity that only the displacements in the horizontal direction are restrained at joints and the two beam ends can rotate freely. As shown in Fig. 4.12b, the upper and lower column ends on both sides are fixed and specific values are imposed to the boundary conditions at the column ends. When the displacements and rotations at the column ends are equal to these imposed specific values, there is no bending moment in the columns, although the equivalent structure is modelled as fixed-connected. The rotations of the upper and lower ends of columns are equal to those of beam ends. In Figs. 4.12b, 4.13b and 4.14b, the absolute value of the rotations imposed at the left column ends and the right beam end is given by

$$a_1 = \frac{PL^2}{9EI} = \frac{90\times10^3\times9^2}{9\times2\times10^{11}\times4.5770\times10^{-4}} = 0.008849rad$$

and the absolute value of the horizontal translations imposed at the left column ends is given by

$$d = a_1 h = 0.008849 \times 3 = 0.02655m$$

where the concentrated loads are $P = 90 \times 10^3 N$, the length of the span $L = 9m$, the flexural rigidity $EI = 2 \times 10^{11} \times 4.5770 \times 10^{-4} Nm^2$, and the storey height $h = 3m$.

These horizontal translations and rotations are imposed as boundary conditions here, instead of being measured. Of course, one can allow the column and beam ends to rotate freely and the column ends to translate without restraint in the horizontal direction, measure these values, and then fix these ends in the next step. However, once these ends are simply fixed without assigning these specific values, these horizontal translations and the rotations in boundary conditions will return to zero again in the subsequent steps. In order to avoid this unwanted result, at the beginning of the second step, one should assign these values of the end of the first step and fix these DOF; then ABAQUS will keep these values in the second and subsequent steps.

In the second step, the two concentrated loads will change from 90kN to 180kN, and the boundary conditions remain unchanged. For the real structure, the beam-to-column connection is converted from a pin-connected joint shown in Fig. 4.12a to a fixed-connected joint in Fig. 4.13a. In Fig. 4.13, $a_2 = a_1 + Da_1$, where Da_1 is the increment of angle in step 2.

The third step is intended to impose a displacement. In this step, other boundary conditions are the same as those of the first two steps, but

vertical displacements of values of 1.0m and 1.1m are imposed on the right end for the original structure and the retrofitted structures, respectively. In Fig. 4.14, $a_3 = a_2 + Da_3$, where Da_2 is the increment of angle within step 3. In Figs. 4.12a, 4.13a and 4.14a, the relative angle between left beam end and left upper column is $90^0 + a_1$, whereas in Figs. 4.12b, 4.13b and 4.14b, the angle remains 90^0. In all these figures, the angle at the right beam end remains equal to a_1 and the translations and rotations of the left column ends are unchanged.

For the original structure, some of the simulation results are shown in Figs. 4.15-16. The relationship between the reaction force and the imposed vertical displacement is shown in Fig. 4.15. To check the effect of the element type and the element size on accuracy, two different elemets S4 and S4R with two different element sizes have been used: (1) Size=0.05m: 0.05m×0.05m in the joint part, and 0.05m×0.2m in the rest of the structure; and (2) Size=0.025m: 0.025m×0.025m in the joint part, and 0.025m×0.1m in the rest. The curves of the vertical reaction and the vertical displacement for the elements S4 and S4R with the mesh sizes 0.05m and 0.025m are shown in Fig. 4.15. Although obvious discrepancy can be observed when the displacement is larger than 0.8m, the four curves almost coincide when the displacement is smaller than 0.648m, at which the failure stress and strain are roughly reached. For clarity, only the results of the element S4R with the size 0.025m are shown in Fig 4.16.

To investigate the stress and strain distributions, the Mises equivalent stress and the equivalent plastic strain are plotted. The equivalent plastic

strain is defined as $\bar{\varepsilon}^{pl} = \bar{\varepsilon}^{pl}\Big|_0 + \int_0^t \dot{\bar{\varepsilon}}^{pl} dt$, where $\bar{\varepsilon}^{pl}\big|_0$ is the initial equivalent plastic strain. The definition of $\dot{\bar{\varepsilon}}^{pl}$ depends on the material model. For Mises plasticity, $\dot{\bar{\varepsilon}}^{pl} = \sqrt{\frac{2}{3}\dot{\boldsymbol{\varepsilon}}^{pl} : \dot{\boldsymbol{\varepsilon}}^{pl}}$, where $\dot{\boldsymbol{\varepsilon}}^{pl}$ is the plastic strain rate tensor. In Figs. 4.16, 4.18 and 4.19, element boundary edges (the edges on the boundaries between two adjacent elements) are not shown in the figures of the global stress and strain distributions, because the element mesh sizes are too fine for the distributions of whole beam to be seen clearly.

With the aim of bounding the likely values at failure, only a best case scenario is considered here for the shell model. In this scenario, the fin plate and the beam web are linked together by butt-welding instead of bolting. As shown in Fig. 4.16, a simplified shell element model is adopted. Even from this best case scenario model, it can be seen that yielding only occurs at the connection parts and the rest of the structure remains elastic. Fig. 4.16 shows that the stress and strain are rather large at the beam-to-column connections. When the imposed vertical displacement reaches a value of 0.648m, the maximum Mises stress reaches the assumed failure stress of 490.8MPa and the maximum equivalent plastic strain of 0.4039 exceeds the assumed failure strain of 0.4; and it can be seen from Fig. 4.15 that an upward force of 82kN is still needed to support the beam at this time. Consequently, rupture will occur at the connection for this best case scenario model, even if no concentrated load is considered at the damaged column.

Quite different from the best case scenario, however, a shear joint can fail in four ways in a real structure: (1) by shear on the bolt shank; (2) by

bearing on the member or bolt; (3) by tension in the member; (4) by shear at the end of the member (MacGinley and Ang 1987). The resistant capacity of these four failure modes is lower than that of this best case scenario model. Consequently, the real structure will fail at its beam-to-column connection.

During the entire loading process, the beam flange does not contact with the column flange face and no prying action (Byfield and Paramasivam 2007; Stoddart, Byfield and Tyas 2014; Stoddart et al. 2013) occurs for this static model. The model is an only very simplified one for global behaviour. The distance between the beam flange and column flange is 0.05m. This problem will investigated in Section 5.2 further with the much more detailed 3D model for the local behaviours of the flexible end plate connections. In that model, the distance between the beam flange and column flange is only 0.008m.

For the structures retrofitted by the Flange Plate Scheme and the Vertical Plate Scheme, some of the simulation results are shown in Figs. 4.17-19. To check the effect of the element type and the element size on accuracy, two different elements S4 and S4R with two different element sizes have been used: (1) Size=0.05m: 0.05m×0.05m in the joint part, and 0.05m×0.2m in the rest of the structure; and (2) Size=0.025m: 0.025m×0.025m in the joint part, and 0.025m×0.1m in the rest. The curves of the vertical reaction and the vertical displacement for the elements S4 and S4R with the mesh sizes 0.05m and 0.025m are shown in Fig. 4.17a. It can be seen that the four curves almost coincide. For clarity, only the results of element S4R with size 0.025m are shown in figures afterwards. It can also be seen

from Fig. 4.17b that the force-displacement curves of the two retrofitting schemes are very close as well. The vertical reaction force on the right damaged column is upward at the beginning. With increasing vertical displacement, the force will decrease. Because there is a concentrated load on the damaged column, the damaged column continues to move down, and then the direction of the vertical reaction becomes downward. With further increasing vertical displacement, the vertical force will increase. When the vertical reaction force is equal to the value of the concentrated load, a new equilibrium configuration will be reached and the downward movement will be stopped by the catenary action. If a concentrated load of 100kN is applied to the failed column, for both the Flange Plate Scheme and the Vertical Plate Scheme, when the vertical displacement reaches roughly at a value of 0.7m, the downward movement can be arrested.

The stress and strain distributions are shown in Figs. 4.18 and 4.19 respectively for the Flange Plate Scheme and the Vertical Plate Scheme. In Figs. 4.19b and 4.19e, the front vertical plates are not visualised to show the stress and strain distributions in the beam web, fin plates and column webs behind the front vertical plates. As shown in Figs. 4.18 and 4.19, the proposed two retrofitting schemes can move the weakest part away from the column flange face. When the vertical displacement is 1.1m, the maximum equivalent plastic strains are 0.1818 for the Flange Plate Scheme and 0.1853 for the Vertical Plate Scheme, much smaller than the assumed failure strain of 0.4. For the Flange Plate Scheme, as shown in Figs. 4.17 and 4.18, to reach this displacement, Mises equivalent stress and equivalent plastic strain, a concentrated load of 323kN is needed to be applied at the

damaged column; and for the Vertical Plate Scheme, as shown in Figs. 4.17 and 4.19, a concentrated load of 335kN is needed. As compared with the loads applied in the span, these loads applied at the damaged column are much larger. Consequently, these two retrofitted structures can prevent collapse by catenary action.

The evaluation of the results obtained from the nonlinear numerical analysis leads to the following conclusions.

As a result of the removal of a column, the double span beam becomes overstressed. For the original structure, plastic deformation is concentrated at the fin plate joint. The beam remains elastic and its deformation is almost negligible as compared with the deformation developed at the fin plate. If not appropriately retrofitted, the original structure will possibly rupture at the fin plate joint.

The finite element analysis reveals that the two retrofitting schemes can yield the optimal stress and strain distributions. By strengthening the beam-to-column connection, joint continuity is greatly improved. This connection continuity and the plastic strain hardening characteristics of the steel would allow plastic deformation to develop in the long middle beam segment. The strains in the middle segment are relatively large, but are still low compared to the failure strain. Through the large plastic elongation of the beams, the retrofitting schemes would optimise structural geometric shape and allow catenary action to develop between the columns located on each side of the failed column, thereby providing an alternative load path to resist progressive collapse.

The models used for evaluating the retrofitted structures are simplified. However, similar with the conclusions obtained from the truss model in Chapter 3, as long as the joint becomes strong enough to drive the weak cross-section away from the connection part, the relative strength of the beam end becomes less important. Plastic deformation will occur in the middle beam segment, and therefore the local behaviour of the strengthened joint cannot significantly affect the global performance of the structure. As a result, the simplified shell models can still provide useful results.

It is through welds that the tensions in beam flanges are transferred to the strengthening plates. The stress and strain levels depend on the area of welds between the beam flanges and the strengthening plates. If the weld area reduces, the Mises stress and strain in welds will increase. The weld area depends on the length and the thickness of the strengthening plates. If those of the strengthening plates are too small, the Mises stress and strain in welds will be very large, and therefore the weld failure may occur. As a result, in order to reduce the Mises stress and strain levels in welds and to avoid the weld failure, the length and the thickness of the strengthening plates cannot be too small, particularly for the Vertical Plate Scheme.

In the models in this thesis, a nonlinear static analysis with a dynamic load factor of 2.0 is used to model an intrinsical dynamic event. The dynamic load factor being equal to 2.0 is true only on the condition when a structure is a linear elastic undamped system that has a single degree of freedom, and the support under this single mass is suddenly removed (Clough et al. 1993). However, if a key supporting column is suddenly

destroyed, the dynamic load factor may be different from the value 2.0 for a real structure (Liu, Davison and Tyas 2005; Tsai 2000; Tsai and You 2012). The structural behaviour after the sudden column removal is a dynamic process with very complicated internal force redistribution, involved both the material and geometric nonlinearities. As compared to those by the nonlinear static analysis, the results obtained by the nonlinear dynamic analysis are much more accurate and reliable (Liu, Davison and Tyas 2005). However, the nonlinear dynamic analysis is much more expensive than the nonlinear static analysis because computationally intensive time history calculation is needed to directly simulate the dynamic behaviour of the damaged structure. As a result, only the nonlinear static analysis method is utilised here as the first step in order to reduce computational effort. This research will be developed by using the nonlinear dynamic step-by-step method in the future.

It can be seen from Figs. 4.18 and 4.19 that the columns may still be in the elastic range at the end of loading. This is because the cross-sections of the columns are very large due to being located at the lower part of a high-rise building. When columns are located at upper parts of the building, the column sections will be much smaller than those at lower parts, whereas the beam sections may not change greatly, and therefore the result may be different. As mentioned in Chapter 3, the simple beam-to-column connection changes to a rigid one due to retrofitting, and thus the variation of live load will induce additional bending moment to the columns from the beams. The effect of this additional bending moment on a weak column is investigated in Model 4.4.

Model 4.4. As shown in Fig. 4.20, the single-storey frame is similar to the structure retrofitted by the flange cover plates used in Model 4.3. The structure consists of two equal bays, each one spanning a distance of 9m, and three columns of height 3m. Taking advantage of symmetry, only half of the assemblage is simulated. The side columns used here are 152x152UC23, the smallest section of universal column available in a steel designer's manual (Owens and Knowles 1992), and much weaker than the column used in Model 4.3. The simulation consists of three steps. The first step is intended to simulate the case when the middle column is not damaged, four original design concentrated loads of values of 50kN, 90kN, 90kN, and 45kN are applied at the top of the left column, two at the third points of the span, and the top of the middle column, respectively. In the second step, the restraint of the vertical displacement is released at the middle column and its boundary condition changes from fixed end to vertical slide. In the third step, the load applied at the top of the left column remains at 50kN because the secondary beams borne directly by the left column do not move, however the other three concentrated loads, at the two third points of the span and the top of the damaged middle column, are amplified to 180kN, 180kN, and 90kN, respectively, to consider the dynamic effect.

In Model 4.3, if the loads applied before retrofitting do not change, there will be no bending moment in the column after strengthening. To simulate this case, specific non-zero values of translations and rotations are assigned as the boundary conditions to the beam and column ends. Different from Model 4.3, in Model 4.4, no such specific non-zero values are

assigned to the beam and column ends. All loads acting on the structure can be regarded as variable, and the variation of these loads can cause additional bending moment in the column. Other conditions are the same as those in Model 4.3.

The structure retrofitted by the Flange Plate Scheme is modelled and some of the simulation results are given in Figs. 4.21-23. The adopted element sizes are the same as those used in Model 4.3. At the end of the first step, as shown in Fig. 4.21, the maximum von Mises stress is 113.2MPa, much less than the yield strength of 235MPa. The maximum equivalent plastic strain is zero. It is demonstrated that if the middle column is not removed, the change of live load cannot damage the originally designed column, even though all loads are variable here. At the end of the second step, as shown in Fig. 4.22, plastic hinges are formed at the top of the left column and the right low part of the middle beam segment under the original design loads due to the removal of the middle column. The von Mises equivalent stress and equivalent plastic strain distributions at the end of the third step are shown in Fig. 4.23. Significant plastic deformation develops in the right lower part and the left upper part of the middle beam segment. Compared to those at the end of the second step as shown in Fig. 4.22, yielding develops further at the left connection. The increase of vertical loads and rotation of the plastic hinge causes plasticity to develop extensively. From Fig. 4.23b, considerable distortion of the cross-section is evident with the compression-flange being deformed out of its original flat shape near the top end of the column. It can be seen from Fig. 4.23 that although plasticity develops extensively at the top and bottom ends of the

left column, the column does not collapse under the amplified loads. This fact demonstrates that the proposed retrofitting schemes can prevent collapse by catenary action, even in the very unfavourable case where the columns are very weak.

4.3 Summary

In this chapter, catenary action was investigated by means of finite element analyses. Firstly, the validity and the accuracy of the proposed finite element models were demonstrated by comparing the results between Jetteur et al (1991) and the present study. Secondly, based on the verified models, assemblages of 2D solid elements subjected to catenary tension were evaluated. Finally, 3D shell model were used to perform the simulation of the behaviour of damaged structures. The strengthening effects of the Flange Plate Scheme and the Vertical Plate Scheme have been investigated using the finite element method, and their advantages have been demonstrated. It is also shown that even though the plastic hinges form at the ends of very weak columns, the columns may still support the beam.

Chapter 5: Comparing the performance of different retrofitting schemes

It was shown in the previous chapter that the structural behaviour is quite different before and after retrofitting. Through strengthening the simple beam-to-column joints by the Flange Plate Scheme and the Vertical Plate Scheme, the collapse of a structure can be resisted by developing catenary action of the beams if a column is removed.

In this chapter, the strengthening effects of four different retrofitting schemes are investigated. These four retrofitting schemes are the Traditional Moment Connection Scheme (Bruneau et al. 1998, Houghton and Karns 2001), the Flange Plate Scheme, the SidePlate Connection Scheme (Houghton and Karns 2001) and the Vertical Plate Scheme, respectively. The behaviours of these four retrofitting schemes are compared, and their advantages and drawbacks are analysed. The finite element method is employed for conducting this investigation.

5.1 Investigation of the performance of different schemes for retrofitting fin plate connection by using shell element models

In the previous chapter, finite element analyses were conducted to investigate the retrofitting effects of the Flange Plate Scheme and the Vertical Plate Scheme. Structures perform quite differently at the removal of a column before and after they are retrofitted by the two schemes. In this section, the same commercial multipurpose finite element software

package ABAQUS is utilised for investigating the performance of four different beam-to-column connections.

Model 5.1. As shown in Fig. 5.1a, the single storey frame consists of four equal bays, each spanning a distance of 6m, and five columns of height 4m. The concentrated loads are applied at the two third points of the four beams and the top of the five columns. The centre column has been destroyed by a blast, triggering the collapse. The loss of the centre column has effectively modified the two middle spans into a single span of 12m, and therefore the loads must now be carried by the rest of the structure. This loading condition is more severe than the initial condition, and the beam will likely develop plastic deformation.

Taking advantage of symmetry, the analytic model can be reduced to only half of the whole structure, as shown in Fig. 5.1b. To decrease computational effort further, the left beam is cut in the middle and the left part of left beam and the left column is taken away, and only half of the left beam, the right column, and the right beam in Fig. 5.1b are considered in the following finite element analyses. As shown in Fig. 5.1c, the bottom of the column is fixed end; the left beam at the left end and right beams at the right end are vertical slide, i.e., their rotation and horizontal displacement are restrained but their vertical displacement is not restrained. For the structures retrofitted by the four schemes, the boundary conditions and the load locations are the same as those of the original structure shown in Fig. 5.1c when the finite element analyses are carried out.

The beams have a 406x178UB74 cross-section, and the columns 254x254UC73 (Owens and Knowles 1992). The beams and the columns are

modelled using shell finite elements positioned along the mid-planes of the flange and web components. It is also assumed that the mid-plane of the fin plate is at the same plane as that of the column and the beam webs and the fin plate is welded to the column and the beam. The thickness, the length and the depth of the fin plate are 0.01m, 0.05m and 0.24m, respectively. The Young's modulus is $E = 2 \times 10^{11}$ Pa. The constitutive law in terms of the Mises equivalent stress as a function of the equivalent plastic strain is given by Table 5.1. The failure stress and strain are assumed to be 480.0MPa and 0.1800, respectively.

Table 5.1.

Stress and strain relationship in Model 5.1

Point	1	2	3	4	5	8
Stress(MPa)	200.2	246.0	294.0	374.0	437.0	480.0
Strain	0	0.0235	0.0474	0.0935	0.1377	0.1800

The concentrated loads applied on each one of the primary beams are transferred from the secondary beams. The original values for each of these point loads are 58.0kN for dead load and 37.2kN for live load, respectively. According to ASCE 7(2002) and DoD (2005), when a column is removed and the alternative path method is used, the following load combination is applied to bays immediately adjacent to the removed element.

$$(0.9 \text{ or } 1.2)D + (0.5L \text{ or } 0.2S) + 0.2W$$

D is the dead load and the 0.9 load factor is used when the dead load enhances the overall building stability. The 0.5*L* corresponds to the mean value of maximum live load. *S* and *W* represent the snow and the wind

loads, respectively. As a result, for this structure, the concentrated loads employed for structural assessment are

$$1.2D+0.5L=1.2\times 58.0+0.5\times 37.2=88.2\,\text{kN}$$

Due to taking the advantage of symmetry, only half of the load applied at the damaged middle column is considered, and this concentrated load is 44.1 kN. For both the original and the strengthened structures, force-controlled loading is employed.

For the original structure, the numerical simulation consists of single step. In the step, the concentrated loads applied at the left beam, the column, the two third points of the right beam and the damaged half middle column are proportionally increased from 0 to 88.2kN, 88.2kN, 88.2kN, 88.2kN and 44.1kN, respectively.

The shell element S4R is employed. An element size 0.015m×0.015m is used for modelling the beam-to-column connection part, and an element size 0.015m×0.06m is utilized for modelling the rest of the structures. Some simulation results are shown in Fig. 5.2. To investigate the stress distribution, the Mises equivalent stress is plotted. It can be seen that the stress at the beam-to-column connection is much larger than the stress of other parts of structure. To investigate the strain distribution, the equivalent plastic strain is plotted as well.

Fig. 5.2 shows that when the vertical load scaling factor reaches a value of 0.3686, the maximum Mises stress 480.0MPa and equivalent plastic strain 0.1808 are roughly equal to the assumed corresponding failure values of 480.0MPa and 0.1800 at the fin plates, while the vast majority of the

structure remains below its elastic limit. This type of simple beam-to-column connection part acts like a "fuse". Because yielding only occurs at the connection part, internal forces in the middle segments of the beams are rather limited and cannot increase excessively, and therefore the middle beam segments remain elastic and no plastic deformation occurs there. Because the failure scaling factor of gravity loads is as low as 0.3686, fracture will develop further, and rupture will occur finally at the simple beam-to-column connection even under the static gravity loads without considering dynamic effect induced by the sudden removal of a column.

After strengthening, the beam-to-column connection becomes a rigid one. For the strengthened structures, the numerical simulation consists of three steps. In the first step, the concentrated loads applied at the left beam, the column, the two third points of the right beam and the damaged half middle column are proportionally increased from 0 to 88.2kN, 88.2kN, 88.2kN and 44.1kN, respectively. In the second step, the loads applied at the two third points of the right beam and the damaged half middle column are changed to 176.4kN, 176.4kN and 88.2kN respectively, as a result of accounting for the dynamic effect with an amplification factor of 2.0 (ASCE 7 2002; DoD 2005); while the concentrated loads applied on the left beam and the column remain at 88.2kN, because the left beam and the column remain intact, the secondary beams supported by the left beam and the column do not fall down and no dynamic effect is involved. In the third step, the loads applied at the two third points of the right beam and the damaged half middle column are

increased to 264.6kN, 264.6kN and 132.3kN respectively; while the concentrated load applied at the left beam and the column are still 88.2kN.

For the Traditional Moment Connection Scheme (Bruneau et al. 1998, Houghton and Karns 2001), the beam flanges are butt-welded to the faces of column flanges. For the purpose of the axial forces of the beam flanges being fully-transferred across the column, column stiffeners are added. The width and the thickness of the column stiffeners are assumed to be the same as those of the beam flanges.

Some obtained results are given in Fig. 5.3. Yielding first occurs at the weld part and then happens in the panel zone. The panel zone is the zone enclosed with the two column flanges and the two column stiffeners (Bruneau et al. 1998). Through comparison of stress and strain figures at different loading stages, it can be seen that the stress and the strain distributions change significantly as the loads increase.

As shown in Figs. 5.3c-d, the maximum Mises equivalent stress and the maximum equivalent plastic strain are 434.4MPa and 0.1385 respectively when the scaling factor is 2. In spite of yielding, the maximum equivalent plastic strain is still smaller than the assumed failure strain of 0.1800. It is demonstrated that this retrofitting scheme can prevent the collapse of the structure even considering the dynamic amplification effect. If the imposed vertical loads continue to increase, the stress and strain will also increase further. When the load scaling factor increases to 2.8650, as shown in Figs. 5.3e-f, the maximum Mises equivalent stress and the maximum equivalent plastic strain are 469.6MPa and 0.1799, respectively; approximating the corresponding failure values. These maximum stress and strain occur in the

site butt weld that links the upper beam flange to the column, instead of the beam middle segment.

By comparing to the original structure shown in Fig. 5.2, it can be seen that the stress and strain in the normal beam segment of the strengthened structure are larger than those of the original structure. The ability to prevent the collapse of the structure is enhanced noticeably by this retrofitting scheme. It is because the beam flanges on one side are linked across the column to the beam flanges on the opposite side, and the tensile resistance of the strengthened connections is much larger than that of the original fin plate connections.

The beam flanges are directly attached to the face of a column flange using site butt welds. The welds are the places where the stress and strain demands are maximum. The quality of site butt weld is usually not as good as that of shop weld. The strength of site butt weld is also lower than that of beam flange. Although the resistance of the retrofitted structure increases significantly as compared to the original structure, this strengthened structure is still not perfect. Rather than the weakest part being driven away from the column face, the failure mode appears to be controlled by failure of the weld connecting the beam flange to the face of the column flange. This failure mode is also observed following the Northridge earthquake and is documented by FEMA (2000b). The fractures can rupture completely through the thickness of the weld during a strong earthquake. However, this drawback can be overcome by the following retrofitting scheme.

By adding cover plates on the flanges at the beam ends, the tensile resistance of the beam-to-column connections can be enhanced further. For the structure retrofitted by the Flange Plate Scheme, the length and the thickness of the strengthening cover plate are 0.35m and 0.02m, respectively, and its width is assumed to be equal to that of the beam flange. Through assigning different flange thicknesses at the beam end segments and the beam middle segment, the strengthening effect of the cover plates is considered. The flange thickness is assigned to be 0.036m at the beam ends and 0.016m in the beam middle segment. The width and the thickness of the column stiffener are assumed to be the same as those of the strengthened flange at the beam end.

Some simulation results are given in Fig. 5.4. The maximum Mises equivalent stress and the maximum equivalent plastic strain distributions are 378.7MPa and 0.0968 respectively when the load scaling factor is 2. When the scaling factor increases to 3, the maximum Mises equivalent stress and the maximum equivalent plastic strain are 423.1MPa and 0.1280, respectively. It can be seen that by increasing the thickness of the flanges at beam ends, the weakest part is driven away from the beam-to-column connection to the middle beam segment. The stress and strain in the normal middle segment develop much more, as compared to those for the Traditional Moment Connection Scheme. The middle beam segment is extended significantly and a large amount of the plastic deformation develops there. By so doing, the collapse of the structure can be prevented by catenary action.

For structures retrofitted by the Traditional Moment Connection Scheme and the Flange Plate Scheme, there is obviously plastic deformation in the panel zone if the thickness of the column web is not large enough. Plastic deformation of this panel also contributes the relative rotation between the beam and column. The plastic deformation contributed by the panel zone can be reduced or eliminated by the SidePlate Connection Scheme and the Vertical Plate Scheme.

For structures retrofitted by the SidePlate Connection Scheme (Houghton and Karns 2001) shown in Fig. 5.5, the length and the thickness of the cover plates on the top and bottom beam flanges are 0.35m and 0.016m, respectively, and their width is assumed to be equal to the column width. Different flange thicknesses are assigned at different parts of the beam flange. At the beam end segment, the flange thickness is 0.032m where the cover plates and the beam flanges overlap, and is 0.016m where the cover plates extend out of the range of the beam flanges. In the beam middle segment, the flange thickness is 0.016m. The length extending from the column face and the thickness of the strengthening side plates are 0.35m and 0.02m, respectively, and their depth is equal to the beam depth. Beam stiffeners are added among the two beam flanges, the side plates and beam web. The thickness of the beam stiffeners is 0.01m. Column stiffeners are put among the two column flanges, the side plates and column web. The thickness of the column stiffeners is 0.016m. Some computational results are given in Fig. 5.5. The maximum Mises equivalent stress and the maximum equivalent plastic strain are 383.7MPa and 0.1003 respectively when the scaling factor is 2. When the load scaling factor

increases to 3, the maximum Mises equivalent stress and the maximum equivalent plastic strain are 430.7MPa and 0.1333, respectively. In Fig. 5.5g, the front side plate is removed to show the internal strain distribution behind the front side plate. It can be seen that, differently from the cases of the Traditional Moment Connection Scheme and the Flange Plate Scheme, the strain in the panel zone is negligibly small even when the load scaling factor is 3.

For the Vertical Plate Scheme, the length and the thickness of the strengthening vertical plates are 0.35m and 0.02m, respectively, and their depth is assumed to be equal to that of the beam. The Mises equivalent stress and the equivalent plastic strain distributions at the ends of the first, the second and the third stages are given in Fig. 5.6. Like the cases of the SidePlate Connection Scheme shown in Fig. 5.5, because the sizes of column are small and the strengthened panel zone is too stiff, the column also yields due to retrofitting. Although this structure yields in the vertical plates near the column face; the stress and strain levels in the middle beam segment are higher than those in the vertical plates, and the maximum stress and plastic strain will also first occur in the middle beam segment. As shown in Figs. 5.6c-d, the maximum Mises equivalent stress and the maximum equivalent plastic strain are 401.1MPa and 0.1126 respectively when the scaling factor is 2. When the scaling factor increases to 3, the maximum Mises equivalent stress and the maximum equivalent plastic strain are 449.6MPa and 0.1525, respectively. These stress and strain are very large, but still smaller than their corresponding failure values of 480MPa and 0.1800 respectively. Instead of occurring at the beam end segment

immediately adjacent to the column face, the maximum Mises equivalent stress and the maximum equivalent plastic strain are driven away from the column flange face to the beam middle segment. In Fig. 5.6g, the front vertical plate is removed to show the strain distribution behind the front vertical plate. It can be seen that, similar to the SidePlate Scheme, the strain in the panel zone is very small even when the load scaling factor is 3.

The SidePlate Connection Scheme and the Vertical Plate Scheme use two continuous strengthening steel plates in the vertical direction to retrofit the original simple beam-to-column connection geometry. Different to the early-mentioned two retrofitting schemes of the Traditional Moment Connection and the Flange Plate, these two retrofitting schemes exhibit a physical separation between the face of the column flange and the end of the beam flange, as the beam flanges are connected to the full-depth strengthening plates, instead of being connected directly to the faces of the column. The transference of bending moment, axial tension and shear force from the beam to the column or the beam on the opposite side is provided mainly by these two parallel plates in the vertical direction. These two schemes can force significant plastic behaviour into the normal beam segment adjacent to the connection, if the strengthening steel plates are designed with adequate strength and stiffness.

For the structure strengthened by the SidePlate Connection Scheme, it can be seen by comparing the stresses and strains of different loading stages shown in Fig. 5.5 that, in addition to the increase of the maximum values of stress and strain, the distribution of stress and strain also changes significantly as the vertical concentrated loads increase. For the structure

retrofitted by the Vertical Plate Scheme shown in Fig. 5.6, the same conclusions can be reached. The sizes of the side plates of the SidePlate Connection Scheme are identical to the sizes of the vertical plates of the Vertical Plate Scheme. It can also be seen that the stress distributions of the structure retrofitted by the SidePlate Connection Scheme are similar to those by the Vertical Plate Scheme at the end of three different load stages. The maximum Mises Stress ratios of the structure retrofitted by the Vertical Plate Scheme to that by the SidePlate Connection Scheme are 235.2/234.4=1.003, 401.1/383.7=1.045 and 449.6/430.7=1.044 when the load scaling factors are 1, 2 and 3, respectively. The maximum equivalent plastic strain ratios of the two structures are 0.01798/0.02239=0.8030, 0.1126/0.1003=1.123 and 0.1525/0.1333=1.145 for the corresponding three scaling factors. It can also be seen that the differences in magnitude and distribution of stress and strain are not very large for the same load scaling factor. With the variation of the load scaling factor, redistribution of stress and strain will occur.

Although the differences in mechanical behaviour are not so significant between these two retrofitting schemes, the proposed Vertical Plate Scheme has many advantages on other aspects as compared to the SidePlate Connection Scheme. Usually, the SidePlate Connection is used for new construction, and is shop-welded. By so doing, all welds can be down-hand, and the quality of the welds can be well-controlled. For the SidePlate Scheme, it is only through the cover plates that the axial forces in beam flanges are transferred to the side plates; and through the beam stiffeners that most of the shear force of beam is transferred from the beam

web to the side plates. For a new construction no fin plate is required, but for the retrofitted structure used here the fin plates may exist. Differently from the SidePlate Scheme, for the Vertical Plate Scheme the axial forces of beam flanges are transferred to the vertical plates directly without the cover plates. A portion of shear force is transferred through the existing fin plate to column straightforwardly, in addition to the rest of shear force being transferred through vertical plates. Without cover plates, column stiffeners and beam stiffeners, with no need of overhead-welds on site (Owens and Knowles 1992) between the top cover plate and beam flange, devoid of the requirement of the removal of the concrete floor slab on the top of the beam-to-column connection, the proposed Vertical Plate Scheme can save in the cost of material and labour significantly, but without affecting negatively the mechanical behaviour to a great extent, as compared to the SidePlate Connection Scheme.

For a structure strengthened by the Vertical Plate Scheme or for a structure strengthened by the SidePlate Connection Scheme, due to the existence of strengthening plates in the vertical direction, deformation contributed by the panel zone is negligibly small, but a very obvious relative angle exists between the strengthened beam end segment and the normal beam middle segment. All rotation between the beam and the column is contributed by the plastic deformations of the beam and the column, and the retrofitted beam-to-column connection part becomes almost a rigid one.

5.2 Investigation of the performance of different schemes for retrofitting end plate connection by using 3D solid element models

In recent years, bolted connections, especially end plate types (Jenkins et al. 1986; Sherbourne et al. 1994; Shi et al. 2008; Tyas et al. 2012, Stoddart et al. 2013; Stoddart et al. 2014), have increased in popularity. They have the advantages of requiring less supervision and a shorter assembly time than welded joints. They also have a geometry that can accommodate minor discrepancies in the dimensions of beams and columns. Today, bolted end plate connection is used widely in steel frames as connections between steel members. For the purpose of more reliable designs and economies in construction, great attention has been attracted to the investigation of the connection of steel structures. In addition to the traditional experimental method, numerical simulation can also be used and much of knowledge of the real behaviour of the connection has been derived form detailed finite element analysis. Most of available literatures concerning numerical simulation of the beam-to-column connections are concentrated on the end plate connections.

By adopting eight-node parametric brick elements in order to reproduce the behaviour of bolted end plate connections, Krishnamurthy (1976) was regarded as the pioneer in the field of 3D modelling of connections. The finite element models have been widely used to develop generalized force and displacement (For example, the moment and rotation) curves, to verify design methodologies based on plastic design

concepts, and to assess local behaviour in the connection components, such as bolts and end plates.

The finite element simulation of bolted connections is generally complicated because the problem is three-dimensional (3D) in nature. In addition, combined nonlinear phenomena like material and geometrical nonlinearities, friction, slippage, contact and bolt-plate interaction have to be reproduced. Therefore, Computational models must be validated to insure that they can reproduce real physical behaviour. For this purpose, the research results of Jenkins et al. (1986) and Sherbourne et al. (1994) are employed here.

By using finite element based theoretical modelling (Owen 1980), Jenkins et al. (1986) established the necessary joint characteristics. For the purpose of verification, their theoretical results were compared with experimental observations. The general view of test rig is shown in Fig. 5.7. The beam and column used in the connection was a 305×164 UB54 and 254×254 UC 132. Column web stiffeners were used at the beam flange locations for which the same thickness and width of beam flange was assumed.

As shown in Fig. 5.8, the typical configuration studied consisted of a rectangular plate welded to the beam cross section and bolted by two rows, each of two bolts at the tension flange of the beam and one row of bolts above compression flange. The bolts were all M20 grade 8.8 in 22 mm diameter drilled holes. End plate thickness is a parameter that varied from 12 to 25 mm. 18 tests were carried out. However, the only one test that the end plate thickness is 12mm is compared at present. For extended end

plate connection used in this study, the dimensions shown in Fig. 5.8 are given as the following

$D_P = 440$, $W_P = 200$, $H = 115$, $S1 = 60$, $S2 = 180$, $S3 = 355$, and $G1 = 120$.

In Sherbourne et al. (1994) paper, the finite element analysis software ANSYS was employed. As shown in Fig. 5.9, due to symmetry about a plane passing through the beam and column webs and assuming a symmetric two-way connection, only one-half of the connection is needed to consider for finite element analysis. It is assumed that no buckling failure occur in web. Plastic quadrilateral shell elements are used to model beam web and flange, end plate, column web flange and related stiffeners. The bolt shank is modelled using six 3D spar elements. Bolt head and nut are idealized using eight-node isoparametric solid elements.

To reduce difficulty caused by complicated contact problem, head and nut were believed to stay in close contact with their connection plates through all load steps, they were defined as continuous with column flange and end plate nodes, respectively, i.e., bolt head and nut brick elements share one of their faces with column flange and end plate, respectively. As a result, the number of contact surfaces was greatly reduced.

Fig. 5.10 is taken from Sherbourne et al. (1994) paper. The stress-strain relationship for the elements of the end plate, beam and column web, and flanges is taken as elastic-strain hardening as shown in Fig. 5.10a. The tangential stiffness after the yield point is defined as 5% of the initial modulus of elasticity. For the bolt material, including the shank, head and nut, a tri-linear stress-strain curve shown in Fig. 5.10b is used in which the

initial work hardening is considered to be 10% of the initial modulus of elasticity; after $3\varepsilon_y$, the stiffness decreases to 5% of the initial value.

The moment-rotation curves for the experimental versus finite-element results are shown in Fig. 5.11. For this end plate, the results (Sherbourne et al. 1994) correlate very well over the entire load history.

In the present study, the finite element analysis software ABAQUS is employed to determine the complete moment-rotation relationships for the beam to column connections so that direct comparison with experimental and numerical results is possible. For this purpose, the geometric and physic characteristics of the present model is the entire same as those of Sherbourne et al. (1994). By using a model in a 3D framework, one can take into account interactions between various structural elements. Through considering contact actions between column flange and end plate, between bolt and column flange, and between bolt and end plate, one can simulate real behaviour of the beam to column connection.

As shown in Fig. 5.13b, the deformation is very large in this study, so that complicated material, geometric and boundary nonlinearities are involved. The problems caused by the boundary nonlinearity are much more complicated than those by the material and geometric nonlinearities. In the model of Sherbourne et al., to reduce the difficulty caused by complicated contact problem, head and nut were defined as continuous with column flange and end plate nodes, and bolt head and nut brick elements share their faces with column flange and end plate, like they are "glued" or "welded" together. Different to the shell model used before and the model of Sherbourne et al., contact between all parts is explicitly

modelled in the present models. The contact areas are the end plate-to-column flange, the bolt shank-to-bolt holes and bolt head-to-components. The bolts clamp the components together in order to resist the applied rotation. The hex bolt heads are modelled as cylinders, taking into account the washers by averaging the diameter. The bolt holes are modelled as 22 mm, 2 mm larger than the bolt shaft diameter. The general contact formulation used in ABAQUS involves a "master-slave" type algorithm (ABAQUS 2014). This formulation recognizes the surfaces that are in contact or interpenetrate or slip and imposes constraints on the nodes of the slave surface such that they do not penetrate the master surface. For the contact properties, penalty friction formulation is used. A coefficient of friction equal to 0.5 is defined for sliding resistance while the interface is closed.

For the contact simulation, it is generally better to use linear elements as compared to use quadratic elements (ABAQUS 2014). In the ABAQUS library, three eight-node hexahedral linear elements are available: (1) The C3D8 conforming element with full integration, adopting a 2 × 2 × 2 array of Gauss integration points in the element. This element may experience the shear locking phenomenon. (2) The C3D8I element with full integration (also 8 Gauss points) and incompatible modes. This element has additional degrees of freedom, and it is conceived to overcome the shear locking phenomenon that is observed in bending-dominated problems. Incompatible mode element C3D8I can produce results in bending problems that are comparable to quadratic elements but at significantly lower computational cost. However, they may be sensitive to element

distortions. (3) The C3D8R linear element with reduced integration, adopting only 1 Gauss point. This element provides a remedy for shear locking but the rank-deficiency of the stiffness matrix may engender spurious singular (hourglassing) modes. These modes are controlled in the ABAQUS code with the artificial stiffness method. In addition, a hybrid element formulation is available for all three abovementioned element types. Elements using this formulation have the letter "H" in their names. Hybrid elements can be used when the material behaviour is incompressible (Poisson's ratio = 0.5).

In order to investigate the relative merits of each, this connection is simulated by using these different elements with different mesh sizes. One can compare these results with the stress and strain curves given by test of Jenkins et al. (1986) and simulation of Sherbourne et al. (1994) shown in Fig. 5.11.

Some results given by these brick elements are given in Fig. 5.12. It can be seen from Fig. 5.12a that conforming element C3D8 is too stiff and its result is not as good as others. The results given by C3D8R are almost the same as those by C3D8RH, and therefore they are not shown herein. In order to reduce computation effort, one can try to combine the shell element and brick element as shown in Fig. 5.12d. But obtained results are not desirable. As shown in Fig. 5.12d, the ABAQUS cannot complete computation for fine mesh size 0.005m due to complicated contact problem. In this study, eight-node brick element C3D8I, full integration and incompatible modes, will be mainly used because it performs better in

contact simulation than C3D8RH and C3D8R when the strain become very large.

It can be seen from Fig. 5.11 that the moment-rotation curves of this study show good agreement with the results of experiment by Jenkins et al. (1986) and the finite element analysis by Sherbourne et al. (1994) over the entire load history. It indicates the reliability of the present model in accurately predicting the behaviour of bolted end plate beam to column connections. For the C3D8I element with mesh size of 0.005m, the results of equivalent plastic strain distribution are shown in Fig. 5.13.

In the following, the behaviour of a sub-structure after the column removal will be investigated. In numerical investigations, the modelling assumptions are very important, the more assumptions adopted, the less realistic the modelling may be. Therefore, different from the previous shell models in this thesis, the present modelling will adopt as less assumptions as possible in this section. Also different from the shell element models where two connections are modelled, the only one connection can be modelled herein like most of research involving bolts and connections, due to the difficulty of numerical simulation for contact.

Model 5.2. As shown in Fig. 5.14a, the sub-structure investigated here consists of two equal bays, each spanning a distance of 6.3m. The left end of the left beam and the right end of the right beam are pinned, i.e., the horizontal and vertical displacements are restrained but the rotations are not restrained. A uniformly distributed load is applied at the sub-structure. The lower centre column support has been removed, triggering the collapse under gravity. The loss of the centre column support has

effectively modified the structural geometry into a single span of 12.6m. By so doing, the catenary action after a column removal can be simulated. Similar device was also used by Yang et al. (2012). In this study, the beams, column and bolts are adopted from Shi et al (2008). Their models of sub-structure with an extended end plate connection, bolts and their mesh densities are shown in Fig. 5.15. The depth and width of the built-up beams are 0.3m and 0.2m. The depth and width of the built-up column is 0.3m and 0.25m, respectively. The thicknesses of flange and web are 0.012m and 0.008m for both the beams and column. The details of the flexible end plate connection of this study are shown in Fig. 5.14c. The width, depth and thickness of the flexible end plate are 0.15m, 0.18m and 0.008m, respectively. The bolt holes are modelled as 0.022m, 0.002m larger than the bolt shaft diameter. Uniformly distributed load applied at the beams is 44.40 kN/m, after accounting for the dynamic effect with an amplification factor of 2.

By taking advantage of symmetry, only a half of the sub-structure is considered. The originally considered span of 12.6m becomes a half-span of 6.3m now, only the half of the middle built-up column is considered and the considered shape of the half middle column changes from an I-shape to a T-shape. By taking advantage of symmetry again about the mid-planes passing through beam and column webs, only a quarter of the assemblage is modelled for the finite element analysis. As a result of taking advantage of symmetry twice, the shape of the I-beam changes to a channel, and shape of the middle column changes to an angle finally. By so doing, the computation effort can be reduced significantly. Fig. 5.16a

show the model used in the computational simulation. At this time, the boundary condition at the left side of column becomes vertical slide, i.e., the horizontal displacement and the rotation are restrained but the vertical displacement is not restrained; and the uniformly distributed load applied at the beam becomes 22.20 kN/m.

Finite element model of high strength bolts are shown in Fig. 5.16c. It can be seen through comparison of Fig. 5.16c with Fig. 5.15b that, the bolt sizes are similar to those of Shi et al., except the shank length, due to different thicknesses of the steel plates clamped. The stress and strain relationship for the high strength bolts (including the bolt heads, shanks and nuts) is a tri-linear, with the points defining the curve being given in Table 5.2. The pretension force applied to the bolts is 155 kN. The coefficient of friction for the contact surface between the end plate and column flange was taken as 0.44. They are the same as those of Shi et al. (2008)

Table 5.2.

Stress and strain relationship for high strength bolts in Model 5.2

Point	0	1	2	3
Stress(MPa)	0	990	1160	1160
Strain	0	0.00484	0.136	0.15

Typical steel properties are utilised in the models to describe the elastic material characteristics. For the inelastic material behaviour, a nonlinear isotropic hardening plasticity model with a von Mises yield criterion and associated flow rule is used. Such plasticity model can describe the characteristics of steel and weld subjected to monotonic loading. Since tests are not performed in this study, the following data are adopted to

determine appropriate values of the plasticity material model parameters for welds, bolts and steel plates, respectively.

Majority of the research in this field, including those of Sherbourne et al. (1994) and Shi et al (2008), did not model the welds. Different from them, the welds are modelled herein both geometrically and with different material properties from steel plates. The leg length of the welds that are located between the end plate and the beam web is 6mm. As shown in Fig. 5.17, the stress and strain relationship of this weld is given by modifying that of Chao et al. (2006). In the research of Chao et al, the yielding stress of the steel plates that are welded together is 398MPa, while the corresponding value is 264MPa in this study. Therefore, all of the stresses of Chao et al. (2006) are reduced by a factor of 0.66 and the stress and strain relationship used herein is given as tri-linear.

Shi et al. (2008) have taken the stress–strain relationship for the steel plates as elastical–perfectly plastic. However, this elastical–perfectly plastic relationship cannot be utilised here. Otherwise, if the steel member is elastical–perfectly plastic without strain-hardening stage, the strain may concentrate within only small part of structural member after yielding occurs, and in this small part the strain will fully develop and become large and large under the catenary action of the beams, while the majority of the structural member is still in elastic stage. The strain hardening can cause the plasticity to distribute much more evenly in the majority of structural steel member and can enhance the structural ability of energy-dissipation. In order to avoid this strain localisation phenomenon and realistically predict the structural behaviour after the column removal, the material

properties utilised here are much more detailed than those used in this thesis before. The stress-strain constitutive law for the steel plates is shown in Fig. 5.18 and Table 5.3, which are adopted from Dowling (2013). In Table 5.3, the stress and strain relationship begins with an elastic stage from the origin 0 to point 1. Point 1 is yield point. The stage from point 1 to point 2 is perfectly plastic stage. After point 2, the strain hardening stage begins. The engineering stress reaches its maximum value at point 6. The necking occurs in the vicinity of this point and further increasing engineering strain is accompanied by a reduction in the engineering stress. This reduction of the engineering stress after point 6 is due to decrease in cross-sectional area and not due to a loss in strength of the material itself. Contrasting to the engineering stress, the current stress continues to increase with the current strain up to failure value at point 11.

Because the deformation and strain are very large and significant material and geometrical nonlinearities are involved due to catenary action, the current stress and strain should be adopted herein instead of the engineering stress and strain, which can be used only when deformation and strain are small. Before necking, the current stress σ and strain ε are given by

$$\sigma = \sigma_E\left(1+\varepsilon_E\right),\ \varepsilon = \ln\left(\frac{l}{L}\right) = \ln\left(1+\varepsilon_E\right) \qquad (5.1a,b)$$

where σ_E and ε_E are engineering strain and engineering strain, respectively

After necking at point 6, the current strain is given by

$$\varepsilon = \ln\left(\frac{l}{L}\right) = -\ln\left(\frac{a}{A}\right) = -\ln(1 - PRA) \tag{5.2}$$

Table 5.3.

Structural steel's stress and strain relationship and their conversions in Model 5.2

Point	Engin. Stress (σ_E)	Engin. Strain (ε_E)	Reduct. Area (PRA)	Current Stress (σ)	Current Strain (ε)	Plastic Strain (ε_{plast})
0	0	0		0	0	
1	264.0	0.00131		264.0	0.00131	0
2	264.0	0.01745		268.6	0.01730	0.0160
3	318.6	0.0490		334.3	0.0478	0.0462
4	372.0	0.1250		418.5	0.1178	0.1157
5	394.4	0.2180		480.4	0.1972	0.1949
6	395.0	0.2340		487.5	0.2103	0.2079
7	384.2	0.3060	30.04%	549.1	0.3572	0.3547
8	360.4	0.3300	41.13%	612.1	0.5298	0.5271
9	327.5	0.3480	51.41%	674.2	0.7218	0.7190
10	290.0	0.3600	60.58%	735.5	0.9308	0.9278
11	266.8	0.3660	66.41%	794.2	1.0909	1.0877

where L and A are initial length and cross-sectional area, l and a are current length and cross-sectional area, PRA is percentage reduction area and defined by

$$PRA = \frac{A - a}{A} \tag{5.3}$$

The current plastic strain is given by

$$\varepsilon_{plast} = \varepsilon - \frac{\sigma}{E} \tag{5.4}$$

where E is the Young's modulus.

In ABAQUS, the nonlinear stress and strain relationship is defined by current stress and the current plastic strain. The current plastic strain, called the equivalent plastic strain (PEEQ) in ABAQUS, is given at the last column in Table 5.3.

The implementation of the analysis and the solution of the finite element modelling involve two load steps. Firstly, all displacement restraints are applied at two ends of the structure and the pretension forces are applied to the bolts. After solving the first load step, the second load step implemented consists of an uniformly distributed load being applied on the beam, for which the general static analysis type with geometrical nonlinearity is chosen to consider the effect of large deformation and strain appear after the column removal.

For the original structure with flexible end plate connection, some of the simulation results are shown in Figs. 5.19-20. To check the effect of the element size on accuracy, three different element sizes have been used in the structural member: (1) Size=0.035m: 0.035m×0.035m in the joint part, and 0.035m×0.14m in the rest of the structure; (2) Size=0.02m: 0.02m×0.02m in the joint, and 0.02m×0.08m in the rest; and (3) Size=0.01m: 0.01m×0.01m in the joint part, and 0.01m×0.04m in the rest. The element size used in bolts is 0.004m. Some of meshes can be seen in Fig. 5.16. The relationship between the vertical reaction force at right end hinge support versus the vertical displacement at the left slide end is shown in Fig. 5.19 for these three mesh sizes. It can be seen the difference between different meshes is not very large because the used element sizes are small.

The equivalent plastic strain (PEEQ) distribution is plotted. In Fig. 5.20, element boundary edges are not shown in the figures for the strain distributions to be seen clearly. Fig. 5.20a shows that the plastic strain distribution around the bolt holes. It can be seen from Fig. 5.20 that yielding only occurs at the connection parts, particularly at flexible end plate, while the vast majority of the structure remains below its elastic limit. When the load scaling factor reaches a value of 0.1471, the maximum equivalent plastic strain reaches the value of 1.031, roughly equal to the assumed failure plastic strain of 1.0877. At this time, the maximum plastic strain at weld part is also very large, reaching the value of 0.7881. Consequently, rupture will occur at the connection part and the structure will collapse if the original structure is not strengthened.

This model can also be used for investigating whether or not the lower beam flange can contact the column flange and the prying force action (Byfield and Paramasivam 2007; Stoddart, Byfield and Tyas 2014; Stoddart et al. 2013) can occur. The applied load is the same, but the boundary conditions at two supports change. Instead of the left support, the right support moves downwards now. The left end of column web becomes fixed. At the right end of the beam, the horizontal displacement is restrained, but the vertical displacement and rotation are not restrained. By so doing, the destroyed middle column that is connected to beams by hinges can now be simulated by this boundary condition at the right end, while the destroyed middle column is represented by the left end support in the previous simulation.

Some results are shown in Fig. 21. At the beginning, the distance between the beam lower flange and the column flange decrease as the load increase. This distance reaches the minimum value when load scaling factor is 0.0403. However, the beam lower flange does not contact the column flange even at this moment, as shown in Fig. 5.21a. After this moment, the beam is pulled away from the column and the distance between the beam lower flange and column flange increases as the load scaling factor increase. When the load scaling factor is 0.2024, the distance is shown in Fig. 5.21b. It is can be seen that as predicated by Byfield and Paramasivam (2007), after the middle column support removal, the prying force action does not occur for this static model.

For the structure retrofitted by the Flange Plate Scheme, the length and the thickness of the strengthening cover plate are 0.2m and 0.012m, respectively, and the widths of upper cover plate and lower cover plate are 0.176m and 0.224m, respectively. The width and the thickness of the column stiffeners are 0.996m and 0.012m, respectively.

Some simulation results are given in Figs. 5.22-23. To check the effect of the element size on accuracy, three different element sizes, the same as the sizes adopted for the original structure, have been used in the strengthened structure. The relationship between the vertical reaction force at the right hinge support versus the vertical displacement at the left slide support is shown in Fig. 5.22 for these three mesh sizes. It can be seen the curves of three mesh sizes almost coincide for this model. Fig. 5.23 shows that the maximum equivalent plastic strain is 0.04183 when the load scaling factor is 2. In spite of yielding, this maximum equivalent plastic strain is much

smaller than the assumed failure strain. It is demonstrated that this retrofitting scheme can prevent the collapse of the structure even considering the dynamic amplification effect. As compared to Fig. 5.20, the large strain and deformation at the end plate of original structure disappear here, and they are now very small as shown in Fig 5.23a. Fig 5.23c-d shows strain distributions of some welds and their location at the connection part. The maximum equivalent plastic strain in these welds is only 0.004975. It can be seen that by strengthening the flanges at beam ends, the maximum equivalent plastic strain is driven away from the beam-to-column flexible end plate connection to the middle beam segment. The strain in the normal middle segment develops fully, as compared to that of original structure. The middle beam segment is extended significantly and a large amount of the plastic deformation develops there. By so doing, the collapse of the structure can be prevented by catenary action.

For the Traditional Moment Connection Scheme, the beam flanges are butt-welded to the faces of column flanges. For the purpose of the axial forces of the beam flanges being fully-transferred across the column, column stiffeners are added. The width and the thickness of the column stiffeners are the same as those of the beam flanges. As shown in Fig. 5.24, the maximum equivalent plastic strain is 0.1217, occurring at the lower part of the connection, when the scaling factor is 2. This value is much larger than the corresponding 0.04183 of the structure retrofitted by flange cover plate. Although the collapse can also be prevented, this scheme is less conservative than the Flange Plate Scheme.

For the Vertical Plate Scheme, the length, the depth and the thickness of the strengthening vertical plates are 0.20m, 0.276m and 0.016m, respectively. Relationship between the catenary tension at the left end and the vertical reaction force at the right end versus the vertical displacement at left end are given in Fig. 5.25. When load scaling factor is 2, the vertical displacement at the left end reaches 0.472m. The catenary tension is much larger than the vertical reaction at the later stage of loading. The equivalent plastic strain distributions at the ends of the loading are given in Fig. 5.26. Fig. 5.26a shows that the maximum equivalent plastic strain occurs at lower beam flange adjacent to the vertical plate. In Fig. 5.26b, only the beam and the end plate remain in order to show the strain distribution behind the front vertical plate. It can be seen that the strain of the flexible end plate is very small. Fig. 5.26c shows that the strain level in the middle beam segment is much higher than that in the vertical plates. The maximum equivalent plastic strain is 0.03371 when the scaling factor is 2. This strain is much smaller than its corresponding failure value of 1.0877. Instead of occurring at the beam end segment immediately adjacent to the column face, the maximum equivalent plastic strain are driven away from the column flange face to the beam middle segment.

If the load scaling factor is increased to 4, some computational results are shown in Figs. 5.27-28. The relationships between the catenary tension at the left and the vertical reaction force at the right end versus the vertical displacement at the left end are given in Fig. 5.27a, and the relationship between the bending moment versus the vertical displacement at the left end is given in Fig. 5.27b.

When load scaling factor is 4, the maximum vertical displacement reaches 0.864m. When the vertical displacement is 0.55m, the catenary tension is 923kN. After this point, the catenary tension almost becomes a constant value as the vertical displacement increases, as if it is in a perfectly plastic stage. The fact the catenary tension is unable to increase and the beam reaches perfectly plastic stage does not mean that the structure reaches its ultimate limit state and the final failure of the structure will occur immediately.

As illustrated in Fig. 5.29, taking moments about the right pinned support B and considering counter-clockwise as positive, the equation of moment equilibrium is given as

$$\sum M_B = -M_A - N_A y_A + \frac{1}{2} pL^2 = 0 \tag{5.5}$$

where L is the original span length; M_A, N_A and y_A are respectively the bending moment, catenary tension, and vertical displacement at the left vertical slide support A; p is the uniformly distributed load.

Eq. (5.5) can be rewritten as the following

$$M_A + N_A y_A = \frac{1}{2} pL^2 \tag{5.6}$$

At the beginning, the load p is resisted mainly by the bending action, the bending moment M_A increases as the load p and the vertical displacement y_A increase, while the catenary tension N_A is small. When the load p and the vertical displacement y_A become adequately large, the load p is resisted mainly by the catenary action, and the bending moment

M_A decreases significantly and becomes negligibly small, as mentioned in Chapter 3 and shown in Fig. 5.27b. Then Eq. (5.6) becomes

$$N_A y_A \approx \frac{1}{2} pL^2 \tag{5.7}$$

The horizontal reaction N_B at the right support B is equal to the tension N_A at the left support. Even if the catenary tension N_A cannot increase furthermore, the resistance to structural collapse can still increase because the vertical displacement y_A increases.

The equivalent plastic strain distributions at the ends of the loading are given in Fig. 5.28. Fig. 5.28a shows that the maximum equivalent plastic strain occurs at lower beam flange adjacent to the vertical plate. In Fig. 5.28b, only the beam and the end plate remain, to show the strain distribution behind the front vertical plate. It can be seen that the strain of the flexible end plate is still very small. Fig. 5.28c shows that the strain level in the middle beam segment is still much higher than that in the vertical plates. The maximum equivalent plastic strain is 0.05630 when the scaling factor is 4. This strain is still smaller than its corresponding failure value of 1.0877. It can also be seen by comparing Fig. 5.28c to Fig. 5.26c that, in addition to the increase of the maximum value of plastic strain, the distribution extent of plastic strain also increases significantly as a result of load increasing. The strain distribution is rather even over a very long middle segment of the beam. Even at this time, this structure still has some conservation because the strain level is still very low in the upper part of the beam.

For structures retrofitted by the SidePlate Connection Scheme, the length, the width and the thickness of the cover plates on the top and bottom beam flanges are 0.24m, 0.25m and 0.012m, respectively. The length, the depth and the thickness of the strengthening side plates are 0.74m, 0.4m and 0.016m, respectively. Beam stiffeners of 0.01m thick are added among the two beam flanges, the side plates and beam web. Column stiffeners of 0.012m thick are put among the two column flanges, the side plates and column web. The equivalent plastic strain distributions at the ends of the loading are given in Fig. 5.30. Similar with the structure retrofitted by the vertical plate, the maximum equivalent plastic strain occurs at lower beam flange adjacent to the vertical plate, the strain of the flexible end plate is very small, and the strain level in the middle beam segment is much higher than that in the SidePlate Connection. The maximum equivalent plastic strain is 0.04762 and the vertical displacement at the left end reaches 0.473m when the scaling factor is 2. As a result, this SidePlate Scheme can enhance significantly the ability of the original structure to resist collapse following the column removal.

5.3 Summary

From the above investigation, the following conclusions can be drawn:

The Traditional Moment Connection Scheme can improve the ability of a structure to survive without collapse due to the removal of a column, but the maximum stress and strain still occur near the column flange face and

the enhanced ability to prevent structural progressive collapse is not as good as that of other three retrofitting schemes.

When retrofitted by the Flange Plate Scheme, the SidePlate Connection Scheme and the Vertical Plate Scheme, although yielding also occurs in the strengthened beam ends bordering on the column face in some situations, the stress and strain in the strengthened beam ends are smaller than those in the middle beam segment. These retrofitted structures still have resistant capacity even when the load scaling factor is much larger than 2.

At the beginning of loading, the load is resisted mainly by the bending action, while the catenary tension is very small. As the load increases, the bending moment will decrease significantly and becomes negligibly small, and the catenary tension will increase if the load scaling factor increase. When the load scaling factor becomes adequately large, the catenary tension cannot increase furthermore as the load increases, but the structural resistance to collapse can still increase through the increasing of the beam plastic deformation.

Through comparing structures before and after retrofitting, it can be seen that these three schemes can effectively strengthen the original weakest beam-to-column connection part near the column flange face and can prevent collapse by developing catenary action. Therefore, the safety of people in the structure can be guaranteed at the removal of a column by a blast.

The reason why the structural collapse can be prevented is because the strengthening steel plates are strong enough in these structures. The sizes of the strengthening plates play a crucial role in the distributions of stress and strain. This role will be discussed and the strengthening plate sizes will be parametrically studied in the next chapter for the Flange Plate Scheme and the Vertical Plate Scheme.

Chapter 6: Minimising Weight of Strengthening Plates for Flange Plate Scheme and Vertical Plate Scheme

Usually, a beam is designed to resist lateral loads only. Due to the removal of a column, a very large catenary tension will be involved in the beams, in addition to continuing to be subjected to the lateral loads. In some special cases, the exact solution of the nonlinear structural problem is available. As one of these special cases, when only axial tension exist without lateral loads, the pure catenary tension analyses can be carried out and exact solutions have been obtained for the trusses with strong or weak end segments in Chapter 3. As another of these special cases, the optimal analyses of the beams retrofitted by the Flange Plate Scheme and the Vertical Plate Scheme can be conducted and exact solutions of optimisation can be given in Section 6.1.

Generally speaking, however, the general exact solution of the material and geometrical nonlinear structural problem under the combined bending moment and axial force is extremely difficult, if not impossible, to obtain. Habitually, the finite element method could be used for such cases. This thesis will utilise the software ABAQUS to conduct the parametric study of the structures retrofitted by the two proposed schemes in Section 6.2.

6.1 Exact optimal elastic and elasto-plastic analyses of retrofitted structures under bending, shear and tension

The effect of different thicknesses and lengths of strengthening plates on the resistance of the retrofitted structures will be examined here in order to conduct the optimisation. These thicknesses and lengths can affect the performance of the retrofitted structures significantly. Under the condition that the applied loads remain constant, the behaviour of a structure may be totally different when the size of the strengthening plates is changed.

The weight of the strengthening plates is determined by their sizes. The cost of retrofitting depends on the weight of retrofitting plates. The larger the weight, the better for the reserve capacity of the structure; but the retrofitting cost will be higher; and vice versa. The retrofitted part will experience subsequently from elastic state to elasto-plastic state until final failure, as its stress and strain levels increase with the decrease of size and weight of the strengthening plates. Therefore, two resisting capacities: elastic and elasto-plastic, can be used. Using higher resisting capacity of elasto-plastic state can provide a saving in strengthening material, as compared to that of elastic state. Thereby, the weight of retrofitting plates can be decreased. As the weight of retrofitting plates reduces gradually, the stress and strain levels will increase progressively and, of course, the safety and reserve capacity of the structure will decrease gradually.

6.1.1 *Optimisation of the Beam Retrofitted by the Flange Plate Scheme*

When designing a structural steelwork; there are usually two strength limit states, or criteria, that can be used: (1) elastic, and (2) inelastic. When the thickness of the strengthening plates reduces gradually, the retrofitted cross-section of an I-beam will experience sequentially from elastic state to inelastic state until final failure. In this section, the stress and strain

relationship is assumed to be elastic-perfectly plastic for simplicity. For a strengthened cross-section with I-shape or similar, the stress distribution curves across the section can also be divided into two states. These two states are illustrated in Fig. 6.1 for the cross-section retrofitted by the Flange Plate Scheme. In this figure, the width of the flange cover plates is assumed to be equal to that of the beam flange for simplicity. As shown in Fig. 6.1, the two states are: (1) elastic state, the whole retrofitted cross-section is elastic. When the stress on the cross-section reaches its corresponding yield value, the limit state of elastic stage is arrived. (2) elasto-plastic state, the cross-section is elasto-plastic. The outer portions of the strengthened cross-section become plastic but the inner portion is still elastic. When the stress on the fibre at the neutral axis of the cross-section reaches its corresponding yield value and the elastic inner core on the cross section disappears, the ultimate limit state of elasto-plastic stage is arrived at, and the strengthened cross section reaches its plastic capacity.

Because distinct boundaries between the two states exist, in order to give structural engineers more choice, two criteria of optimisation are used here, instead of a single criterion. The limit state of the elastic stage is adopted as the first criterion. However, if the ultimate limit state of the elasto-plastic stage is adopted as the second criterion, the deflection of the retrofitted beam will be significant and the strains on the outermost fibres of the cross-section will become extremely large. Therefore, the elastic inner core should remain sufficiently large and the strains on the outermost fibres should not assume very large values.

For a structure strengthened by flange cover plates, the optimisation problem consists of finding the minimum weight of retrofitting plates for these two different optimisation criteria. The objective function of the weight is expressed as

$$W(t_c, l_c) \propto \rho b l_c t_c \tag{6.1}$$

where ρ is the density of steel, b the width of beam flanges, t_c and l_c are the thickness and the length of the flange cover plates. The aim of optimisation is to reduce this retrofitting plate weight W.

Design variables considered in the optimisation are the thickness t_c and the length l_c of the retrofitting plates. Although they are usually discrete in real designs and constructions, the thickness and the length of the retrofitting plates are regarded as continuum variables in Section 6.1.

The state constraints are that the maximum or minimum absolute values of the stress or other physical quantities must not exceed their corresponding maximum or minimum allowable values for the two different stages when optimising the strengthening plates. In the elastic stage, the stress is adopted as a constraint condition, and is expressed as

$$|\sigma| \le \sigma_{\max} \tag{6.2}$$

which acts as an indicator of the safe reserve capacity of the retrofitted structure.

Sometimes, one may need partial derivatives of the constraint conditions with respect to the design variables. To find such partial derivatives is the goal of sensitivity analysis (Bendsoe 1995, Choi and Kim

2005a,b; Christensen and Klarbring 2009). In the form of sensitivity analysis, the stress constraint condition can be expressed as

$$-\sigma_{\max} \le \sigma(t_c, l_c) = \sigma(t_{c0}, l_{c0}) + \frac{\partial \sigma(t_{c0}, l_{c0})}{\partial t_c}(t_c - t_{c0}) + \frac{\partial \sigma(t_{c0}, l_{c0})}{\partial l_c}(l_c - l_{c0}) \le \sigma_{\max} \quad (6.3)$$

In the following model, the influence of different thicknesses and lengths of the flange cover plates on enhancing the moment resisting capacity of an I-beam is evaluated. For decreasing weight of flange cover plates, the magnitude of stress and strain will increase and the retrofitted beam will experience two different stages. The beam retrofitted by flange cover plates will be optimised according to the above mentioned two criteria.

Model 6.1. A cantilever beam is adopted for this structural optimisation problem. As shown in Fig. 6.2, the beam is fixed at right end and subjected to a horizontal load and a vertical load at the left free end. The length, the width and the depth of the beam are $L = 1.5m$, $b = 0.2m$ and $h = 0.4m$, respectively. The thicknesses of flange and web are $t_f = 0.02m$ and $t_w = 0.014m$, respectively. The Young's modulus is $E = 2 \times 10^{11} Pa$. The used stress-strain relationship is assumed to be elastic-perfectly plastic. The yield stress is $\sigma_y = 2.35 \times 10^8 Pa$.

One can take a left section at any horizontal distance x along the length of the cantilever beam from its left free end. Taking moments about this section, the bending moment under the vertical concentrated load at this section is given as

$$M(x) = P_y x$$

In the original design, the magnitude of both horizontal and vertical loads is $1.763\times10^5 N$, the maximum Mises stress under these two loads is $167.4MPa$, less than the yield stress $\sigma_y = 235.0MPa$, and therefore the structure is safe. However, the two applied loads are doubled and increase significantly to a new value of $P_x = P_y = 3.526\times10^5 N$. After checking, it is found that this original structure is not safe. As shown in Fig. 6.3, the Flange Plate Scheme is used to retrofit the segments where the stresses are higher than the yield strength.

In Fig. 6.3, the bending moment reaches its maximum value at the right fixed support. This maximum bending moment under the new load is

$$M(L) = P_y L = 3.526\times10^5 \times 1.5 = 5.289\times10^5 Nm$$

The variation of the thickness of flange cover plates can cause the redistribution of the stress across the strengthened section. As illustrated in Figs. 6.1, with the decrease of the thickness t_c of flange cover plates, the strengthened cross section at the extreme right end experiences elastic state and elasto-plastic state sequentially. When the thickness is still large, as shown in Fig. 6.1, the whole cross section is in the elastic state. The normal stress distribution due to the axial tensile and lateral loads can be obtained by superimposing the uniform stress distribution corresponding to the centric tension P_x and the linear distribution corresponding to the bending moment $M(x) = P_y x$, or

$$\sigma(t_c, x, y) = \frac{P_x}{A(t_c)} + \frac{P_y}{I(t_c)} xy \quad \left(L - l_c \le x \le L, -\frac{h}{2} - t_c \le y \le \frac{h}{2} + t_c \right) \tag{6.4}$$

where x is measured from the left free end where P_x and P_y are applied, y is measured from the centroidal axis of the cross section, $A(t_c)$ is the area of the strengthened cross section, and $I(t_c)$ is the moment of inertia of the section with respect to the centroidal axis. The expressions of $A(t_c)$ and $I(t_c)$ are given by

$$A(t_c) = 2b(t_f + t_c) + t_w(h - 2t_f) \tag{6.5a}$$

$$I(t_c) = \frac{1}{12}\left[b(h + 2t_c)^3 - (b - t_w)(h - 2t_f)^3\right] \tag{6.5b}$$

On the outermost tensile fibre of the cross section at the extremely right end, where $x = L$ and $y = \frac{h}{2} + t_c$, the normal stress reaches maximum value and is given by

$$\sigma\left(t_c, L, \frac{h}{2} + t_c\right) = \frac{P_x}{A(t_c)} + \frac{P_y L}{I(t_c)}\left(\frac{h}{2} + t_c\right) \tag{6.6a}$$

At the same location, the partial derivative of the stress with respect to the cover plate thickness t_c is given by

$$\begin{aligned} \frac{\partial}{\partial t_c}\sigma\left(t_c, L, \frac{h}{2} + t_c\right) &= \frac{\partial}{\partial t_c}\left[\frac{P_x}{A(t_c)} + \frac{P_y L}{I(t_c)}\left(\frac{h}{2} + t_c\right)\right] \\ &= -\frac{2bP_x}{[A(t_c)]^2} + \frac{P_y L}{I(t_c)} - \frac{P_y L b(h + 2t_c)^3}{4[I(t_c)]^2} \end{aligned} \tag{6.6b}$$

The initial thickness of the flange cover plate is assumed to be $t_{c0} = 0.02m$. Let $t_c = t_{c0} = 0.02m$, then the area of the cross section and the moment of inertia are given by Eq. (6.5) as

$$A(t_c) = 2b(t_f + t_c) + t_w(h - 2t_f)$$
$$= 2 \times 0.2(0.02 + 0.02) + 0.014(0.4 - 2 \times 0.02) = 0.02104 m^2$$

$$I(t_c) = \frac{1}{12}\left[b(h + 2t_c)^3 - (b - t_w)(h - 2t_f)^3\right]$$
$$= \frac{1}{12}\left[0.2(0.4 + 2 \times 0.02)^3 - (0.2 - 0.014)(0.4 - 2 \times 0.02)^3\right] = 6.966 \times 10^{-4} m^4$$

The maximum normal stress of the whole strengthened segment and its t_c-derivative are given by Eq. (6.6) as

$$\sigma(t_c) = \sigma\left(t_c, L, \frac{h}{2} + t_c\right) = \frac{P_x}{A(t_c)} + \frac{P_y L}{I(t_c)}\left(\frac{h}{2} + t_c\right)$$
$$= \frac{3.526 \times 10^5}{0.02104} + \frac{3.526 \times 10^5 \times 1.5}{6.966 \times 10^{-4}}\left(\frac{0.4}{2} + 0.02\right)$$
$$= 1.838 \times 10^8 Pa$$

$$\frac{\partial \sigma(t_c)}{\partial t_c} = \frac{\partial}{\partial t_c}\sigma\left(t_c, L, \frac{h}{2} + t_c\right) = -\frac{2bP_x}{A^2} + \frac{P_y L}{I} - \frac{P_y L b(h + 2t_c)^3}{4I^2}$$
$$= -\frac{2 \times 0.2 \times 3.526 \times 10^5}{0.02104^2} + \frac{3.526 \times 10^5 \times 1.5}{6.966 \times 10^{-4}} - \frac{3.526 \times 10^5 \times 1.5 \times 0.2(0.4 + 2 \times 0.02)^3}{4 \times \left(6.966 \times 10^{-4}\right)^2}$$
$$= -4.202 \times 10^9 Pa/m$$

Because this maximum stress is lower than the yield stress, the structure is safe for the thickness of 0.02m. To reduce the weight of the strengthening plates, the thickness can be reduced. With this reduction of cover plate thickness the stress will increase. When the thickness is small enough, the outermost fibre of the upper tensile flange cover plate can reach its yield strength, i.e., the limit state of elastic stage and the first criterion of optimisation.

In the right strong segment, the stress depends only on the thickness of the flange cover plates and does not relate to the length of the plates. The

stress $\sigma(t_c, l_c)$ in Eq. (6.3) becomes a function of t_c only. By letting $\sigma_{\max} = \sigma_y$, Eq. (6.3) can be rewritten as

$$\sigma(t_c) = \sigma(t_{c0}) + \frac{d\sigma(t_{c0})}{dt_c}(t_c - t_{c0}) \le \sigma_y \tag{6.7}$$

Table 6.1.

Results for the Flange Plate Scheme in elastic stage by sensitivity analysis for Model 6.1

	$A(t_{c0})$ (m²)	$I(t_{c0})$ (m⁴)	$\sigma(t_{c0})$ (MPa)	$\frac{d\sigma(t_{c0})}{dt_c}$ (MPa/m)	t_c (m)
1	0.02104	0.0006966	183.8	-4202	0.00782
2	0.01617	0.0004735	253.9	-7891	0.01022
3	0.01713	0.0005155	236.3	-6852	0.01040
4	0.01720	0.0005188	235.0	-6779	0.01041
5	0.01720	0.0005188	235.0	-6779	0.01041

By assuming equality in the above expression, the thickness of the cover plates can be given as

$$t_c = \frac{\sigma_y - \sigma(t_{c0})}{\frac{d\sigma(t_{c0})}{dt_c}} + t_{c0} = \frac{2.350\times10^8 - 1.838\times10^8}{-4.202\times10^9} + 0.02 = 0.007817m$$

Assuming $t_{c0} = t_c = 0.007817m$ and repeating the above process, the following results are obtained.

$$A(t_{c0}) = 0.01617m^2,\ I(t_{c0}) = 4.735\times10^{-4}m^4,\ \sigma(t_{c0}) = 2.539\times10^8 Pa,$$

$$\frac{d\sigma(t_{c0})}{dt_c} = -7.891\times10^9 Pa/m,\ t_c = 0.01022m$$

The process continues until t_c converges to a value. The calculation processes and results are given in Table 6.1. It can be seen that the outermost fibre of the upper flange cover plate will reach the yield stress when $t_c = 0.01041m$.

In addition to the normal stress, the contribution of the shear stress should also be considered. The formulation of shear stress is based on equilibrium and the relationship between the shear stress and normal stress. Consider the isolated element of a strengthened I-beam shown in Fig. 6.4, which is of infinitesimal length in the x direction and of finite length in the y direction. The top of the element is the top of the I-beam at $\frac{h}{2}+t_c$ and the bottom of the element is at an isolation break located at y. The strengthened cross section from y to $\frac{h}{2}+t_c$ is shown in the right part of the figure. For clarity, only force distributions in the x direction are shown on the isolated element. The shear stress $\tau(t_c,x,y)$ is uniform in the x direction as it acts over the infinitesimal distance Δx. From equilibrium of forces in the x direction for the isolated element, the following is derived.

$$\begin{aligned}\sum F_x &= \int_y^{\frac{h}{2}+t_c} \sigma(t_c,x+\Delta x,y)dA - \int_y^{\frac{h}{2}+t_c} \sigma(t_c,x,y)dA - \tau(t_c,x,y)t_w\Delta x \\ &= \int_y^{\frac{h}{2}+t_c} [\sigma(t_c,x+\Delta x,y)-\sigma(t_c,x,y)]dA - \tau(t_c,x,y)t_w\Delta x = 0\end{aligned} \tag{6.8}$$

Thereby, the shear stress can be given by

$$\tau(t_c,x,y) = \frac{1}{t_w}\lim_{\Delta x\to 0}\int_y^{\frac{h}{2}+t_c} \frac{\sigma(t_c,x+\Delta x,y)-\sigma(t_c,x,y)}{\Delta x}dA = \frac{1}{t_w}\int_y^{\frac{h}{2}+t_c} \frac{\partial\sigma(t_c,x,y)}{\partial x}dA \tag{6.9}$$

According to the pairing principle of shear stresses, this value is the magnitude of the transverse shear stress as well. When the normal stress $\sigma(t_c, x, y)$ is expressed by Eq. (6.4), then the shear stress of the web can be expressed as

$$\tau(t_c, x, y) = \frac{1}{t_w} \int_y^{\frac{h}{2}+t_c} \frac{\partial}{\partial x}\left(\frac{P_x}{A(t_c)} + \frac{P_y}{I(t_c)} xy \right) dA = \frac{1}{t_w} \int_y^{\frac{h}{2}+t_c} \frac{P_y}{I(t_c)} y dA \tag{6.10}$$

The x-derivative of $\frac{P_x}{A(t_c)}$ is zero since the terms P_x and $A(t_c)$ are not functions of x. The terms P_y and $I(t_c)$ are factored out of the integral since they are not functions of y. Solving for $\tau(t_c, x, y)$ results in

$$\tau(t_c, x, y) = \frac{P_y}{I(t_c) t_w} \int_y^{\frac{h}{2}+t_c} y dA = \frac{P_y S(y)}{I(t_c) t_w} \tag{6.11}$$

The integral $S(y)$ is defined as the first moment of area with respect to the centroidal axis of the cross section isolated from y to $\frac{h}{2} + t_c$. When y is located within the web, it can be given by

$$S(y) = \int_y^{\frac{h}{2}} y dA = \frac{1}{2}\left\{ b(t_f + t_c)(h - t_f + t_c) + t_w\left[\left(\frac{h}{2} - t_f \right)^2 - y^2 \right] \right\}, \quad \left(|y| \le \frac{h}{2} - t_f \right) \tag{6.12}$$

It is demonstrated by this equation that the transverse shear stress varies in a parabolic fashion with respect to the distance of y from the centroidal axis. The maximum value of shear stress occurs when $y = 0$.

Occurring on the extremely right strengthened cross section $x = L$ and at the centroidal axis $y = 0$, the maximum shear stress is given by

$$\tau(t_c,L,0)=\frac{P_y}{t_w I(t_c)}S(0)=\frac{P_y}{t_w I(t_c)}\frac{1}{2}\left[b(t_f+t_c)(h-t_f+t_c)+t_w\left(\frac{h}{2}-t_f\right)^2\right]$$
$$=\frac{3.526\times10^5}{0.014\times5.188\times10^{-4}}\frac{1}{2}$$
$$\left[0.2(0.02+0.01041)(0.4-0.02+0.01041)+0.014\left(\frac{0.4}{2}-0.02\right)^2\right] \quad (6.13a)$$
$$=6.865\times10^7\,Pa$$

At the same point, the normal stress is contributed by the centric tension P_x only and is given by

$$\sigma(t_c,L,0)=\frac{P_x}{A(t_c)}=\frac{3.526\times10^5}{0.01720}=2.050\times10^7\,Pa \quad (6.13b)$$

The Mises stress is

$$\sigma^{Mises}(t_c,L,0)=\sqrt{[\sigma(t_c,L,0)]^2+3[\tau(t_c,L,0)]^2}$$
$$=\sqrt{(2.050\times10^7)^2+3\times(6.865\times10^7)^2} \quad (6.14)$$
$$=1.207\times10^8\,Pa$$

The yield strength is $\sigma_y=2.350\times10^8\,Pa$, and therefore this Mises stress is much smaller than the yield strength.

In addition to the maximum normal stress on the top fibre and the Mises stress at the centroidal axis, the Mises stress should also be checked at the junction surface between flange and web, where both the normal stress and the shear stress are quite large. The normal and the shear stresses at that surface are given respectively by

$$\sigma\left(t_c,L,\frac{h}{2}-t_f\right)=\frac{P_x}{A(t_c)}+\frac{P_y L}{I(t_c)}\left(\frac{h}{2}-t_f\right)$$
$$=\frac{3.526\times10^5}{0.01720}+\frac{3.526\times10^5\times1.5}{5.188\times10^{-4}}\left(\frac{0.4}{2}-0.02\right) \quad (6.15a)$$
$$=2.040\times10^8\,Pa$$

$$\tau\left(t_c, L, \frac{h}{2}-t_f\right)=\frac{P_y}{t_w I(t_c)} S\left(\frac{h}{2}-t_f\right)=\frac{P_y}{t_w I(t_c)} \frac{1}{2} b\left(t_f+t_c\right)\left(h-t_f+t_c\right)$$
$$=\frac{3.526\times10^5}{0.014\times5.188\times10^{-4}} \frac{1}{2} 0.2(0.02+0.01041)(0.4-0.02+0.01041) \quad (6.15b)$$
$$=5.764\times10^7\, Pa$$

The Mises stresses at this junction point is

$$\sigma^{Mises}\left(t_c, L, \frac{h}{2}-t_f\right)=\sqrt{\left[\sigma\left(t_c, L, \frac{h}{2}-t_f\right)\right]^2+3\left[\tau\left(t_c, L, \frac{h}{2}-t_f\right)\right]^2}$$
$$=\sqrt{\left(2.040\times10^8\right)^2+3\times\left(5.764\times10^7\right)^2} \quad (6.16)$$
$$=2.271\times10^8\, Pa$$

Because the maximum Mises stress is smaller than the yield strength $\sigma_y=2.350\times10^8\, Pa$, the junction point is safe. To examine whether there is any other Mises stress larger than this value within the web, the derivative of the Mises stress is used to search for the maximum value, but it is found that no such larger stress exist. Therefore, this Mises stress at the junction point is also the largest in the whole web.

Among these three possible points, the stress at the top fibre of the strengthened cross section is the maximum stress. Because the maximum stress of the whole section just reaches the yield strength and no plastic region is developed in the cross section, the requirement on strength is satisfied for this thickness. Because of the limit state of the elastic stage being reached, the thickness of 0.01041m is the mathematical solution for the first optimisation criterion, and the adopted steel plates can be 11mm thick for realistic structure.

The above discussions are only for a pure mathematical model. In this model, the links between the cover plates and the beam flanges are not

regarded as a potential problem. For a real structure, however, the cover plates and beam flanges are linked by welds. Therefore, these welds should be adequately large. Otherwise, failure may occur in these welds.

For the left normal beam segment, the normal stress distribution can be obtained by superimposing the uniform stress distribution corresponding to the centric tension P_x and the linear distribution corresponding to the bending moment $M = P_y x$, or

$$\sigma(x,y) = \frac{P_x}{A} + \frac{P_y}{I} xy \quad \left(0 \le x \le L - l_c, -\frac{h}{2} \le y \le \frac{h}{2}\right) \tag{6.17}$$

where x is measured from the left free end at which P_x and P_y are applied, y is measured from the centroidal axis of the cross section, A is the area of the cross section, and I is the moment of inertia of the section with respect to the centroidal axis. The expressions and values of A and I are given by

$$\begin{aligned} A &= 2bh - (b - t_w)(h - 2t_f) \\ &= 2 \times 0.2 \times 0.02 + 0.014(0.4 - 2 \times 0.02) \\ &= 0.01304 m^2 \end{aligned} \tag{6.18a}$$

$$\begin{aligned} I &= \frac{1}{12}\left[bh^3 - (b - t_w)(h - 2t_f)^3\right] \\ &= \frac{1}{12}\left[0.2 \times 0.4^3 - (0.2 - 0.014)(0.4 - 2 \times 0.02)^3\right] \\ &= 3.435 \times 10^{-4} m^4 \end{aligned} \tag{6.18b}$$

Occurring at the uppermost flange fibre at the junction cross section between the left normal segment and right strengthened segment, the maximum normal stress of the left normal segment can be given by

$$\sigma\left(L - l_c, \frac{h}{2}\right) = \frac{P_x}{A} + \frac{P_y (L - l_c) h}{2I} \tag{6.19}$$

If the flange plate length l_c decreases, this maximum stress will increase. When the length l_c is adequately short, this maximum stress can reach the yield strength.

In the left normal segment, the strain associates only with the length of the flange plates, the number of design variables decrease from two to one, and the expression involves ordinary, rather than partial, differentiation. Thus, Eq. (6.3) becomes

$$\sigma(l_c) = \sigma(l_{c0}) + \frac{d\sigma(l_{c0})}{dl_c}(l_c - l_{c0}) \le \sigma_{\max} = \sigma_y \tag{6.20}$$

in which $\sigma(l_c)$ is given by Eq. (6.19) and

$$\frac{d\sigma(l_c)}{dl_c} = -\frac{P_y h}{2I} \tag{6.21}$$

By substituting Eqs. (6.19) and (6.21) into Eq. (6.20) and assuming equality in Eq. (6.20), the length of the cover plates can be given as

$$\begin{aligned} l_c &= \frac{\sigma_y - \sigma(l_{c0})}{\frac{d\sigma(l_{c0})}{dl_c}} + l_{c0} = \frac{\sigma_y - \left[\frac{P_x}{A} + \frac{P_y(L - l_{c0})h}{2I}\right]}{-\frac{P_y h}{2I}} + l_{c0} = L - \left(\sigma_y - \frac{P_x}{A}\right)\frac{2I}{P_y h} \\ &= 1.5 - \left(235.0\times10^6 - \frac{3.526\times10^5}{0.01304}\right)\frac{2\times3.435\times10^{-4}}{3.526\times10^5\times0.4} \\ &= 0.4870m \end{aligned} \tag{6.22}$$

This result of l_c is the exact solution, and no further iteration is needed.

Similar to the case of the strengthened cross section, the contribution of the shear stress should be considered as well. Occurring at the centroidal axis, the maximum shear stress is given by

$$\tau(L-l_c,0)=\frac{P_x}{t_w I(t_c)}\frac{1}{2}\left[bt_f(h-t_f)+t_w\left(\frac{h}{2}-t_f\right)^2\right]$$
$$=\frac{3.526\times10^5}{0.014\times3.435\times10^{-4}}\frac{1}{2}\left[0.2\times0.02(0.4-0.02)+0.014\left(\frac{0.4}{2}-0.02\right)^2\right] \quad (6.23a)$$
$$=7.235\times10^7\,Pa$$

At the same location, the normal stress, contributed by the tension P_x only, is given by

$$\sigma(L-l_c,0)=\frac{P_x}{A}=\frac{3.526\times10^5}{0.01304}=2.704\times10^7\,Pa \quad (6.23b)$$

The Mises stress is

$$\sigma^{Mises}(L-l_c,0)=\sqrt{[\sigma(L-l_c,0)]^2+3[\tau(L-l_c,0)]^2}$$
$$=\sqrt{(2.704\times10^7)^2+3\times(7.235\times10^7)^2} \quad (6.24)$$
$$=1.282\times10^8\,Pa$$

This Mises stress is much smaller than the yield strength of $\sigma_y=2.350\times10^8\,Pa$.

In addition to the maximum normal stress on the top fibre and the Mises stress at the centroidal axis, the Mises stress at the junction surface between flange and web should also be checked. The normal and shear stresses at this surface are respectively

$$\sigma\left(L-l_c,\frac{h}{2}-t_f\right)=\frac{P_x}{A(t_c)}+\frac{P_y(L-l_c)}{I(t_c)}\left(\frac{h}{2}-t_f\right)$$
$$=\frac{3.526\times10^5}{0.01304}+\frac{3.526\times10^5(1.5-0.4870)}{3.435\times10^{-4}}\left(\frac{0.4}{2}-0.02\right) \quad (6.25a)$$
$$=2.142\times10^8\,Pa$$

$$\tau\left(L,\frac{h}{2}-t_f\right)=\frac{P_x}{t_w I(t_c)}S\left(\frac{h}{2}-t_f\right)=\frac{P_x}{t_w I(t_c)}\frac{1}{2}bt_f(h-t_f)$$
$$=\frac{3.526\times10^5}{0.014\times5.188\times10^{-4}}\frac{1}{2}0.2\times0.02(0.4-0.02) \quad (6.25b)$$
$$=5.572\times10^7\,Pa$$

The Mises stress at this junction point is

$$\begin{aligned}\sigma^{Mises}\left(L-l_c,\frac{h}{2}-t_f\right)&=\sqrt{\left[\sigma\left(L-l_c,\frac{h}{2}-t_f\right)\right]^2+3\left[\tau\left(L-l_c,\frac{h}{2}-t_f\right)\right]^2}\\&=\sqrt{\left(2.142\times10^8\right)^2+3\times\left(5.572\times10^7\right)^2}\\&=2.349\times10^8\,Pa\end{aligned}\tag{6.26}$$

Because this Mises stresses is roughly the same as, but still not larger than, the yield strength $\sigma_y=2.350\times10^8\,Pa$, the first optimisation criterion is still not exceeded at the junction point. To examine whether there is any other Mises stress larger than this value within the web, the derivative of the Mises stress is used to search for the maximum value, but no such stress is found. Therefore, this Mises stress at the junction point is also the largest in the whole web.

Among these three possible points, the stress at the top fibre of the normal cross section and the Mises stress at the junction point are the maximum stress. Because these maximum stresses of the whole section just reach the yield strength and the corresponding maximum strains are not larger than the yield strain, the requirement on strength is satisfied for this length. Therefore, the length of 0.4870m is the optimal solution for the first optimisation criterion.

The weight of the flange cover plates for the first optimisation criterion is

$$W\left(t_c,l_c\right)=2\rho bl_ct_c=2\times7850\times0.2\times0.4870\times0.01041=15.92kg\tag{6.27}$$

The weight of the original beam is

$$W_o=\rho AL=7850\times0.01304\times1.5=153.5kg\tag{6.28}$$

The ratio between them is

$$15.92/153.5 = 10.37\%$$

Under the original load case when $P_x = P_y = 1.763 \times 10^5 N$, the maximum stress of the whole original structure is given as

$$\sigma\left(L, \frac{h}{2}\right) = \frac{P}{A} + \frac{PLh}{2I} = \frac{1.763 \times 10^5}{0.01304} + \frac{1.763 \times 10^5 \times 1.5 \times 0.4}{2 \times 3.435 \times 10^{-4}} = 167.4 \times 10^6 Pa \quad (6.29)$$

If these two horizontal and vertical loads increase proportionally, when the magnitude of these two loads increases to

$$\frac{235.0 \times 10^6}{167.4 \times 10^6} 1.763 \times 10^5 = 2.475 \times 10^5 N$$

the original structure will reach its elastic limit resisting capacity. The increase of resisting capacity for elastic limit state is

$$(3.526 \times 10^5 - 2.475 \times 10^5)/2.475 \times 10^5 = 42.47\%$$

It can be seen that through the increase of retrofitting material by only 10.37%, the elastic limit resisting capacity increases by 42.47% for the first optimisation criterion.

Because steel is a ductile material, it is able to withstand deformation under loads without material fracture or structural collapse even if the first optimisation criterion, based on the elastic limit state, is exceeded. For the upper portion of the extremely right strengthened cross section, any further decrease in the thickness of the flange cover plates will cause the outermost fibres to develop plastic flow but at the same time maintain the yield stress. Consequently, the adjacent upper fibre undergoes an increase

in strain with corresponding increase in stress up to a maximum of σ_y. With the further reduction of the thickness, the lowermost fibre may also yield, and a compressive plastic zone may also form in the lower portion in addition to the tensile plastic zone in the upper portion of the cross section.

Because the stress will have a constant value of σ_y after yielding, it is difficult for the stress to be adopted as the optimisation criterion now. This is quite different from the elastic stage. The strain is better than the stress in this respect, but is not as good as the yield strain distance. The yield strain distance z_y, from the neutral axis to the fibre on which the yield strain ε_y just occurs, defines the boundary between the elastic and the plastic zones and represents half the depth of the elastic inner core. Any fibre located beyond the yield strain distance will behave plastically. This yield strain distance z_y will reduce with the thickness of flange cover plates. If the thickness t_c decreases without limit, the stress will continue to develop in the section until the entire section is stressed up to σ_y, the elastic inner core vanishes completely and the pure plastic resisting capacity is reached.

For a certain value of strain, the elastic inner core may be very large and at the same time the vertical displacement may be very small when a beam depth is large. When a beam depth is small, the elastic inner core may be very small and therefore the deflection may be very large for the same value of strain. In order to prevent the vertical displacement being out of control, the yield strain distance, instead of the strain, is adopted as the constraint condition for optimisation.

However, according the theory of plasticity (Chakrabarty 1986), the shear stress is zero on the plastic portions of the cross-section. This conclusion can also be demonstrated straightforwardly by letting $\sigma(t_c, x, y) = \sigma_y$ in Eq. (6.9) and Fig. 6.4. Therefore, the shear force across the beam is entirely resisted by the elastic portion of the cross-section only. Even though the shear force is very small, the curvature will be infinite, the deflection will be very large and material fracture and structural collapse will occur for a real structure if this pure plastic state is adopted as the second optimisation criterion. Therefore, an adequately large elastic core should remain and the thickness t_c can not decrease without any limit.

In this model, the elastic core is located within the web on the cross section at the right fixed support, and the shear load P_y is resisted by the elastic inner core only. The shear stress distribution on the elastic core can be given by Eq. (6.9) as

$$\tau(z) = \frac{3P_y}{4t_w z_y}\left(1 - \frac{z^2}{z_y^2}\right) \tag{6.30}$$

where z represents the distance of the point considered from the neutral surface, and the yield strain distance is the maximum value of z. The maximum value of the shear stress occurs when $z = 0$ and is given by

$$\tau_{\max} = \tau(0) = \frac{3P_y}{4t_w z_y} \tag{6.31}$$

It can be seen from the above two equations that the distribution and the maximum value of the shear stress over the elastic inner core is the same as in an elastic rectangular beam of width t_w and depth $2z_y$.

With the thickness t_c decreasing, the yield strain distance z_y will reduce. When the yield strain distance z_y reaches its minimum value, the maximum shear stress will reach the yield strength. This minimum yield strain distance cannot be exceeded, otherwise, the shear force cannot be resisted. The yield shear strength is $\tau_y = \frac{\sigma_y}{\sqrt{3}}$ in this situation (Chakrabarty 1986). Therefore, the minimum yield strain distance can be given by

$$z_{y\min} = \frac{3P_y}{4t_w\tau_y} = \frac{3\sqrt{3}P_y}{4t_w\sigma_y} \tag{6.32}$$

The second optimisation criterion in the elasto-plastic stage is that under any combined bending moment, shear force and axial tension, the yield distance must not be smaller than the minimum yield distance. Like Eq. (6.2) for elastic stage, this constraint condition can be written simply as

$$z_y \geq z_{y\min} \tag{6.33}$$

According to horizontal force equilibrium, the following expression can be written.

$$\sigma_y t_w \left(y_{tens} - y_{comp}\right) = P_x \tag{6.34a}$$

where y_{tens} is the distance from the neutral axis to the web-flange junction fibre on tension, and y_{comp} is the distance from the neutral axis to the web-flange junction fibre on compression. The sum of these two distances is equal to the depth of the web.

$$y_{tens} + y_{comp} = h - 2t_f \tag{6.34b}$$

From Eq. (6.34), the following expressions about the neutral axis location can be given.

$$y_{tens} = \frac{h}{2} - t_f + \frac{P_x}{2\sigma_y t_w} \tag{6.35a}$$

$$y_{comp} = \frac{h}{2} - t_f - \frac{P_x}{2\sigma_y t_w} \tag{6.35b}$$

The plastic moment of the flange portions is

$$M_p^f(t_c) = \sigma_y b(t_f + t_c)(h + t_c - t_f) \tag{6.36a}$$

The elasto-plastic moment of the web portion about the centroidal axis is

$$\begin{aligned} M_{ep}^w(z_y) &= t_w \int_{-y_{comp}}^{-z_y} z(-\sigma_y)dz + t_w \int_{-z_y}^{z_y} z\left(\frac{\sigma_y}{z_y}z\right)dz + t_w \int_{-z_y}^{y_{tens}} z\sigma_y dz - \frac{1}{2}\sigma_y t_w (y_{tens} - y_{comp})^2 \\ &= \sigma_y t_w \left[\frac{1}{2}(y_{tens}^2 + y_{comp}^2) - \frac{1}{3}z_y^2\right] - \frac{1}{2}\sigma_y t_w (y_{tens} - y_{comp})^2 = \sigma_y t_w \left(y_{tens} y_{comp} - \frac{1}{3}z_y^2\right) \\ &= \sigma_y t_w \left[\left(\frac{h}{2} - t_f\right)^2 - \left(\frac{P_x}{2\sigma_y t_w}\right)^2 - \frac{1}{3}z_y^2\right] \end{aligned} \tag{6.36b}$$

When $z_y = z_{y\min}$, $M_{ep}^w(z_y)$ will reach its maximum value. By substituting Eq. (6.32) into Eq. (6.36b), then

$$\begin{aligned} M_{ep\max}^w &= \sigma_y t_w \left[\left(\frac{h}{2} - t_f\right)^2 - \left(\frac{P_x}{2\sigma_y t_w}\right)^2 - \frac{1}{3}z_{y\min}^2\right] \\ &= \sigma_y t_w \left[\left(\frac{h}{2} - t_f\right)^2 - \frac{13}{16}\left(\frac{P_x}{\sigma_y t_w}\right)^2\right] \end{aligned} \tag{6.37}$$

Therefore, the maximum total elasto-plastic resisting moment with respect to the centroidal axis can be given as

$$M_{ep\max}(t_c) = M_p^f(t_c) + M_{ep\max}^w$$
$$= \sigma_y b(t_f + t_c)(h + t_c - t_f) + \sigma_y t_w \left[\left(\frac{h}{2} - t_f \right)^2 - \frac{13}{16} \left(\frac{P_x}{\sigma_y t_w} \right)^2 \right] \quad (6.38)$$

It can be demonstrated by the above equation that the reduction in bending moment $M_{ep\max}(t_c)$ is proportional to the square of the axial tension P_x. Enlarging the tension can reduce the elasto-plastic bending resisting capacity.

When the structure is within the elastic stage, the first order derivative methods such as the sensitivity analysis can be used. Because the elastic inner core is now reduced to such extent as a result of the reduction of the strengthening plate thickness, however, the sensitivity method may not work very well. On the other hand, an exact solution can be given for this optimisation problem of the nonlinear continuum structure. Considering the moment equilibrium condition $M_{ep\max}(t_c) = P_y L$ and Eq. (6.38), the expression of the optimal thickness t_c can be given explicitly as

$$t_c = -\frac{h}{2} + \sqrt{\left(\frac{h}{2} - t_f \right)^2 \left(1 - \frac{t_w}{b} \right) + \frac{13P_x^2}{16\sigma_y^2 b t_w} + \frac{P_y L}{\sigma_y b}} = -\frac{0.4}{2} +$$
$$\sqrt{\left(\frac{0.4}{2} - 0.02 \right)^2 \left(1 - \frac{0.014}{0.2} \right) + \frac{13 \times \left(3.526 \times 10^5 \right)^2}{16 \left(235.0 \times 10^6 \right)^2 0.2 \times 0.014} + \frac{3.526 \times 10^5 \times 1.5}{235.0 \times 10^6 \times 0.2}} \quad (6.39)$$
$$= 0.005033m$$

The maximum strain, occurring on the uppermost tensile fibre of the strengthened cross section, is

$$\varepsilon(y_{tens}, t_c) = \frac{\varepsilon_y}{z_{y\min}} \left(y_{tens} + t_f + t_c \right) \quad (6.40)$$

where ε_y is the yield strain given by

$$\varepsilon_y = \frac{\sigma_y}{E} \tag{6.41}$$

The minimum yield distance is given by Eq. (6.32) as

$$z_{y\min} = \frac{3\sqrt{3}P_y}{4t_w\sigma_y} = \frac{3\sqrt{3}\times 3.526\times 10^5}{4\times 0.014\times 235.0\times 10^6} = 0.1392m$$

The distance from the neutral axis to the web-flange junction fibre on tension is given by Eq. (6.35a) as

$$y_{tens} = \frac{h}{2} - t_f + \frac{P_x}{2\sigma_y t_w} = \frac{0.4}{2} - 0.02 + \frac{3.526\times 10^5}{2\times 2.35\times 10^8\times 0.014} = 0.2336m$$

The yield strain is given by Eq. (6.41) as

$$\varepsilon_y = \frac{\sigma_y}{E} = \frac{2.35\times 10^8}{2\times 10^{11}} = 0.001175$$

Therefore, the maximum strain is given by Eq. (6.40) as

$$\varepsilon(y_{tens}, t_c) = \frac{\varepsilon_y}{z_{y\min}}\left(y_{tens} + t_f + t_c\right) = \frac{0.001175}{0.1392}\left(0.2336 + 0.02 + 0.005033\right) = 0.002108$$

This maximum strain on the cross section at the right fixed support is also the maximum strain of the whole strengthened structure. Although it is larger than the yield strain, the maximum strain is still smaller than the failure strain of steel, and therefore the retrofitted structure is safe.

For the left normal segment, if the strengthening plate length l_c decreases without limit, the stress will continue to develop on the junction section between the left normal and right strengthened segments until the entire junction section is stressed up to σ_y and the elastic inner core fades

away completely. To avoid this situation, an adequately large elastic inner core should remain and the length l_c can not decrease without limit. For the junction cross section between the two segments, the second optimisation criterion in elasto-plastic stage, based on the minimum yield strain distance of $z_{y\min} = 0.1392m$, is the same as that for the right strengthened cross section.

The plastic moment of the flange portions is

$$M_p^f = \sigma_y b t_f \left(h - t_f\right) \tag{6.42}$$

The elasto-plastic moment of the web portion and its maximum value are the same as those of the strengthened cross section, and they are given by Eqs. (6.36b) and (6.37). Therefore, the maximum total elasto-plastic resisting moment can be given as

$$\begin{aligned} M_{ep\max} &= M_p^f + M_{ep\max}^w \\ &= \sigma_y b t_f \left(h - t_f\right) + \sigma_y t_w \left(\frac{h}{2} - t_f\right)^2 - \frac{13P_x^2}{16\sigma_y t_w} \\ &= 235.0\times10^8 \times 0.2 \times 0.02(0.4 - 0.02) \\ &+ 235.0\times10^8 \times 0.014\left(\frac{0.4}{2} - 0.02\right)^2 - \frac{13\left(3.526\times10^5\right)^2}{16\times235.0\times10^8\times0.014} \\ &= 4.331\times10^5\, Nm \end{aligned} \tag{6.43}$$

Considering the equilibrium condition about the moments $M_{ep\max} = P_y(L - l_c)$, the optimal length l_c can be given as

$$\begin{aligned} l_c &= L - \frac{M_{ep\max}}{P_y} = 1.5 - \frac{4.331\times10^5}{3.526\times10^5} \\ &= 0.2717m \end{aligned} \tag{6.44}$$

The weight of the flange cover plates for the second optimisation criterion is

$$W = 2\rho b l_c t_c = 2 \times 7850 \times 0.2 \times 0.2717 \times 0.005033 = 4.294kg \qquad (6.45)$$

The weight of original beam given by Eq. (6.28) is $W_o = 153.5kg$. The ratio between these two weights is

$$4.294/153.5 = 2.797\%$$

For the first optimisation criterion, the weight of the strengthening plates given by Eq. (6.27) is $15.92kg$. The weight ratio between these two optimisation criteria is

$$4.294/15.92 = 26.97\%$$

As compared to the first criterion, the second criterion can result in significant saving in material.

If the original structure is not retrofitted by the Flange Plate Scheme and these two horizontal and vertical forces increase proportionally to the magnitude of $P_x = P_y = P$, the maximum elasto-plastic moment at the right fixed support is given by

$$\begin{aligned} M_{ep\max} &= M_p^f + M_{ep\max}^w \\ &= \sigma_y b t_f \left(h - t_f\right) + \sigma_y t_w \left(\frac{h}{2} - t_f\right)^2 - \frac{13P^2}{16\sigma_y t_w} \\ &= PL \end{aligned} \qquad (6.46)$$

By solving the above equation, the expression of P can be given explicitly as

$$
\begin{aligned}
P &= \frac{8}{13}\sigma_y t_w\left[-L+\sqrt{L^2+\frac{13}{4}\left[\frac{b}{t_w}t_f(h-t_f)+\left(\frac{h}{2}-t_f\right)^2\right]}\right] \\
&= \frac{8}{13}2.35\times10^6\times0.014 \\
&\left[-1.5+\sqrt{1.5^2+\frac{13}{4}\left[\frac{0.2}{0.014}0.02(0.4)+\left(\frac{0.4}{2}-0.02\right)^2\right]}\right] \\
&= 2.949\times10^5\,N
\end{aligned}
\tag{6.47}
$$

If the magnitude of these two forces increases to this value of P, the original structure will reach its elasto-plastic limit resisting capacity. The increase of resisting capacity due to retrofitting is

$$(3.526\times10^5-2.949\times10^5)/2.949\times10^5=19.57\%$$

Through the increase of retrofitting material by 2.794%, the elasto-plastic limit resisting capacity increases by 19.57% for the second optimisation criterion.

By substituting this value of P into Eq. (6.32), the new maximum yield strain distance is given as

$$z_{y\min}=\frac{3\sqrt{3}P}{4\sigma_y t_w}=\frac{3\sqrt{3}\times2.949\times10^5}{4\times2.35\times10^8\times0.014}=0.1164m$$

As compared to the old value of $0.1392m$, this new yield strain distance is reduced due to the load decrease.

6.1.2 *Optimisation of the Beam Retrofitted by the Vertical Plate Scheme*

In addition to the Flange Plate Scheme, the beam can also be retrofitted by the Vertical Plate Scheme. When the beam segments are retrofitted by vertical plates, the optimisation process is similar to the above mentioned process of the Flange Plate Scheme. As illustrated in Fig. 6.5, the cross-

section retrofitted by the Vertical Plate Scheme may experience two different stages sequentially as the thickness of vertical plates reduces gradually.

Different from the weight expression about the flange plates given by Eq. (6.1), the total weight of the strengthening vertical plates is

$$W \propto \rho(h-2t_f)l_v t_v \tag{6.48}$$

where ρ is the density of steel, h is the depth of the original beam, t_f is the thickness of the original beam flanges, t_v and l_v are the thickness and the length of the retrofitting vertical plates.

The density ρ of steel, the depth h of beam and the thickness t_f of the original beam flanges are constants. Design variables considered in the optimisation are the thickness t_v and the length l_v of the retrofitting plates. To reduce cost, the total weight should be as small as possible.

For the beam segment strengthened by vertical plates, if the thickness of the vertical plates is large enough, the cross section is in the elastic state. In this state, the stress should not be more than the corresponding maximum allowable value when reducing the thickness t_v and the length l_v. In the form of sensitivity analysis, the stress constant condition can be expressed as

$$-\sigma_{\max} \le \sigma(t_v,l_v) = \sigma(t_{v0},l_{v0}) + \frac{\partial\sigma(t_{v0},l_{v0})}{\partial t_v}(t_v - t_{v0}) + \frac{\partial\sigma(t_{v0},l_{v0})}{\partial l_v}(l_v - l_{v0}) \le \sigma_{\max} \tag{6.49}$$

As mentioned in Model 6.1, the original beam does not satisfy the strength requirement after doubling the loads. This original beam can also

be retrofitted by vertical plates. In Model 6.2, the beam retrofitted by the vertical plates will be optimised and its exact solutions will be given.

Model 6.2. All other conditions are the same as those in Model 6.1, except for the adopted retrofitting scheme which is different. As shown in Fig. 6.6, the Vertical Plate Scheme is used to strengthen the beam segments, where the internal forces are very large and the yield strain is exceeded. For the model shown in Fig. 6.6, the structure consists of two segments: the right strengthened end segment and the left normal segment.

In the left normal segment, as mentioned in Model 6.1, the maximum stress and strain associate only with the length of the strengthening plates and does not relate to the thickness of the plates. The solution procedure of optimisation, and the obtained results according to the first and the second optimisation criteria for the structure retrofitted by the vertical plates are the same as those retrofitted by the flange cover plates. Therefore, they are not repeated here. Only the procedure and results associated with the right retrofitted segment are given.

The variation of the thickness of vertical plates can cause change of the stress distribution across the strengthened section. When the thickness is still large, as shown in Fig. 6.5a, the whole cross section is in the elastic state. Similar to the case of the structure strengthened by the flange cover plates, an adequately large initial thickness can be adopted first. Then this thickness can be reduced. With the gradual decrease of the thickness of vertical plates, the cross-section at the extreme right end experiences elastic stage, and elasto-plastic stage sequentially, as shown in Fig. 6.5.

The normal stress distribution due to the axial tensile and lateral loads can be given by

$$\sigma(t_v, x, y) = \frac{P_x}{A(t_v)} + \frac{P_y}{I(t_v)} xy \quad \left(L - l_v \le x \le L, -\frac{h}{2} \le y \le \frac{h}{2} \right) \tag{6.50}$$

where x is measured from the left free end where P_x and P_y are applied, y is measured from the centroidal axis of the strengthened cross section. The area of the cross section, and the moment of inertia of the section with respect to the centroidal axis are given by

$$A(t_v) = 2bt_f + (t_w + 2t_v)(h - 2t_f) \tag{6.51a}$$

$$I(t_v) = \frac{1}{12}\left[bh^3 - (b - t_w - 2t_v)(h - 2t_f)^3 \right] \tag{6.51b}$$

When $x = L$ and $y = \frac{h}{2}$, the normal stress reaches its maximum value and is given by

$$\sigma\left(t_v, L, \frac{h}{2} \right) = \frac{P_x}{A(t_v)} + \frac{P_y L h}{2I(t_v)} \tag{6.52a}$$

Its partial derivative of with respect to the vertical plate thickness t_v is given by

$$\begin{aligned} \frac{\partial}{\partial t_v} \sigma\left(t_v, L, \frac{h}{2} \right) &= \frac{\partial}{\partial t_v} \left[\frac{P_x}{A(t_v)} + \frac{P_y L h}{2I(t_v)} \right] \\ &= -\frac{2P_x(h - 2t_f)}{[A(t_v)]^2} - \frac{P_y L h (h - 2t_f)^3}{12[I(t_v)]^2} \end{aligned} \tag{6.52b}$$

The initial thickness of the vertical plates is assumed to be $t_{v0} = 0.02m$. Let $t_v = t_{v0} = 0.02m$, then the area and the moment of inertia of the cross section are given by Eq. (6.51) as

$$\begin{aligned} A(t_v) &= 2bt_f + (t_w + 2t_c)(h - 2t_f) \\ &= 2 \times 0.2 \times 0.02 + (0.014 + 2 \times 0.02)(0.4 - 2 \times 0.02) \\ &= 0.02744m^2 \end{aligned}$$

$$\begin{aligned} I(t_v) &= \frac{1}{12}\left[bh^3 - (b - t_w - 2t_v)(h - 2t_f)^3\right] \\ &= \frac{1}{12}\left[0.2 \times 0.4^3 - (0.2 - 0.014 - 2 \times 0.02)(0.4 - 2 \times 0.02)^3\right] \\ &= 4.990 \times 10^{-4} m^4 \end{aligned}$$

The maximum normal stress of the whole strengthened segment and its t_v-derivative are given by Eq. (6.52) as

$$\begin{aligned} \sigma\left(t_v, L, \frac{h}{2}\right) &= \frac{P_x}{A(t_v)} + \frac{P_y L h}{2I(t_v)} \\ &= \frac{3.526 \times 10^5}{0.02744} + \frac{3.526 \times 10^5 \times 1.5}{4.990 \times 10^{-4}}\left(\frac{0.4}{2}\right) \\ &= 2.248 \times 10^8 Pa \end{aligned}$$

$$\begin{aligned} \frac{\partial}{\partial t_v}\sigma\left(t_v, L, \frac{h}{2}\right) &= -\frac{2P_x(h - 2t_f)}{[A(t_v)]^2} - \frac{P_y L h(h - 2t_f)^3}{12[I(t_v)]^2} \\ &= -\frac{2 \times 3.526 \times 10^5 (0.4 - 2 \times 0.02)}{0.02744^2} - \frac{3.526 \times 10^5 \times 1.5 \times 0.4(0.4 - 2 \times 0.02)^3}{12 \times \left(4.990 \times 10^{-4}\right)^2} \\ &= -2.580 \times 10^9 Pa/m \end{aligned}$$

Because this maximum stress is lower than the yield stress, the structure is safe for the thickness of 0.02m. This thickness can be reduced to decrease the weight of strengthening plates. With this reduction of vertical plate thickness the stress will increase. When the thickness is small enough, the outermost fibre of the upper tensile flange reaches its yield stress, i.e., the elastic limit state and the first optimisation criterion.

In the right strong segment, the stress depends only on the thickness of the vertical plates and not on their length. The stress $\sigma(t_v, l_v)$ in Eq. (6.49) becomes a function of t_v only. As a result, Eq. (6.49) can be rewritten as

$$\sigma(t_v) = \sigma(t_{v0}) + \frac{d\sigma(t_{v0})}{dt_v}(t_v - t_{v0}) \le \sigma_{\max} = \sigma_y \tag{6.53}$$

By assuming equality in the above expression, the thickness of the vertical plates is given as

$$t_v = \frac{\sigma_y - \sigma(t_{v0})}{\frac{d\sigma(t_{v0})}{dt_v}} + t_{v0} = \frac{2.350\times10^8 - 2.248\times10^8}{-2.580\times10^9} + 0.02 = 0.01606m$$

Assuming $t_{v0} = t_v = 0.01606m$ and repeating the above process, the following results are obtained.

$$A(t_{v0}) = 0.02460m^2,\ I(t_{v0}) = 4.864\times10^{-4}m^4,\ \sigma(t_{v0}) = 2.402\times10^8 Pa,$$

$$\frac{d\sigma(t_{v0})}{dt_v} = -3.040\times10^9 Pa/m,\ t_v = 0.01776m$$

The process continues until t_v converges to a value. The calculation processes and results are given in Table 6.2. It can be seen that the outermost fibre of the upper tensile flange will reach the yield strength when $t_v = 0.01733m$.

Similar to the case of the Flange Plate Scheme, the contribution of the shear stress should be considered as well. The maximum shear stress occurs at the centroidal axis and is given by

$$\tau(t_v,L,0)=\frac{P_x}{(t_w+2t_v)I(t_v)}\left[bt_f\frac{1}{2}(h-t_f)+(t_w+2t_v)\left(\frac{h}{2}-t_f\right)^2\right]$$
$$=\frac{3.526\times10^5}{(0.014+2\times0.01733)\times4.782\times10^{-4}}\left[0.2\times0.02\frac{1}{2}(0.4-0.02)+(0.014+2\times0.01733)\left(\frac{0.4}{2}-0.02\right)^2\right] \quad (6.54a)$$
$$=1.495\times10^7\,Pa$$

Table 6.2.

Results for the Vertical Plate Scheme in elastic stage by sensitivity analysis for Model 6.2

	$A(t_{v0})$ (m²)	$I(t_{v0})$ (m⁴)	$\sigma(t_{v0})$ (MPa)	$\frac{d\sigma(t_{v0})}{dt_c}$ (MPa/m)	t_v (m)
1	0.02744	0.0004990	224.8	-2580	0.01606
2	0.02460	0.0004864	240.2	-3040	0.01776
3	0.02583	0.0004816	233.3	-2828	0.01716
4	0.02539	0.0004769	235.7	-2901	0.01739
5	0.02347	0.0004788	234.7	-2872	0.01730
6	0.02550	0.0004781	235.1	-2883	0.01734
7	0.02552	0.0004783	235.0	-2879	0.01733
8	0.02552	0.0004782	235.0	-2880	0.01733

At the same point, the normal stress, contributed by the tension P_x only, is given by

$$\sigma(t_v,L,0)=\frac{P_x}{A(t_v)}=\frac{3.526\times10^5}{0.02552}=1.382\times10^7\,Pa \quad (6.54b)$$

The Mises stress is

$$\sigma^{Mises}(t_v,L,0)=\sqrt{[\sigma(t_v,L,0)]^2+3[\tau(t_v,L,0)]^2}$$
$$=\sqrt{(1.382\times10^7)^2+3\times(1.495\times10^7)^2} \quad (6.55)$$
$$=2.935\times10^7\,Pa$$

The yield strength is $\sigma_y = 2.350\times10^8\,Pa$, so this Mises stress is much smaller than the yield strength.

In addition to the maximum normal stress on the top fibre and the Mises stress at the centroidal axis, the Mises stress at the junction surface between web, vertical plates and flange should also be checked. The normal and shear stresses at that junction surface are respectively

$$\begin{aligned}\sigma\left(t_v, L, \frac{h}{2}-t_f\right) &= \frac{P_x}{A(t_v)} + \frac{P_y L}{I(t_v)}\left(\frac{h}{2}-t_f\right)\\ &= \frac{3.526\times10^5}{0.02552} + \frac{3.526\times10^5\times1.5}{4.782\times10^{-4}}\left(\frac{0.4}{2}-0.02\right)\\ &= 2.129\times10^8\,Pa\end{aligned} \tag{6.56a}$$

$$\begin{aligned}\tau\left(t_v, L, \frac{h}{2}-t_f\right) &= \frac{P_x}{(t_w+2t_v)I(t_v)} S\left(\frac{h}{2}-t_f\right) = \frac{P_x}{(t_w+2t_v)I(t_v)}\frac{1}{2}bt_f\left(h-t_f\right)\\ &= \frac{3.526\times10^5}{(0.014+2\times0.01733)\times4.782\times10^{-4}}\frac{1}{2}0.2\times0.02(0.4-0.02)\\ &= 1.151\times10^7\,Pa\end{aligned} \tag{6.56b}$$

The Mises stresses at that junction point is

$$\begin{aligned}\sigma^{Mises}\left(t_v, L, \frac{h}{2}-t_f\right) &= \sqrt{\left[\sigma\left(t_v, L, \frac{h}{2}-t_f\right)\right]^2 + 3\left[\tau\left(t_v, L, \frac{h}{2}-t_f\right)\right]^2}\\ &= \sqrt{\left(2.129\times10^8\right)^2 + 3\times\left(1.151\times10^7\right)^2}\\ &= 2.138\times10^8\,Pa\end{aligned} \tag{6.57}$$

Because this Mises stress is smaller than the yield strength $\sigma_y = 2.350\times10^8\,Pa$, the junction point is safe. To examine whether the Mises stress is larger elsewhere within the web and the vertical plates, the derivative of the Mises stress is used to search for the maximum value, but it is found that no such location exists. This Mises stress at the junction point is also the largest in the whole web.

Among these three possible points, the normal stress at the top fibre of the cross section is the maximum stress. Because this maximum stress of the whole section just reaches the yield strength and the corresponding maximum strain is not larger than the yield strain, the requirement on strength is satisfied for this thickness. The thickness of 0.01733m is the optimal solution for the first optimisation criterion.

Similar to that of the flange cover plates in Model 6.1, the optimal length of vertical plates is 0.4870m. The weight of the vertical plates for the first optimisation criterion is

$$W = 2\rho(h - 2t_f)l_v t_v = 2 \times 7850 \times (0.4 - 2 \times 0.02) \times 0.4870 \times 0.01733 = 47.70kg \quad (6.58)$$

The weight of the original beam is given by Eq. (6.28) as $W_o = 153.5kg$. The ratio between them is

$$47.70/153.5 = 31.07\%$$

Similar to Model 6.1, the increase of the resisting capacity for the elastic limit state is 42.47%. It can be seen that through an increase of retrofitting material by 31.07%, the limit resisting moment increases by 42.47% for the first optimisation criterion.

For the right strengthened segment, after the elastic limit state is reached, any further decrease in the thickness of the vertical plates will cause the outermost fibre to change as earlier but at the same time maintain the yield stress, and the adjacent fibres undergo an increase in strain with corresponding increase in stress up to a maximum of σ_y. The yield strain distance z_y will reduce with the thickness of the vertical plates.

However, an adequately large elastic inner core should remain and the thickness t_v can not decrease without limit.

In this model, the elastic core is located within the beam web and the vertical plates on the cross section at the right fixed support. The shear load P_y is resisted by the elastic core only. The shear stress distribution on the elastic inner core can be given by

$$\tau(z)=\frac{3P_y}{4(t_w+2t_v)z_y}\left(1-\frac{z^2}{z_y^2}\right) \tag{6.59}$$

The maximum value of the shear stress occurs when $z=0$ and is

$$\tau_{\max}=\tau(0)=\frac{3P_y}{4(t_w+2t_v)z_y} \tag{6.60}$$

As the thickness t_v decreases, the yield strain distance z_y will reduce. When the yield strain distance z_y reaches its minimum value, the maximum shear stress and strain will reach their corresponding yield values. This minimum yield distance cannot be reduced further. The yield shear strength is $\tau_y=\frac{\sigma_y}{\sqrt{3}}$ in this situation. Considering Eq. (6.60), the minimum yield strain distance can be given as

$$z_{y\min}=\frac{3P_y}{4(t_w+2t_v)\tau_y}=\frac{3\sqrt{3}P_y}{4(t_w+2t_v)\sigma_y} \tag{6.61}$$

The second optimisation criterion in elasto-plastic stage is based on the constraint condition on this minimum yield strain distance. The same as Eq. (6.33), $z_y \geq z_{y\min}$, under any combined action of bending moment, shear

force and axial tension, the yield strain distance z_y must not exceed the limit of the minimum yield strain distance $z_{y\min}$.

According to the force equilibrium condition in horizontal direction, the following expression can be given.

$$\sigma_y\left(t_w + 2t_v\right)\left(y_{tens} - y_{comp}\right) = P_x \tag{6.62a}$$

where y_{tens} and y_{comp} are the distances from the neutral axis to the flange inner surface fibres on tension and on compression, respectively. The sum of these two distances is the depth of the web and the vertical plates.

$$y_{tens} + y_{comp} = h - 2t_f \tag{6.62b}$$

From Eq. (6.62), the following expressions about the neutral axis location can be given by

$$y_{tens} = \frac{h}{2} - t_f + \frac{P_x}{2\sigma_y\left(t_w + 2t_v\right)} \tag{6.63a}$$

$$y_{comp} = \frac{h}{2} - t_f - \frac{P_x}{2\sigma_y\left(t_w + 2t_v\right)} \tag{6.63b}$$

The plastic moment of the flange portions is

$$M_p^f = \sigma_y b t_f\left(h - t_f\right) \tag{6.64a}$$

The elasto-plastic moment of the web and vertical plate portions is

$$
\begin{aligned}
&M_{ep}^{w}\left(t_v, y_y\right)=\left(t_w+2t_v\right) \\
&\left[\int_{-y_{comp}}^{-z_y} z\left(-\sigma_y\right)dz+\int_{-z_y}^{z_y} z\left(\frac{\sigma_y}{y_y}z\right)dz+\int_{-z_y}^{y_{tens}} z\sigma_y dz-\frac{1}{2}\sigma_y\left(y_{tens}-y_{comp}\right)^2\right] \\
&=\sigma_y\left(t_w+2t_v\right)\left(y_{tens}y_{comp}-\frac{1}{3}z_y^2\right) \\
&=\sigma_y\left(t_w+2t_v\right)\left[\left(\frac{h}{2}-t_f\right)^2-\left(\frac{P_x}{2\sigma_y\left(t_w+2t_v\right)}\right)^2-\frac{1}{3}z_y^2\right]
\end{aligned}
\tag{6.64b}
$$

When $z_y=z_{y\min}$, $M_{ep}^{w}\left(t_v, y_y\right)$ reaches its maximum value. By substituting Eq. (6.61) into Eq. (6.64b), then

$$
\begin{aligned}
M_{ep\max}^{w}\left(t_v\right)&=\sigma_y\left(t_w+2t_v\right)\left[\left(\frac{h}{2}-t_f\right)^2-\left(\frac{P_x}{2\sigma_y\left(t_w+2t_v\right)}\right)^2-\frac{1}{3}z_{y\min}^2\right] \\
&=\sigma_y\left(t_w+2t_v\right)\left[\left(\frac{h}{2}-t_f\right)^2-\frac{13}{16}\left(\frac{P_x}{\sigma_y\left(t_w+2t_v\right)}\right)^2\right]
\end{aligned}
\tag{6.65}
$$

Thereby, the maximum total elasto-plastic resisting moment can be given as

$$
\begin{aligned}
&M_{ep\max}\left(t_v\right)=M_p^f+M_{ep\max}^{w}\left(t_v\right) \\
&=\sigma_y bt_f\left(h-t_f\right)+\sigma_y\left(t_w+2t_v\right)\left[\left(\frac{h}{2}-t_f\right)^2-\frac{13}{16}\left(\frac{P_x}{\sigma_y\left(t_w+2t_v\right)}\right)^2\right] \\
&=P_y L
\end{aligned}
\tag{6.66}
$$

The expression of the optimal thickness t_v can be given explicitly as

$$t_v = -\frac{t_w}{2} + \frac{-\left[\sigma_y b t_f \left(h - t_f\right) - P_y L\right] + \sqrt{\left[\sigma_y b t_f \left(h - t_f\right) - P_y L\right]^2 + 4\left(\frac{h}{2} - t_f\right)^2 \frac{13P_x^2}{16}}}{2\sigma_y \left(\frac{h}{2} - t_f\right)^2}$$

$$= -0.5 \times 0.014 + \frac{1}{2 \times 235.0 \times 10^6 \left(0.5 \times 0.4 - 0.02\right)^2} \tag{6.67}$$

$$\left\{ -\left[235.0 \times 10^6 \times 0.2 \times 0.02 \times \left(0.4 - 0.02\right) - 3.526 \times 10^5 \times 1.5\right] \right.$$

$$+ \left\{ \left[235.0 \times 10^6 \times 0.2 \times 0.02 \times \left(0.4 - 0.02\right) - 3.526 \times 10^5 \times 1.5\right]^2 \right.$$

$$\left. \left. + 4\left(0.5 \times 0.4 - 0.02\right)^2 0.8125 \left(3.526 \times 10^5\right)^2 \right\}^{\frac{1}{2}} \right\}$$

$$= 0.005412m$$

The maximum strain, occurring on the outermost tensile fibre of the extremely right strengthened cross section, is

$$\varepsilon\left(y_{tens}, t_v\right) = \frac{\varepsilon_y}{z_{y\min}} \left(y_{tens} + t_f\right) \tag{6.68}$$

where ε_y is the yield strain given by Eq. (6.41).

The minimum yield strain distance is given by Eq. (6.61) as

$$z_{y\min} = \frac{3\sqrt{3}P_y}{4\left(t_w + 2t_v\right)\sigma_y} = \frac{3\sqrt{3} \times 3.526 \times 10^5}{4\left(0.014 + 2 \times 0.005412\right) \times 235.0 \times 10^6} = 0.07852m$$

This minimum yield strain distance is much less than the corresponding value $0.1392m$ of the Flange Plate Scheme. The distance from the neutral axis to the web-flange junction surface on tension is given by Eq. (6.63a) as

$$y_{tens} = \frac{h}{2} - t_f + \frac{P_x}{2\sigma_y \left(t_w + 2t_v\right)} = \frac{0.4}{2} - 0.02 + \frac{3.526 \times 10^5}{2 \times 2.35 \times 10^8 \left(0.014 + 2 \times 0.005412\right)}$$

$$= 0.2102m$$

The yield strain is given by Eq. (6.41) as $\varepsilon_y = 0.001175$. Therefore, the maximum strain is given by Eq. (6.68) as

$$\varepsilon(y_{tens}, t_v) = \frac{\varepsilon_y}{z_{y\,\min}}(y_{tens} + t_f) = \frac{0.001175}{0.07852}(0.2102 + 0.02) = 0.003445$$

This maximum strain on the cross section at the right fixed support is also the maximum strain of the whole strengthened structure. It is more than the corresponding value 0.002108 of the Flange Plate Scheme, but this retrofitted structure is still safe. Because the deformation is still very small, geometrical nonlinearity is not involved.

As mentioned before, the optimal length of vertical plates is the same as that of flange cover plates in Model 6.1. The length of 0.2717m is the optimal solution. The weight of the vertical plates for the second optimisation criterion is

$$W = 2\rho(h - 2t_f)l_v t_v = 2 \times 7850 \times (0.4 - 2 \times 0.02) \times 0.2717 \times 0.005412 = 8.311kg \quad (6.69)$$

The weight of the original beam is given by Eq. (6.28) as $W_o = 153.5kg$. The ratio between them is

$$8.311/153.5 = 5.414\%$$

For the first optimisation criterion, the weight of the strengthening plates given by Eq. (6.58) is $47.70kg$. The weight ratio between these two optimisation criteria is

$$8.311/47.70 = 17.42\%$$

As compared to the first criterion, the second criterion can result to significant savings in material.

Similar to Model 6.1, the increase of the elasto-plastic limit resisting capacity due to retrofitting is 19.57%. It can be seen that by increasing

retrofitting material by 5.414%, the limit resisting moment increases by 19.57% for the second optimisation criterion.

6.1.3 *Discussion and summary*

For the first- and the second- optimisation criteria, the weight ratios of the Flange Plate Scheme to the Vertical Plate Scheme are, respectively

$$\frac{15.92kg}{47.70kg} = 33.38\%\,,\ \frac{4.294kg}{8.311kg} = 51.67\%$$

For the same optimisation criterion, the weight of the flange cover plates is much less than that of the vertical plates. It is because their different location. The flange cover plates are located on the outer sides of the beam flanges, where the stress and strain reach roughly their corresponding maximum values, so the area is utilised fully. Whereas, the vertical plates are located between the two beam flanges, the stress and strain are very small in most of the cross section, and the area is utilised inadequately. Therefore, strengthening beam flanges is more effective than strengthening the web.

In the above two models, the magnitude of the axial tensile load P_x is the same as that of the lateral load P_y, the elastic core is located entirely within the beam web, the upper and the lower portions of the cross section are in the plastic state. However, if the axial tensile load P_x becomes much larger than the lateral load P_y, only the upper portion of the cross section will be in the plastic state and the lower portion will be in the elastic state. For such a case, a closed form solution of optimal analysis may also be given in a way similar to the above.

Although the steel yields, the displacements and strains of the structures are still very small, the assumption of small deformation remains to be valid, geometric nonlinearity is not involved, and only material is nonlinear in this section. In the next section, because both material and geometric nonlinearities are involved due to the catenary action following column removal, a closed form solution will be impossible and finite element analysis will be needed.

Finding the optimal strengthening plate thickness is a sizing problem, but finding the optimal strengthening plate length is a shape optimisation problem. The latter problem is more complicated than the former one (Bendsoe 1995). In this section, the sizes of the retrofitting plates are treated as continuum design variables, the sensitivity analysis method is used in the elastic stage, and exact optimal results are given. On the contrary, in the next section, the thickness and length of strengthening plates will be regarded as discrete design variables. For the finite element analyses, the explicit expression of the gradient of stress can not be given as easily as in this section. Therefore, the sensitivity method will not be used in the next section.

6.2 Minimising weight of strengthening plates through finite element parametric study

In this section, the finite element analysis software ABAQUS is utilised to simulate the structural behaviours after the column removal. Because even the newest the ABAQUS version 2016 cannot optimise nonlinear structures

now, only the parametric study is carried out to minimise weight of the strengthening plates of the structures retrofitted by the two proposed schemes. Once the functions of ABAQUS develop and can optimise the nonlinear structural steelworks or other methods are available in the future, this parametric study can be developed to the structural optimisation of the proposed retrofitting schemes.

Table 6.3.

Stress and strain values in Model 6.3

Point	1	2	3	4
Stress(MPa)	235.0	236.0	360.0	490.8
Strain	0.001175	0.01446	0.03653	0.4

Different from the cases of retrofitted beams subjected to axial tensile and lateral loads, for which exact results of optimisation are given in the previous section, in this section the structure modelled is subjected to the sudden removal of a column. Therefore catenary tension is involved in the beams connected to the failed column. If the same elastic-perfectly plastic relationship used in the previous section is adopted in this section, the strain will concentrate in very short beam segments, and the strain level in the majority of the structure will be very low. In order to prevent the structural collapse by developing adequately the catenary action in the beams, the stress and strain relationship used in this section will be a more appropriate one of strain-hardening instead of the simplistic elastic-perfectly plastic. The stress and strain curve adopted in Model 6.3 is the Mises stress and equivalent plastic strain relationship given by Table 6.3, which is adopted from Faella et al. (2000).

At the strengthened connection parts, the situation is different from that of the normal beam segments. The steel members are connected by welding. Nevertheless, welding is a complex metallurgical process, which may cause many negative effects on the connection. For example, the welding process may embrittle the steel material located in the heat-affected zone if the base metal is not properly preheated and cooling is too rapid in high-strength steel. Located between the weld fusion zone and the base metal, the heat-affected zone consists of steel whose grain structure has been modified by the high heat imparted during welding process (Bruneau et al. 1998). The stress state is also very complex in the connection parts. For these reasons and others not-mentioned herein, the allowable stress and strain levels at the connections should much lower than those in the beam segments.

In the previous section there were two optimisation criteria, and there will also be two criteria in this section. The first criterion used in the previous section is yield strength. From Table 6.3, it can be seen that the yield Mises stress is 235.0MPa. However, due to the removal of a column, the peak stress in a beam subjected to the combined action of both the very large axial catenary tension and the lateral loads will be much larger than the peak stress of the beam subjected to the ordinary lateral loads only. It is difficult, if not impossible, for the peak stress to remain below the elastic limit. At the same time, to retain certain reserve capacity, the allowable stress and strain levels cannot be too high for the first criterion. At the second point in Table 6.3, although the yield strain is exceeded, the stress level is still low, only 236.0MPa, and large reserve capacity still remains. Therefore, the

stress of 236.0MPa at the end point of the yield plateau is used as the first criterion, instead of the stress of 235.0MPa at the end point of the elastic stage.

The second criterion adopted herein has two requirements. The first one is that of "strong connection, weak beam". This means that the local maximum Mises stress and equivalent plastic strain at the strengthened connection parts must smaller than those in the un-strengthened normal beam segments. The second one is that the local maximum Mises stress at the strengthened connection cannot exceed the values of 360.0MPa, the third point of Table 6.3. The reason for doing so is that the tangential modulus of the stress and strain curve before the third point of Table 6.3 is much larger than that after this point. By so doing, the reserve capacity can be retained.

The procedure for minimising weight of strengthening plates according to the above mentioned two criteria is given in Fig. 6.7. In this figure, for the i_l th length and the i_t th thickness of strengthening steel plates, the function $f_w(i_l, i_t)$ is the plate weight. The expression $\sigma_c(i_l, i_t) \leq 236.0\text{MPa}$ means that the local maximum Mises stress $\sigma_c(i_l, i_t)$ at the connection parts is smaller than or equal to the assumed value 236.0MPa of the first criterion. $w_{l1\min}$ is the minimum weight of strengthening plates for the i_l th length and the first criterion. $w_{1\min}$ is the minimum plate weight of one beam-to-column connection for the first criterion.

The expression $\sigma_c(i_l, i_t) \leq \sigma_b(i_l, i_t)$ means that that the local maximum Mises stress $\sigma_c(i_l, i_t)$ of the connection parts is smaller than or equal to the

local maximum Mises stress $\sigma_b\ (i_l, i_t)$ of the normal beam segments for the i_l th length and the i_t th thickness of the plates, and it is the first requirement of the second criterion. The expression $\sigma_c\ (i_l, i_t) \leq 360.0\text{MPa}$ means that the local maximum Mises stress $\sigma_c\ (i_l, i_t)$ at the strengthened connection cannot exceed the value of 360.0MPa; and it is the second requirement of the second criterion. $w_{l2\min}$ is the minimum plate weight for the i_l th length and the second criterion. $w_{2\min}$ is the minimum weight of strengthening plates of one beam-to-column connection for the second criterion.

In the following model, the structures retrofitted by flange cover plates and vertical plates will be parametrically studied according to the above two criteria respectively. The influence of different thicknesses and lengths of the strengthening plates on preventing the collapse of the structure is evaluated.

Model 6.3. In this model, a steel structure retrofitted by the Vertical Plate Scheme and the Flange Plate Scheme will be parametrically studied. As shown in Fig. 6.8a, the building structure investigated here is a braced steel frame with 15 storeys. Each storey is 4.2m high and the building is 63m high. The building contained five 9m bays spanning east-west and three 9m bays spanning north-south, and its plan dimensions are 45m east-west and 27m north-south. Each floor slab spanning east-west is furthermore divided equally to three by two secondary beams. All of beams and columns are connected by fin plate connection. As shown in Fig. 6.8a, one column on north side is destroyed by a blast on the ground level. Therefore, all floors supported by this column will collapse. The compressions reduce

significantly and become very small in the columns just above and supported by this damaged column. The loss of the column has effectively modified the two spans of 9m into a single span of 18m, and the loads originally supported by the damaged column must now be carried by the rest of the structure.

Because the floor loads, slabs and steel beams are the same for every storey, all floors above the damaged column behave in a rather similar way. As a result, a model of one-storey part frame shown in Fig. 6.8b can be used for investigating this problem. In this figure, the two intact beams that are located out of the collapse area and do not fall down with the unsupported column are cut in the middle and the only half of the beam is left and the rest intact part of structure is taken away, in order to reduce computational effort.

As shown in Fig. 6.8c, the analytic model can be further reduced to only the half by taking advantage of symmetry. This half model will be used in the following finite element analyses. The bottom of the lower column is fixed end; the top of the upper column, the left half beam at the left end and the right beam at the right end are vertical slide, i.e., their rotation and horizontal displacement are restrained but their vertical displacement is not restrained. For the original and retrofitted structures, the boundary conditions and the load locations are the same.

The beams have a 457x152UB82 cross-section, and the columns 305x305UC283 (Owens and Knowles 1992). The thickness, length and the depth of the fin plate are 0.011m, 0.05m and 0.36m, respectively. The beam and the column are modelled using shell elements positioned along the

mid-planes of the flange and web components. It is also assumed for simplicity that the mid-plane of the fin plate is at the same plane as that of the column and the beam webs and the fin plate is welded to the column and the beam. The shell element S4R is employed. An element size 0.027m×0.027m is used for modelling the beam-to-column connection parts, and an element size 0.027m×0.108m is utilized for modelling the rest of the structures. This sub-frame is very similar to that of Model 4.3, and the same element type and similar mesh desity are adopted, and therefore the mesh sensitivity study is not conducted here. For both the original and the strengthened structures, the force-controlled loading is employed. The numerical simulation consists of two steps. In the first step, the concentrated loads applied at the left beam, the column, the two third points of the right beam and the damaged half middle column are proportionally increased from 0 to 80kN, 80kN, 80kN, 80kN and 40kN, respectively. In the second step, the loads applied at the two third points of the right beam and the damaged half middle column are changed to 160kN, 160kN and 80kN respectively, as a result of accounting for the dynamic effect with an amplification factor of 2.0 (ASCE 7 2002; DoD 2005); while the concentrated loads applied on the left beam and the column remain 80kN, because the left beam and the column remain intact, the secondary beams supported by the left beam and the column do not fall down and no dynamic effect is involved.

For the original structure, some simulation results are shown in Fig. 6.9. To investigate the stress and the strain distributions, the Mises equivalent stress and the equivalent plastic strain are plotted. It can be seen that the stress

and the strain at the beam-to-column connection are much larger than the stress and the strain of other parts of structure.

Fig. 6.9 shows that when the vertical load scaling factor reaches a value of 0.9275, the maximum Mises stress 488.9MPa and equivalent plastic strain 0.3923 of the whole model, roughly equal to the assumed corresponding failure values of 490.8MPa and 0.4, occur at the fin plates, while the stress and strain levels of the vast majority of the structure are still rather low. This type of simple beam-to-column connection part acts like a "fuse". Because the high stress and strain only occur at the connection part, internal forces in the middle segments of the beams are rather limited and cannot increase excessively. Fracture will develop, and rupture will occur finally at the simple beam-to-column connection. As a result, all above floors, beams and columns will collapse within the two spans originally supported by the damaged column.

Different from that of the original structure, after strengthening, the beam-to-column connection becomes a rigid one. The lengths and the thicknesses of strengthening plates are the variables of parametric study herein. The lengths of reinforcing vertical plates are related with the weld requirements. The minimum allowable plate length out of column flange is assumed to be 25cm herein. The used lengths of the vertical plates extending out of the column face, from the longest to the shortest, are assumed to be 40, 35, 30 and 25cm, respectively. The available steel plate thicknesses, from the thickest to the thinnest, are assumed to be 32, 30, 28, 26, 25, 24, 23, 22, 21, 20, 19, 18, 17, 16, 15, 14, 13, 12, 11, 10, 9 and 8mm,

respectively. The computation is conducted according to the procedure shown in Fig 6.7. In this figure, the plate weight function can be given by

$$f_w(i_l, i_t) = 2md[2l(i_l) + s]t(i_t)$$

Table 6.4.

Maximum Mises equivalent stresses and equivalent plastic strains of connection and whole structure with respect to different lengths (*l*) and thicknesses (*t*) of vertical plates for Model 6.3

l (cm) *t* (mm)	Max. stress of connection (MPa)	Max. strain of connection	Max. stress of whole struct. (MPa)	Max. strain of whole struct.	Weight of Vert. plates (kg)
l=40,*t*=32	235.4	0.0049	388.5	0.1138	240.1
l=40,*t*=25	236.0	0.0127	385.8	0.1064	187.6
l=40,*t*=24	247.8	0.0153	385.3	0.1048	180.1
l=40, *t*=21	334.4	0.0303	382.8	0.0981	157.6
l=40, *t*=20	360.8	0.0368	381.7	0.0948	150.1
l=35, *t*=32	235.4	0.0059	389.6	0.1169	217.8
l=35, *t*=25	236.0	0.0127	386.9	0.1094	170.2
l=35, *t*=24	243.9	0.0147	386.4	0.1078	163.4
l=35, *t*=20	358.2	0.0344	382.8	0.0980	136.1
l=35, *t*=19	362.7	0.0422	381.6	0.0948	129.3
l=30, *t*=32	235.7	0.0099	390.8	0.1202	195.5
l=30, *t*=30	235.8	0.0113	390.1	0.1182	183.3
l=30, *t*=28	236.1	0.0133	389.3	0.1159	171.1
L=30, *t*=21,	340.5	0.0314	384.1	0.1016	128.3
L=30, *t*=20	360.5	0.0360	382.8	0.0980	122.2
l=25, *t*=32	302.3	0.0247	392.0	0.1233	173.2
l=25, *t*=26	356.7	0.0342	388.7	0.1116	140.7
l=25, *t*=25	360.8	0.0370	386.8	0.1090	135.3

where $l(i_l)$) is the i_l th length extending out of column flange; $t(i_t)$ is the i_t th plate thickness; the mass density of steel is m =7850kg/m^3; the plate depth is

d =0.4437m; and the plate length between the two column flanges is s =0.2771m.

Initially, the largest length and thickness can be used. If the adopted sizes of strengthening plates are too large, the sizes can be progressively reduced. Some computational results are given by Table 6.4 and Figs. 6. 10-11. When the initial length l (i_l =1) is 40cm and the initial thickness t (i_t =1) is 32mm, the global maximum Mises stress of 388.5MPa and equivalent plastic strain of 0.1138 of the whole structure occur at the normal beam segment bordering on the strengthened connection part. The local maximum Mises stress σ_c (i_l =1, i_t =1) of the connection parts, occurring at the fin plate between the beam web and column flange, is 235.4MPa, below the assumed value 236.0MPa of the first criterion. The weight of strengthening plates of one beam-to-column connection is f_w (i_l =1, i_t =1)=240.1kg.

Because the thickness of vertical plates is too large, it can be decreased to reduce the weight. When the thickness is progressively reduced to the value of t (i_t =4)=25mm while the length remains, the local maximum Mises stress σ_c (i_l =1, i_t =4) is increased to 236.0MPa, equal to the value of the first criterion. These local maximum stress and strain near the column face occur at the vertical plates. If the thickness is decreased to the next value of t (i_t +1=5)=24mm, the local maximum Mises stress σ_c (i_l =1, i_t +1=5) near the column face is increased to 247.8MPa, larger than the assumed value 236.0MPa of the first criterion. This means that for the length l (i_l =1)=40cm, the thickness of t (i_t =4)=25mm is smallest allowable value for the first criterion.

When the second criterion is adopted, this thickness will be very large, and can be reduced further to decrease the weight of vertical plates. The length remains, and the thickness can be reduced from $t(i_t=5)$=24mm progressively. For all thicknesses that are not less than $t(i_t=9)$=21mm, the requirement of the second criterion will not be violated.

As shown in Table 6.4, if the thickness is $t(i_t=9)$=21mm, the local maximum Mises stress $\sigma_c(i_l=1, i_t=9)$=334.4MPa at the connection part is smaller than the corresponding value $\sigma_b(i_l=1, i_t=9)$=382.8MPa of the normal beam segment and 360.0MPa of the third point of Table 6.3, still satisfying the requirements of the second criterion. If the thickness is further reduced to $t(i_t+1=10)$=20mm, the local maximum Mises stress $\sigma_c(i_l=1, i_t+1=10)$=360.8MPa at the connection part is larger than the value of 360.0MPa , and the second criterion is violated. Therefore, when the length is $l(i_l=1)$=40cm, the minimum thickness is $t(i_t=9)$=21mm for the second criterion.

When the length is progressively reduced to $l(i_l=2{:}4)$=35, 30 and 25cm, the minimum thicknesses for the first and second criteria can also be obtain in the way similar to the case when the length is $l(i_l=1)$=40cm. It can be seen from Table 6.4 that for the four lengths, the corresponding minimum thickness and weight are: (1) $l(i_l=1)$=40cm: $t(i_t=4)$=25mm and $w_{l1\min}=f_w(i_l=1, i_t=4)$=187.6kg for the first criterion, and $t(i_t=9)$=21mm and $w_{l2\min}=f_w(i_l=1, i_t=9)$=156.7kg for the second criterion; (2) $l(i_l=2)$=35cm: $t(i_t=4)$=25mm and $w_{l1\min}=f_w(i_l=2, i_t=4)$=170.2kg for the first criterion, and

t (i_t=10)=20mm and $w_{l2\min} = f_w$ (i_l=2, i_t=10)=136.1kg for the second criterion; (3) l (i_l=3)=30cm: t (i_t=2)=30mm and $w_{l1\min} = f_w$ (i_l=3, i_t=2)=183.3kg for the first criterion, and t (i_t=9)=21mm and $w_{l2\min} = f_w$ (i_l=3, i_t=9)=128.3kg for the second criterion; and (4) l (i_l=4)=25cm: none for the first criterion, and t (i_t=4)=26mm and $w_{l2\min} = f_w$ (i_l=4, i_t=4)=140.7kg for the second criterion. Among them, the weight $w_{l1\min}$ of group (2) is the minimum value $w_{1\min} = f_w$ ($i_{l1\min}$=2, $i_{t1\min}$=4)=170.2kg for the first criterion and the weight $w_{l2\min}$ of group (3) is the minimum value $w_{2\min} = f_w$ ($i_{l2\min}$=3, $i_{t2\min}$=9)=128.3kg for the second criterion.

As a consequence, for the first criterion, the solution is in Group (2), the length and thickness are 35cm and 25mm respectively, and the weight of strengthening plates is 170.2kg; and for the second criterion, the solution is in Group (3), the length and thickness are 30cm and 21mm respectively, and the weight of strengthening plates is 128.3kg. The Mises stress and strain distributions are shown in Figs. 6.10-11 for the results obtained from the requirements of the two criteria. If the second criterion is adopted, as compared to the weight of vertical plates of 170.2kg for the first criterion,

$$\frac{170.2 - 128.3}{128.3} = 32.66\%$$

32.66% of strengthening plate weight is saved, and the economical effect is obvious.

The original structure can also be retrofitted by flange cover plates, in addition to vertical plates. When retrofitted by the Flange Plate Scheme, the available lengths and thicknesses of strengthening plates are the same

as those adopted for the Vertical Plate Scheme. The computation is conducted according to the procedure shown in Fig 6.7. In this figure, the plate weight function can be given by

$$f_w(i_l, i_t) = 2mb_f\{2l(i_l)t(i_t) + s[t(i_t) + t_f]\}$$

where $l(i_l)$) is the i_l th length extending out of column flange; $t(i_t)$ is the i_t th plate thickness; the mass density of steel is m =7850kg/m^3; the beam flange width is b_f =0.1535m; the beam flange thickness is b_f =0.0189m; and the plate length between the two column flanges is s =0.2771m.

Some computational results are given by Figs. 6.12-13 and Table 6.5. The used initial length and thickness are 40cm and 32mm, respectively. The local maximum Mises stress of the connection parts, occurring at the place between beam end and column flange, is 235.7MPa, not exceeding the requirement of the first criterion that the maximum Mises stress near column face should be no more than 236.0MPa. The corresponding local maximum equivalent plastic strain at the same place is 0.0099. The weight of strengthening plates for these sizes is 95.69kg.

To reduce the weight of strengthening plates, the thickness of the cover plates can be decreased. The stress and strain of the connection parts increase monotonically with the decrease of the thickness.

If the length remains and the thickness is reduced to the next one, i.e., 30mm, the local maximum Mises stress at the top weld near column flange is increased to 239.5MPa, larger than the first criterion value of 236.0MPa. The corresponding local maximum equivalent plastic strain at the same location is 0.0139. It means that the thickness of flange cover plates of

32mm would not be reduced further; otherwise the allowable stress of the first criterion will be exceeded.

Table 6.5.

Maximum Mises equivalent stresses and equivalent plastic strains of connection and whole structure with respect to different lengths (*l*) and thicknesses (*t*) of flange cover plates for Model 6.3

l (cm) *t* (mm)	Max. stress of connection (MPa)	Max. strain of connection	Max. stress of whole struct. (MPa)	Max. strain of whole struct.	Weight of cover plates (kg)
l=40,*t*=32	235.7	0.0099	390.9	0.1203	95.69
l=40,*t*=30	239.5	0.0139	390.5	0.1192	90.49
l=40,*t*=19	356.0	0.0340	384.3	0.1020	61.94
l=40,*t*=18	360.4	0.0357	383.0	0.0985	59.35
l=35,*t*=32	245.7	0.0150	390.2	0.1186	87.97
l=35,*t*=19	353.1	0.0335	385.2	0.1045	57.36
l=35,*t*=18	360.1	0.0351	384.1	0.1015	55.01
l=30,*t*=32	267.8	0.0188	389.4	0.1163	80.26
l=30,*t*=18	359.0	0.0346	384.6	0.1030	50.67
l=30,*t*=17	360.5	0.0363	383.4	0.0996	48.56
l=25,*t*=32	296.0	0.0237	388.2	0.1131	72.55
l=25,*t*=18	358,7	0.0345	384.8	0.1034	46.33
l=25,*t*=17	360.6	0.0363	383.8	0.1008	44.46

Therefore, it can be seen from Table 6.5 that for the first criterion the minimum thickness is 32mm for the length of 40cm, and the weight of strengthening flange cover plates of the structure is 95.69kg. The Mises stress and strain distributions are shown in Fig. 6.12.

If the second criterion is adopted, the thickness will be very large, and it can be progressively reduced to decrease the weight of flange cover

plates. For all thicknesses that are not less than 19mm, the requirement of the second criterion will not be violated.

As shown in Table 6.5, if the thickness is reduced to 19mm, the local maximum Mises stress of 356.0MPa at the weld that links the upper beam flange and the strengthening cover plate to the column flange face are smaller than the corresponding value of 384.3MPa of the normal beam segment and 360.0MPa of the third point of Table 6.3, still satisfying the requirements of the second criterion. If the thickness is further reduced to 18mm, the local maximum Mises stress of 360.4MPa at the connection part is larger than the value of 360.0MPa, and the second criterion is violated. Therefore, when the length is 40cm, the minimum thickness is 19mm for the second criterion.

When the length is progressively reduced to 35, 30 and 25cm, the minimum thicknesses for the first and second criteria can also be obtain in the way similar to the case when the length is 40cm. It can be seen from Table 6.5 that for the four lengths, the corresponding minimum thickness and weight are: (1)40cm: 32mm and 95.69kg for the first criterion, and 19mm and 61.94kg for the second criterion; (2) 35cm: none for the first criterion, and 19mm and 57.36kg for the second criterion; (3) 30cm: none for the first criterion, and 18mm and 50.67kg for the second criterion; and (4) 25cm: none for the first criterion, and 18mm and 46.33kg for the second criterion. The weight 95.69kg of group (1) is the only value satisfying the first criterion and the weight 46.33kg of group (4) is the minimum value for the second criterion.

As a consequence, for the first criterion, the solution is in Group (1), the length and thickness are 35cm and 32mm respectively, and the weight of strengthening plates is 95.69kg; and for the second optimisation criterion, the solution is in Group (4), the length and thickness are 25cm and 18mm respectively, and the weight of strengthening plates is 46.33kg. The Mises stress and strain distributions are shown in Figs. 6.12-13 for the results obtained from the requirements of the two criteria. If the second criterion is adopted, as compared to the weight of flange cover plates of 95.69kg for the first criterion,

$$\frac{95.69 - 46.33}{46.33} = 106.5\%$$

106.5% of strengthening plate weight is saved, and the economical effect is significant.

The weight ratio of the Vertical Plate Scheme to the Flange Plate Scheme for the first optimisation criterion is

$$\frac{170.2 - 95.69}{95.69} = 77.87\%$$

This weight ratio for the second optimisation criterion is

$$\frac{128{,}3 - 46.33}{46.33} = 176.9\%$$

The strengthening material weights required by the Vertical Plate Scheme are 77.87% and 176.9% more than those by the Flange Plate Scheme for the first and second criteria, respectively.

Although the Vertical Plate Scheme requires much more strengthening material weight than the Flange Plate Scheme for the same criterion, the Vertical Plate Scheme has the advantage that it does not require removing the floor slab when the strengthening vertical plates are welded to the original structure. Whereas when Flange Plate Scheme is conducted, the portion of floor concrete slab upon the beam-to-column connection needs to be removed in order to weld the upper strengthening flange cover plates to the original structural members. Like the incision of surgical operation, the cut of floor slab will have adverse impact on the structure and reduce its load resistant capacity. Conducting such parametric study can minimise the length of the strengthening flange cover plates, and therefore help to reduce considerably the retrofitting cost.

6.3 Summary

The cost of retrofitting increases with the weight of retrofitting plates. The larger the weight, the better for the reserve capacity of structure; but the retrofitting cost will be higher; and vice versa. As the weight reduces gradually, the stress and strain levels will increase, and the resisting capacity of the structure will progressively decrease. This chapter devocates to minimise strengthening plate weights of the Flange Plate Scheme and the Vertical Plate Scheme. In Section 6.1, the exact analytical optimal solutions were given for retrofitted beams that are subjected to axial tensile and lateral loads. The adopted two optimisation criteria are (1) the entire cross-section must be elastic; (2) an elastic core must exist and

the yield strain distance must not be smaller than the proscribed minimum yield strain distance.

In Section 6.2, where column removal is considered, there are very large axial tensions in the beams, the analysis becomes very complicated, exact solution becomes impossible and so the finite element method software ABAQUS was adopted to conduct the parametric study for minimising the weights of vertical plates and the flange cover plates. Two criteria, based on the requirement that (1) the maximum Mises equivalent stress cannot be larger than 236.0MPa at the connection parts and (2) the maximum Mises stress of the connection parts is smaller than or equal to that of the normal beam segments and the local maximum Mises stress at the strengthened connection cannot exceed its values of 360.0MPa, the third point of Table 6.3.

For the same criterion, the strengthening plate weight of the Vertical Plate Scheme is much more than that of the Flange Plate Scheme. However, the Vertical Plate Scheme does not require removing the concrete floor slab for welding; in addition to the adverse impact to structure, the removal of the thick floor slab is very labour demanding and expensive. For the Flange Plate Scheme, minimising plate weight can reduce significantly the length of strengthening plates. The area of the floor slab required to be removed from the beam-to-column connection depends mainly on the length of strengthening flange cover plates.

Chapter 7: Summary and conclusions

This thesis described the results of an investigation devoted to the analysis of catenary action and the improvement of the catenary behaviour of an existing structure. There were five aspects in the work presented. Firstly, literature on progressive collapse, catenary action, and beam-to-column connections was reviewed. It has been shown in the publications reviewed that the strength, ductility, redundancy and continuity of a structure are very important for resisting local damage and preventing progressive collapse of the structure. The structure should have sufficient local resistance, and it should be able to provide alternative load transfer paths when one of its structural members is destroyed.

Secondly, an analysis of catenary action was conducted, and the effect of strengthening simple beam-to-column connections in an existing steel building structure was discussed. It was demonstrated that plastic deformation and catenary action of the beam can reduce the bending moment significantly through axially restraining the beam. The investigation of catenary action was carried out by using a truss element model. Because there is no lateral load in the span and the boundary condition is pin, exact results can be obtained. For catenary action to fully develop, no weak ends should exist. It is demonstrated that the failure load and global deformation can increase significantly through strengthening the originally weak end segments.

As demonstrated by the truss model, the ultimate strength of a fin plate beam-to-column connection is determined as the lowest value among the

various structural parts. In order to enhance the capability of the structure to withstand a general structural collapse, the requirement of strength and continuity at the beam-to-column connection should be fulfilled, and this connection should be strengthened. After strengthening, the axial force in beam flanges can be transferred across the column, and therefore the retrofitted beam-to-column joint can be qualified as full-strength moment-resisting joint. Based on these principles, two schemes were proposed for retrofitting fin plate beam-to-column connections. Through fully connecting beam flanges, the beam-to-column connection of these steel frames can be strengthened. Thereby, one can greatly improve the structural ductility and the resistance to axial catenary force, increase the entire structural robustness, and enhance the survival capacity of these steel framed structures.

Thirdly, this thesis has attempted to provide reasonable nonlinear finite element models for evaluating different post-column removal performance as a function of the original and retrofitted beam-to-column connection geometries. Finite element analysis is necessary because different from the truss model, when lateral loads and a bending moment exist, the case becomes much more complicated. In Model 4.2, assemblages of two-dimensional solid elements subjected to catenary tension are evaluated. For fully developing catenary action, no weak section should exist in the beam end segments. In Model 4.3, three-dimensional shell model is set to perform the simulation of the catenary behaviour of damaged structures. It has been shown that through fulfilling the requirement of continuity for the beam-to-column connection, one can greatly improve the structural

ductility and the resistance to catenary force, thus increasing the entire structural robustness and enhancing survival capacity of some steel framed structures.

All of the above mentioned simulations were conducted for the original structure, the structures retrofitted by the Flange Plate Scheme and the Vertical Plate Scheme. It has been shown that the original fin plate connection of the existing structure is too weak for catenary action to develop and strengthening the connection is needed. The comparison of the simulation results before and after strengthening highlighted the effectiveness of the two proposed retrofitting schemes.

Due to retrofitting, additional bending moment may be transferred from the beam to the column through the strengthened beam-to-column joint. When the column is weak, it is possible that the additional bending moment causes the column to yield. However, the analyses presented demonstrated that even though plastic hinges occur at its top and bottom ends as a result of the removal of a nearby column, the column may still continue to withstand loads without becoming a mechanism and collapsing.

Fourthly, this thesis has investigated the relative ability of the Traditional Moment Connection Scheme, the Flange Plate Scheme, SidePlate Connection Scheme and the Vertical Plate Scheme. Through the investigation, the relative advantages and shortcomings of these schemes are determined. The Traditional Moment Connection Scheme can improve the ability of structure to prevent progressive collapse, but the enhanced ability is not adequate because the maximum stress and strain still occur

near the column flange face. Performing much better than the Traditional Moment Connection Scheme, the Flange Plate Scheme, the SidePlate Connection Scheme and the Vertical Plate Scheme can prevent the progressive collapse of the structures by developing catenary action in the beams because the original weakest beam-to-column connection part near the column flange face are strengthened effectively and the stress and strain in the middle beam segment are much larger than those in the strengthened beam ends.

In this thesis, the shell element models are mainly adopted to investigate the global behaviour of the structures after the column removal. In order to simplify the models and reduce computational effort, many assumptions have been used. However, the modelling assumptions are very important, the more assumptions adopted, the less realistic the modelling may be. For overcoming the drawbacks of the very simplified shell models and using as less assumptions as possible in modelling, the much more detailed 3D solid element models are adopted in Section 5.2 to investigate the local behaviour of the end plate connections before and after strengthened by the above mentioned four schemes. In the 3D solid element models, the contacts among the bolts and the steel plates and the geometries and the material properties of the welds are simulated. Although demanding much more computational effort, the 3D solid element models can provide much more information about the local performance of the connections, as compare to the shell element models.

Finally, this thesis has attempted to minimise the weights of the flange plates and the vertical plates. For both the retrofitted beams and the

retrofitted frames, the stresses and the strains increase in the strengthening plates with the reduction of the thickness of the strengthening plates. To allow structural engineers more choice, two criteria based on different stress and strain levels were adopted, instead of a single one criterion.

In Section 6.1, the retrofitted beams are subjected to the combined action of bending moment, shear force and axial tension. When the beams are in elastic state, the sensitivity method can be used to find exact optimal solutions for the first criterion. When the beams are in the elasto-plastic state, based on the minimum yield strain distance that defines the boundary of the elastic core, closed form optimal solutions can be given for the second criterion.

For the retrofitted frames with a lot of redundancies in Section 6.2, the finite element analyses are used for the minimisation. Two criteria are adopted. The first criterion is based on the constraint that the maximum stress in the beam-to-column connection part cannot exceed the value 236.0MPa at the end of the perfectly plastic stage. The second criterion has two requirements. The first one that the local maximum Mises stress and equivalent plastic strain at the strengthened connection parts must smaller than or equal to that in the un-strengthened normal beam segments. The second one is that the local maximum Mises stress at the strengthened connection cannot exceed its values of 360.0MPa, the third point of Table 6.3. For both the retrofitted beams and frames, the weigh of retrofitting plates can be saved considerably.

Chapter 8: Future work

Most of people live or work in old buildings, rather than in new ones. The quantity of existing structural steelworks is much larger than new steel construction. The cost of demolishing the old structural steelwork and rebuilding a new one is usually much larger than the cost of retrofitting it to satisfy the new requirement. Because simple steel construction is widely used in UK and other places in the world, the research in this field is very useful.

However, the literature about the structural optimisation of retrofitting existing old steel structures with simple connection is very limited. How to optimise these strengthened existing steel buildings in order both to prevent the collapse of the structure due the removal of a column by blast and to save the retrofitting cost is still a useful research question. Therefore, a gap between knowledge and practice can be identified. This cap should be bridged. Answering this research question is very important, and is the first aim of our future research.

In this thesis, some work has been done in this field. There are two design variables of the length and depth of strengthening plate. Because the number of design variables is small, the software ABAQUS could be employed for minimising the weight of retrofitting plates. But when a structure becomes complicated, number of optimal variables becomes large, and material and geometrical nonlinearities are involved, it will be very difficult, if not impossible, to employ ABAQUS to solve such problems. For this purpose, the other software that is more powerful in the research

field of structural optimisation than ABAQUS should be used. Such software is available now. For examples, the function of structural optimisation of the software ANSYS is much more powerful than that of the ABAQUS. The software ANSYS itself has many very useful methods for finding optimal results, and the number of optimal variables can also be much larger than that used in this thesis now. I already have some ability to utilise the software ANSYS to carry out the structural optimisation.

The second work that can be done in the future is numerical simulation of the Link Bar Retrofitting Scheme, which also be mentioned in Liu (2010a). As shown in Fig. 8.1a, original double angle web connection, a type of simple connection, can be strengthened by the Link Bar Scheme. As shown in Fig. 8.1b, the Link Bar Retrofitting Scheme is proposed by modifying the idea of Hoeckman et al. (2005). By installing bars with high strength near the beam flanges and transferring the flange forces across the column, one can further increase its tension resistance, and greatly strengthen the joint. The difference between the beam and the column web thicknesses can be adjusted by inserting thin plates. In addition to the above mentioned virtues on the mechanical aspect, this retrofitting scheme also has many other merits. For example, it is labor saving because it can be easily conducted without requiring the removal of the part of the floor slab near the column. Different from the above mentioned two retrofitting schemes, this one does not require welding on site, and can avoid the possible brittle damage caused by site-welding.

For the bars to pass through column flanges, rectangular holes are needed to be cut. Instead of mechanical means of cutting, which requires

cutting tools to contact column flanges and is quite labor demanding on site, non-contact cutting can be used here. There are four main non-contact cutting methods: oxy-fuel cutting, plasma cutting, laser cutting and water jet cutting. Among the widely used non-contact site-cutting methods, compared with the oxygen-acetylene cutting, the plasma cutting is preferred here because the plasma-arc has much less heat-affected zone than the oxy-fuel, although the oxy-fuel can cut thick column flanges more easily than the other three methods.

As shown in Fig. 8.2, the left end of the left beam and the right end of the right beam are pinned, i.e., the horizontal and vertical displacements are restrained but the rotations are not restrained, and concentrated loads are applied at the third points and the column. Two spans of 6m change to one span of 12m after losing the middle column support. By so doing, the catenary action after a column removal can be simulated. Similar device was also used by Yang et al. (2012).

By taking advantage of symmetry, only a half of the substructure is considered. The originally considered span of 12m becomes a half-span of 6m now, only the half of the middle universal column is considered and the considered shape of the half middle column changes from an I-shape to a T-shape. By taking advantage of symmetry again about the mid-planes of beam and column webs, only a quarter of the original substructure is considered. By so doing, the shape of the universal beam changes from an original I-shape to a channel, and shape of the middle column changes from T-shape to an angle finally. Fig. 8.3 show this model used in the computational simulation.

The modelling of Link Bar Retrofitting Scheme is much more difficult than the shell element modelling in this thesis. Link bars are made from high strength steel. Different from widely used structural steel, the weldability of high strength steel is rather poor. Therefore bolted connection is necessary. Due to simulating the interactions between various components, including high strength bolts, high strength link bars, beam web and column web, a contact problem is involved. The solution of contact problem is one of the most difficult in finite element analysis due to involving in material, geometric, and boundary nonlinearities (ABAQUS 2014, Belytschko et al. 2000). The evaluation of boundary nonlinearity is much more complex than those of material and geometric nonlinearities. Much time and effort have been taken to try to solve similar contact problems. The modelling of the Link Bar Retrofitting Scheme is much more complicated than the contact problems that have been faced before, but some useful results have been obtained, as shown in Figs. 8.4a-b. These results show that after retrofitted through the Link Bar Scheme, the structural ability to prevent collapse can be enhanced greatly by developing catenary action at the removal of column. If this work can be done, the chance is large about publishing a paper in a good journal.

The third work that can be done in the future is the dynamic analysis of the retrofitted structures. As mentioned in Chapter 4, the actual dynamic load factor may be different from the value 2.0 for a realistic structure (Liu, Davison and Tyas 2005; Tsai 2000; Tsai and You 2012), because of the material and geometric nonlinearities, and the complicated dynamic internal force redistribution process following the sudden column removal.

As compared to the static analysis method by using the dynamic load factor 2, the nonlinear dynamic analysis methods are much more reliable. Because the 3D solid element models, particularly when the contact problems are involved, may be too demanding in computational resource, the shell element, 2D solid element or beam models can be used firstly. This writer has experience in structural dynamics, is familiar with the nonlinear step-by-step methods, and believes that this work can be done.

The above three works can be done within 24 months.

List of References

1. ABAQUS. (2014). *ABAQUS theory guide*, Dassault Systems.
2. Astaneh-Asl, A., Madsen,E. A., Noble, C., Jung, R., McCallen, D., Hoehler, M. S., Li, W., and Hwa, R. (2001a). "Use of catenary cables to prevent progressive collapse of buildings", *Report Number UCB/CEE-Steel-2001/02,* Dept. of Civil and Env. Engrg., Univ. of Calif., Berkeley, US..
3. Astaneh-Asl, A., Jones, B., Zhao, Y., and Hwa, R. (2001b). "Progressive collapse resistance of steel building floors", *Report Number UCB/CEE-Steel-2001/03*, Dept. of Civil and Environmental Engineering., University of California, Berkeley, US.
4. American Concrete Institute (ACI). (2002). *Building code requirements for structural concrete: ACI 318-02*, ACI, Farmington Hills, Mich. US.
5. American Society of Civil Engineer (ASCE). (2002). *Minimum design loads for buildings and other structures: SEI/ASCE 7-02*, ASCE, Reston, Va. US.
6. Bangash, M. Y. H., and Bangash, T. (2006). *Explosion-resistant buildings*, Springer., London, UK.
7. Bazant, Z. P., and Zhou Y. (2002). "Why did the world trade center collapse?—Simple analysis." *J. Eng. Mech.*, 128(1), 2–6.
8. Belytschko, T., Liu, W. K., and Moran, B. (2000). *Nonlinear finite element for continua and structures*, John Wiley & Sons, Chichester, UK.
9. Bendsoe, M. P. (1995). *Optimization of structural Topology, Shape and Material*, Springer, Berlin, Germany.
10. Brockenbrough, R. L., and Merritt F. S. (1999). *Structural steel designer's handbook*, 3rd Ed., McGraw-Hill, New York, USA.

11. Bruneau, M., Uang C. M., and Whitttaker, A. (1998). *Ductile design of steel structures*, McGraw-Hill, New York, US.
12. BS 5950-1 (2000). *Structural use of steelwork in building. Code of practice for design*: *hot rolled and welded section*. BSI, London, UK.
13. Bursi, O. S., and Jaspart, J. P. (1997). "Benchmarks for finite element modelling of bolted steel connections." *Journal of Construction Steel Research*, 43:17-42.
14. Byfield, M. P. (2004). "Design of steel framed buildings at risk from terrorist attack." *The Structural Engineer*, 82(22), 31-38.
15. Byfield, M. P. (2006). "Behaviour and design of commercial multistorey buildings subjected to blast." *Journal of Performance of Constructed Facilities*, 20(4), 324-329.
16. Byfield, M. P., Paramasivam, S. (2007). "Catenary action in steel-framed building." *Structures and building*, 160(SB5), 247-257.
17. Chakrabarty, J. (1986). *Theory of plasticity*, McGraw-Hill, New York, USA.
18. Chen., C., and Lin., C. (2013). "Seismic performance of steel beam-to-column moment connections with tapered beam flanges." *Engineering Structures*, 48, 588-601.
19. Choi, K. K., and Kim, N. H. (2005a). *Structural Sensitivity Analysis and Optimization 1—Linear Systems*, Springer, Berlin, Germany.
20. Choi, K. K., and Kim, N. H. (2005b). *Structural Sensitivity Analysis and Optimization 2—Nonlinear Systems and Applications*, Springer, Berlin, Germany.
21. Christensen, P.W., and Klarbring, A. (2009). *An Introduction to Structural Optimization*, Springer, Berlin, Germany.

22. Clough, R. W., and Penzien, J. (1993). *Dynamics of structures*, 2nd Ed., McGraw-Hill, New York, USA.
23. Corley, W. G. (2004). "Lessons learned on improving resistance of buildings to terrorist attacks." *Journal of Performance of Constructed Facilities*, 18(2), 68-78.
24. Corley, W. G., Mlakar, Sr., P. F., Sozen, M. A., and Thornton, C. H. (1998). "The Oklahoma City bombing: summary and recommendations for multihazard mitigation." *Journal of Performance of Constructed Facilities*, 12(3), 100-112.
25. Department of Defense (DoD). (2002). *DoD minimum antiterrorism standards for buildings. UFC 4-010-01*, Unified Facilities Criteria, Washington, D.C., US.
26. Department of Defense (DoD). (2005). *Design of building to resist progressive collapse*. *UFC 4-023-03*, Unified Facilities Criteria, Washington, D.C., US.
27. Dowling, N. E. (2013). Mechanical behaviour of material, 4th Ed., Preentice Hall, New York, USA.
28. Dusenberry, D. O., and Hamburger, R. O. (2006). "Practical means for energy-based analyses of disproportionate collapse potential." *Journal of Performance of Constructed Facilities*, 20(4), 336-348.
29. Ellingwood, B. R. (2006). "Mitigating risk from abnormal loads and progressive collapse." *Journal of Performance of Constructed Facilities*, 20(4), 315-323.
30. Ellingwood, B. R., and Leyendecker, E.V. (1978). "Approaches for design against progressive collapse." *J. Struct. Div., ASCE*, 104(3), 413-423.

31. Ellingwood, B. R., MacGregor, J. G., Galambos, T. V. & Cornell, C. A. (1982), Probability-based load criteria: Load factors and load combinations, *Journal of the Structural Division*, ASCE, 108(5), 978–97.
32. Ellingwood, B. R. (1994), Probability-based codified design: Past accomplishments and future challenges, *Structural Safety*, 13(3), 159–76.
33. Ellingwood, B. R., and Dusenberry, D. O. (2005). "Building design for abnormal loads and progressive collapse." *Computer-Aided Civil and Infrastructure Engineering*, 20, 194–205.
34. El-Rimawi, J. A., Burgess, I. W., and Plank, R. J. (1995). ''The analysis of semi-rigid frames in fire—A secant approach.'' *J. Constr. Steel Res.,* 22, 125–146.
35. Engelhardt, M. D., and Sabol, T. A. (1995). "Lesson learned from the Northridge earthquake: Steel moment frame performance." *Proceedings, New direction in seismic design*, October, 1-12, Tokyo.
36. Faella, C., Piluso V., and Rizzano, G. (2000). *Structural steel semi-rigid connections – Theory design and software*, CRC Press, London, UK.
37. Federal Emergency Management Agency (FEMA). (1996). "The Oklahoma City bombing: Improving building performance through multi-hazard mitigation." *FEMA 277*, Washington, D.C., US.
38. Federal Emergency Management Agency (FEMA). (2000a). "Prestandard and commentary for the seismic rehabilitation of buildings." *FEMA 356*, Washington, D.C., US.
39. Federal Emergency Management Agency (FEMA). (2000b). "State of art report on connection performance: Program to reduce the earthquake hazards of steel moment-frame structures." *FEMA 355D*, Washington, D.C., US.

40. Federal Emergency Management Agency (FEMA). (2002). "World Trade Center building performance study: Data collection, preliminary observations, and recommendations." *FEMA 403*, Washington, D.C., US.
41. Galambos, T. V., Ellingwood, B., MacGregor, J. G. and Cornell, C. A. (1982) "Probability-based load criteria: Assessment of current design practice." *Journal of the Structural Division*, ASCE, 108(5), 959–77.
42. General Services Administration (GSA). (2003). *Progressive collapse analysis and design guidelines for new federal office buildings and major modernization projects*. Washington, D.C., US.
43. General Services Administration (GSA). (2013). *Alternate path analysis and design guidelines for progressive collapse resistance*. Washington, D.C., US.
44. Griffiths, H., Pugsley, A. G., and Saunders, O. (1968). "Report of the inquiry into the collapse of flats at Ronan Point, Canning Town." *Her Majesty's Stationery Office*, London, UK.
45. Gross, J. L and McGuire, Q. (1983). "Progressive collapse resistant design." *J. Struct. Eng.*, 109(1), 1-15.
46. Gurson, A. L. (1977). "Continuum theory of ductile rupture by void nucleation and growth. Part I: Yield criteria and flow rules for porous ductile media." *J. Eng. Mater. Technol.*, 99(1), 2–15.
47. Hallquist, J. (2005). *LS-DYNA*, Livermore Software Technology corp., Livermore, Calif., US.
48. Hayes Jr., J. R., Woodson, S. C., and Pekelnicky, R. G. (2005). "Can strengthening for earthquake improve blast and progressive collapse resistance?" *J. Struct. Eng.*, 131(8), 1157–1177.
49. Hoeckman, W., Verhaeghe, P., and Obbard, R. (2005). "Extreme event

beam link connection." *4th European conference on steel and composite structures*, 4(10), 139-146.

50. Houghton, D., and Karns, J. (2001). "Effective Mitigation of Progressive Collapse in Steel Frame Buildings using Ductile High-Capacity Beam-to-Column Moment Connections Exhibiting Discrete Structural Continuity Across a Failed Column." *Proceedings of the Society of American Military Engineers (SAME) National Symposium on Comprehensive Force Protection,* Citadel, Charleston, South Carolina, US.
51. Huang, Z. H., Burgess, I. W., and Plank, R. J. (2000). ''Three dimensional analysis of composite steel-framed buildings in fire.'' *J. Struct. Eng.,* 126(3), 389–397.
52. Izzuddin, B. A., Vlassis, A. G., Elghazouli, A. Y., and Nethercot, D. A. (2007). ''Assessment of progressive collapse in multi-storey buildings." *Structures and building*, 160(SB4), 197-205.
53. Izzuddin, B. A., Vlassis, A. G., Elghazouli, A. Y., and Nethercot, D. A. (2008). ''Progressive collapse of multi-storey buildings due to sudden column loss - Part I: Simplified assessment framework.'' *Engineering Structures*, 30, 1308-1318.
54. Jetteur, P., and Cescotto, S. (1991) "A mixed finite element for the analysis of large inelastic strains." *International Journal for Numerical Methods in Engineering*, 31, 229-39.
55. Khandelwal, K., and El-Tawil, S. (2007). "Collapse behaviour of steel special moment resisting frame connections." *J. Struct. Eng.*, 133(5), 646-655.
56. Kim, D., Ball, S., C., Sim, H., and Uang C. (2016). "Evaluation o sloped RBS moment connections." *J. Struct. Eng.*, 142(6)

57. Kim, J., and Kim, T. (2009). "Assessment of progressive collapse-resisting capacity of steel moment frames." *Journal of Constructional Steel Research*, 65 (1), 169-179.

58. Kishi, N., and Chen, W. F. (2007). "Moment-rotations of semi-rigid connections with angles." *J. Struct. Eng.*, 116(7), 1813-1834.

59. Lamonta, S., Gillieb, M., and Usmanib, A. S. (2007). "Composite steel-framed structures in fire with protected and unprotected edge beams." *Journal of Constructional Steel Research*, 63. 1138–1150.

60. Liu, J. L. (2010a). "Preventing progressive collapse through strengthening beam-to-column connection, part1: theoretical analysis." J*ournal of Constructional Steel Research*, 66. 229–237.

61. Liu, J. L. (2010b). "Preventing progressive collapse through strengthening beam-to-column connection, part2: finite element analysis." *Journal of Constructional Steel Research*, 66. 238–247.

62. Liu, R, E., Davison, J. B., and Tyas, A. (2005). "Is caternary action sufficient to resist procressive callapse in a steel framed building?" *4th European conference on steel and composite structures*, 4(10), 155-162.

63. MacGinley, T. J., and Ang, T. C. (1987). *Structural steelwork – Design to limit state theory*, Butterworths, London, UK.

64. Marchand, K. A., and Alfawakhiri, F. (2005). *Facts for steel buildings – Blast and progressive collapse*, American Institute of Steel Construction, US.

65. Marjanishvili, S. M. (2004). "Progressive analysis procedure for progressive collapse." *Journal of Performance of Constructed Facilities*, 18(2), 79-85.

66. Mlakar, Sr., P. F., Corley, W. G., Sozen, M. A., and Thornton, C. H. (1998). "The Oklahoma City bombing: Analysis of blast damage to the Murrah Building." *Journal of Performance of Constructed Facilities*, 12(3), 113-119.

67. Munoz-Garcia, E., Davison, J. B., and Tyas, A. (2005). "Analysis of the response of structural bolts subjected to rapid rates of loading." *4th European conference on steel and composite structures*, 4(10), 147-154.

68. Nair, R. S. (2006). "Preventing Disproportionate Collapse." *Journal of Performance of Constructed Facilities*, 20(4), 309-314.

69. National Research Council (NRC). (2001). *Protecting people and buildings from terrorism*, Committee for Oversight and Assessment of Blast-effects and Related Research, National Academy Press, Washington, D.C.

70. Newland, D. E., and Cebon, D. (2002). "Could the World Trade Center have been modified to prevent its collapse?" *J. Eng. Mech.*, 128(7), 795–800.

71. Norville, H. S., Harvill, N., Conrath, E. J., Shariat S., and Mallonee, S. (1999). "Glass-related injuries in Oklahoma City bombing." *Journal of Performance of Constructed Facilities*, 13(2), 50-56.

72. Osteraas, J. D. (2006). "Murrah building bombing revisited: a qualitative assessment of blast damage and collapse patterns." *Journal of Performance of Constructed Facilities*, 20(4), 330–335.

73. Owens, G. W., and Knowles, P. R. (1992). *Steel designers' manual*, 5th ed., The Steel Construction Institute, Blackwell Scientific Publications, London.

74. Pearson C., and Delatte, N. (2005). "Ronan Point apartment tower collapse and its effect on building codes." *Journal of Performance of Constructed Facilities*, 19(2), 172–177.

75. Popov, E. P., and Pinkney, R. B. (1969). "Cyclic yield reversals in steel building connections." *J. Struct. Div., ASCE*, 95(3), 327-353.

76. Ricles, J. M., Sause, R., Garlock, M. M., and Zhao, C. (2001). "Post-tensioned seismic-resistant connections for steel frames." *J. Struct. Eng.*, 127(2), 113-121.

77. Ricles, J. M., Sause, R., Peng, S. W., and Lu, L. W. (2002). "Experimental evaluation of earthquake resistant post-tensioned connections for steel frames." *J. Struct. Eng.*, 128(7), 850-859.

78. Rittenhouse, T., DiMaggio, P., and Ettouney, M. (2001). "Behaviour of steel structures subjected to blast loading." *Proceedings of 2001 Structures Congress*, Washington D.C., US.

79. Shi, G., Shi, Y., Wang, Y., and Bradford, M. A. (2008) "Numerical simulation of steel pretensioned bolted end-plate connections of different types and details." *Engineering structures*, 30. 2677–2686.

80. Smilowitz, R., and Tennant, D. (2001). "Multi-hazard design to resist progressive collapse." *Proceedings of 2001 Structures Congress*, Washington D.C., US.

81. Smith, P. D., and Hetherington, J. G. (1994). *Blast and ballistic loading of structures*, Butterworth-Heinemann, London, UK.

82. Sozen, M. A., Thornton, C. H., Corley, W. G., and Mlakar, Sr., P. F. (1998). "The Oklahoma City bombing: Structure and mechanisms of the Murrah Building." *Journal of Performance of Constructed Facilities*, 12(3), 120-136.

83. Steel Construction Institute (SCI). (1995). ''Joint in steel construction: Moment connection.'' Silwood Park, Ascot, UK.

84. Steel Construction Institute (SCI). (2002). ''Joint in steel construction: Simple connection.'' Silwood Park, Ascot, UK.

85. Stoddart, E. P., Byfield, M. P., and Tyas, A. (2014). "Blast modelling of steel frames with simple connections." *J. Struct. Eng.*, 140(1)

86. Stoddart, E. P., Byfield, M. P., Davison, J. B., and Tyas, A. (2013) "Strain rate dependent component based connection modelling for use in non-linear dynamic progressive collapse analysis." *Engineering Structures*, 55, 35-43.

87. Taylor, R., L., Beresford, P., J., and Wilson, E., L. (1976) "A non-conforming element for stress analysis." *Int. J. Num. Meth. Eng.,* 10, 1211-1220.

88. Tan, S., and Astaneh-Asl, A. "Cable-based retrofit of steel building floor to prevent progressive collapse", *Report Number UCB/CEE-Steel-2003/02,* Dept. of Civil and Environmental Engineering., University of California, Berkeley, US.

89. Tyas, A., Warren, J. A., Stoddart, E. P., Davison, J. B., Tait, S. J., and Huang, Y. (2012) "A Methodology for Combined Rotation-Extension Testing of Simple Steel Beam to Column Joints at High Rates of Loading." *Experimental Mechanics*, 52(8), 1097-1109.

90. Tsai, M. (2010). "An analytical methodology for the dynamic amplification factor in progressive collapse evaluation of building structures." *Experimental Mechanics Research Communication*, 37, 61-66.

91. Tsai, M., and You, Z. (2012). "Experimental evaluation of inelastic dynamic amplification factor for progressive collapse analysis under sudden column support loss." *Experimental Mechanics Research Communication*, 40, 56-62.

92. Tvergaard, V. (1981). "Influence of voids on shear band instabilities under plane strain conditions." *Int. J. Fract.*, 17(2), 389–407.

93. Tvergaard, V., and Needleman, A. (1984). "Analysis of the cup-cone fracture in a round tensile bar." *Acta Metall.*, 32(1), 157–169.

94. Wang, Y. C., and Kodur, V., K., R. (2000). ''Research towards use of unprotected steel structures.'' *J. Struct. Eng.,* 26(12), 1442–1450.

95. Wang, Y. C., Lennon, T., and Moore, D., B. (1995). ''The behaviour of steel frames subject to fire.'' *J. Constr. Steel Res.,* 35, 291–322.

96. Wu., J., and Feng., Y., T., (2013). "Finite element simulation of new RHS column-to-I beam connections for avoiding tensile fracture.'' *J. Constr. Steel Res.,* 86, 42–53.

97. Yang, B., and Tan, K. H. (2012). "Numerical analyses of steel beam–column joints subjected to catenary action." J*ournal of Constructional Steel Research*, 70. 1–11.

98. Yin, Y. Z., and Wang, Y. C. (2004). "A numerical study of large deflection behaviour of restrained steel beams at elevated temperatures.'' *J. Constr. Steel Res.,* 60, 1029-1047.

99. Yin, Y. Z., and Wang, Y. C. (2005a). "Analysis of catenary action in steel beam using a simplified hand calculation method, part1: theory and validation for uniform temperature distribution.'' *J. Constr. Steel Res.,* 61, 183-211.

100. Yin, Y. Z., and Wang, Y. C. (2005b). "Analysis of catenary action in steel beam using a simplified hand calculation method, part2: Validation for non-uniform temperature distribution.'' *J. Constr. Steel Res.,* 61, 213–234.

101. Zhou, Q., and Yu, T. X. (2004). "Use of high-efficiency energy absorbing device to arrest progressive collapse of tall building." *J. Eng. Mech.*, 130(10), 1177–1187.

102. Zienkiewicz , O. C., and Taylor, R. L., (2000a). *Finite element method, 5ed, vol. 1, the Basis, and vol. 2, Sollid Mechanics*, 5th Ed., Butterworth-Heinemann, Oxford, UK.

103. Zienkiewicz , O. C., and Taylor, R. L., (2000b). *Finite element method, 5ed, vol. 1, the Basis, and vol. 2, Sollid Mechanics*, 5th Ed., Butterworth-Heinemann, Oxford, UK.

Figures

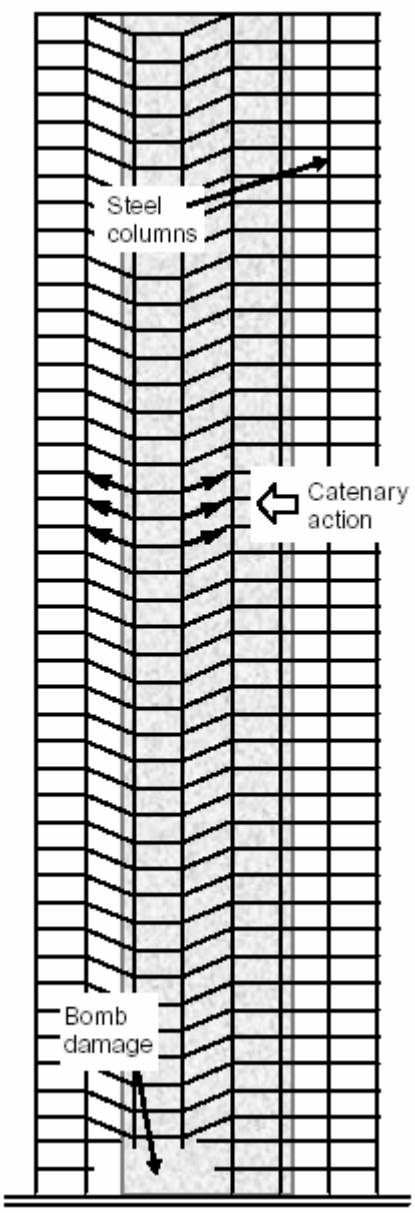

Fig. 1.1. Catenary action (Byfield and Paramasivam 2007)

Fig. 2.1. Ronan Point after collapse (Pearson and Delatte 2005)

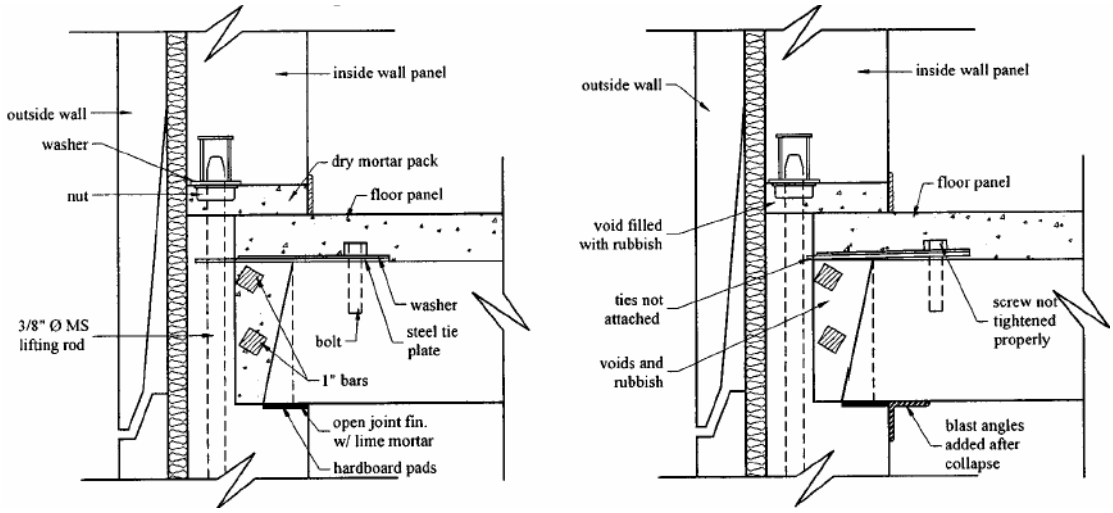

(a) Schematic design of joint (b) As built joint

Fig. 2.2. Connection of wall and floor slabs (Pearson and Delatte 2005)

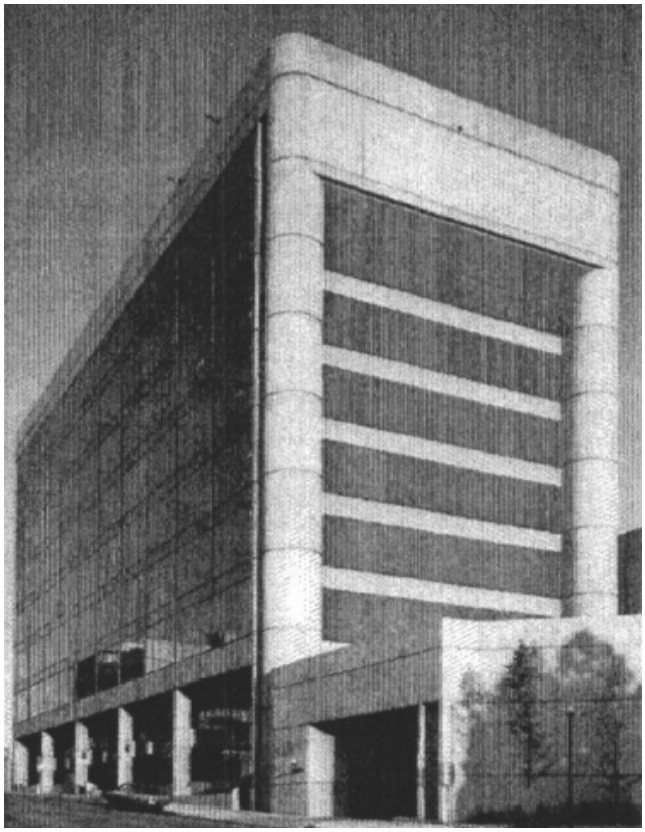

Fig. 2.3. Murrah Building prior to blast (Hayes Jr. et al. 2005)

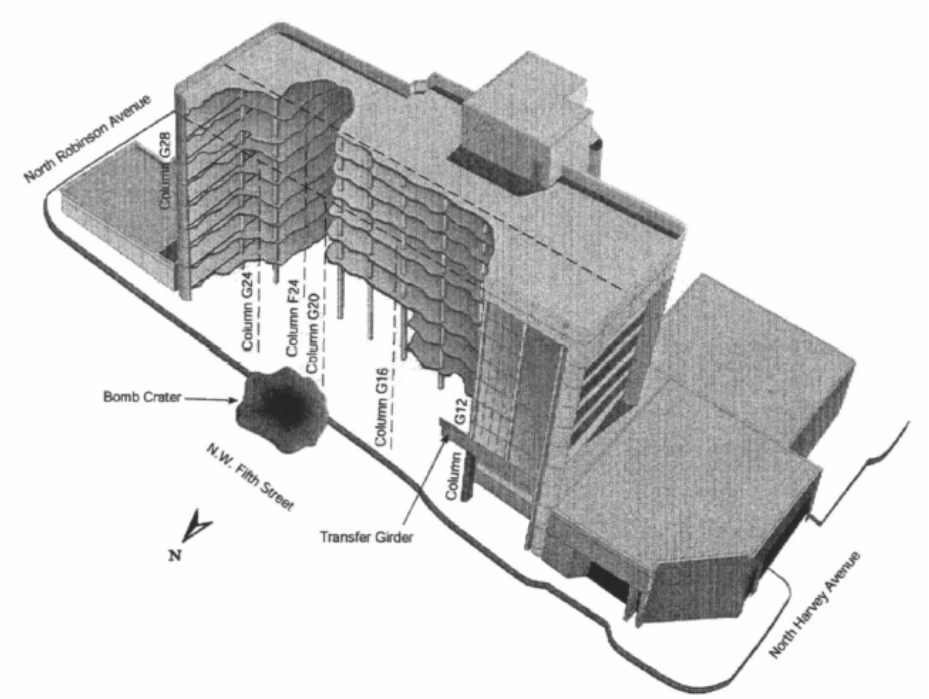

Fig. 2.4. Partially collapsed structure (FEMA 1996)

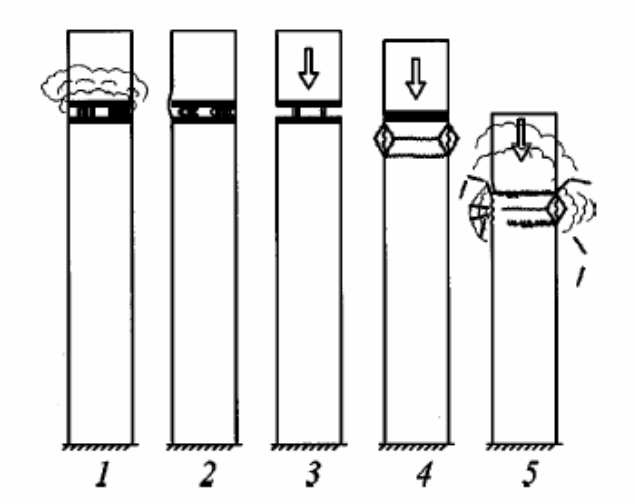

Fig. 2.5. Stages of collapse of the building (floor height exaggerated) (Bazant and Zhou 2002),

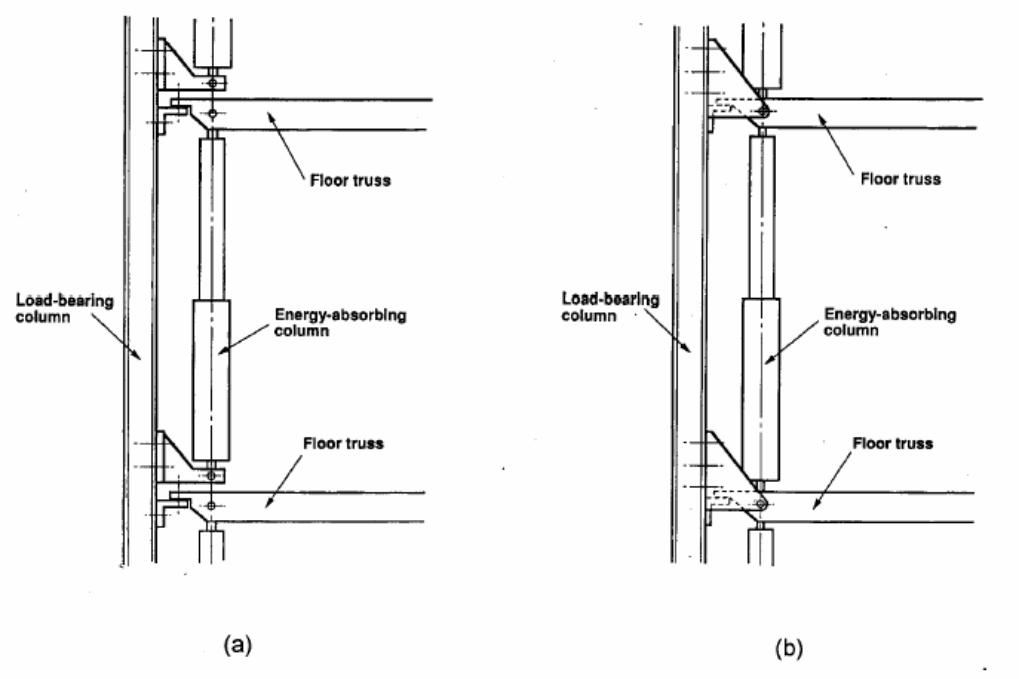

Fig. 2.6. Attachment of energy-absorbing columns (Newland and Cebon 2002)

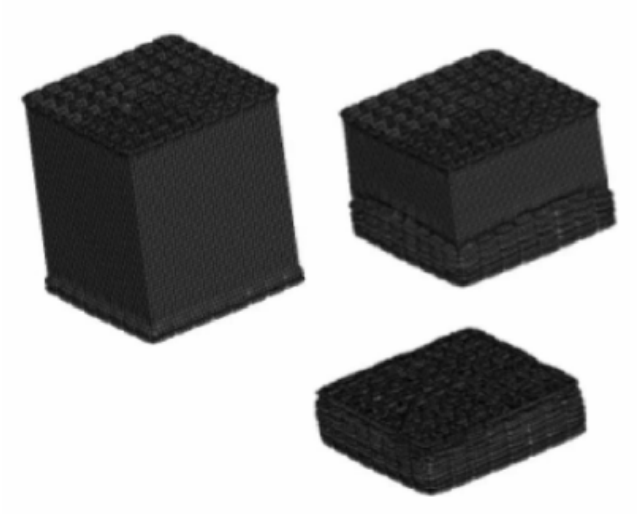

Fig. 2.7. Progressive crush of aluminum-based square cell honeycomb structure (Zhou and Yu 2004)

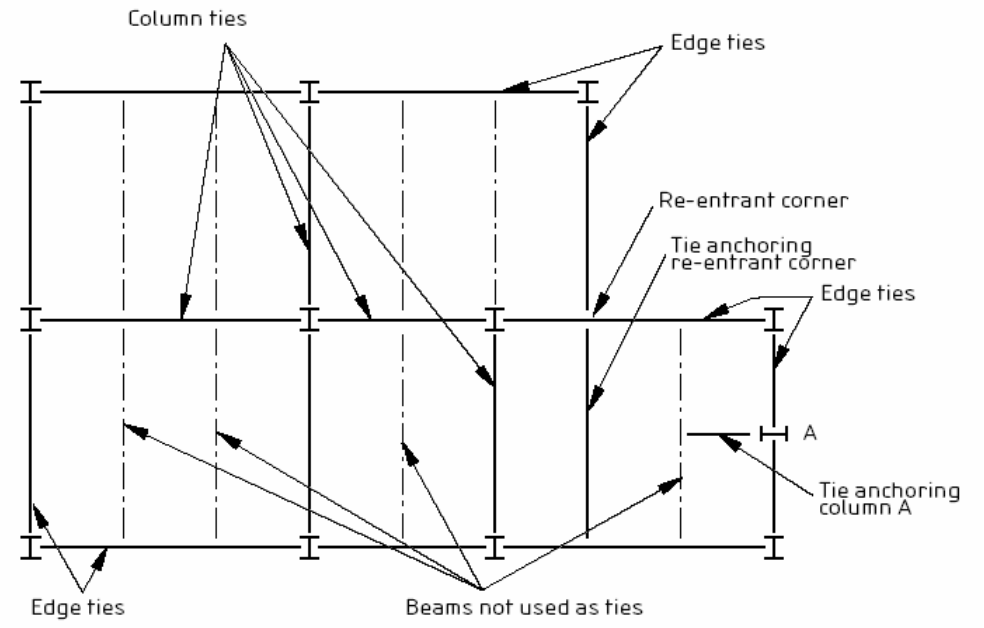

Fig. 2.8. Example of tying the columns of a building (BS5959-1 2000)

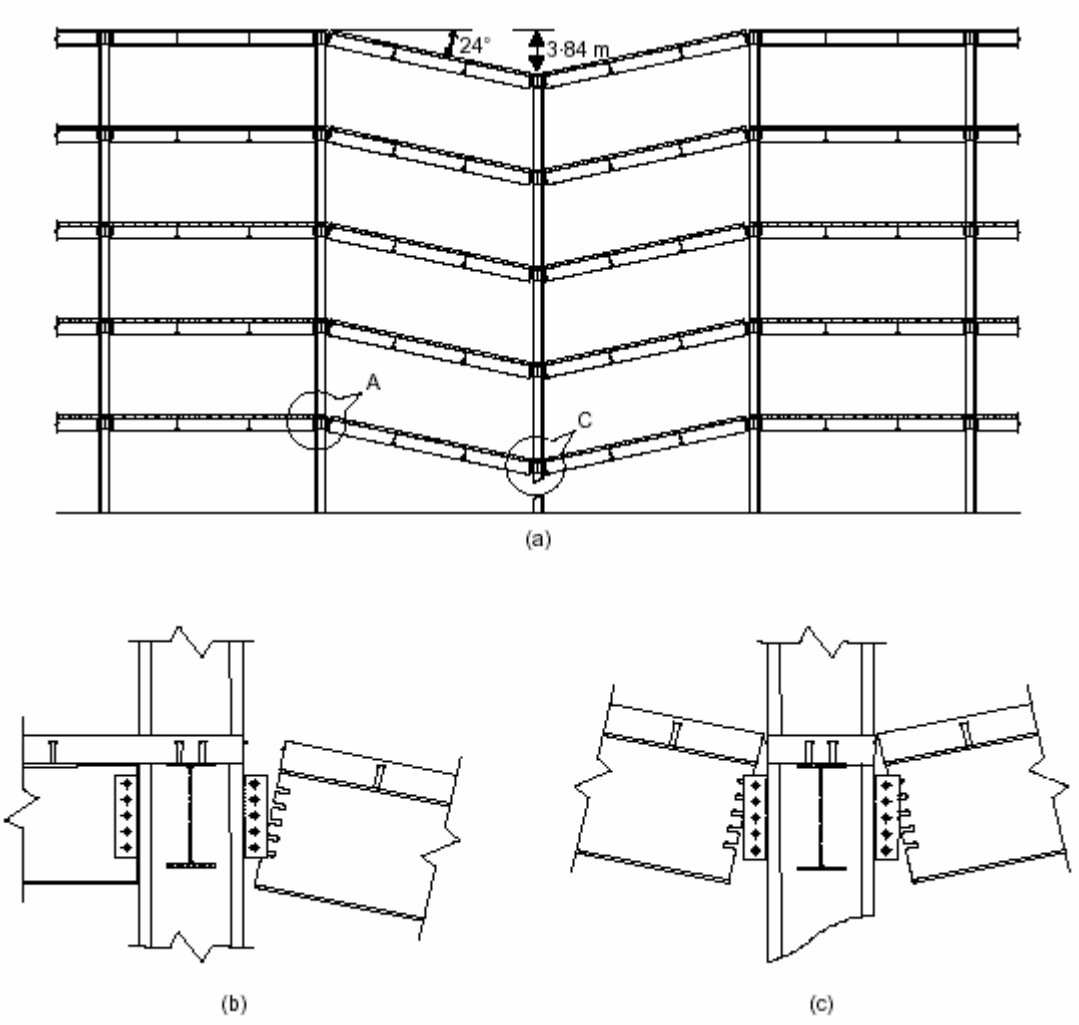

Fig. 2.9. Frame at failure (Byfield and Paramasivam 2007)

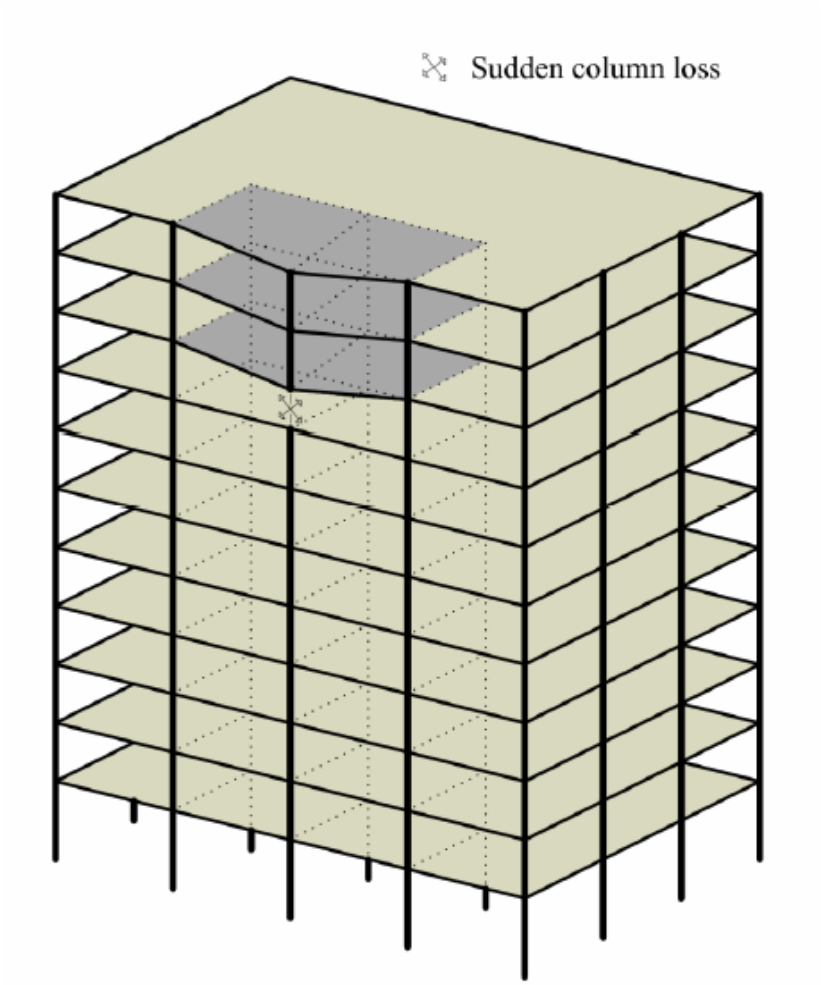

Fig. 2.10. Multi-storey building subject to sudden column loss (Izzuddin et al 2007, 2008)

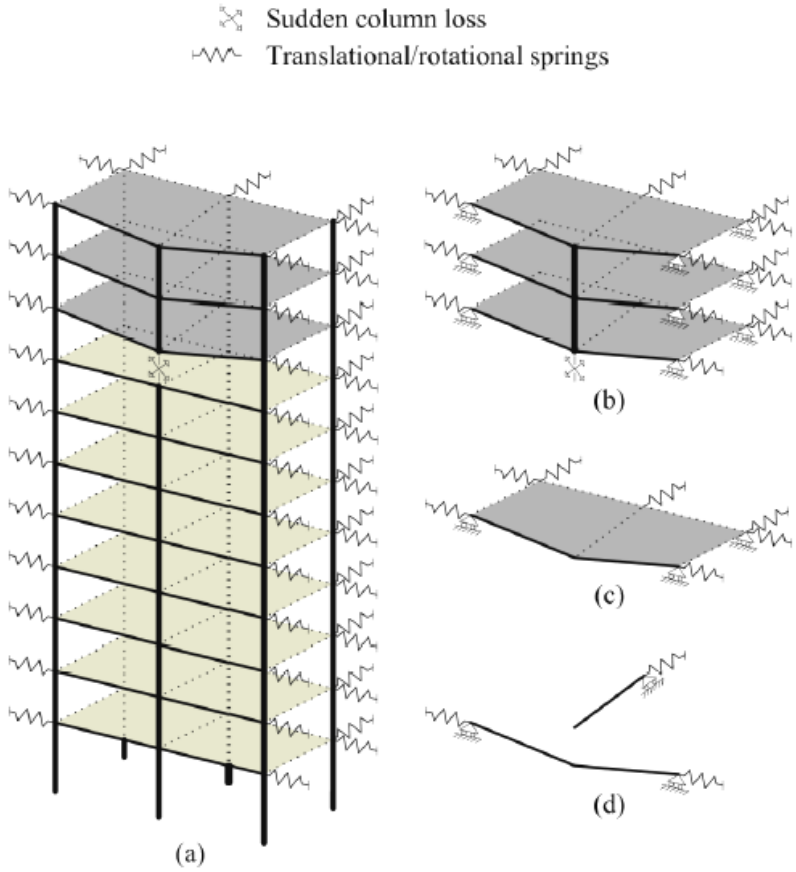

Fig. 2.11. Sub-structural levels for progressive collapse assessment (Izzuddin et al 2007, 2008a)

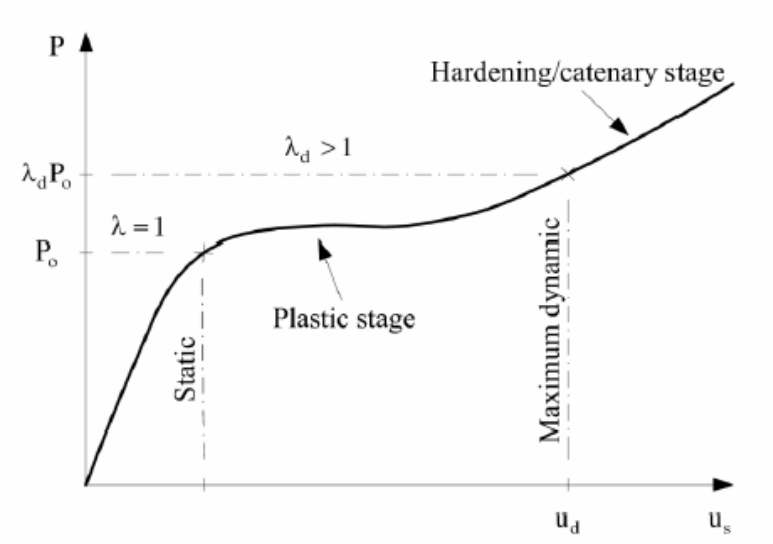

Fig. 2.12. Characteristic nonlinear static response under proportional load ($P = \lambda P_0$) (Izzuddin et al 2007, 2008a)

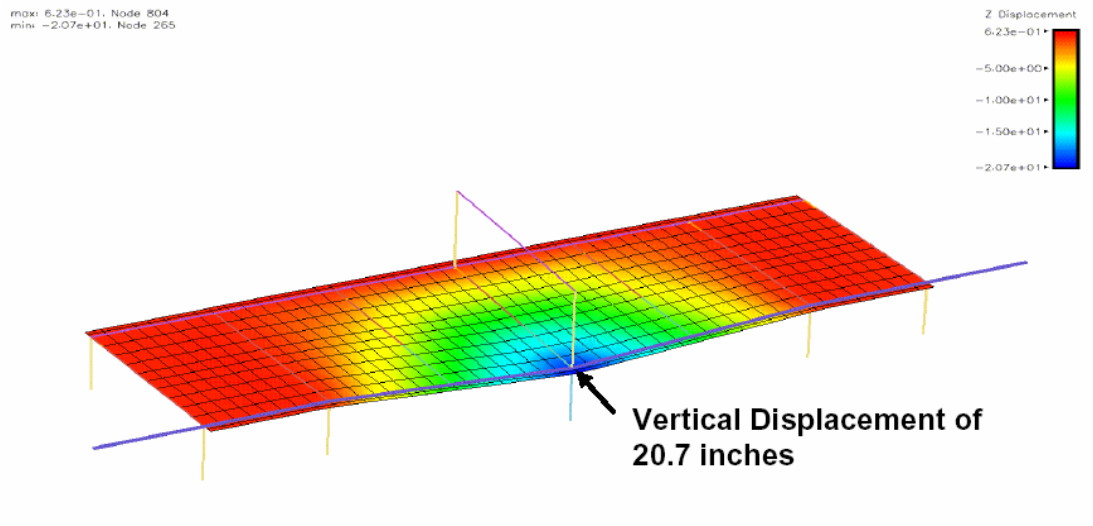

Fig. 2.13. Displacements predicted by analysis (Astaneh-Asl et al. 2001a)

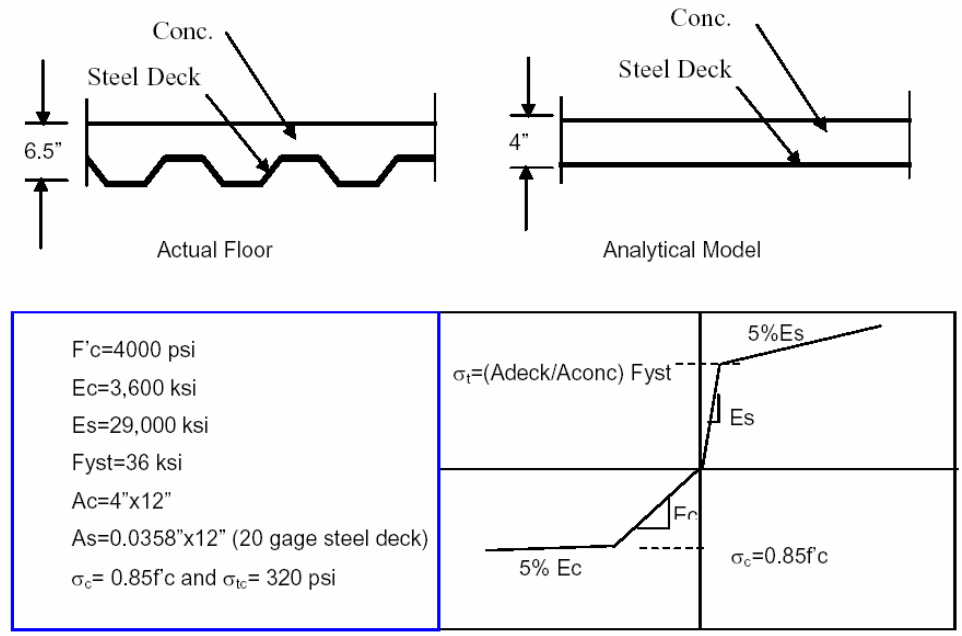

Fig. 2.14. Nonlinear model of steel deck/concrete slab used by Astaneh-Asl et al. (2001a)

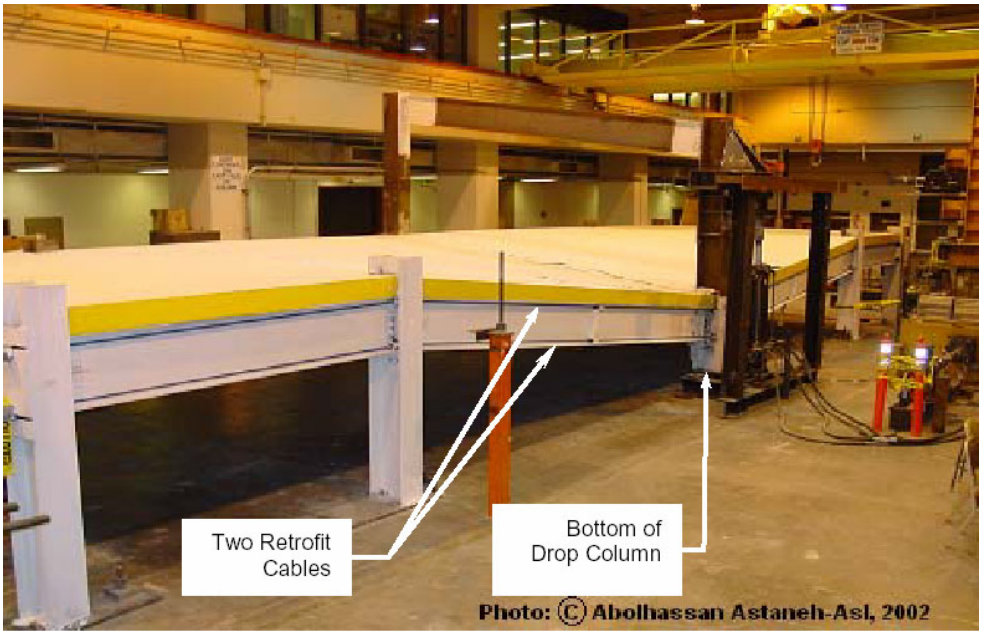

(a) Overall view of test specimen

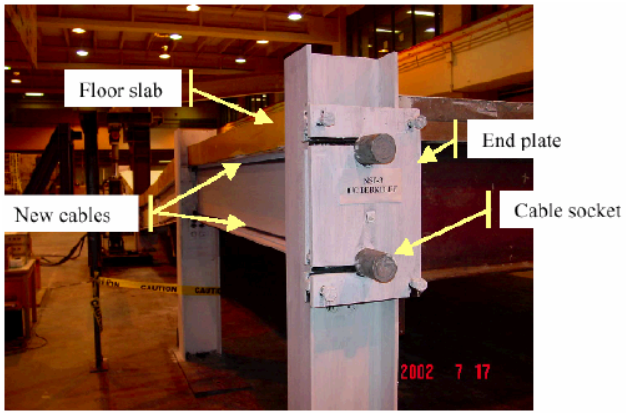

(b) Cable end-fittings at column

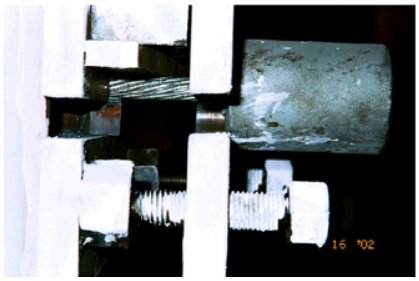

(c) Detail of end-fitting

Fig. 2.15. Sub-structure retrofitted with cable (Tan and Astaneh-Asl 2003)

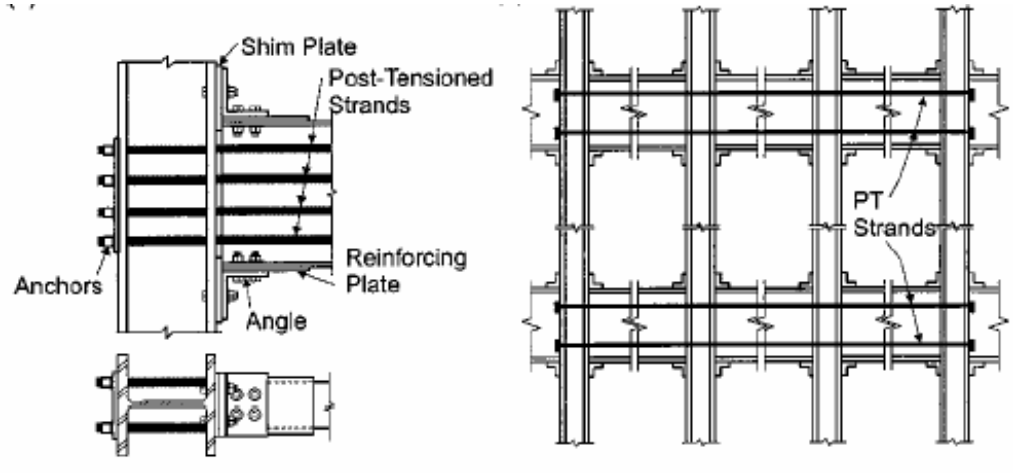

(a) (b)

Fig. 2.16. Schematics of (a) post-tensioned connection and (b) moment resisting frame with post-tensioned connections (Ricles et al. 2002)

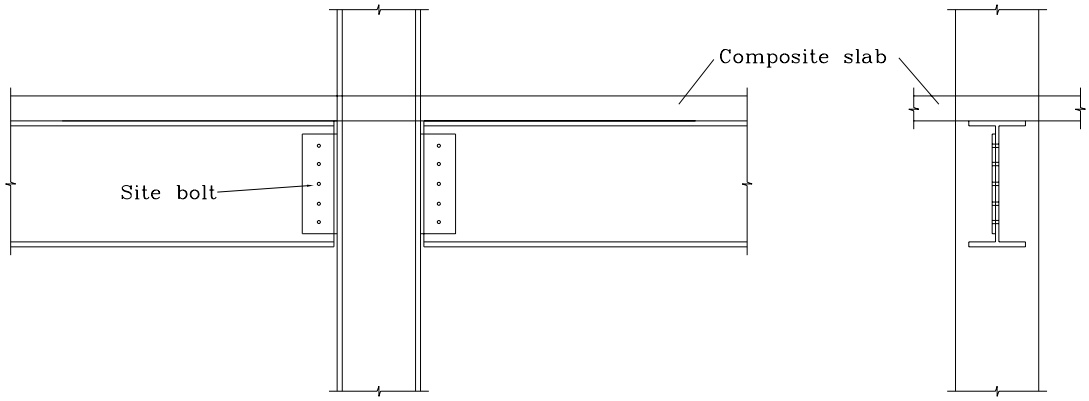

Fig. 2.17. Fin plate connection

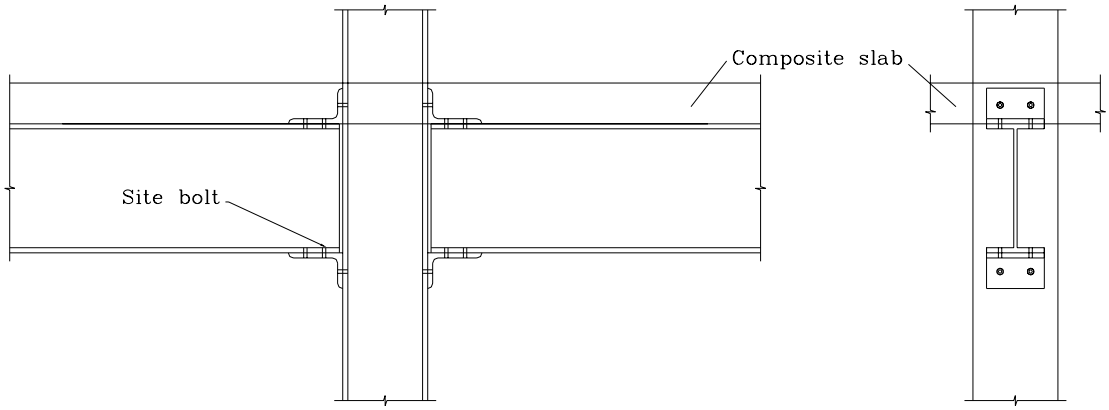

Fig. 2.18. Semi-rigid connection

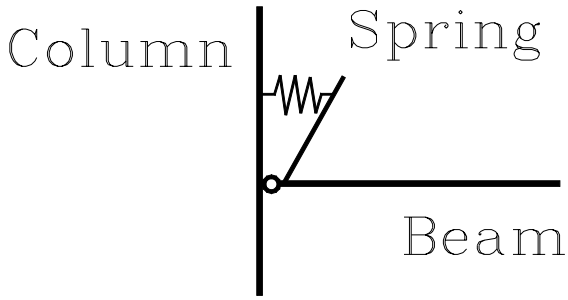

Fig. 2.19. A model for semi-rigid connections

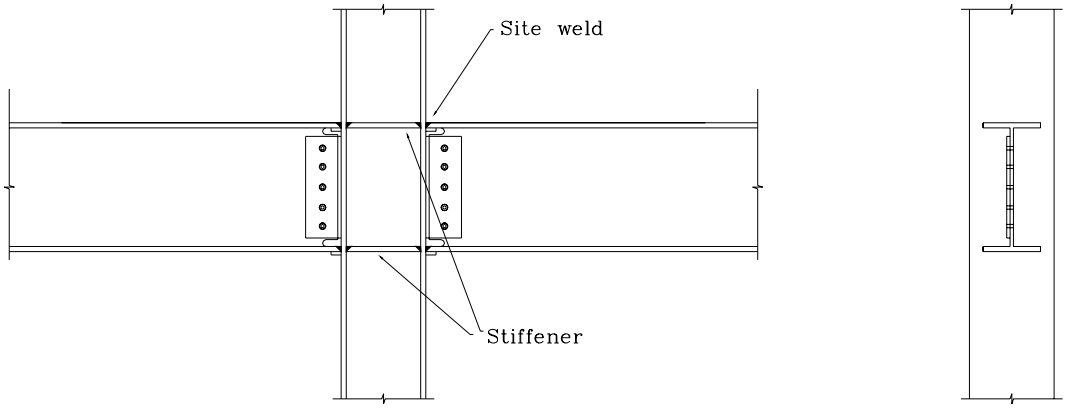

Fig. 2.20. Traditional moment connection detail

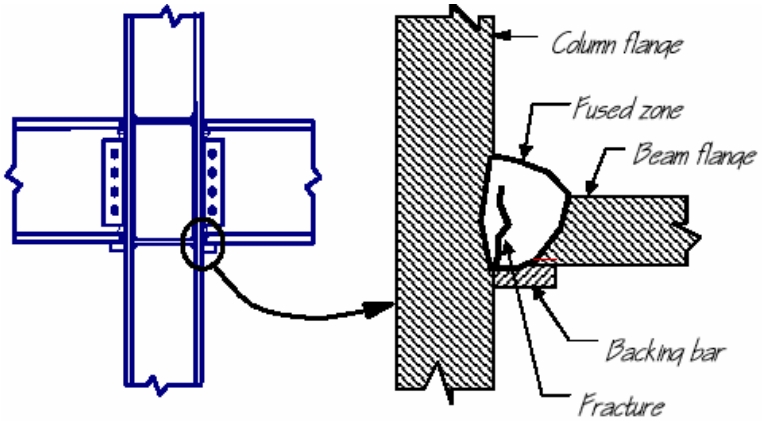

(a) Common zone of fracture initiation in beam-column connection

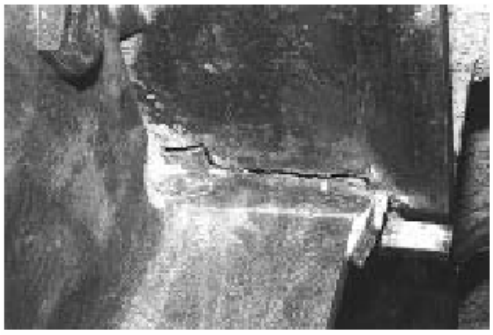

(b) Fracture at fused zone

(c) Column flange "divot" fracture

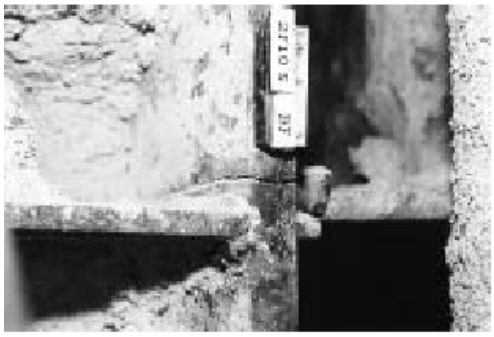

(d) Fractures through column flange

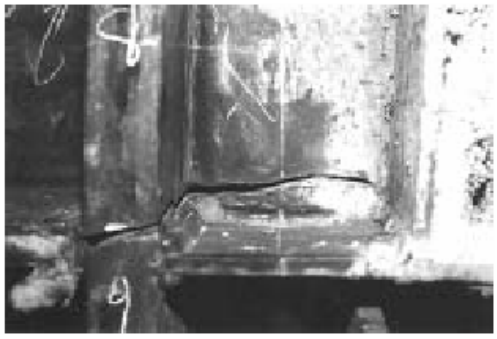

(e) Fracture progresses into column web

(f) Vertical fracture through beam shear plate connection

Fig. 2.21. Fractures in traditional steel moment connection (FEMA. 2000b)

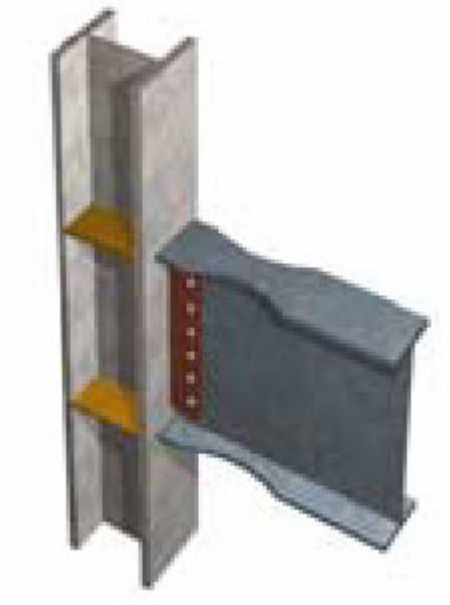

Fig. 2.22. Reduced beam section (RBS) moment connection (Houghton *et al.* 2001)

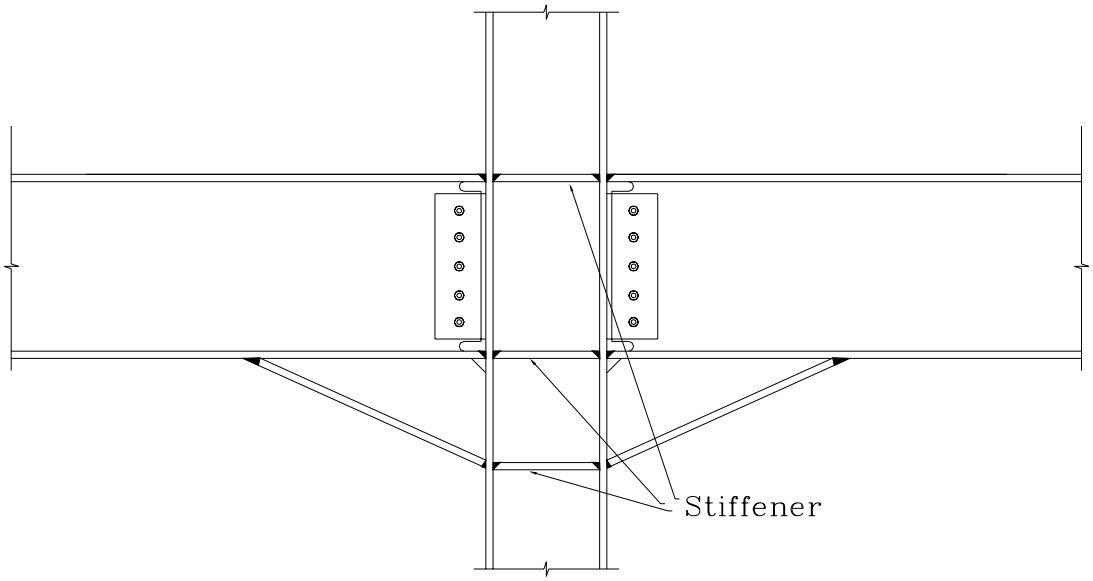

Fig. 2.23. Haunch connection

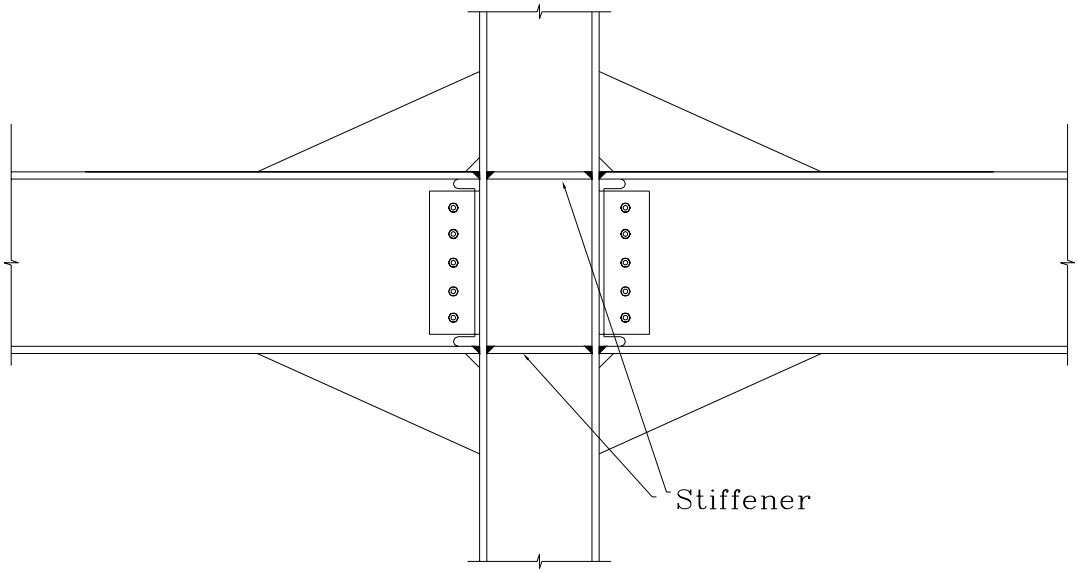

Fig. 2.24. Rib plate connection

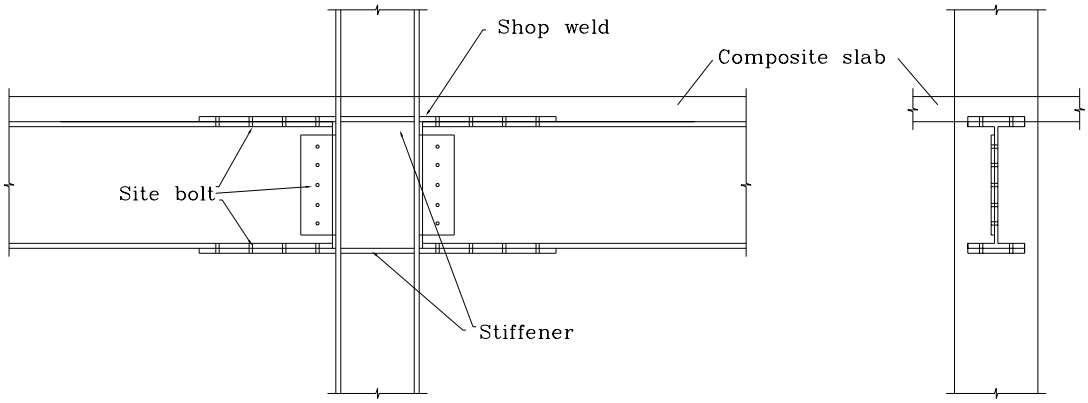

Fig. 2.25. Shop-welded flange plate connection

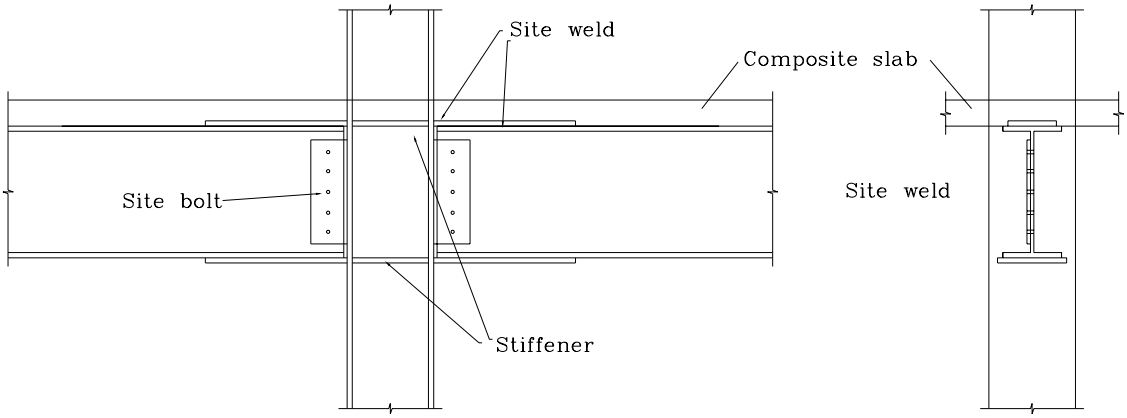

Fig. 2.26. Site-welded flange plate connection

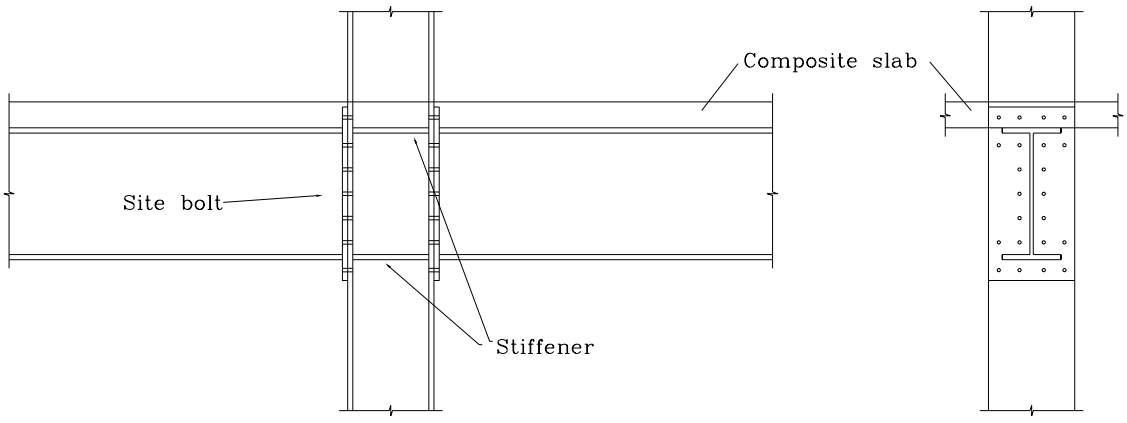

Fig. 2.27. End plate connection

Fig. 2.28. SidePlate connection (Houghton *et al.* 2001)

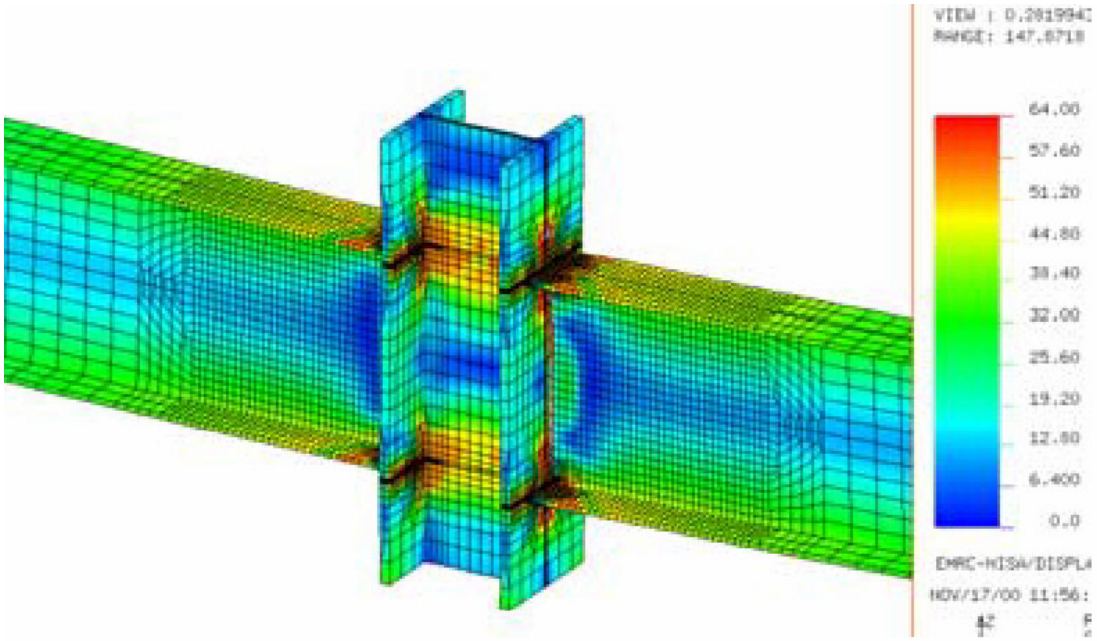

(a) von Mises stress (ksi) of traditional moment connection.

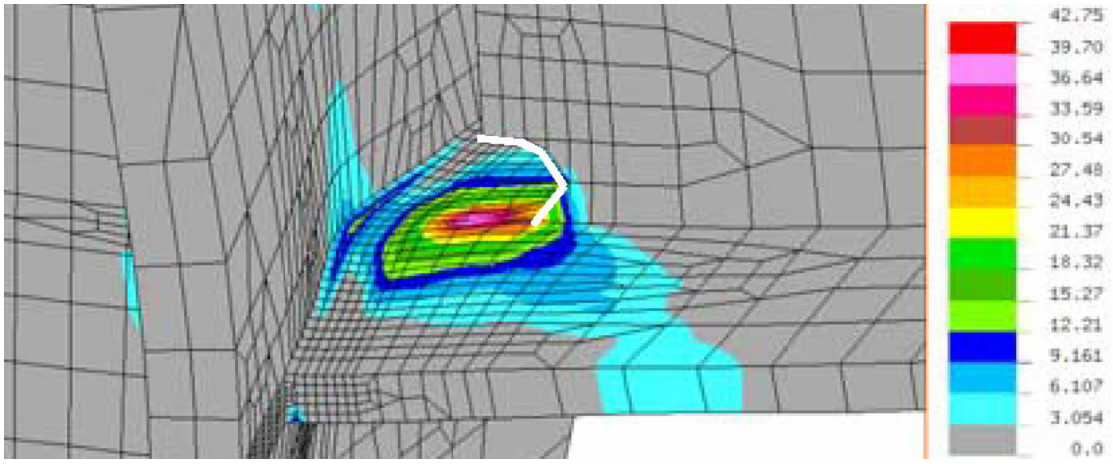

(b) Effective plastic strain at weld root of traditional moment connection

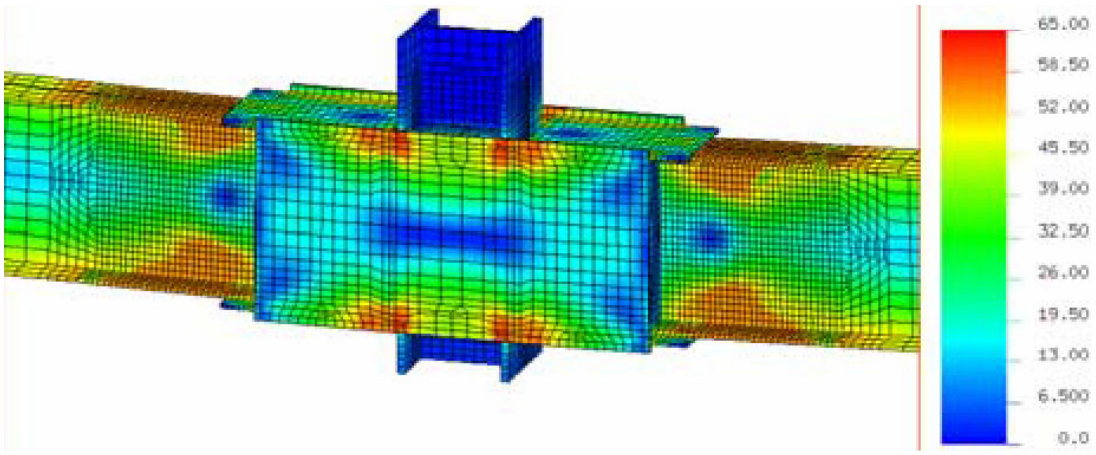

(c) von Mises stress (ksi) of SidePlate moment connection

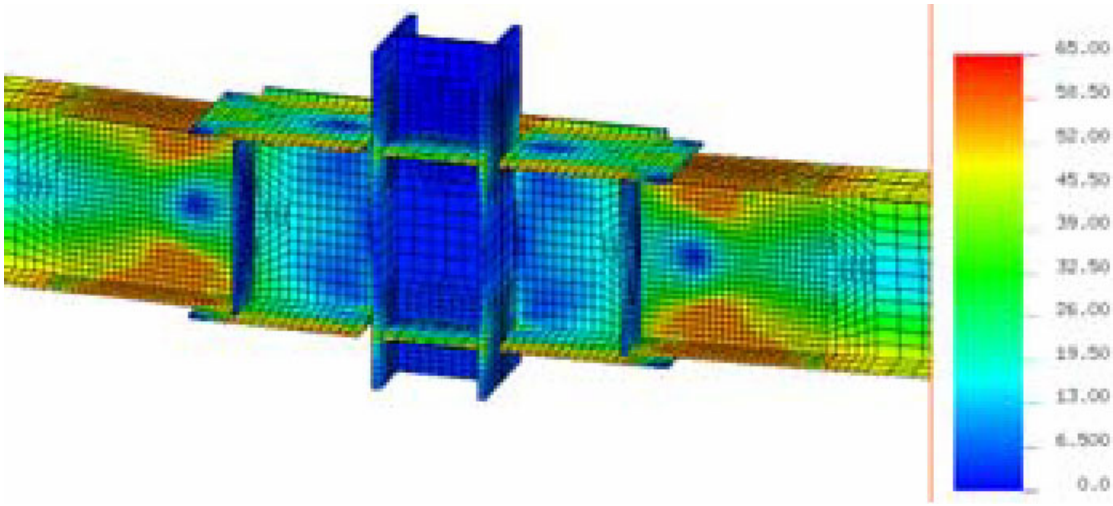

(d) von Mises stress (ksi) of SidePlate moment connection, with one side plate removed

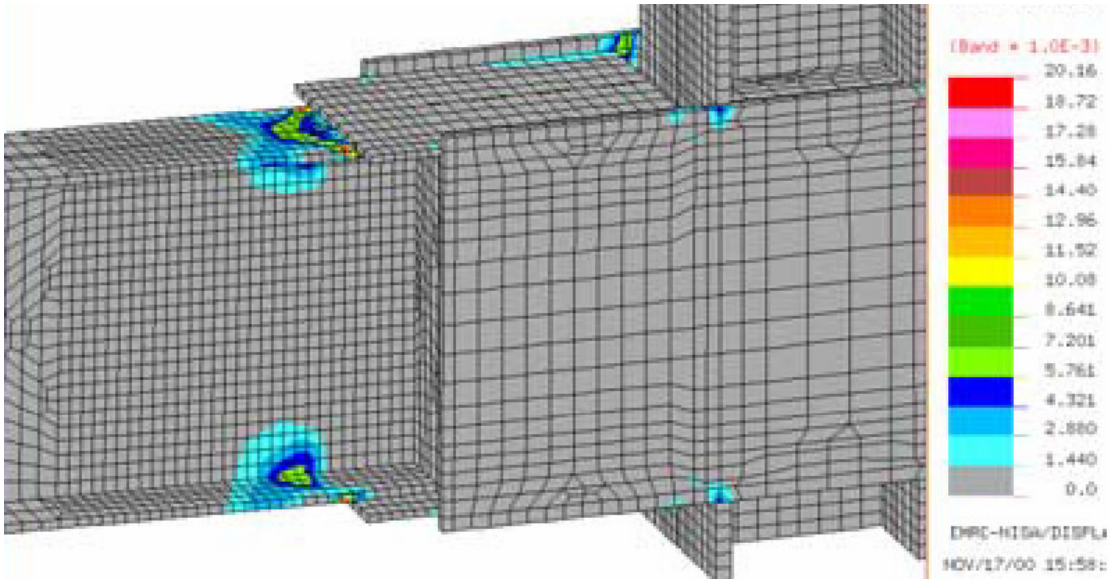

(e) Effective plastic strain of SidePlate moment connection

Fig. 2.29. Stress and strain distributions of traditional moment connection and SidePlate connection (Houghton *et al.* 2001)

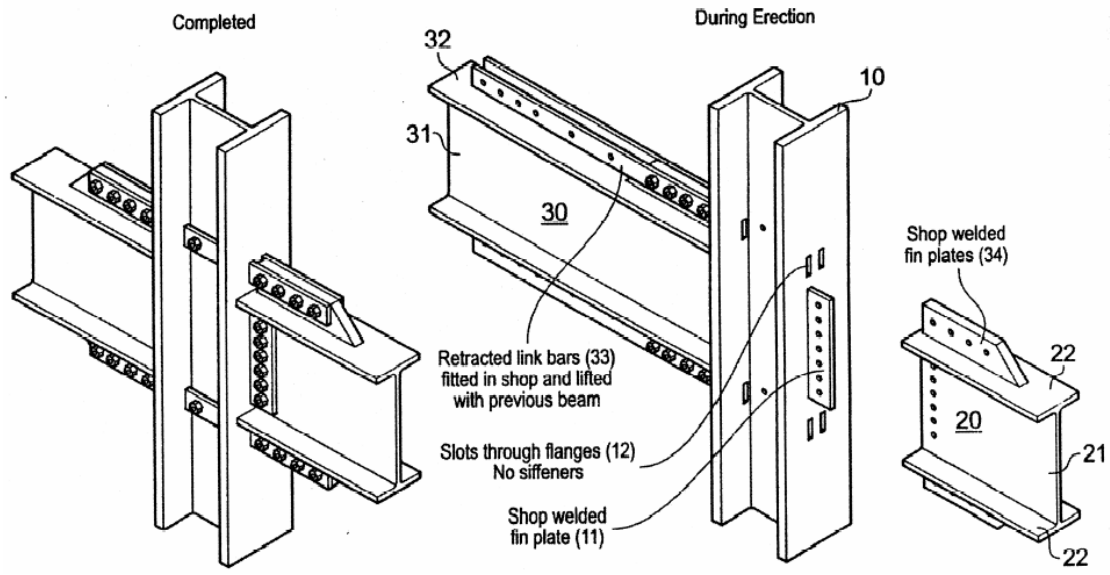

Fig. 2.30. Extreme Event Beam Link Connection (Hoeckman et al. 2005)

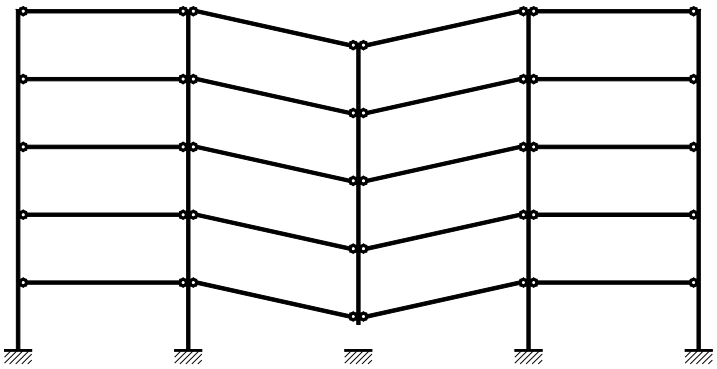

Fig. 3.1. Structural response to removal of column by catenary action

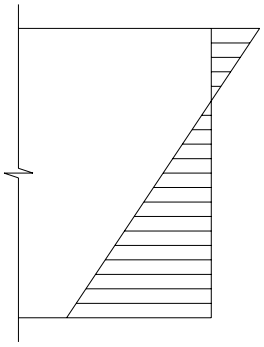

(a) Whole cross-section is elastic with tensile and compressive stresses

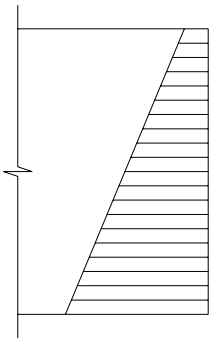

(b) Whole cross-section is elastic with only tensile stress

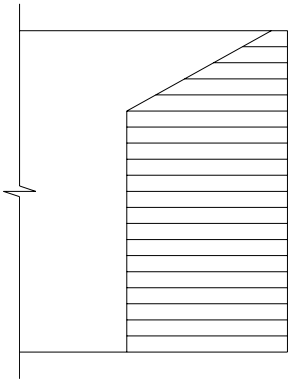

(c) Bottom is yielded without compressive stress in top

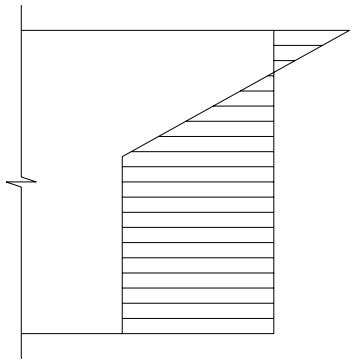

(d) Bottom is yielded with compressive stress in top

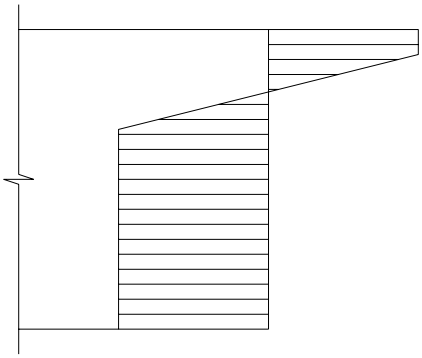

(e) Both bottom and top are yielded with elastic region

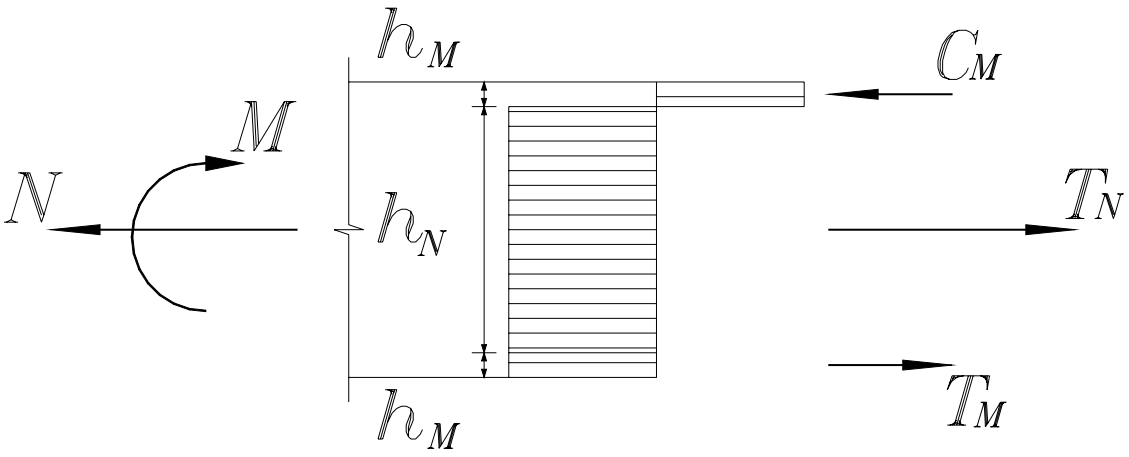

(f) Yielding fully develops in whole cross-section

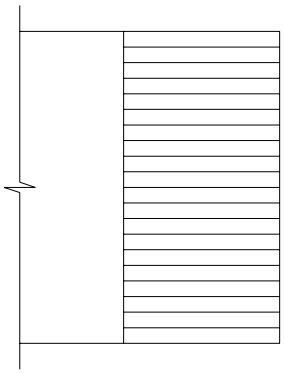

(g) Whole cross-section is in pure tensile plasticity

Fig. 3.2. Stress distribution in cross-section

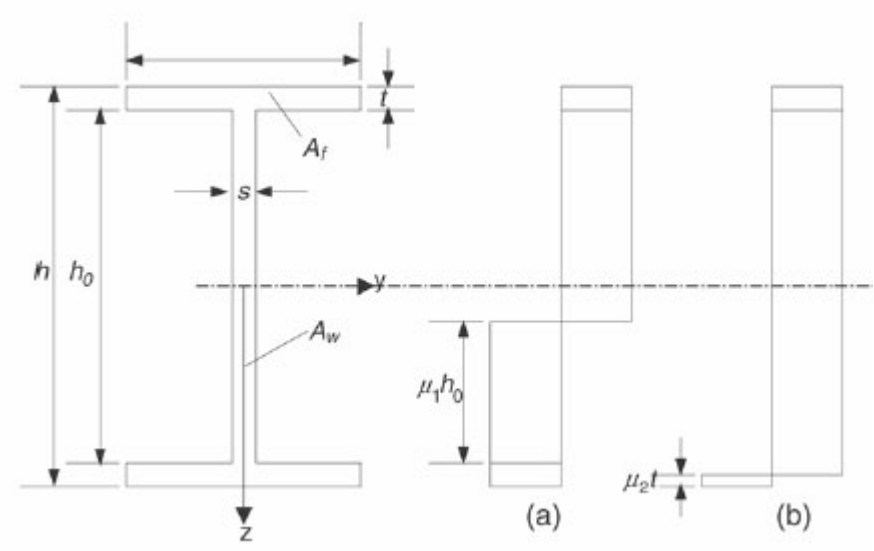

Fig. 3.3. Dimensions and stress diagram of universal beam (Yin and Wang 2005a)

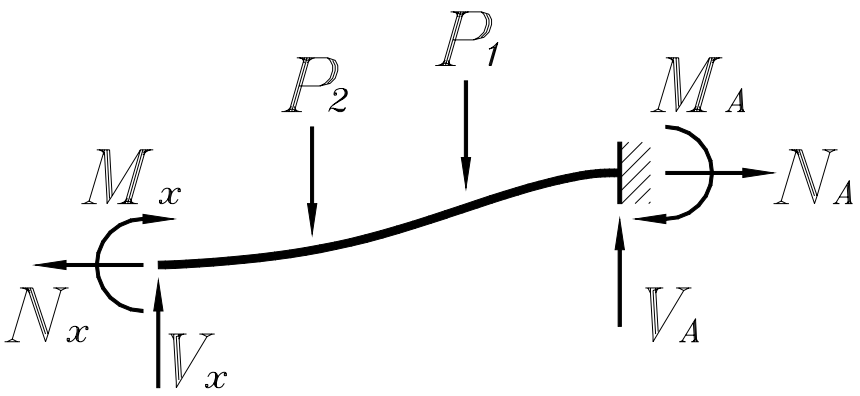

Fig. 3.4. Analysis of catenary action

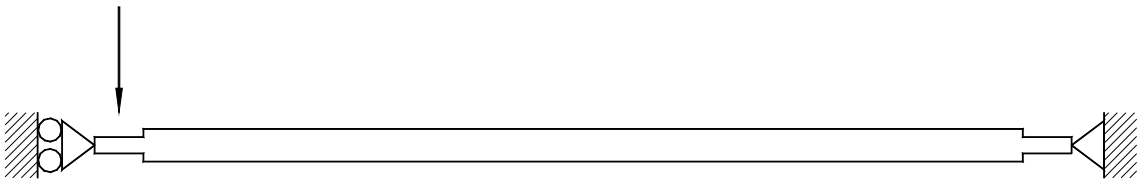

(a) Weak truss ends in Model 3.1

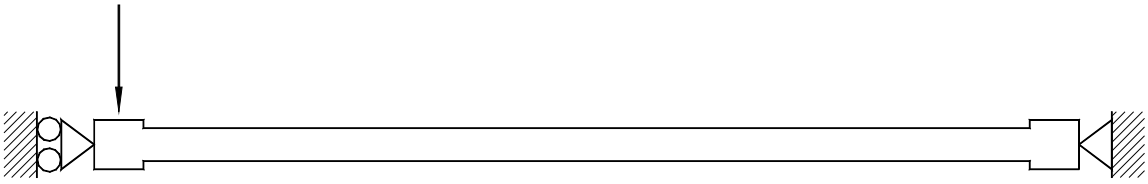

(b) Strong truss ends in Model 3.2

Fig. 3.5. Structures in models

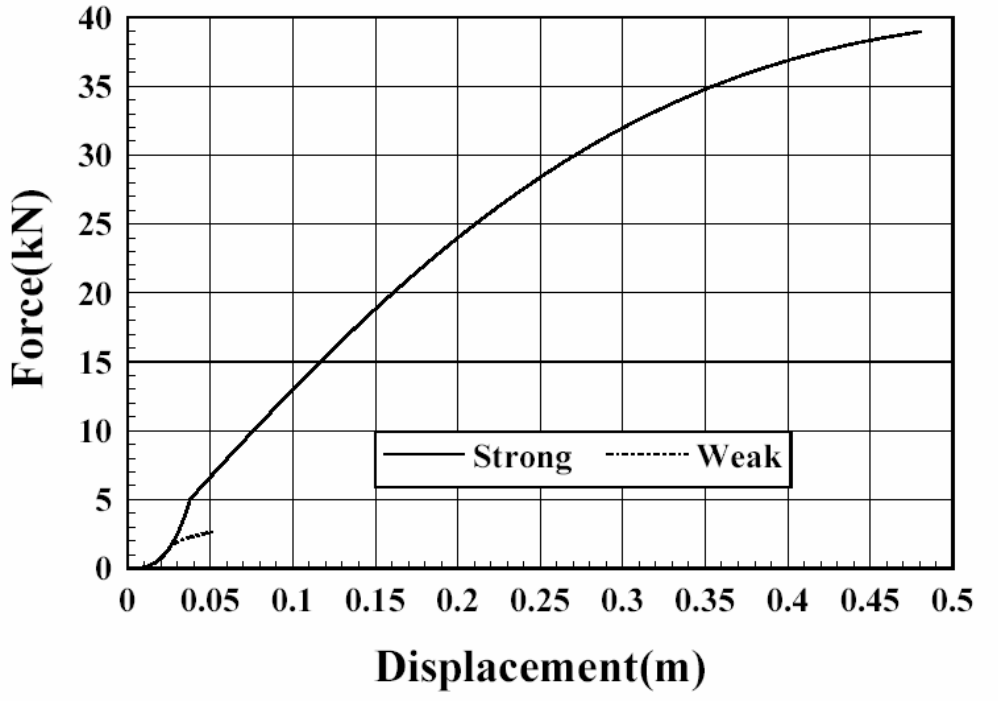

Fig. 3.6. Relationship between load and vertical displacement until failure strain is reached

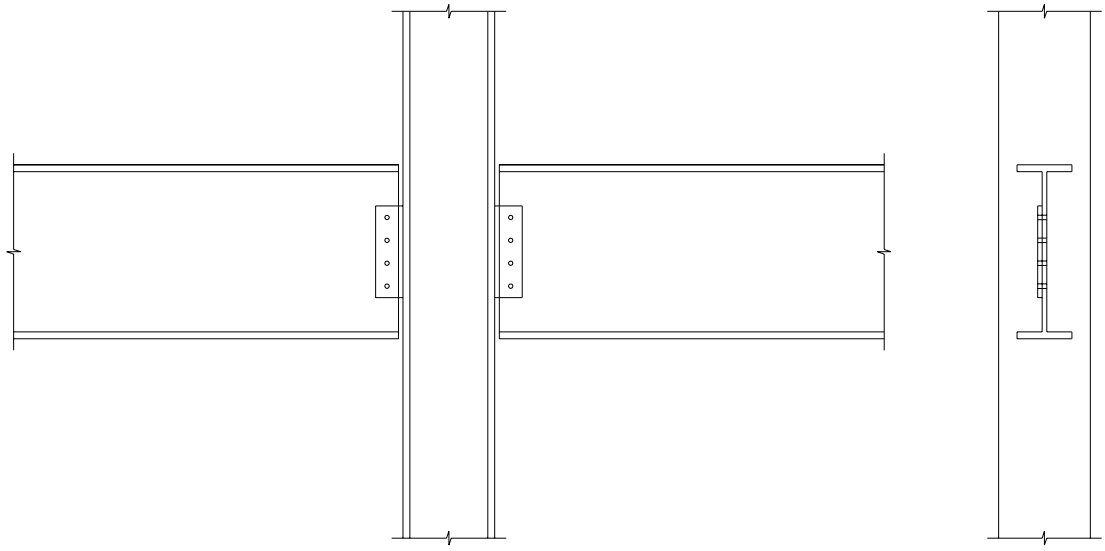

Fig. 3.7. Original design of fin plate joint

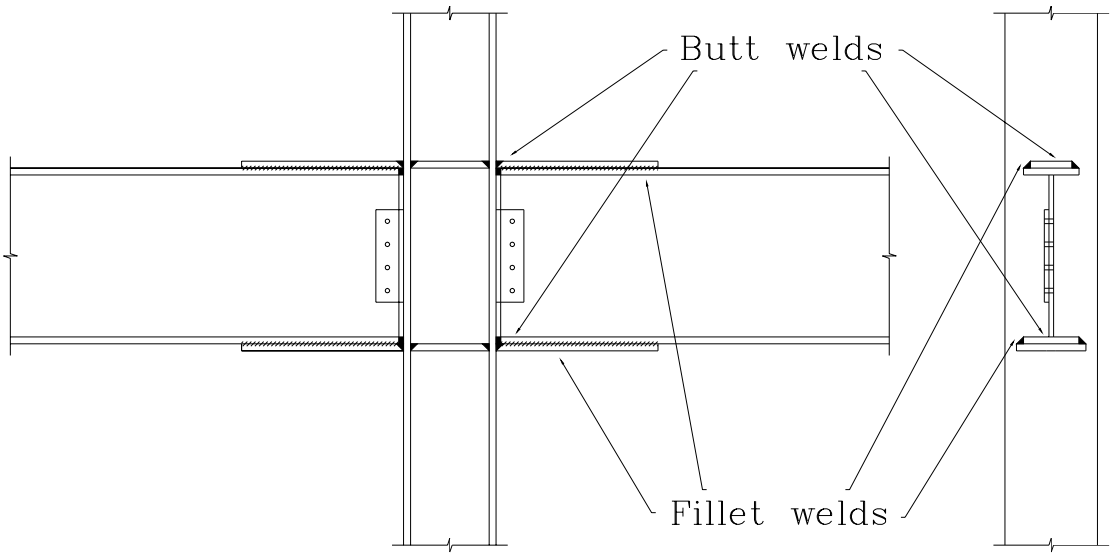

Fig. 3.8. Flange Plate Retrofitting Scheme

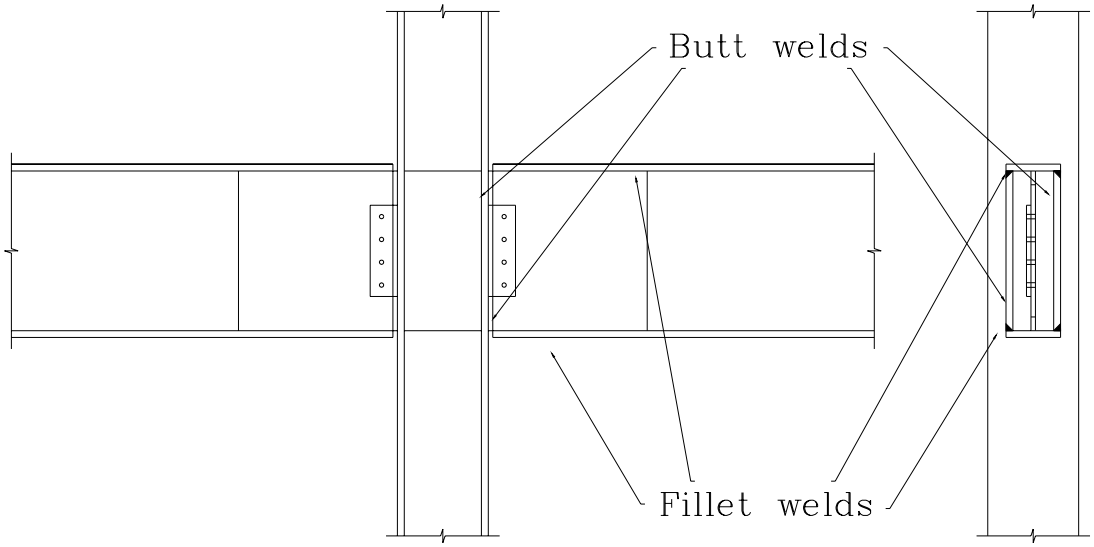

Fig. 3.9. Vertical Plate Retrofitting Scheme

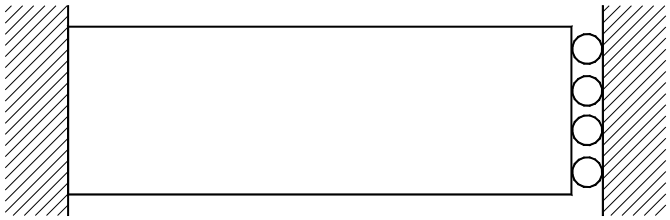

Fig. 4.1. Beam in Model 4.1

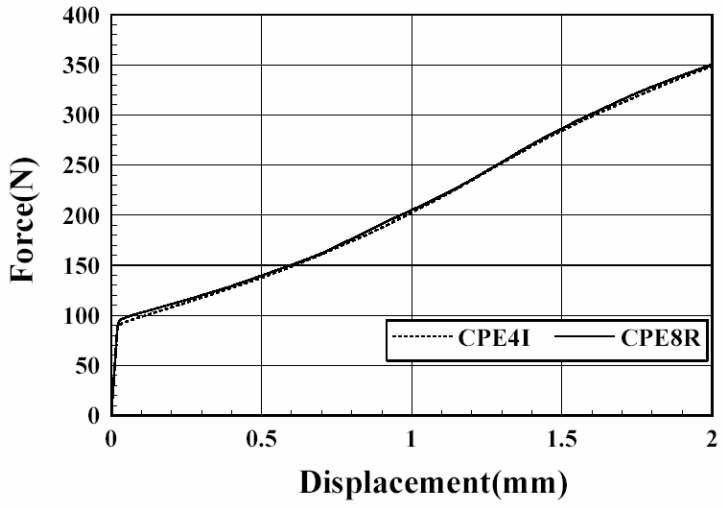

(a) Results of this study by using elements CPE4I and CPE8R

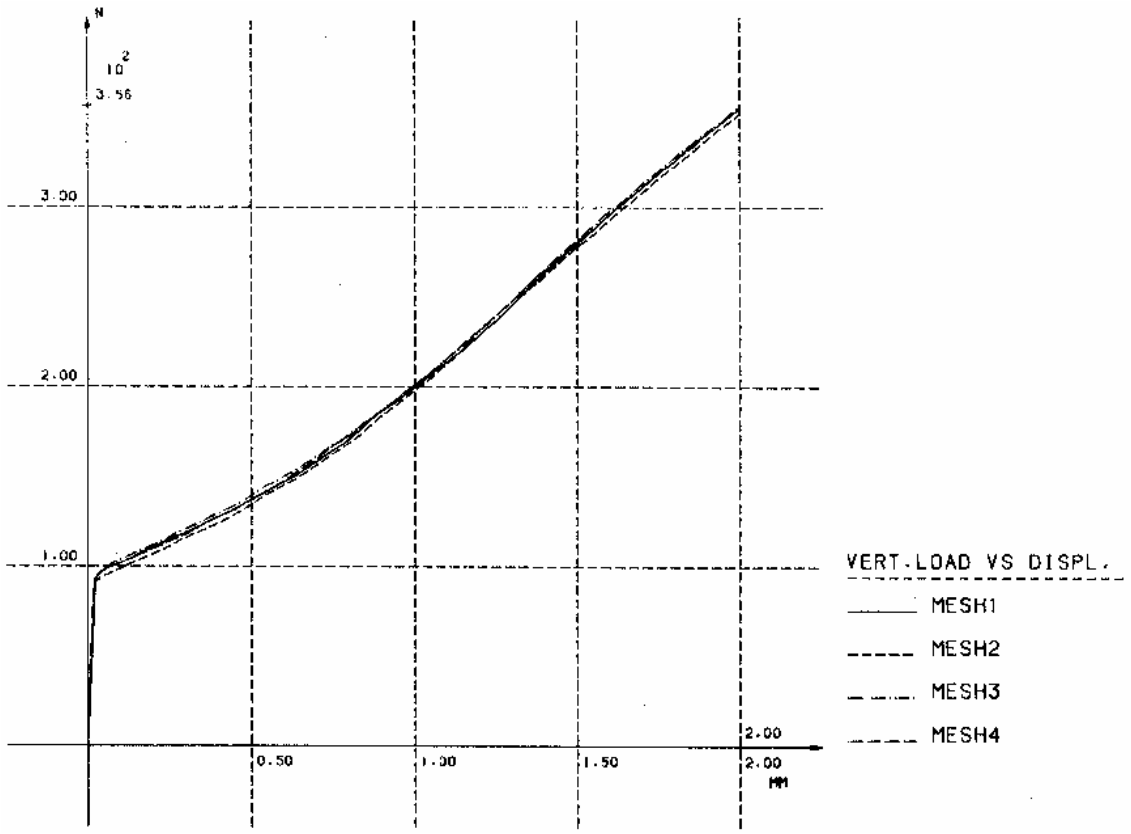

(b) Results of Jetteur and Cescotto (1991)

Fig. 4.2. Computational results of force-displacement relationship

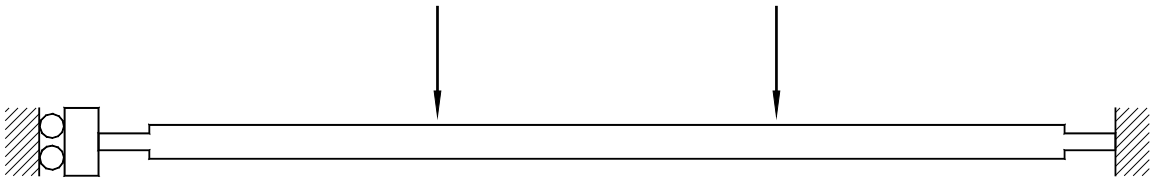

(a) Weak beam ends

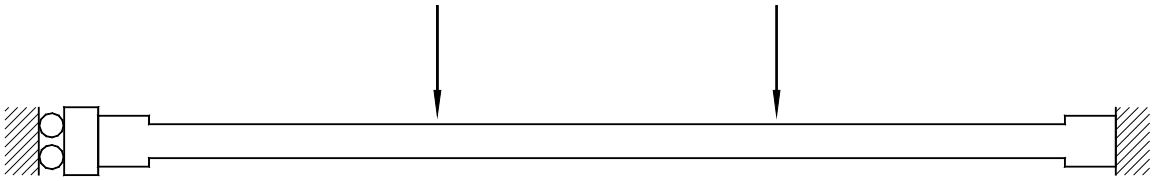

(b) Strong beam ends

Fig. 4.3. Structures in Model 4.2

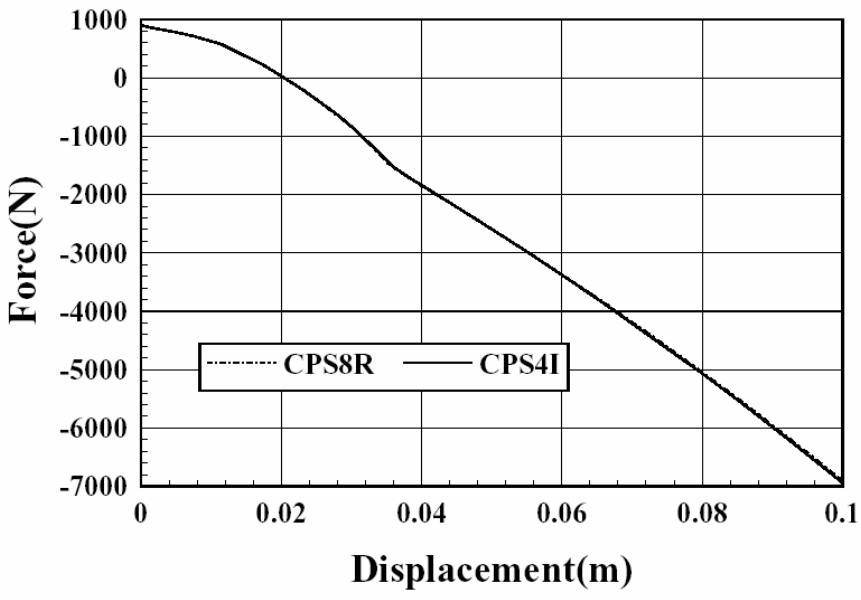

Fig. 4.4. Relationship between vertical reaction and vertical displacement of structure with weak beam end for solid elements CPS8R and CPS4I

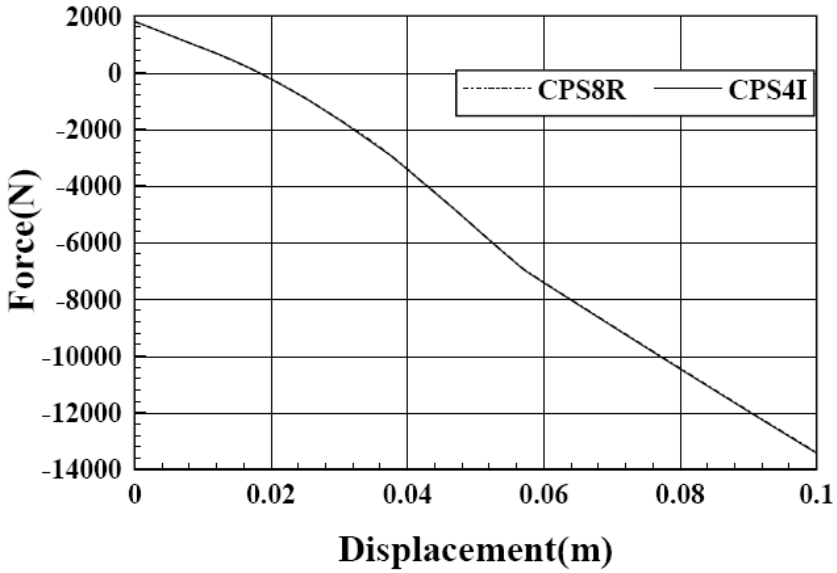

Fig. 4.5. Relationship between vertical reaction and vertical displacement of structure with strong beam ends for solid elements CPS8R and CPS4I

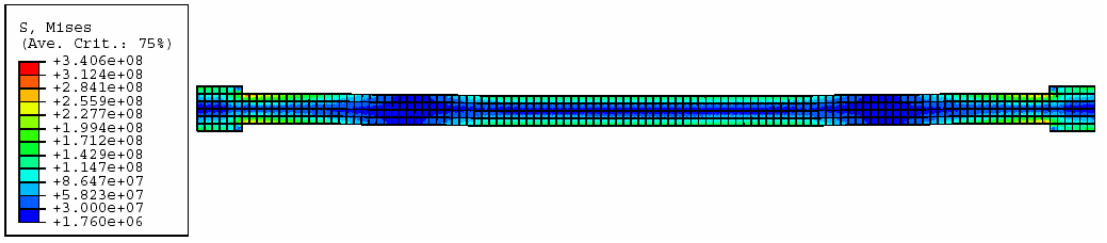

(a) In whole model when displacement =0

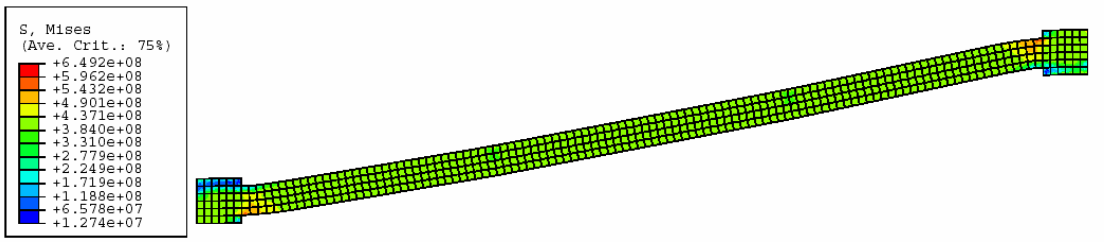

(b) In whole model when displacement =0.1m

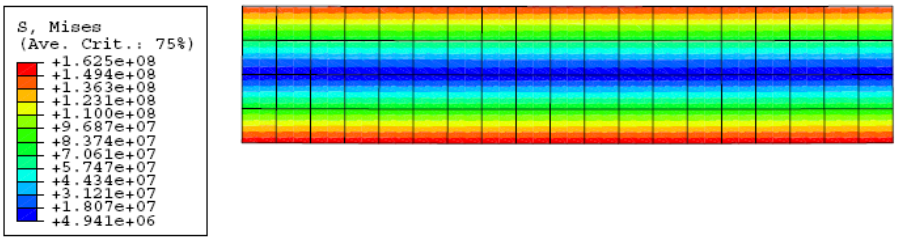

(c) In short middle segment when displacement =0

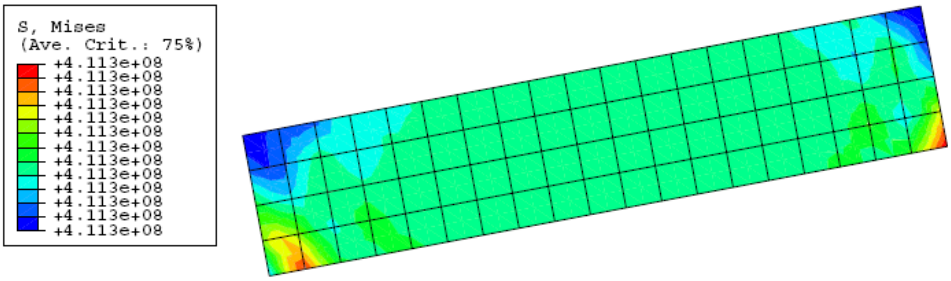

(d) In short middle segment when displacement =0.1m

Fig. 4.6. Mises stress distribution of beam with strong ends

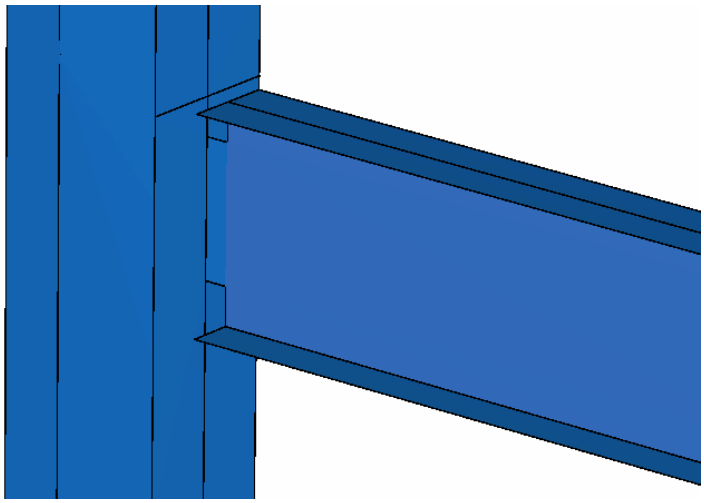

Fig. 4.7. Geometry of original connection in Model 4.3

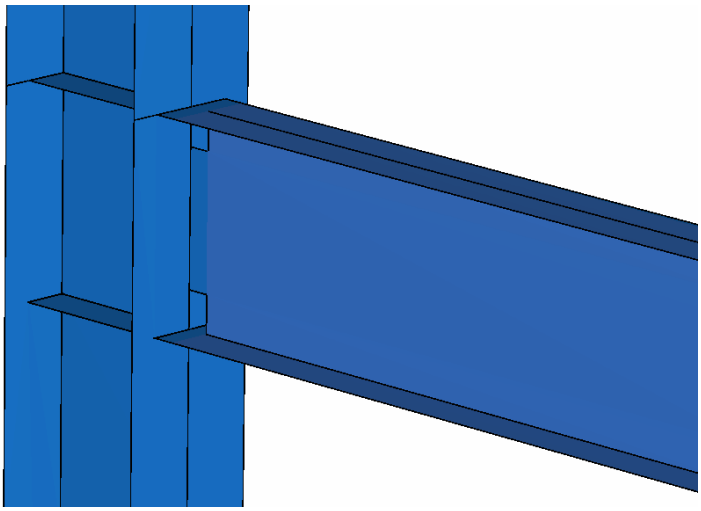

Fig. 4.8. Geometry of connection retrofitted by Flange Plate Scheme in Model 4.3

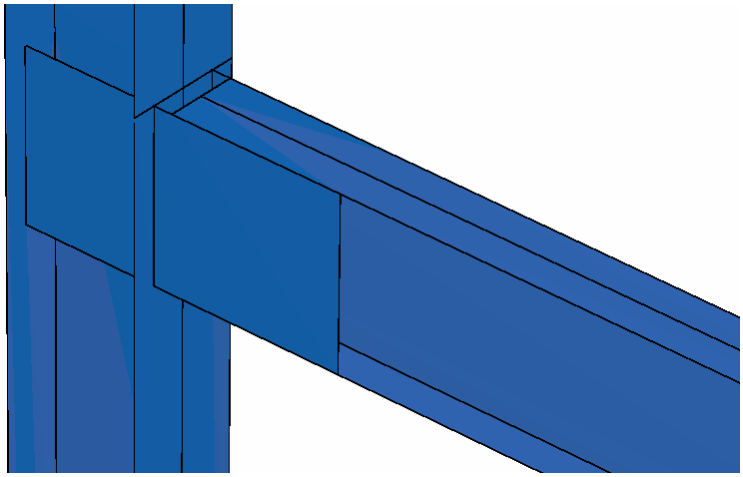

Fig. 4.9. Geometry of connection retrofitted by Vertical Plate Scheme in Model 4.3

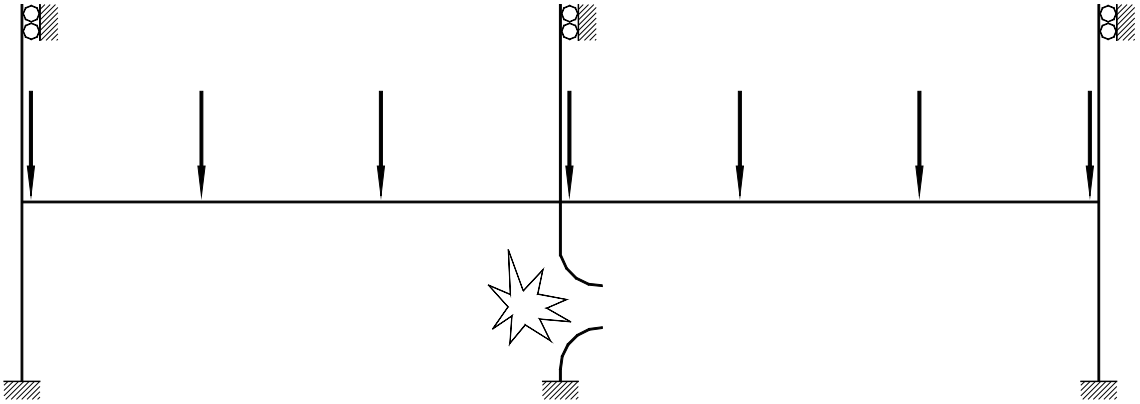

Fig. 4.10. Frame investigated in Model 4.3

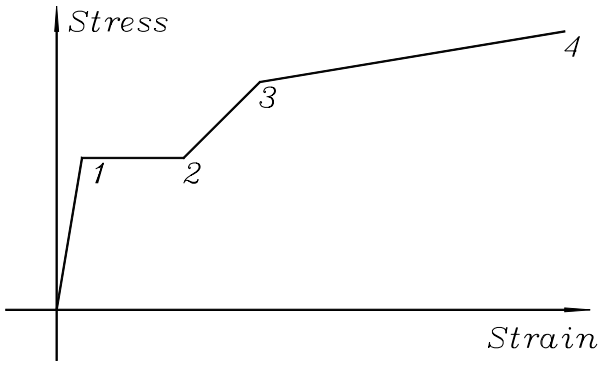

Fig. 4.11. Stress-strain relationship

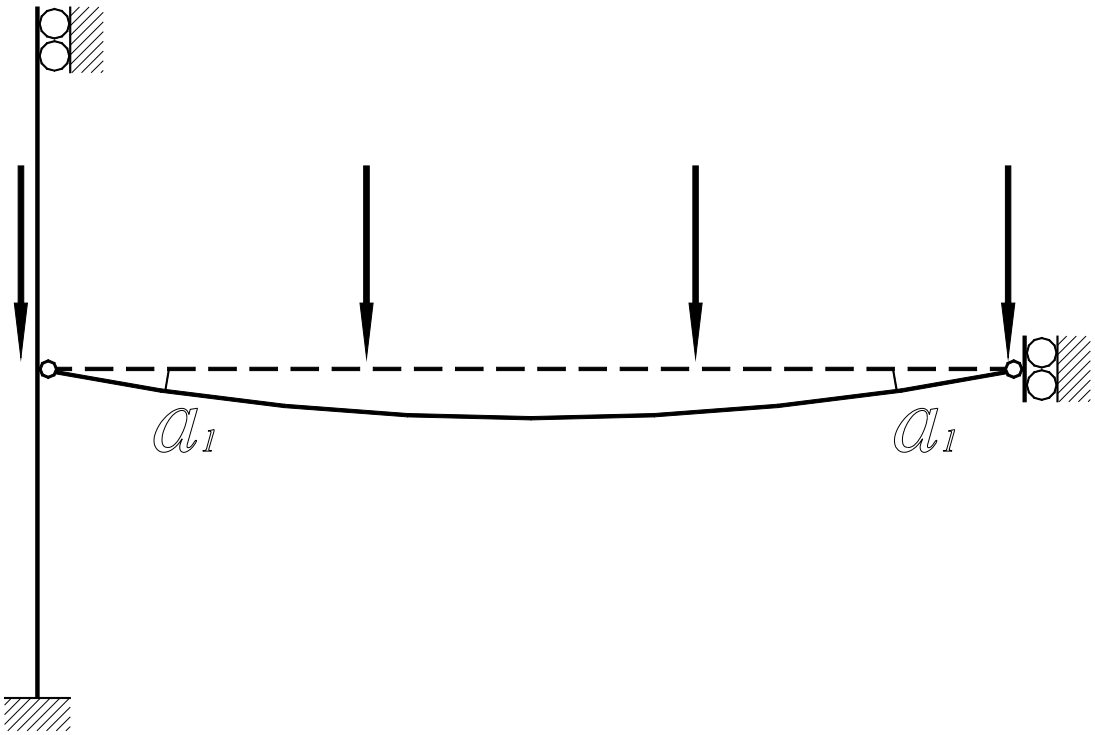

(a) Real pin-connected structure

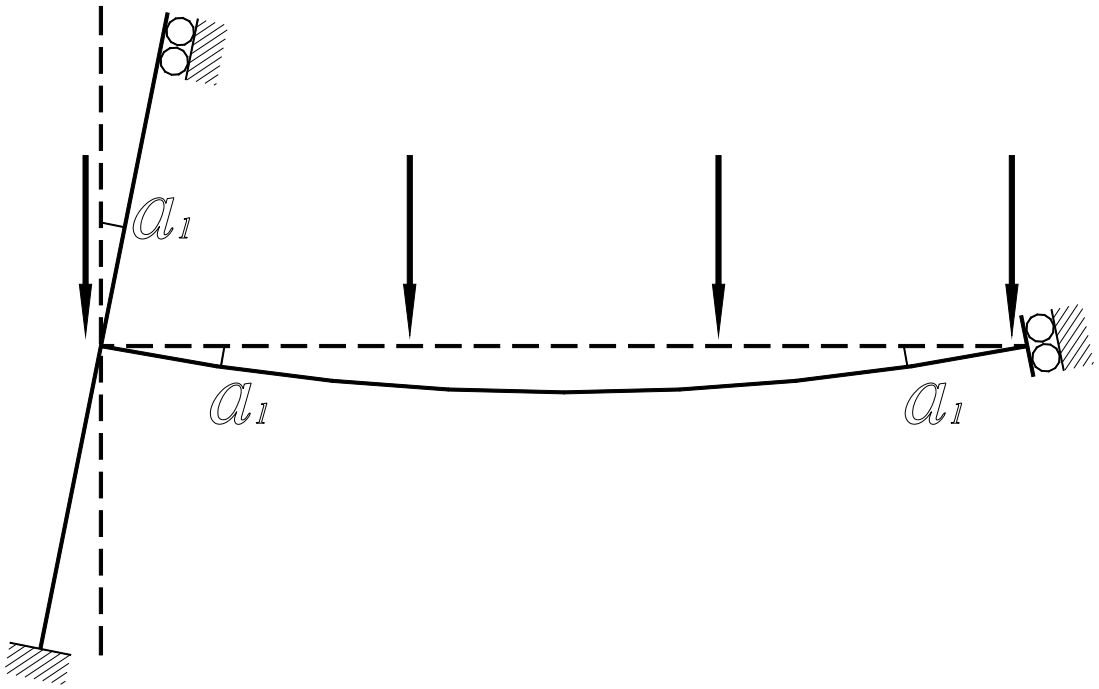

(b) Equivalent fixed-connected structure

Fig. 4.12. Retrofitted structure at the end of first step

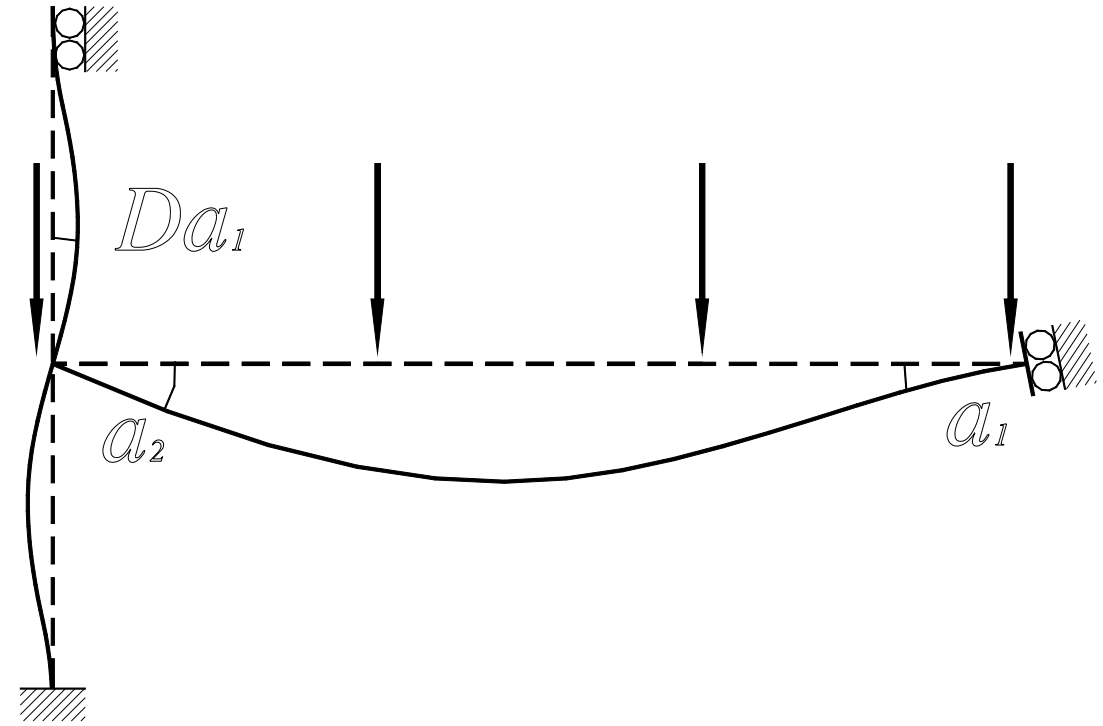

(a) Real structure

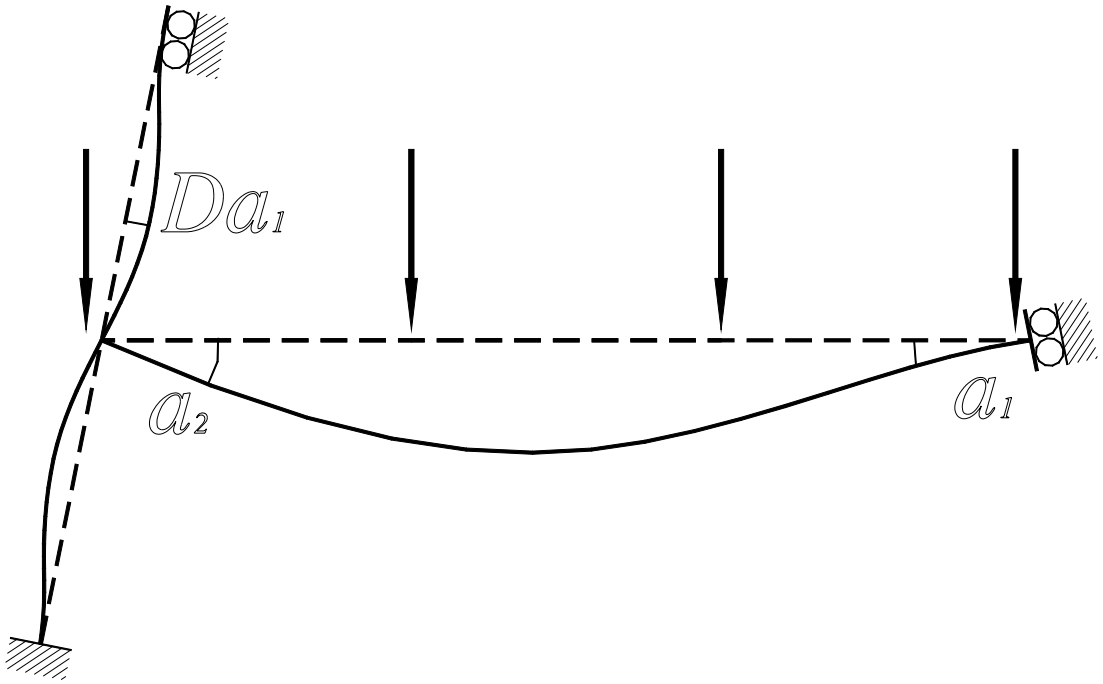

(b) Equivalent structure

Fig. 4.13. Retrofitted structure at the end of second step

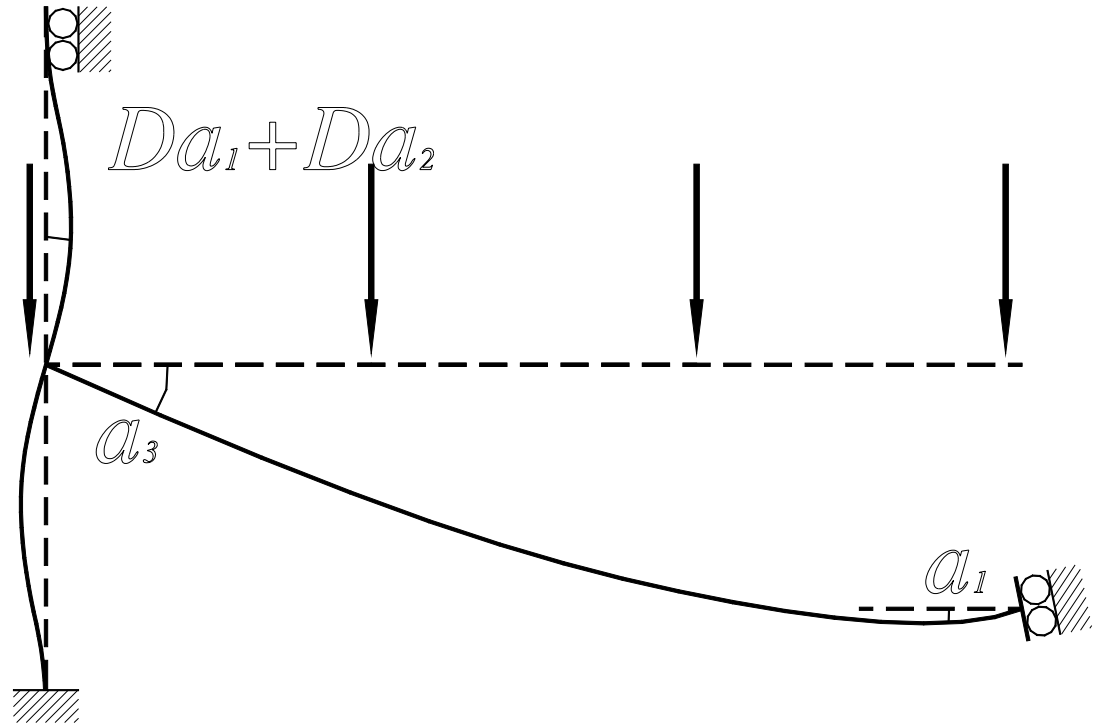

(a) Real structure

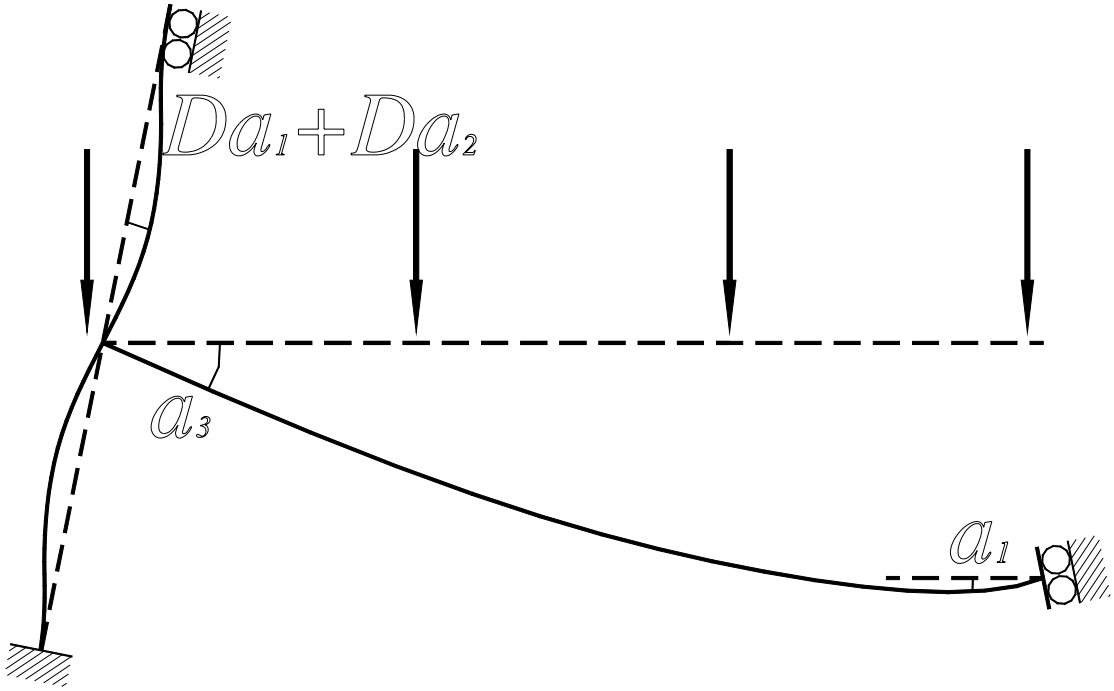

(b) Equivalent structure

Fig. 4.14. Retrofitted structure at the end of third step

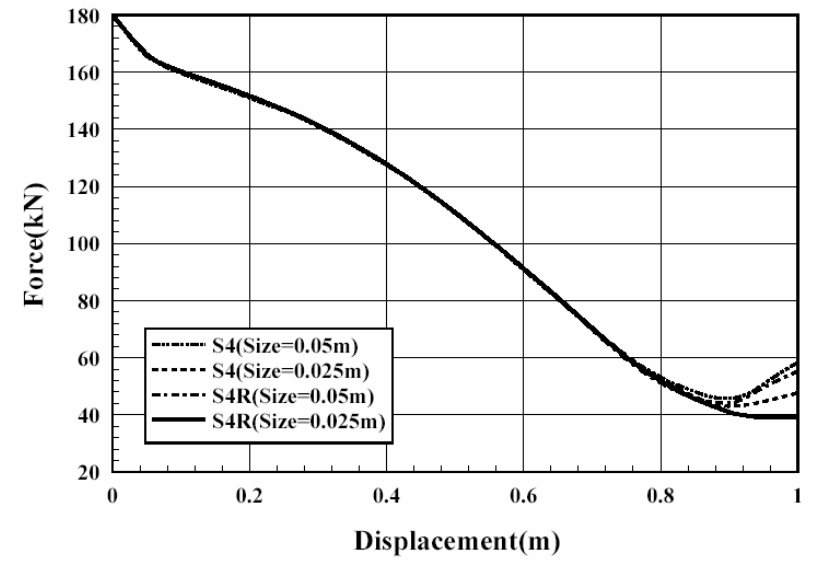

Fig. 4.15. Relationship between vertical reaction and vertical displacement of original structure for elements S4 and S4R with mesh sizes 0.05m and 0.025m

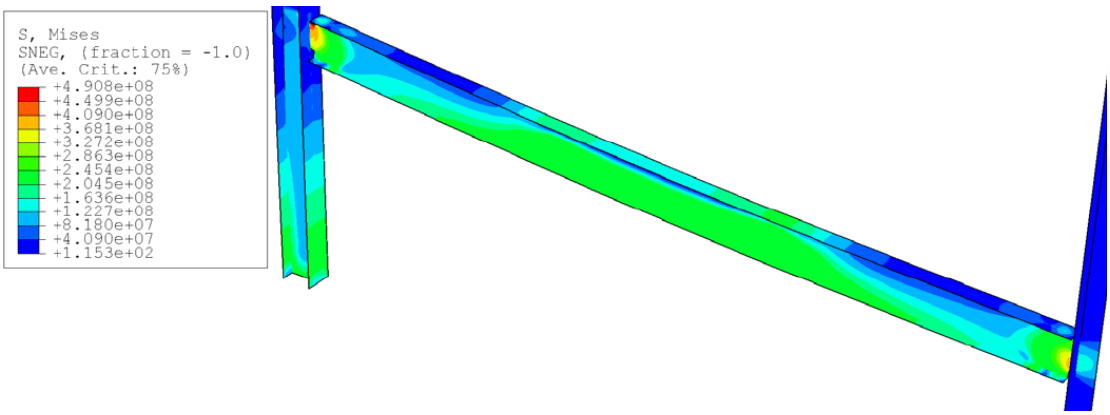

(a) Mises equivalent stress (Pa) distribution of whole beam

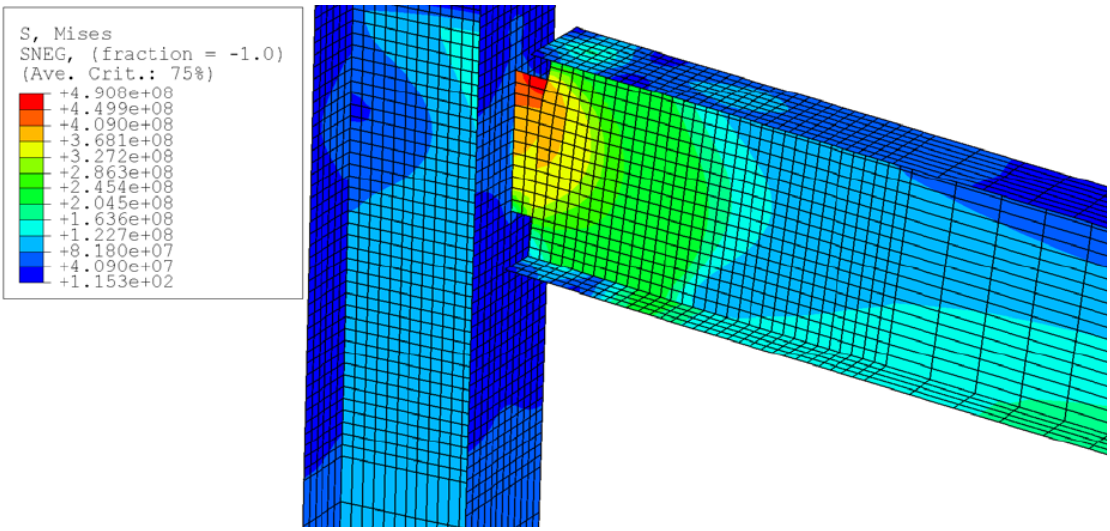

(b) Mises equivalent stress (Pa) distribution at left beam-to-column connection

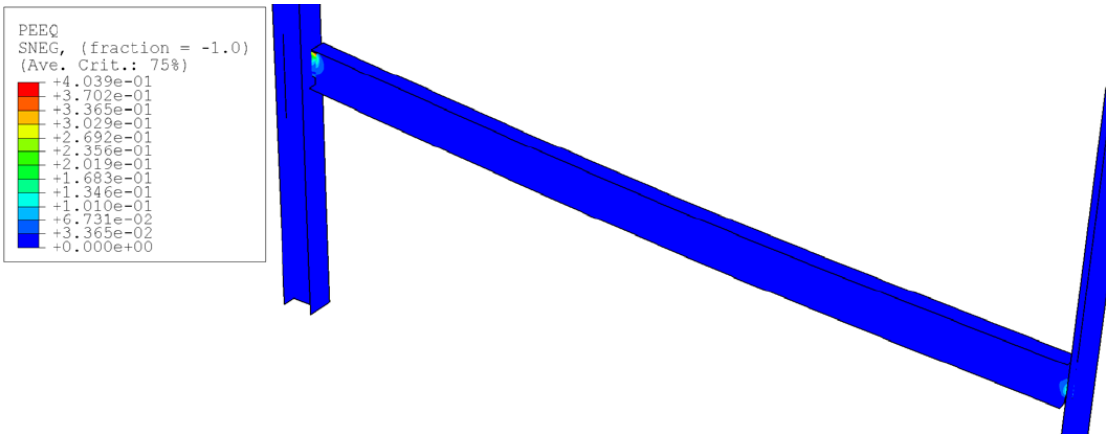

(c) Equivalent plastic strain distribution of whole beam

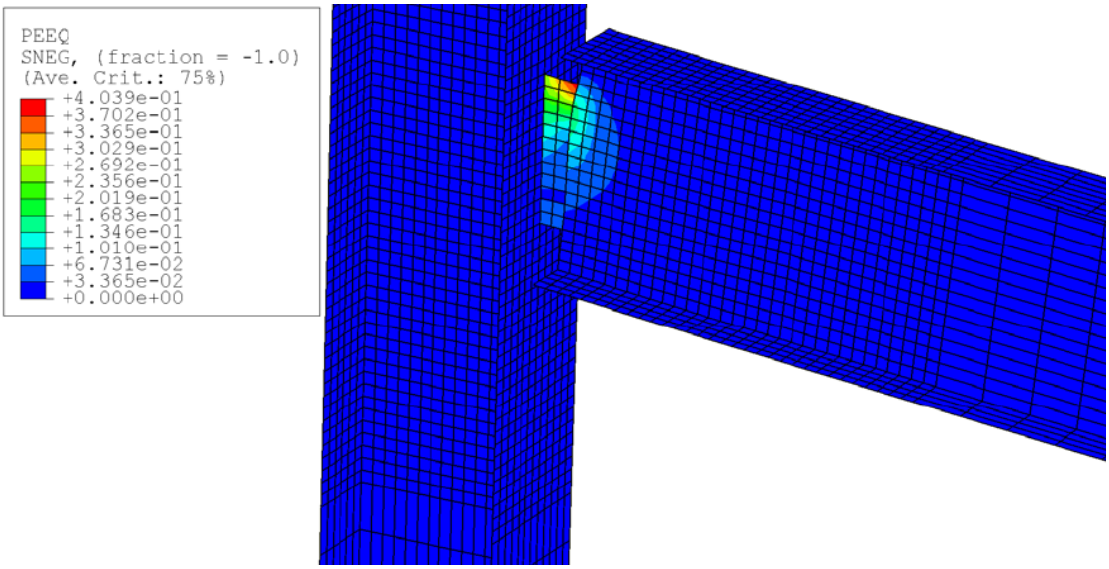

(d) Equivalent plastic strain distribution at left beam-to-column connection

Fig. 4.16. Mises equivalent stress and Equivalent plastic strain distributions when vertical displacement is 0.648m for original structure

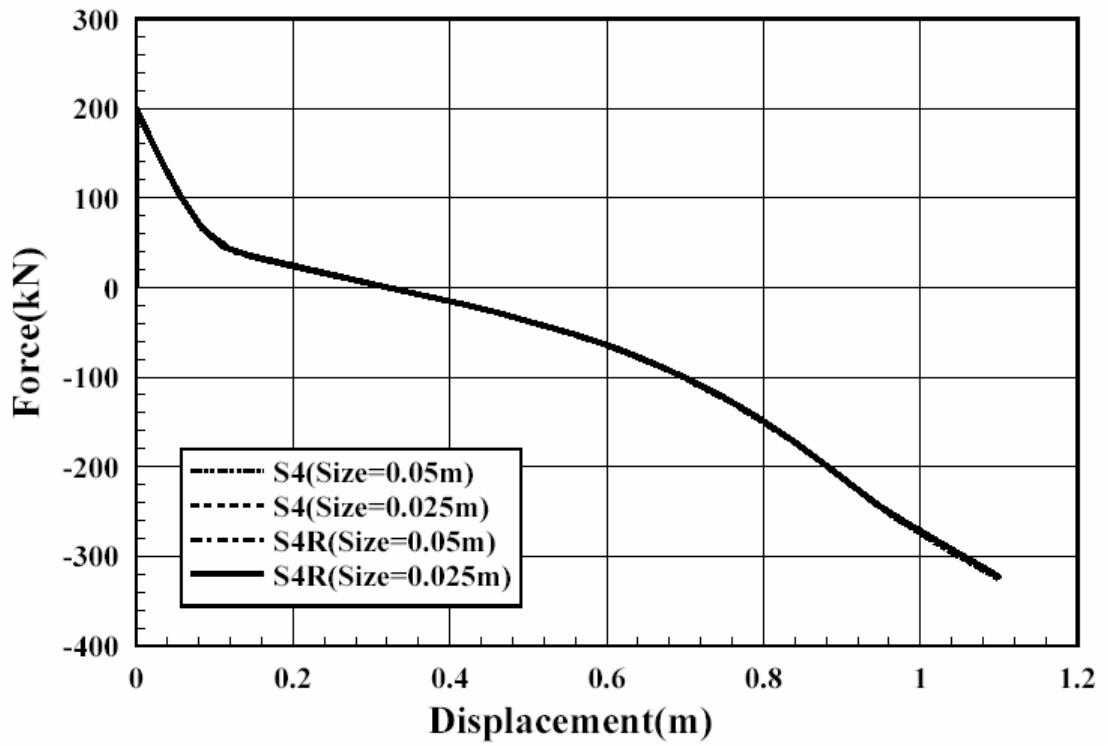

(a) For structure retrofitted by Flange Plate Scheme for elements S4 and S4R with mesh sizes 0.05m and 0.025m

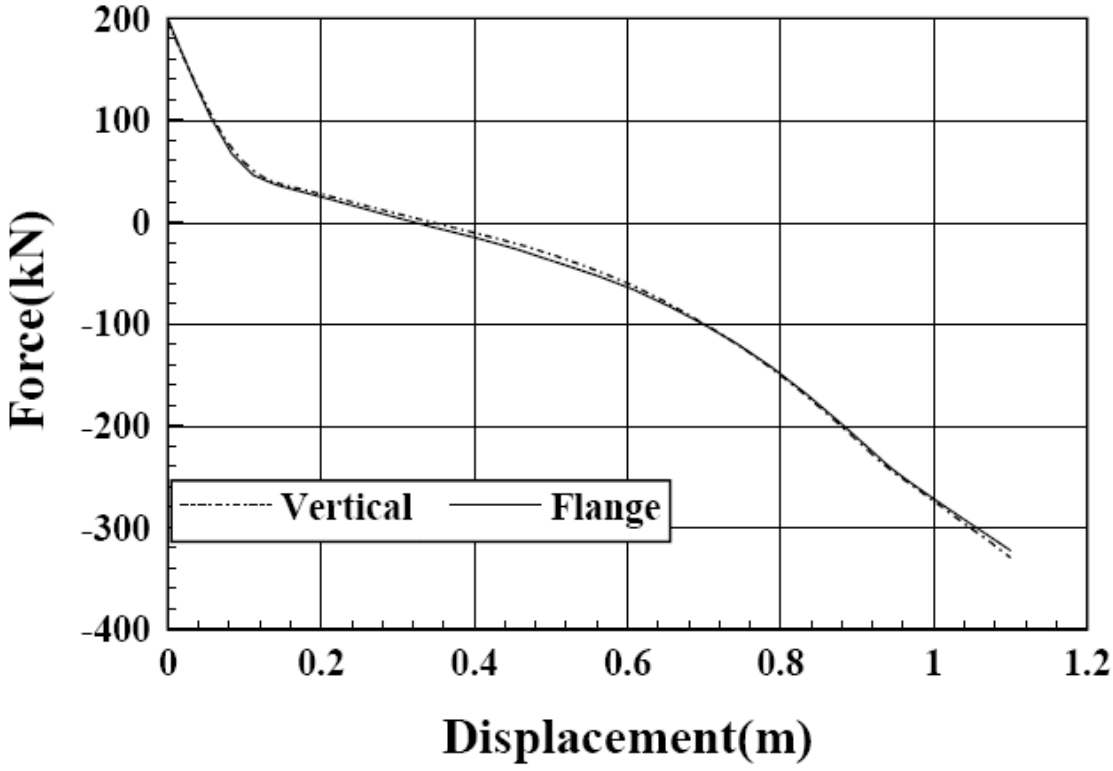

(b) For structures retrofitted by Vertical Plate Scheme and Flange Plate Scheme for for element S4R with mesh size 0.025m

Fig. 4.17. Relationship between vertical reaction and vertical displacement for retrofitted structures

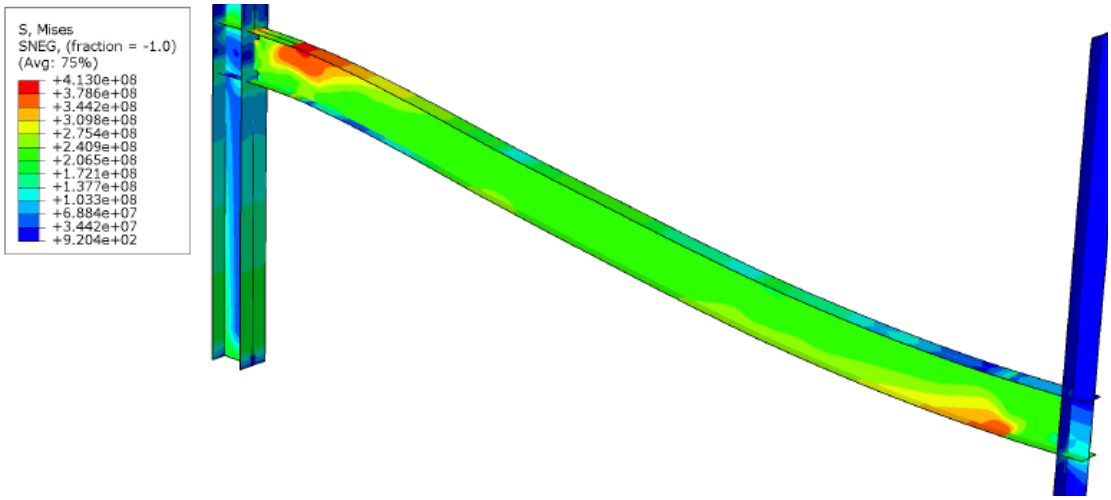

(a) Mises equivalent stress (Pa) distribution of whole beam

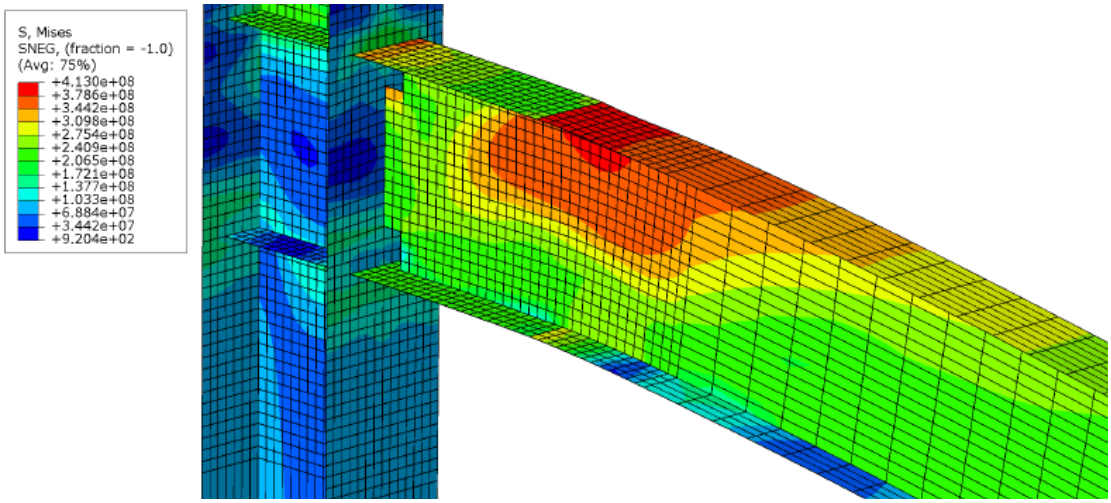

(b) Mises equivalent stress (Pa) distribution at left beam-to-column connection

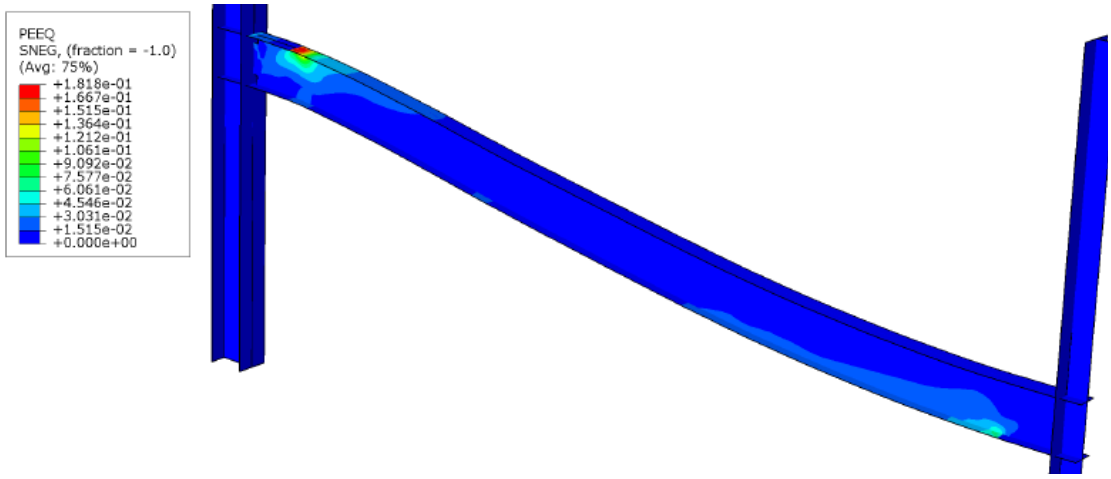

(c) Equivalent plastic strain distribution of whole beam

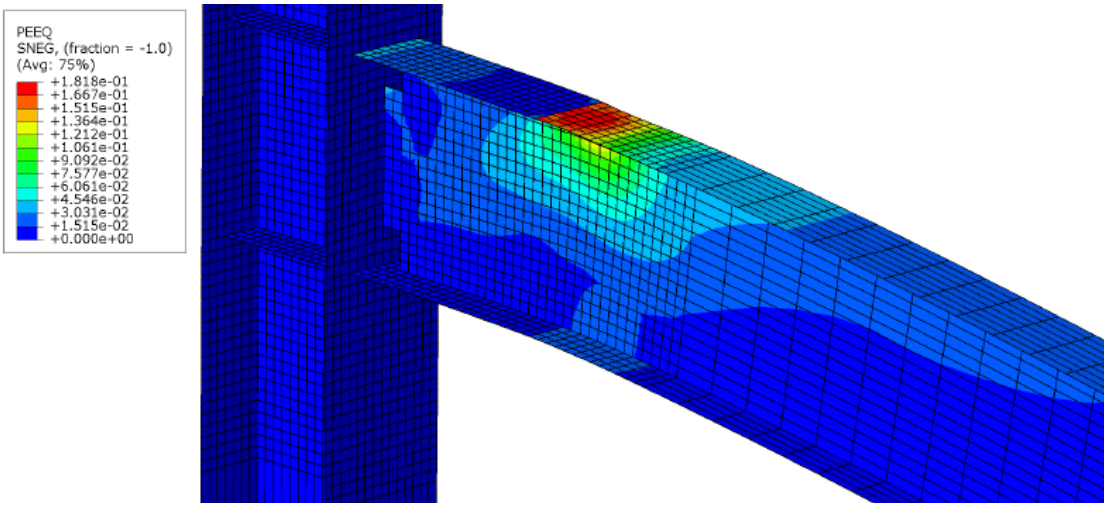

(d) Equivalent plastic strain distribution at left beam-to-column connection

Fig. 4.18. Mises equivalent stress and equivalent plastic strain distribution when vertical displacement is 1.1m for Flange Plate Scheme

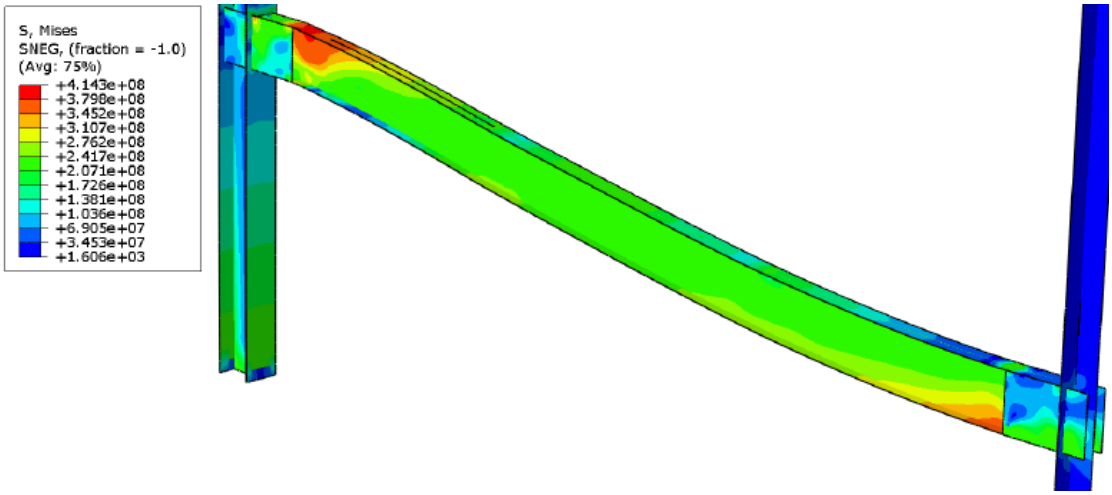

(a) Mises equivalent stress (Pa) distribution of whole beam

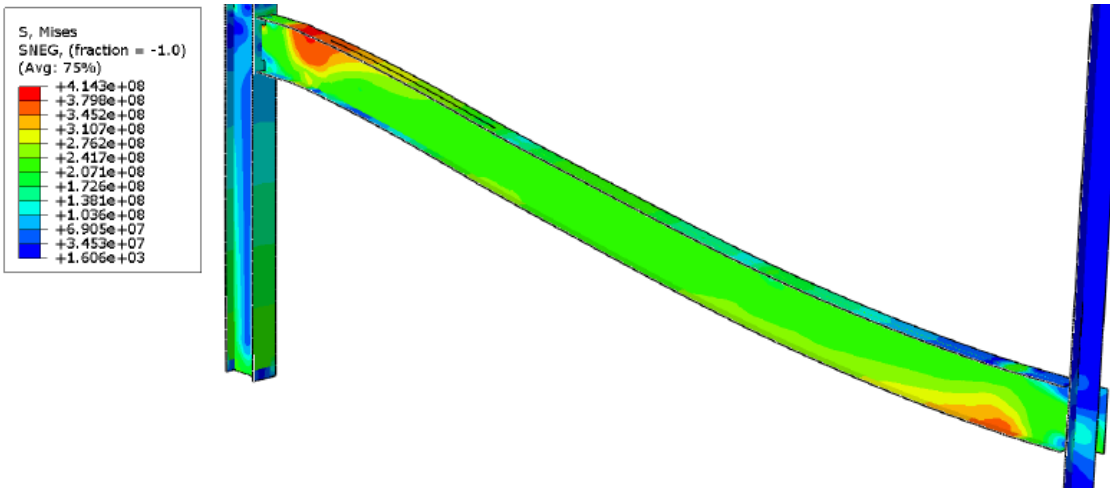

(b) Mises equivalent stress (Pa) distribution of whole beam at removal of front vertical plate

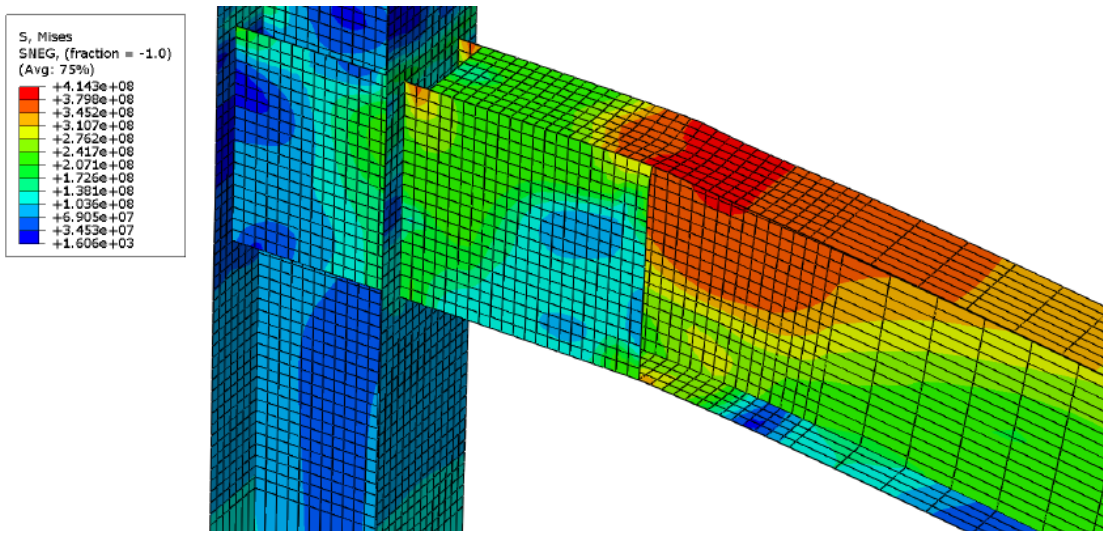

(c) Mises equivalent stress (Pa) distribution at left beam-to-column connection

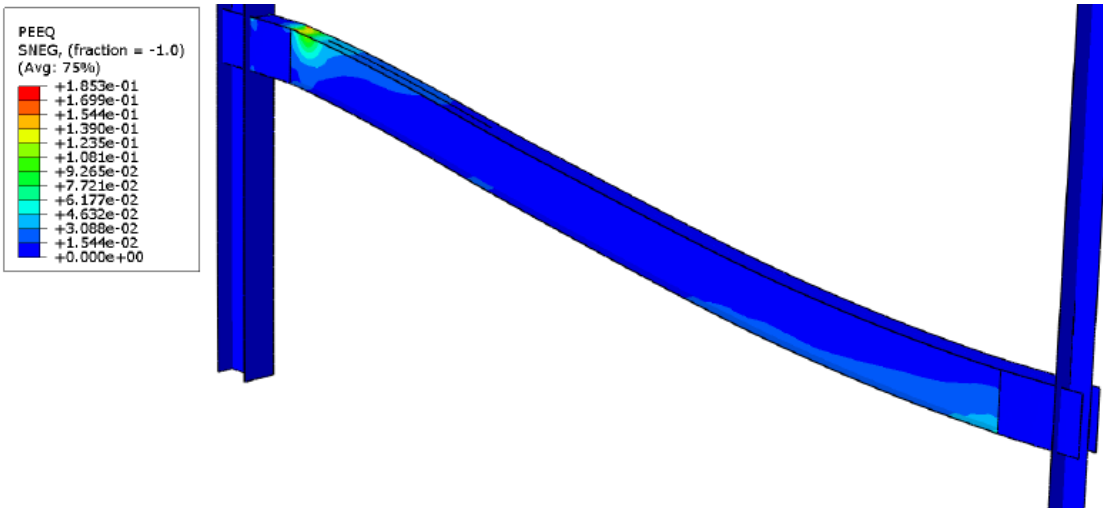

(d) Equivalent plastic strain distribution of whole beam

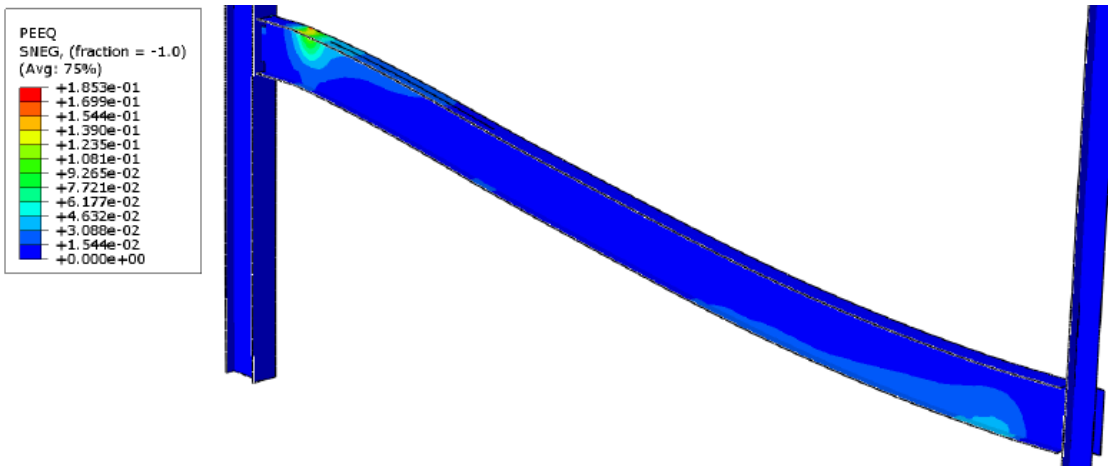

(e) Equivalent plastic strain distribution of whole beam at removal of front vertical plate

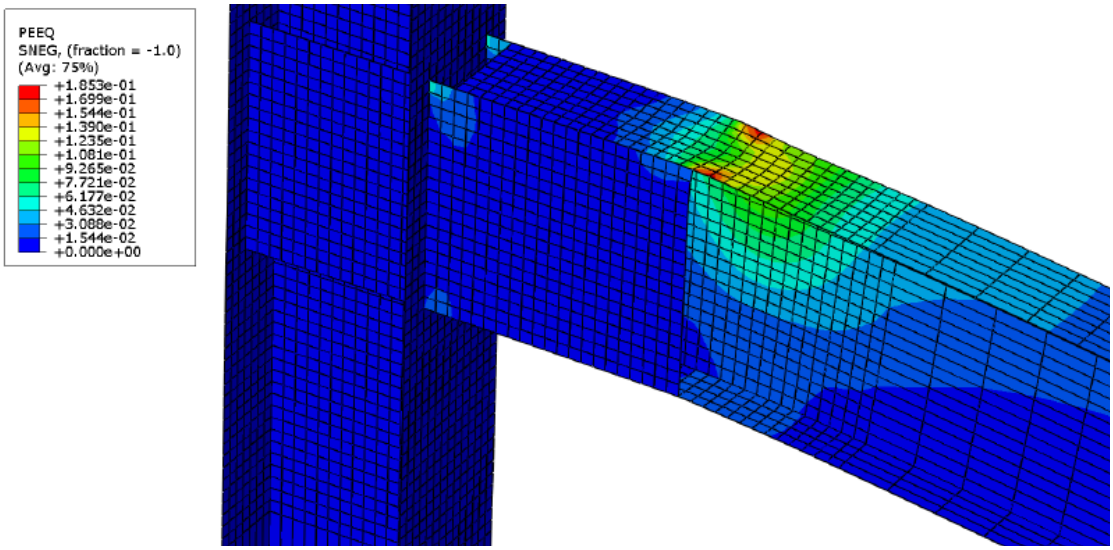

(f) Equivalent plastic strain distribution at left beam-to-column connection

Fig. 4.19. Mises equivalent stress and equivalent plastic strain distribution for vertical plate scheme when vertical displacement is 1.1m for Vertical Plate Scheme

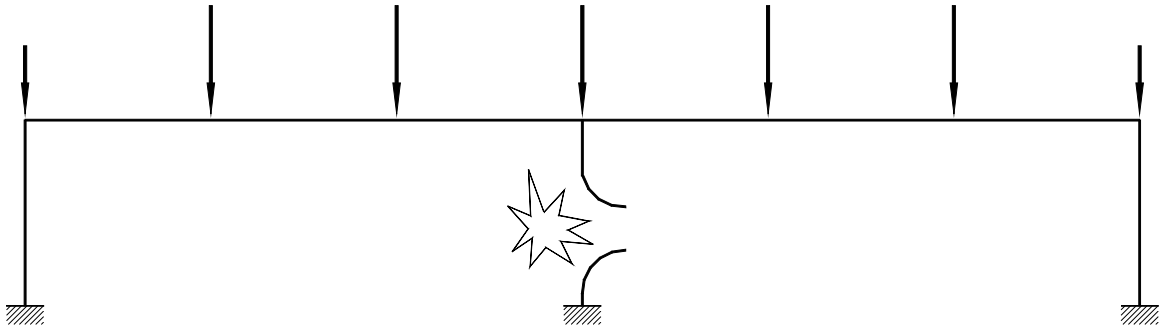

Fig. 4.20. Frame investigated in Model 4.4

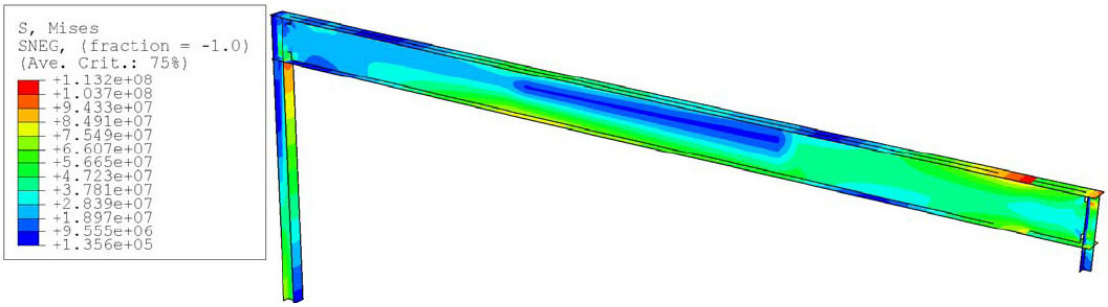

(a) Global distribution of Mises equivalent stress (Pa)

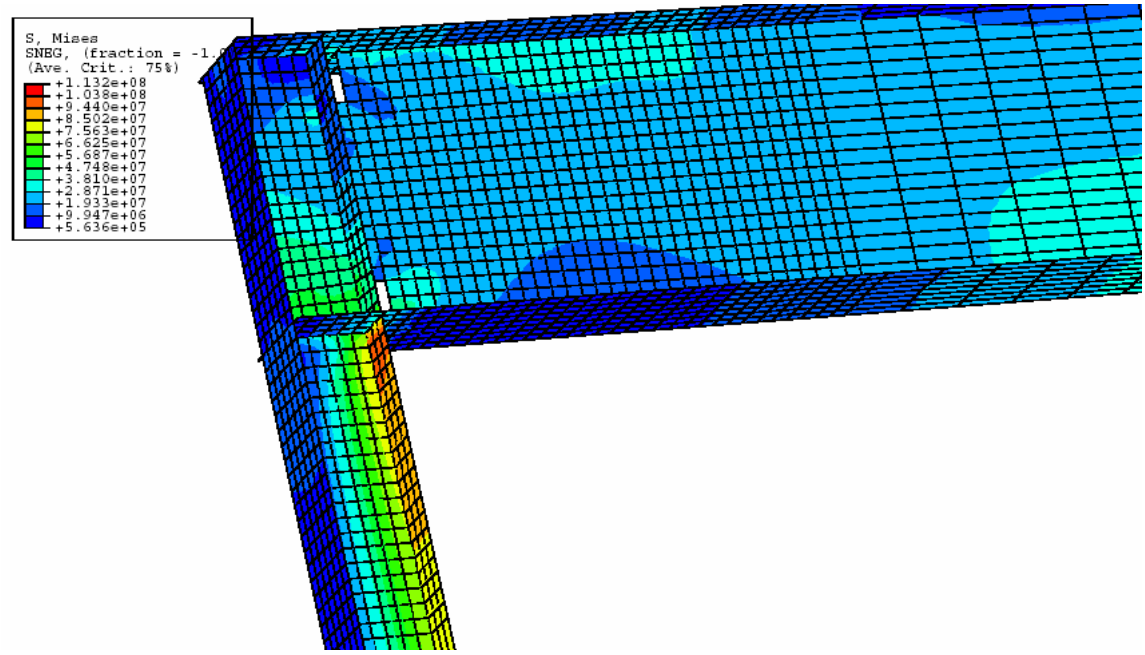

(b) Local distribution of Mises equivalent stress (Pa) at left connection

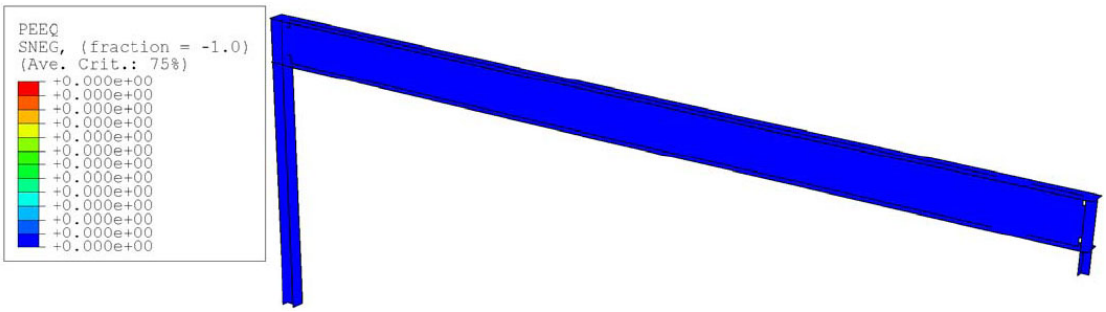

(c) Global distribution of equivalent plastic strain

Fig. 4.21. Distributions of Mises stress and equivalent plastic strain at the end of the first step

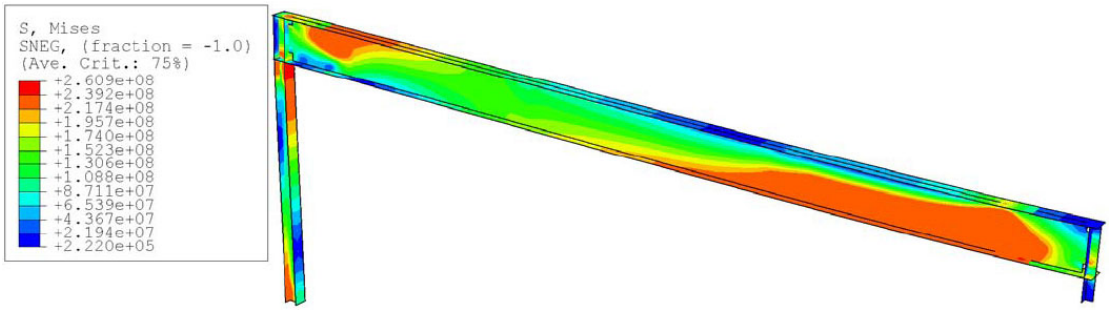

(a) Global distribution of Mises equivalent stress (Pa)

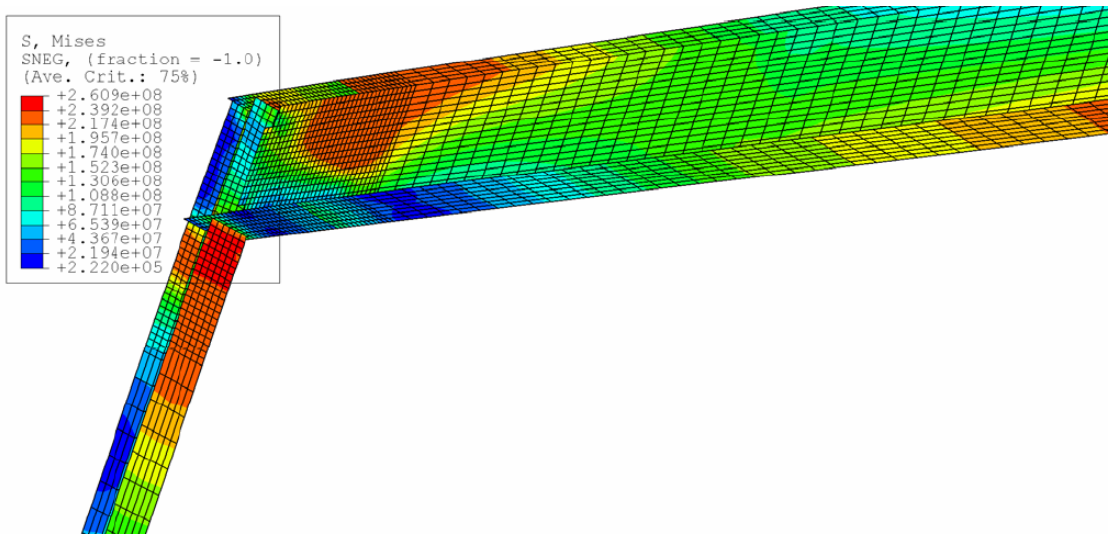

(b) Local distribution of Mises equivalent stress (Pa) at left connection

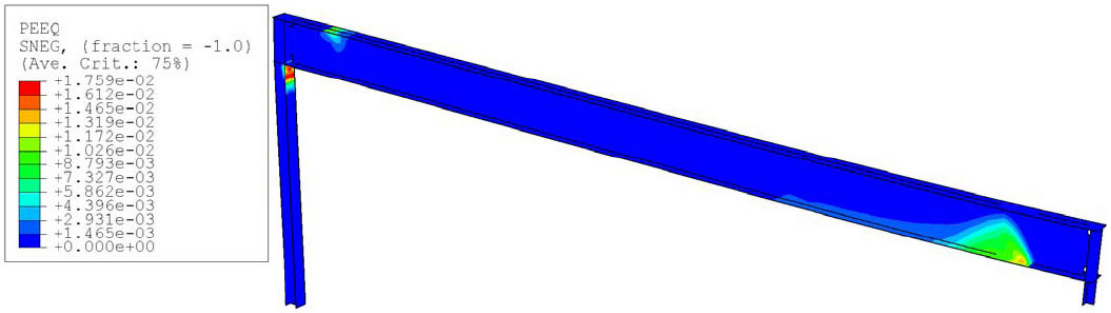

(c) Global distribution of equivalent plastic strain

Fig. 4.22. Distributions of Mises stress and equivalent plastic strain at the end of the second step

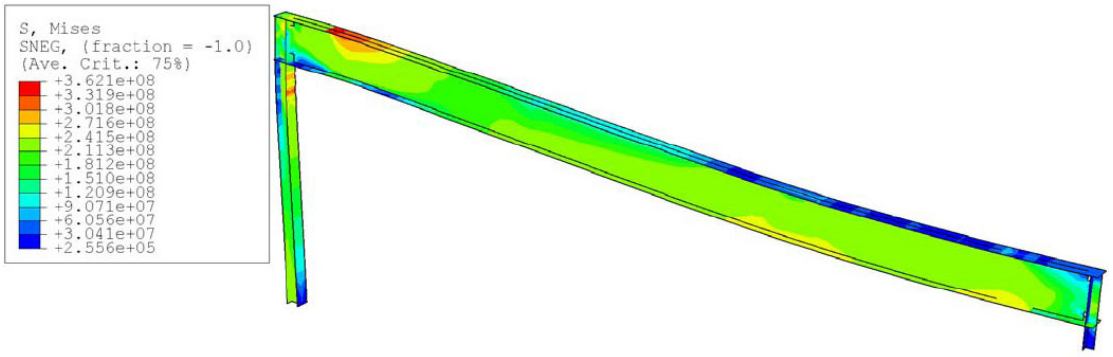

(a) Global distribution of Mises equivalent stress (Pa)

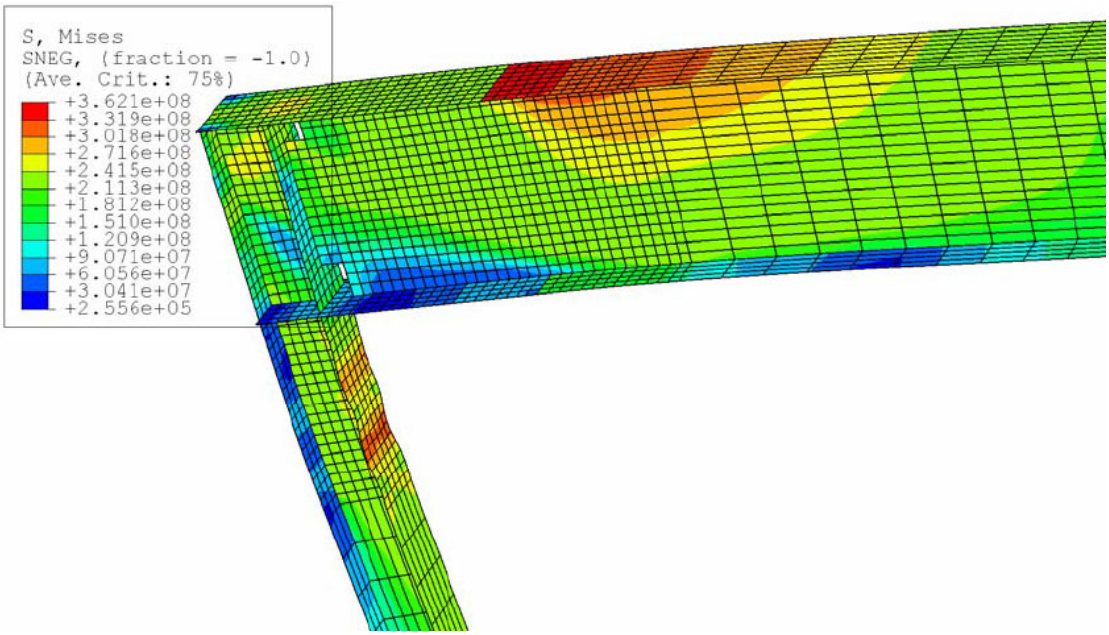

(b) Local distribution of Mises equivalent stress (Pa) at left connection

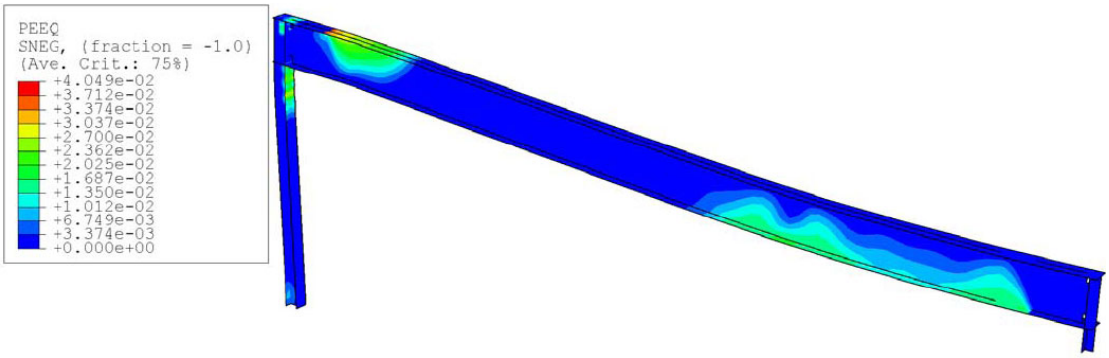

(c) Global distribution of equivalent plastic strain

Fig. 4.23. Distributions of Mises stress and equivalent plastic strain at the end of the third step

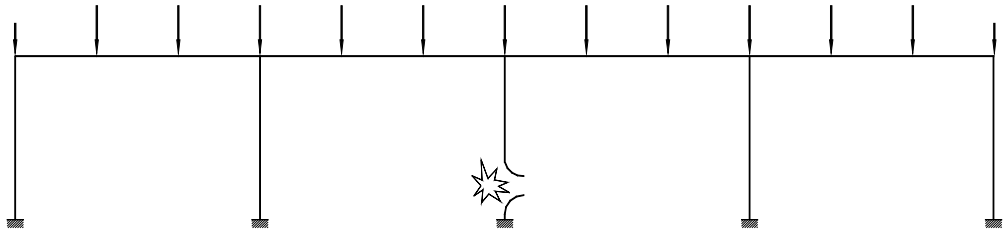

(a) Whole structure

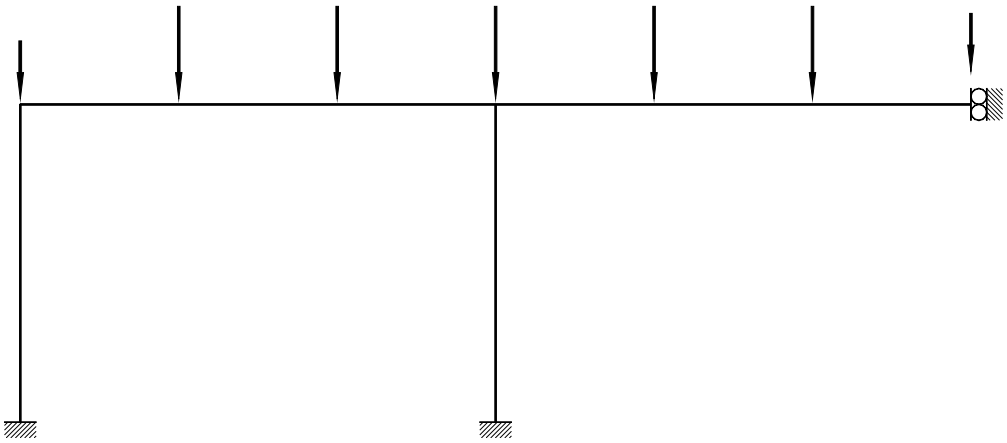

(b) Half of structure by taking advantage of symmetry

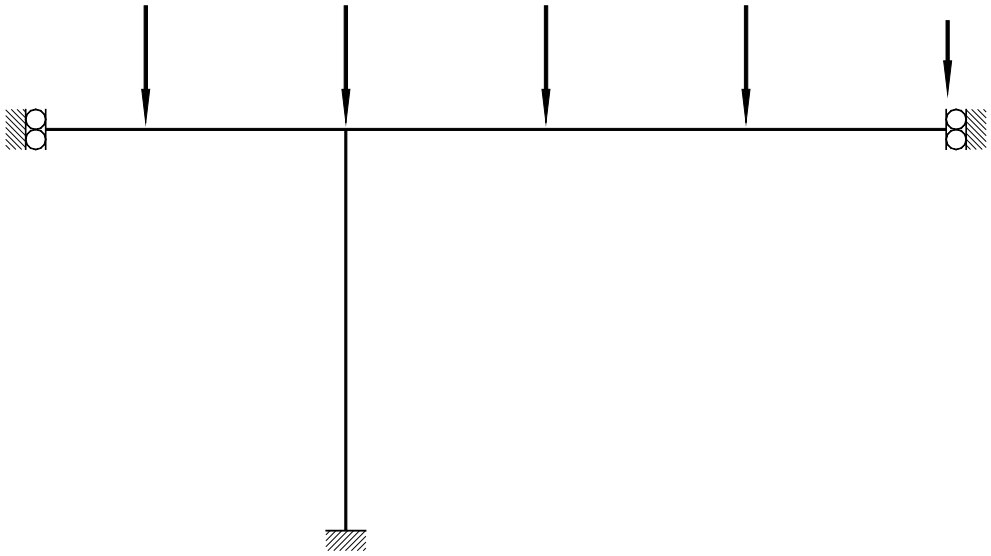

(c) Assemblage used in finite element analyses

Fig. 5.1. Frame investigated in Model 5.1

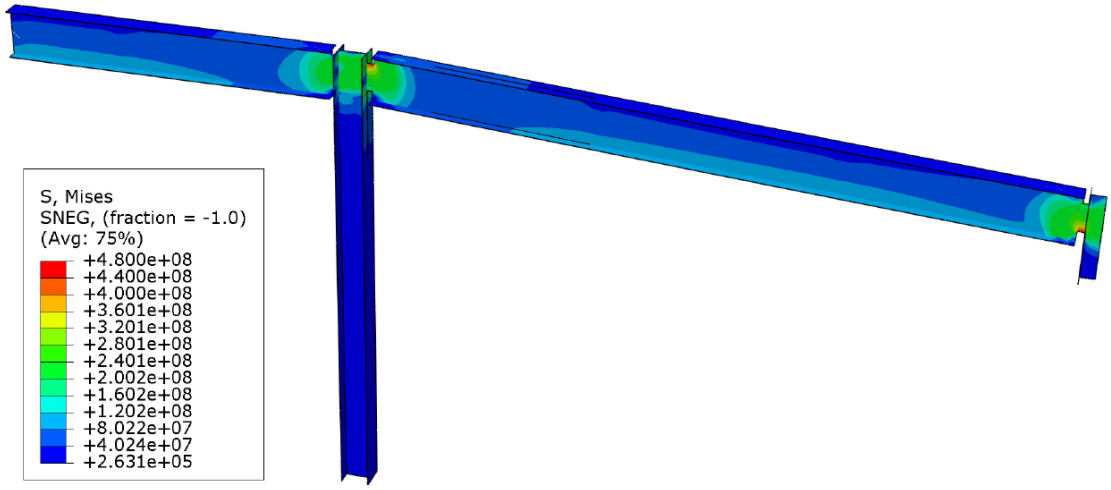

(a) Mises equivalent stress (Pa) distribution

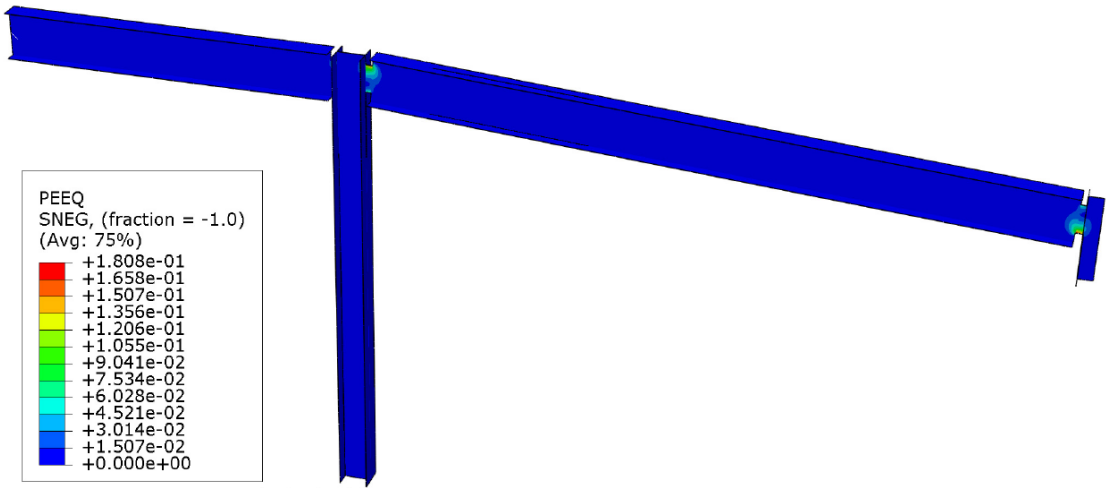

(b) Equivalent plastic strain distribution

Fig. 5.2. Stress and strain distributions of original structure when load scaling factor is 0.3686

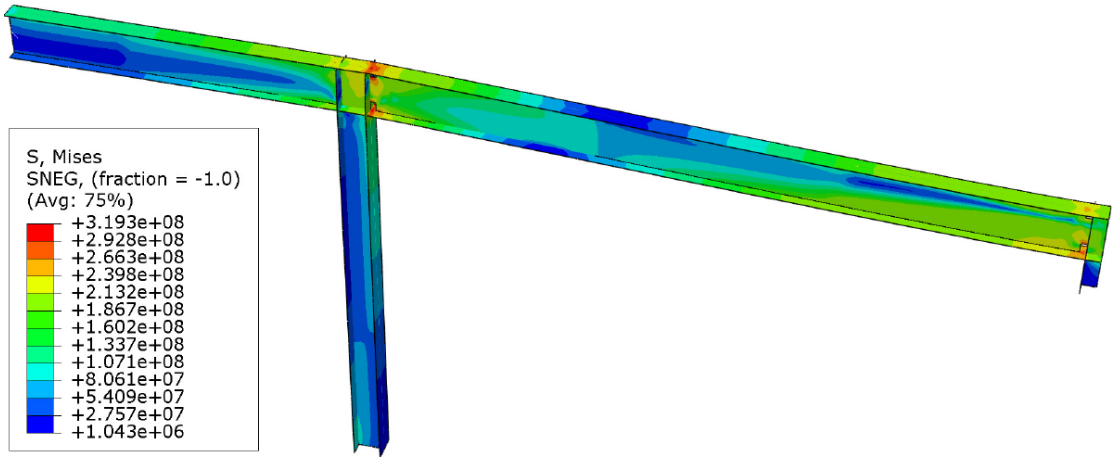

(a) Mises equivalent stress (Pa) distribution when load scaling factor is 1

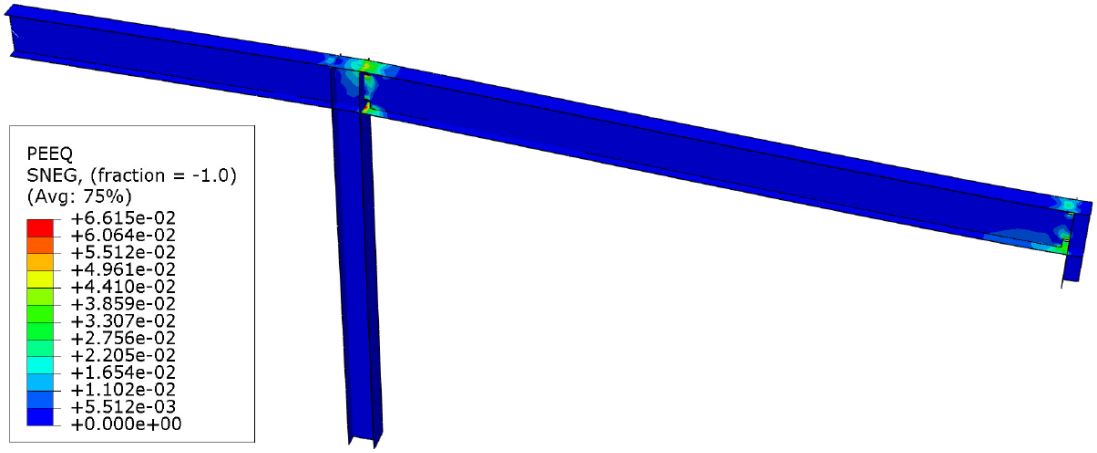

(b) Equivalent plastic strain distribution when load scaling factor is 1

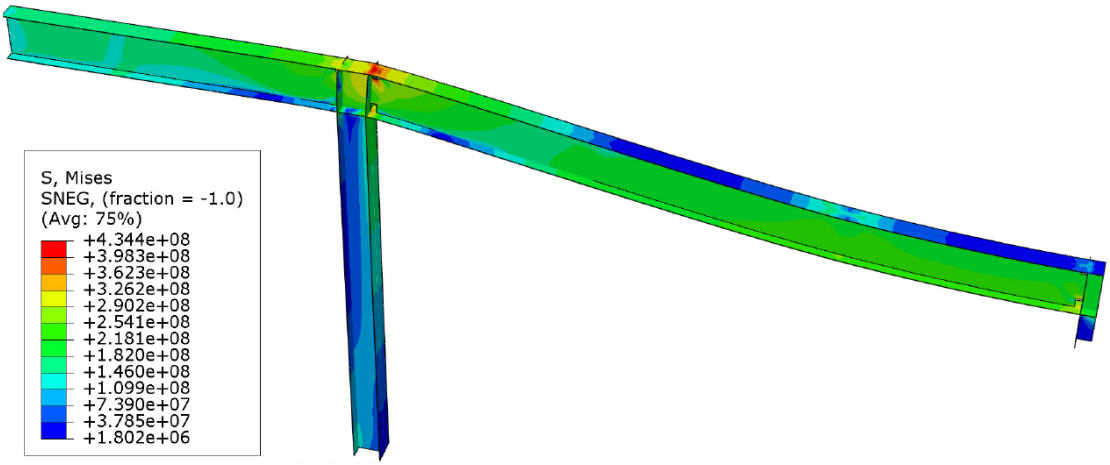

(c) Mises equivalent stress (Pa) distribution when load scaling factor is 2

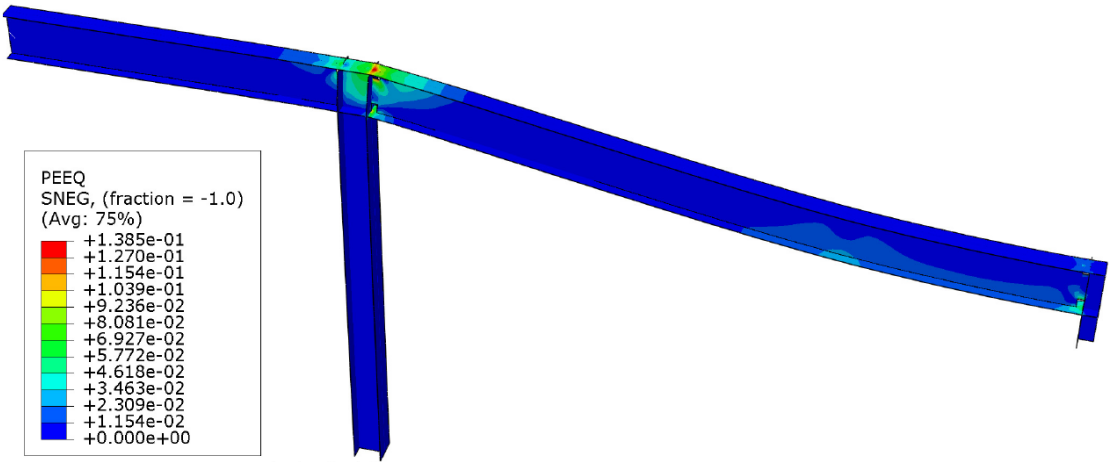

(d) Equivalent plastic strain distribution when load scaling factor is 2

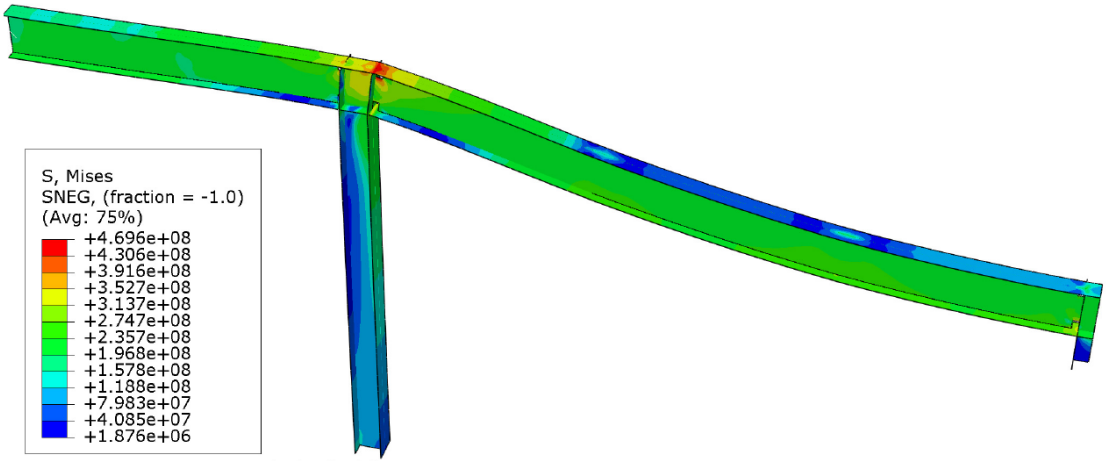

(e) Mises equivalent stress (Pa) distribution when load scaling factor is 2.8650

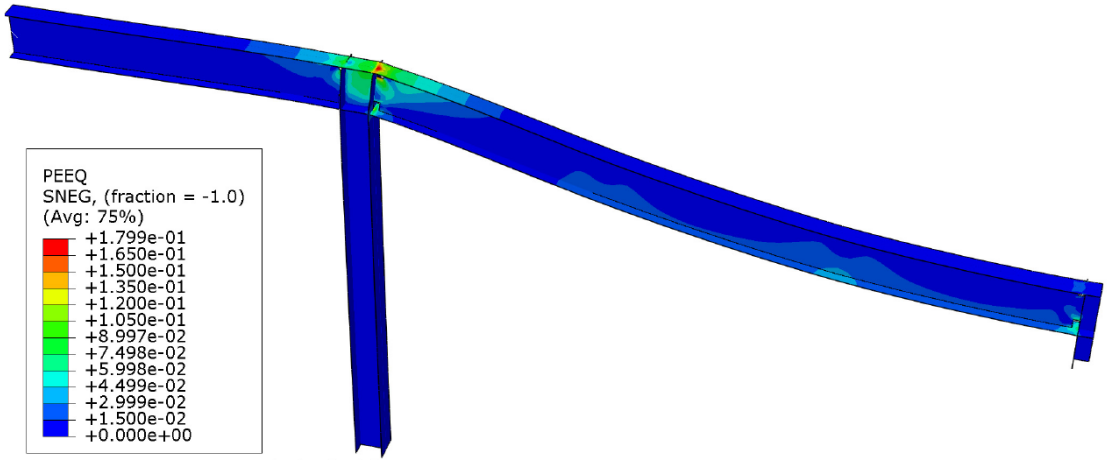

(f) Equivalent plastic strain distribution when load scaling factor is 2.8650

Fig. 5.3. Stress and strain distributions of structure retrofitted by Traditional Moment Connection Scheme

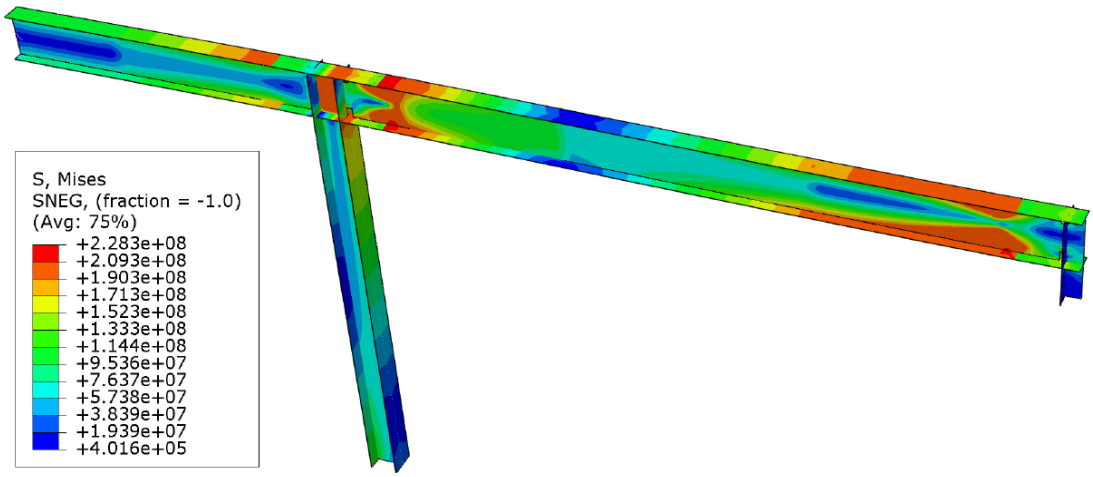

(a) Mises equivalent stress (Pa) distribution when load scaling factor is 1

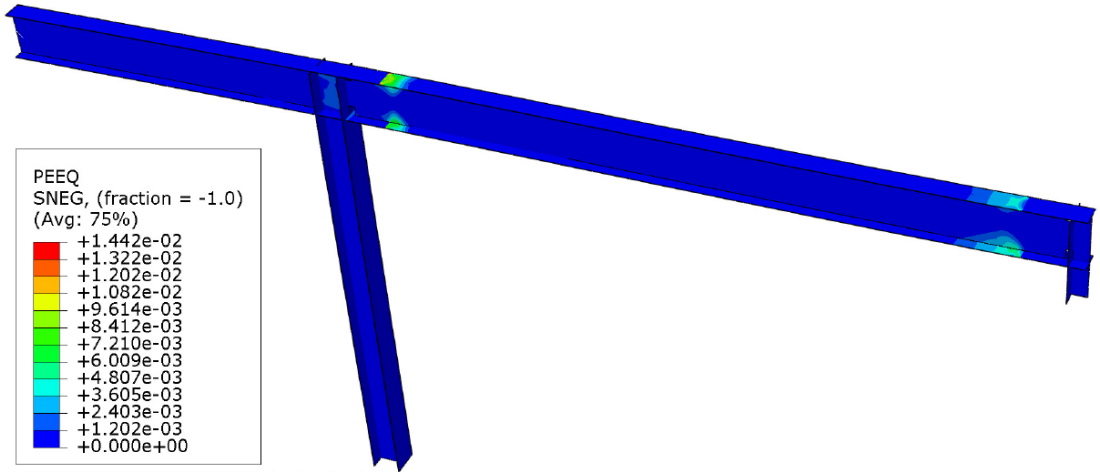

(b) Equivalent plastic strain distribution when load scaling factor is 1

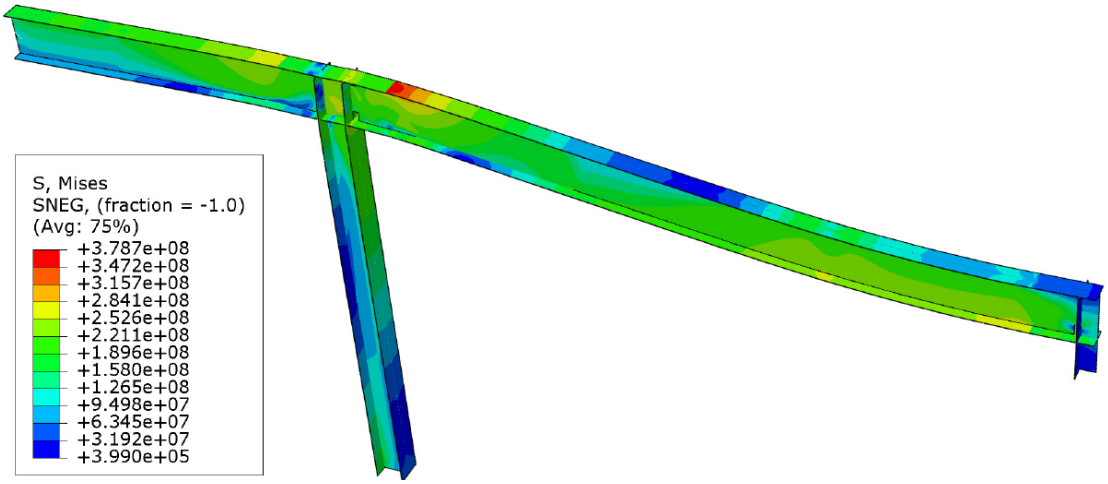

(c) Mises equivalent stress (Pa) distribution when load scaling factor is 2

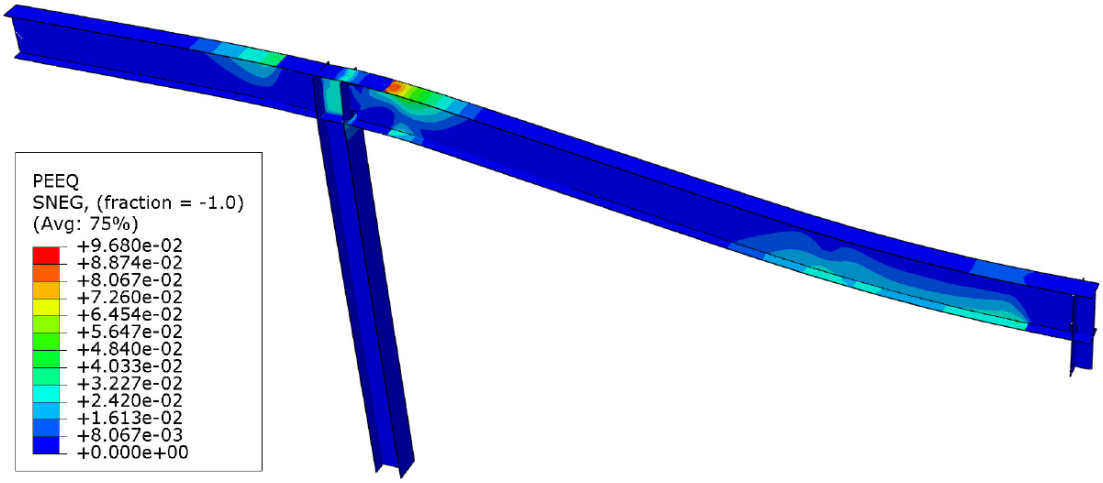

(d) Equivalent plastic strain distribution when load scaling factor is 2

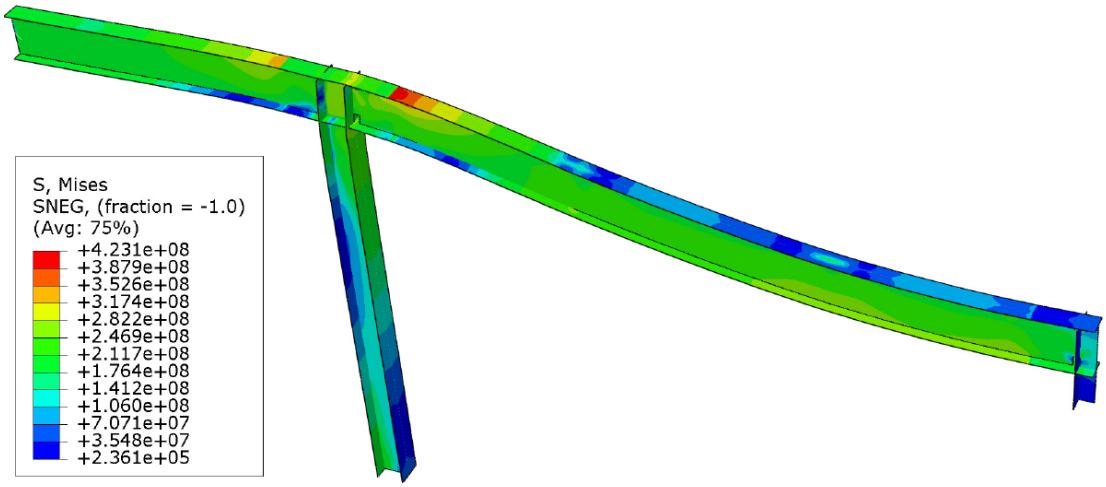

(e) Mises equivalent stress (Pa) distribution when load scaling factor is 3

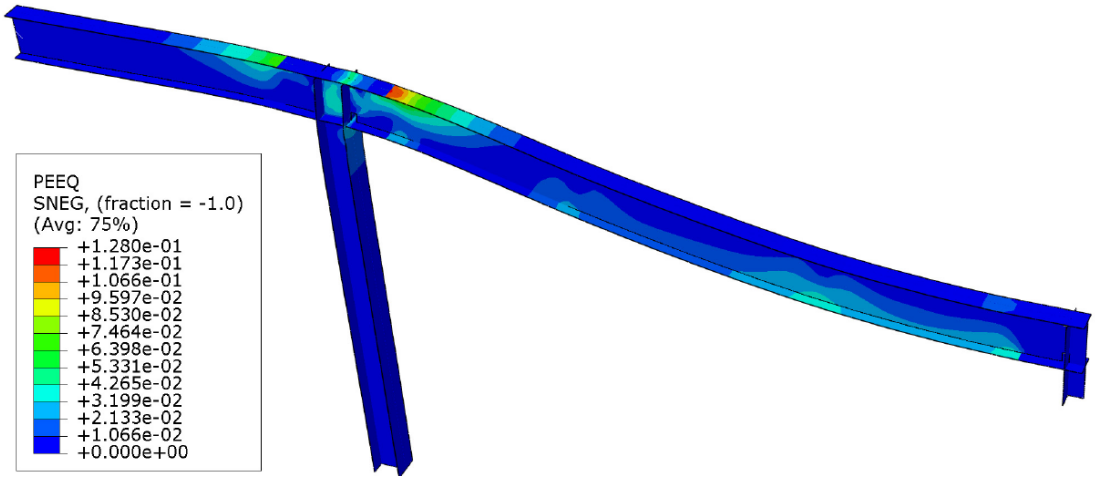

(f) Equivalent plastic strain distribution when load scaling factor is 3

Fig. 5.4. Stress and strain distributions of structure retrofitted by Flange Plate Scheme

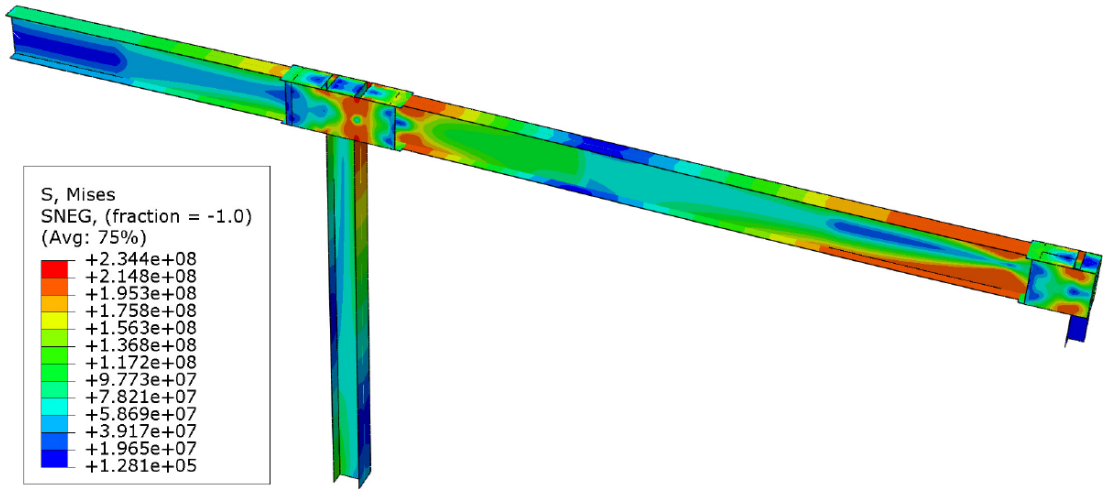

(a) Mises equivalent stress (Pa) distribution when load scaling factor is 1

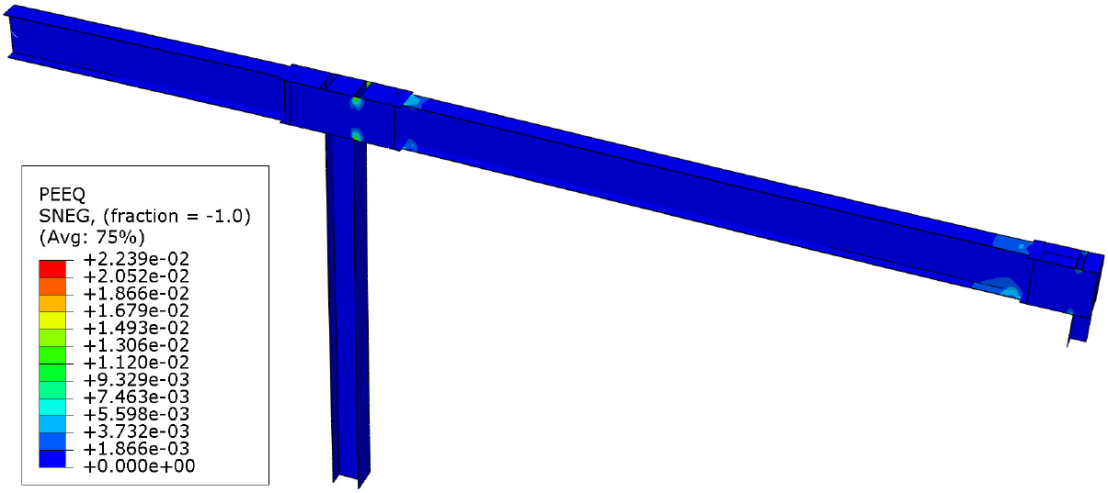

(b) Equivalent plastic strain distribution when load scaling factor is 1

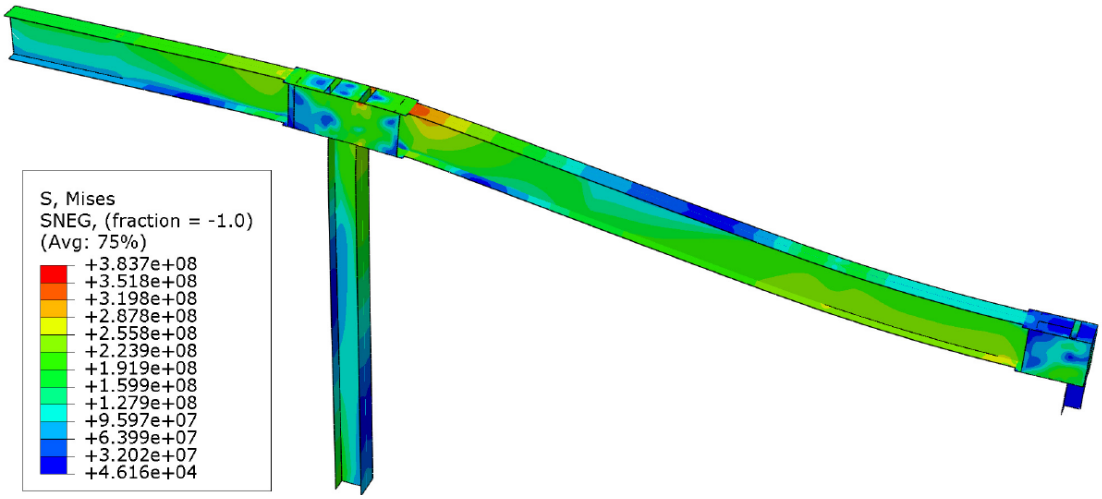

(c) Mises equivalent stress (Pa) distribution when load scaling factor is 2

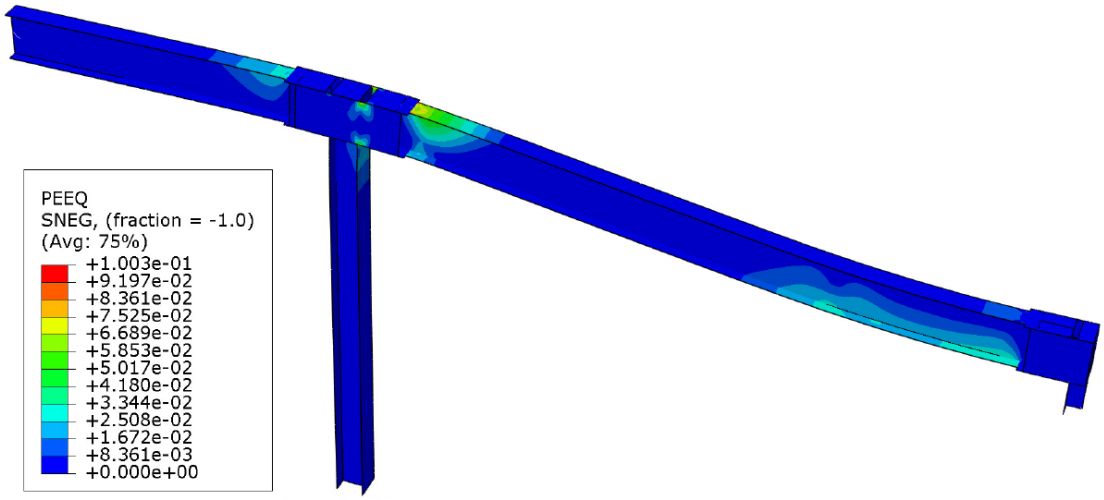

(d) Equivalent plastic strain distribution when load scaling factor is 2

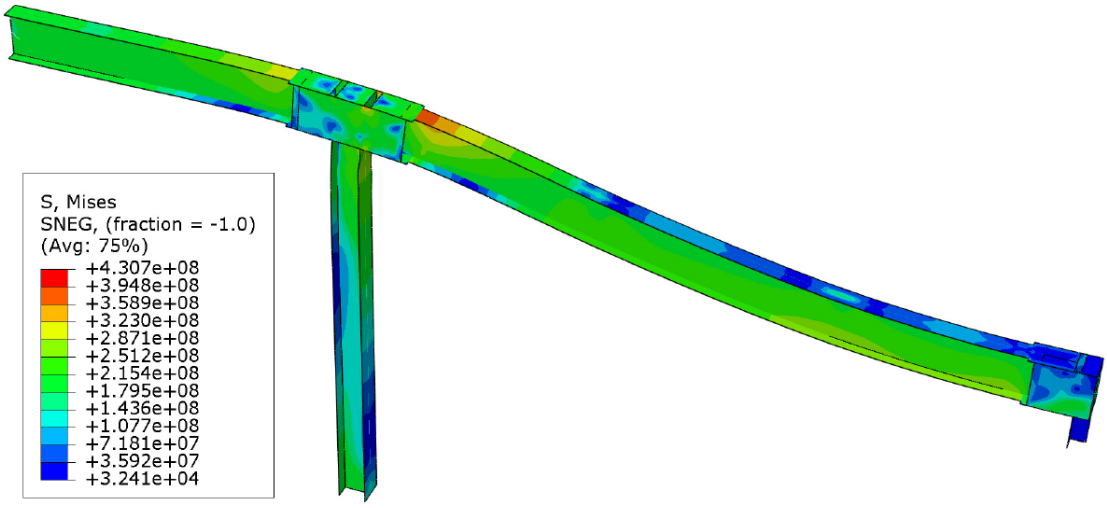

(e) Mises equivalent stress (Pa) distribution when load scaling factor is 3

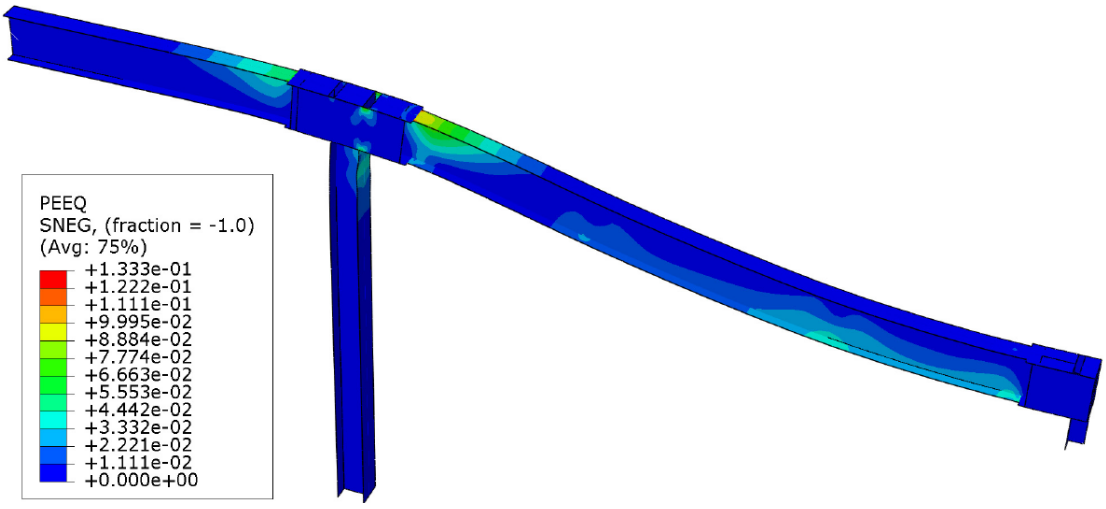

(f) Equivalent plastic strain distribution when load scaling factor is 3

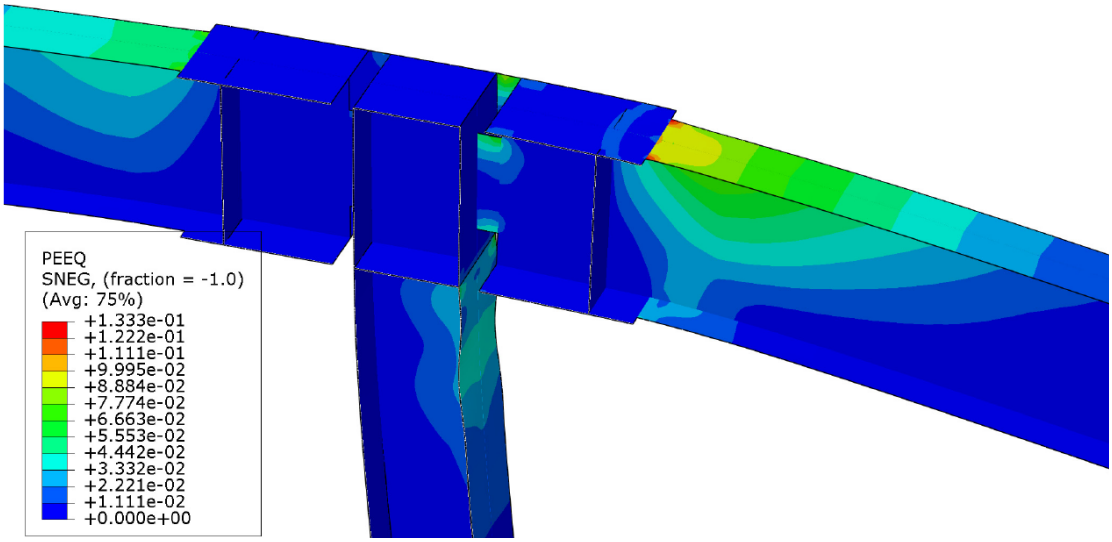

(g) Equivalent plastic strain distribution at beam-to-column connection without front side plate being shown when load scaling factor is 3

Fig. 5.5. Stress and strain distributions of structure retrofitted by SidePlate Connection Scheme

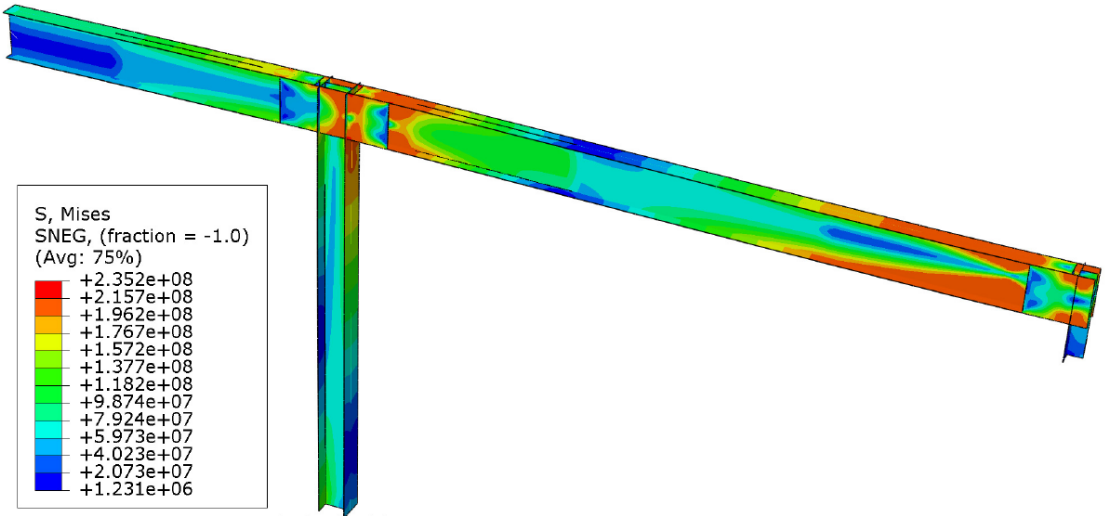

(a) Mises equivalent stress (Pa) distribution when load scaling factor is 1

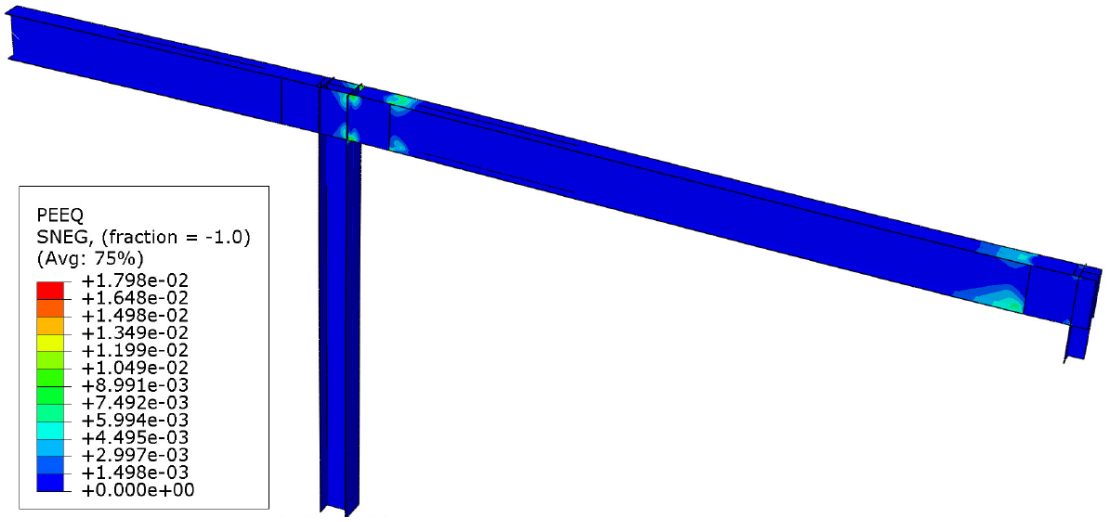

(b) Equivalent plastic strain distribution when load scaling factor is 1

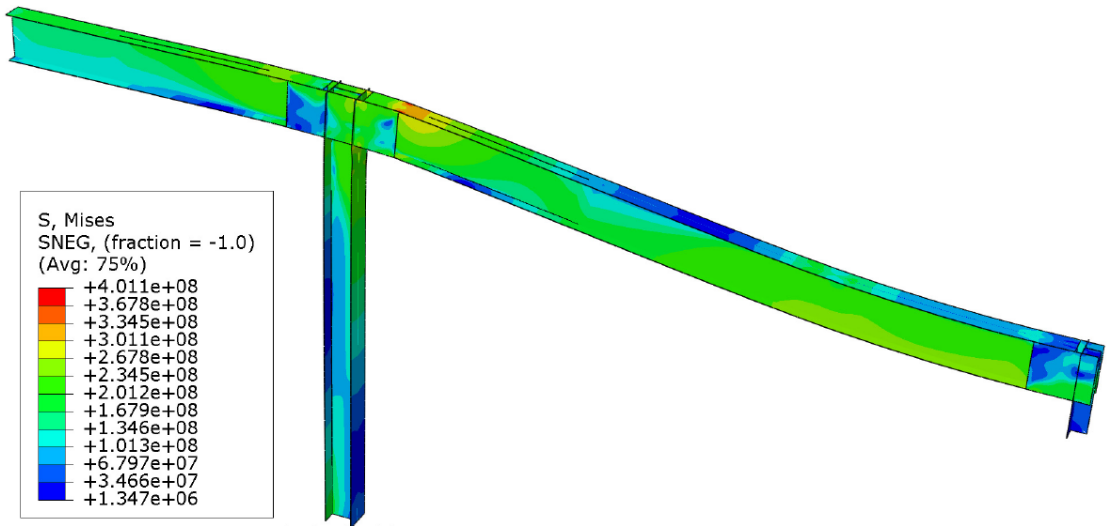

(c) Mises equivalent stress (Pa) distribution when load scaling factor is 2

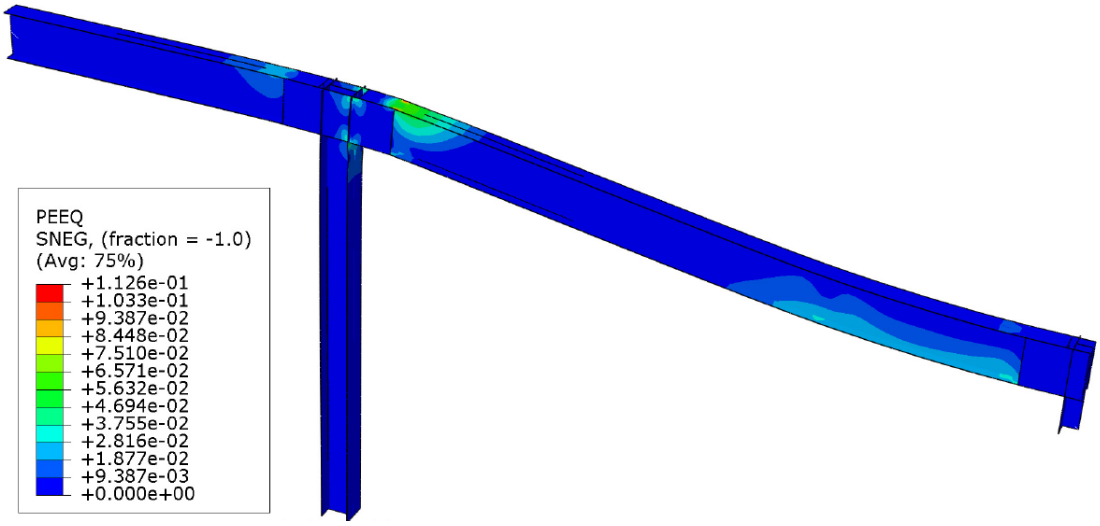

(d) Equivalent plastic strain distribution when load scaling factor is 2

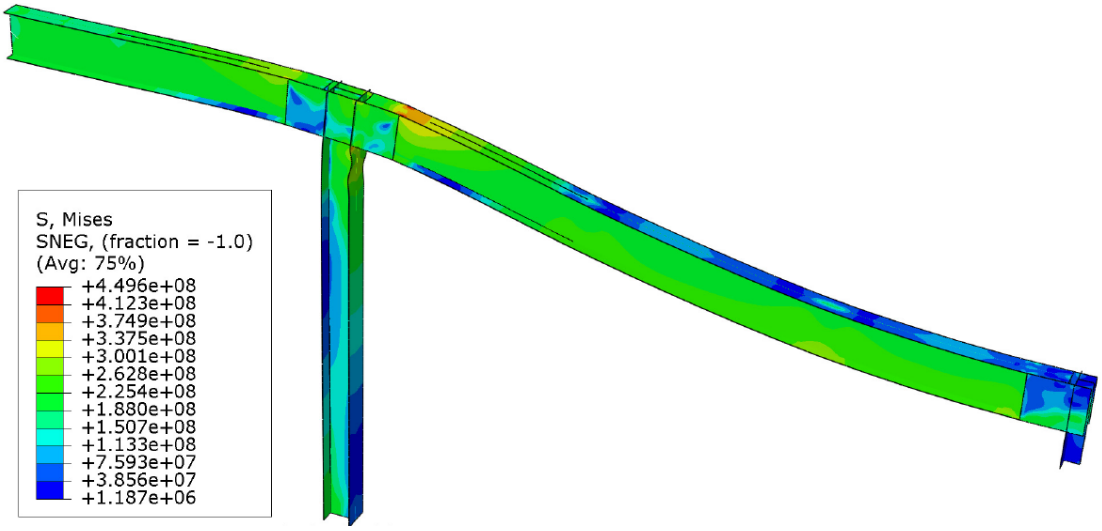

(e) Mises equivalent stress (Pa) distribution when load scaling factor is 3

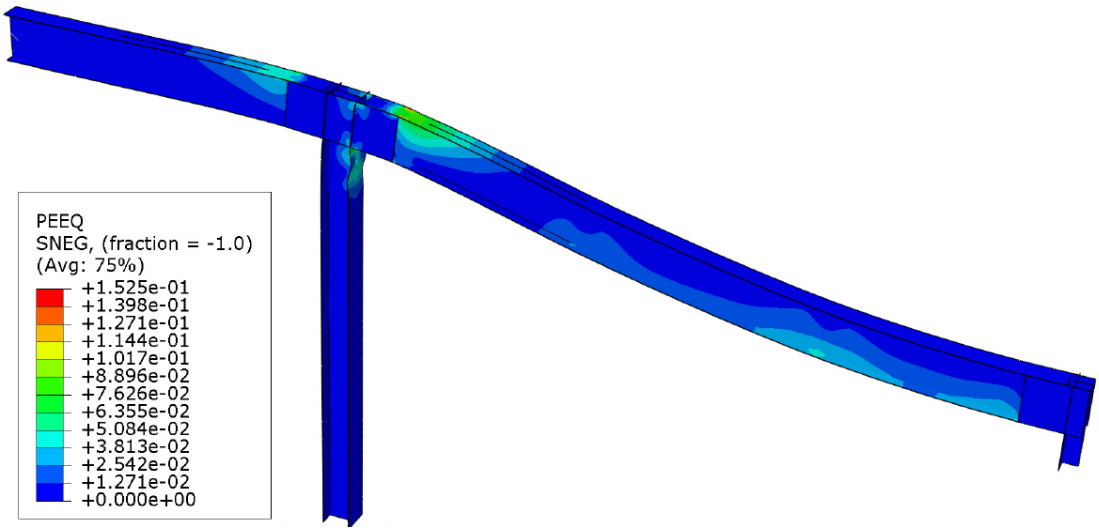

(f) Equivalent plastic strain distribution when load scaling factor is 3

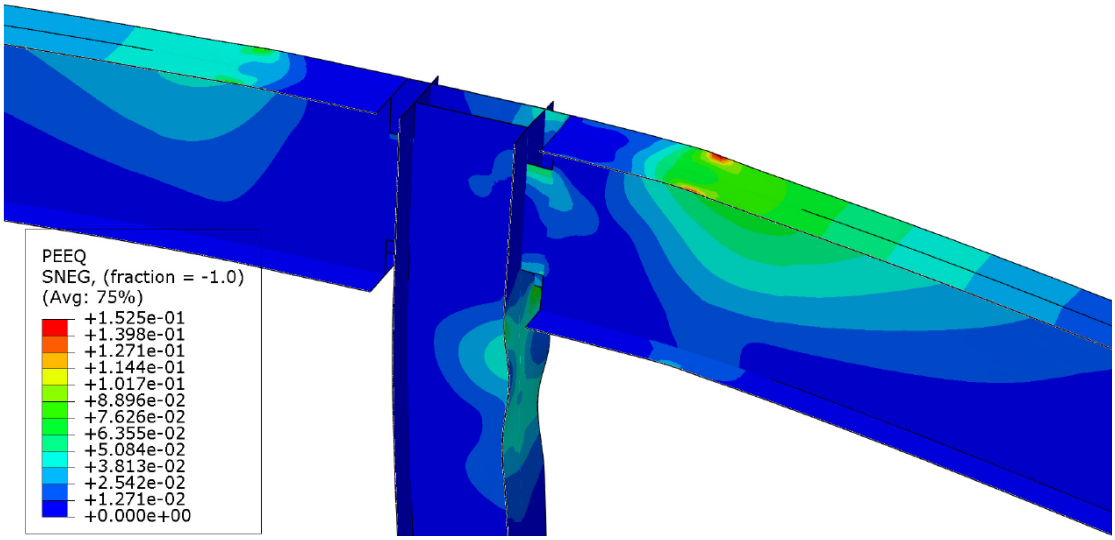

(g) Equivalent plastic strain distribution at beam-to-column connection without front vertical plate being shown when load scaling factor is 3

Fig. 5.6. Stress and strain distributions of structure retrofitted by Vertical Plate Scheme

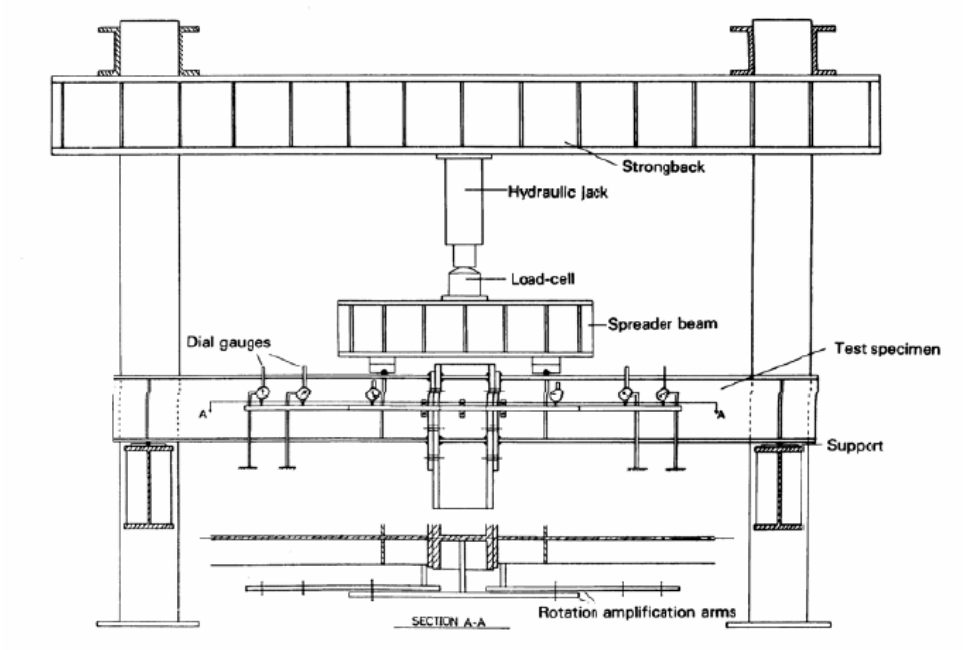

Fig. 5.7. View of test rig adopted by Jenkins et al. (1986)

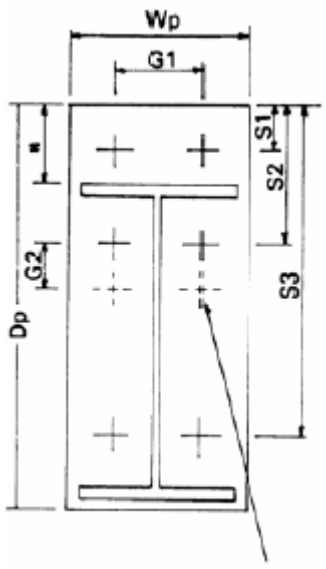

Fig. 5.8. Extended end plate (dimension in mm) used by Jenkins et al. (1986)

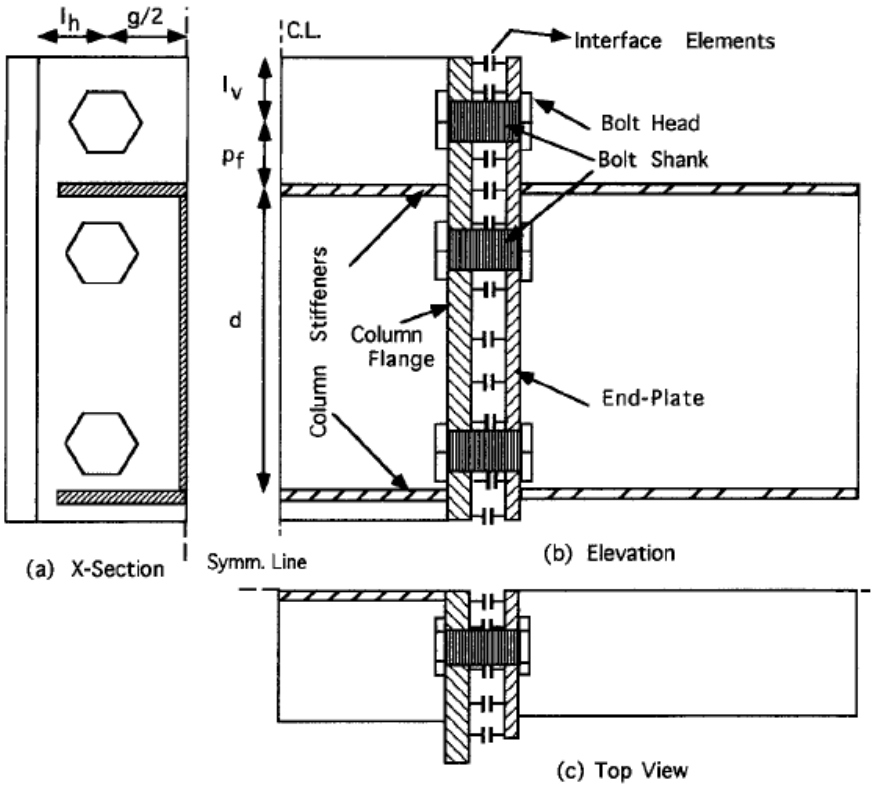

Fig. 5.9. Configuration of 3D finite element model used by Sherbourne et al. (1994)

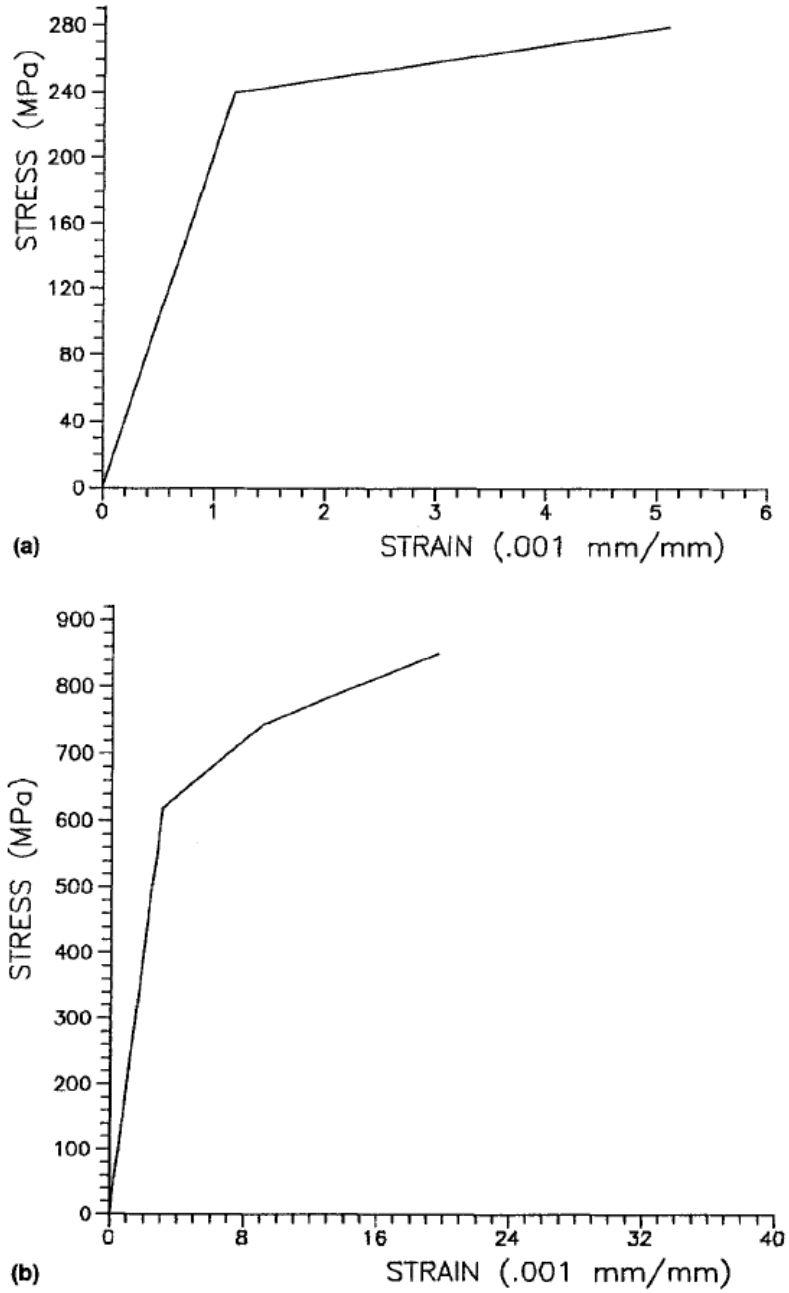

Fig. 5.10. Stress and strain curves used by Sherbourne et al. (1994) (a) for beam, column, and end plate materials; (b) for bolt shank, head, and nut materials

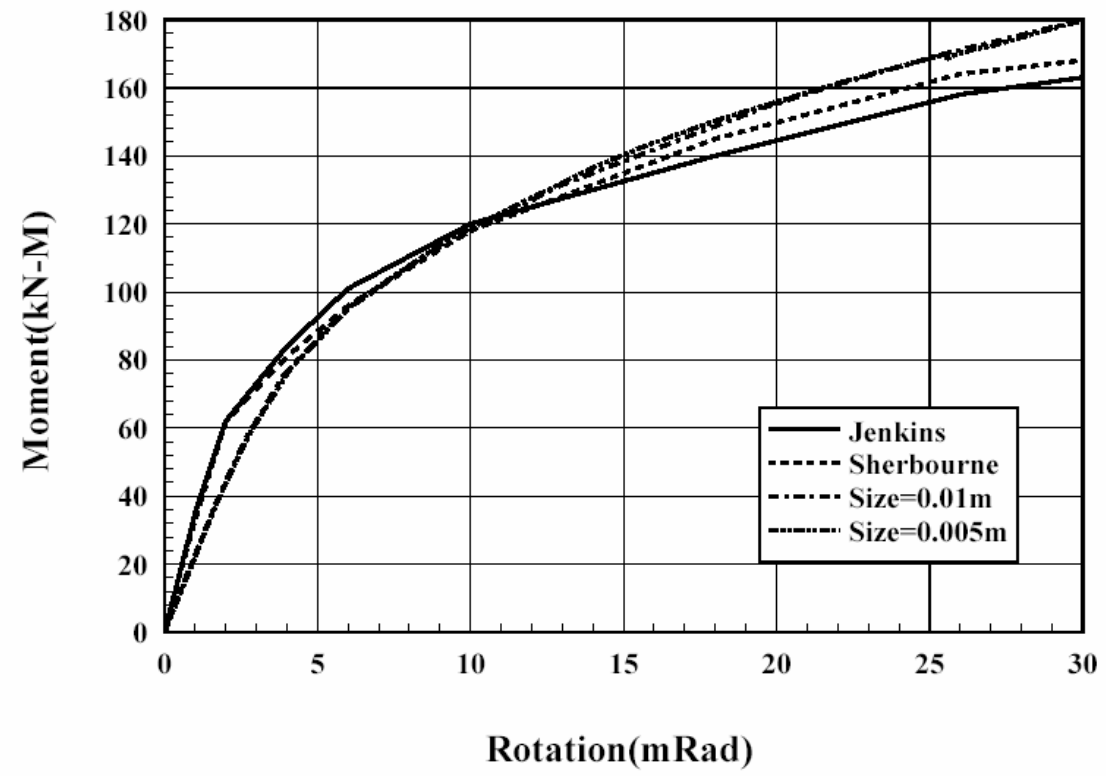

Fig. 5.11. For moment (kN-M) and rotation (0.001 radians) curve, comparison of test result of Jenkins et al. (1986), simulation results of Sherbourne et al. (1994) and ANAQUS simulation results of present study for element C3D8I with mesh sizes of 0.01m and 0.005m

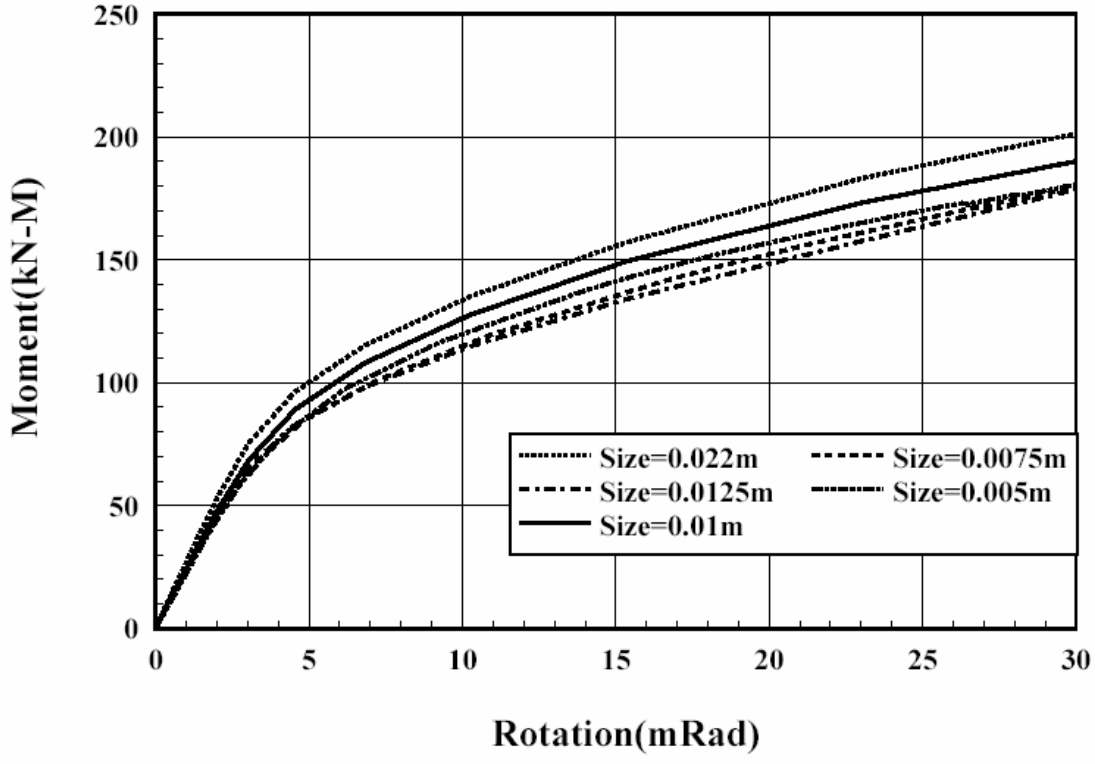

(a) Element C3D8

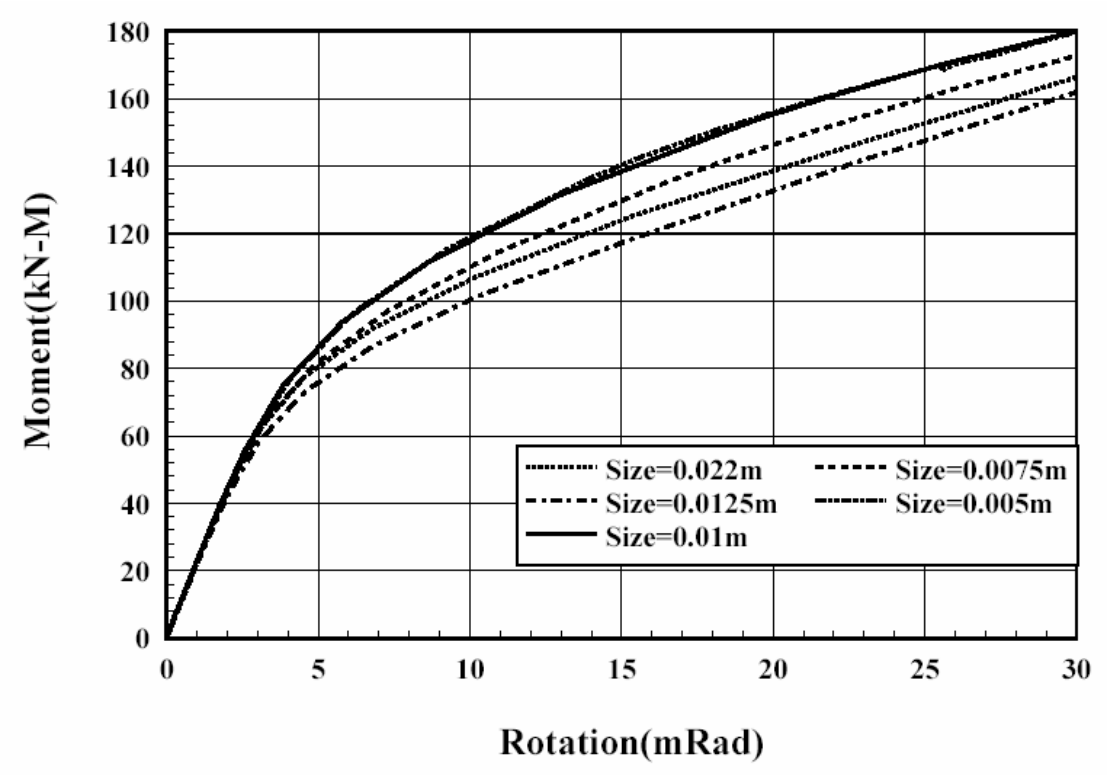

(b) Element C3D8I

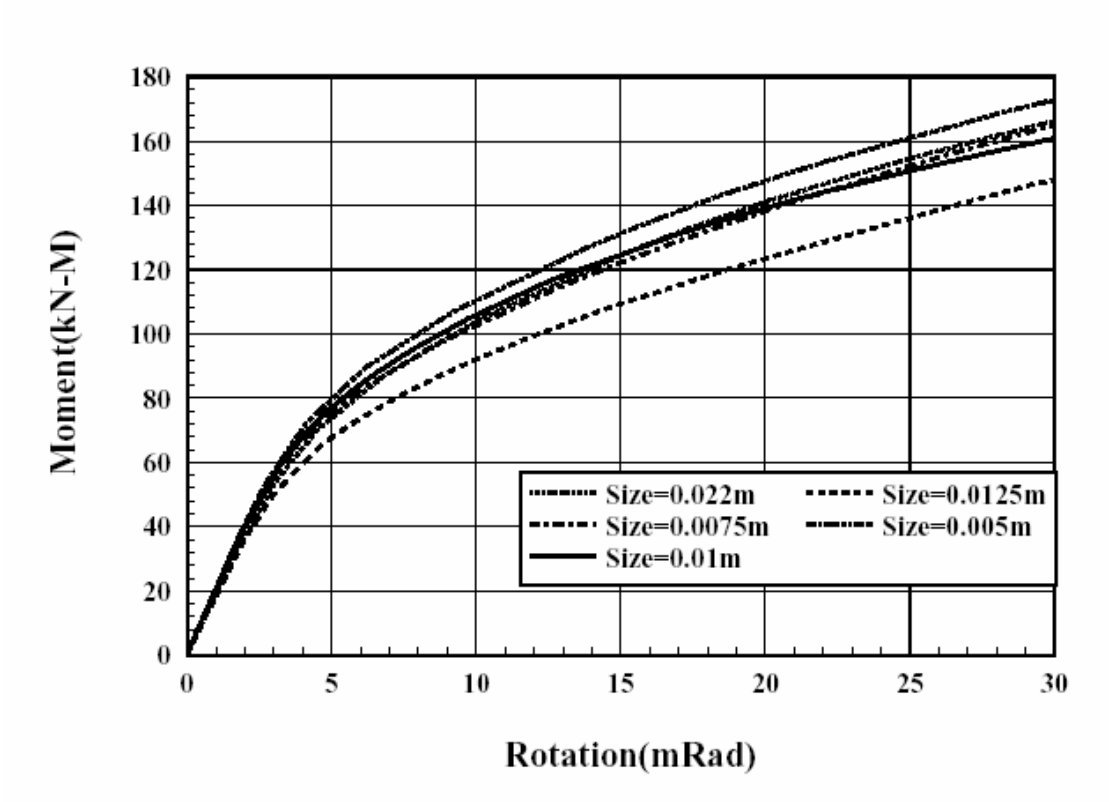

(c) Element C3D8RH

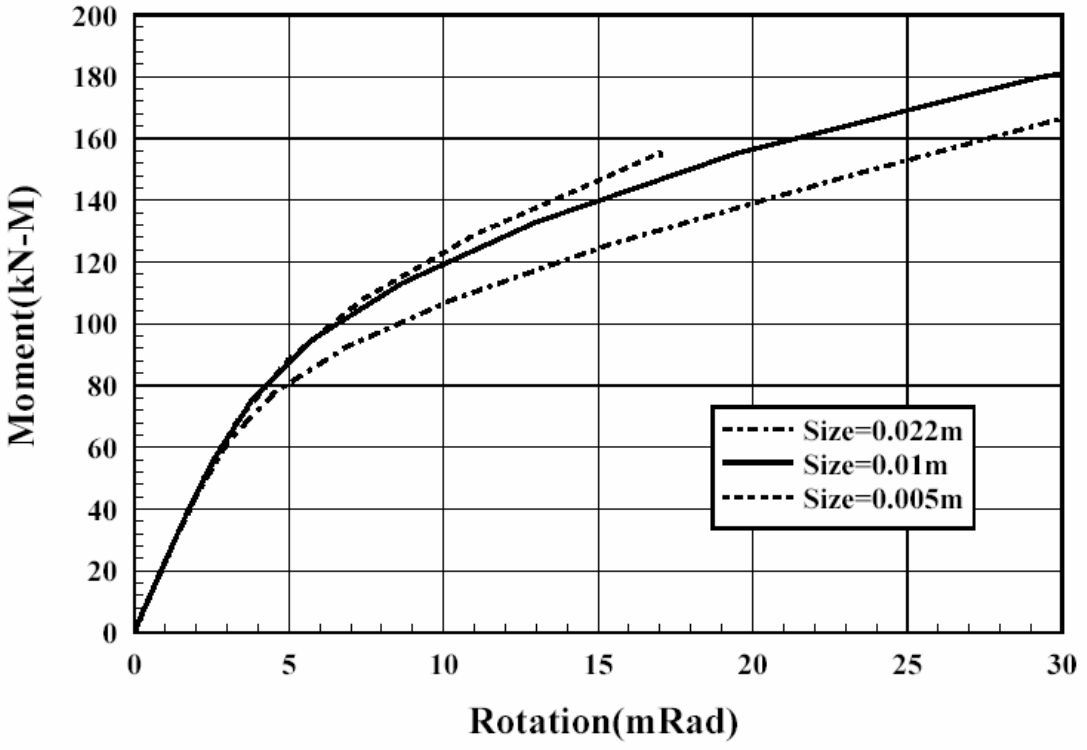

(d) Solid and shell elements

Fig. 5.12. For moment (kN-M) and rotation (0.001 radians) curve, comparison of ABAQUS simulation results of present study for different element types and mesh sizes

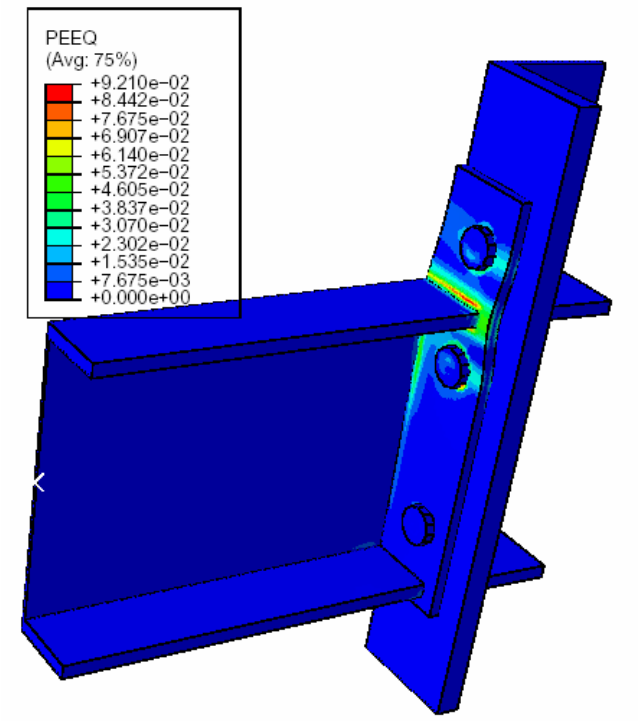

(a) Global

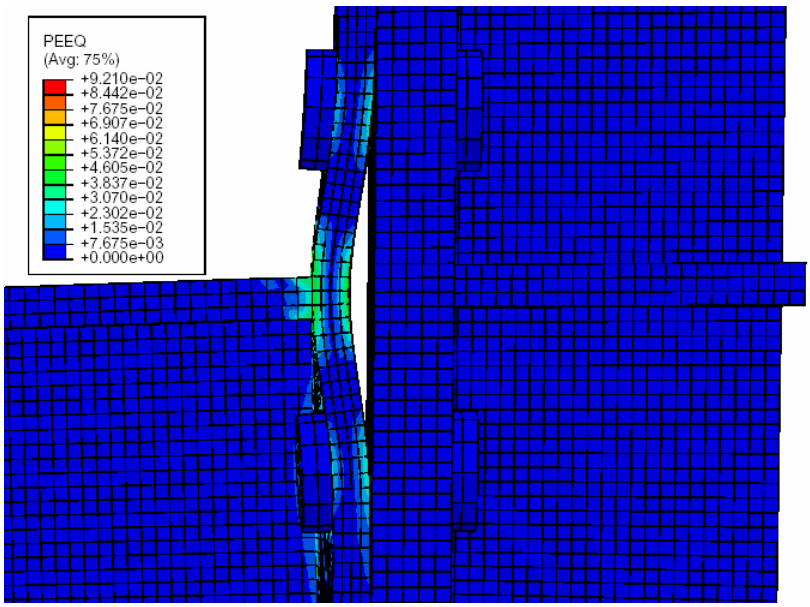

(b) Local at upper beam flange

Fig. 5.13. Simulation results of equivalent plastic strain (PEEQ) distribution by using C3D8I with mesh size of 0.005m

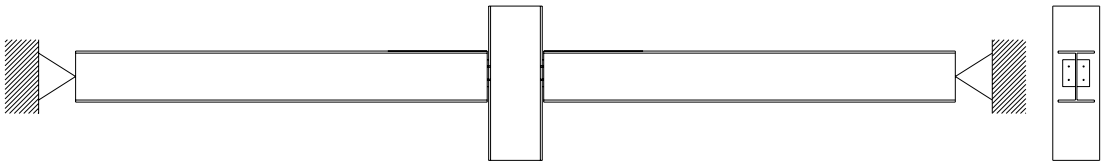

(a) Whole sub-structure

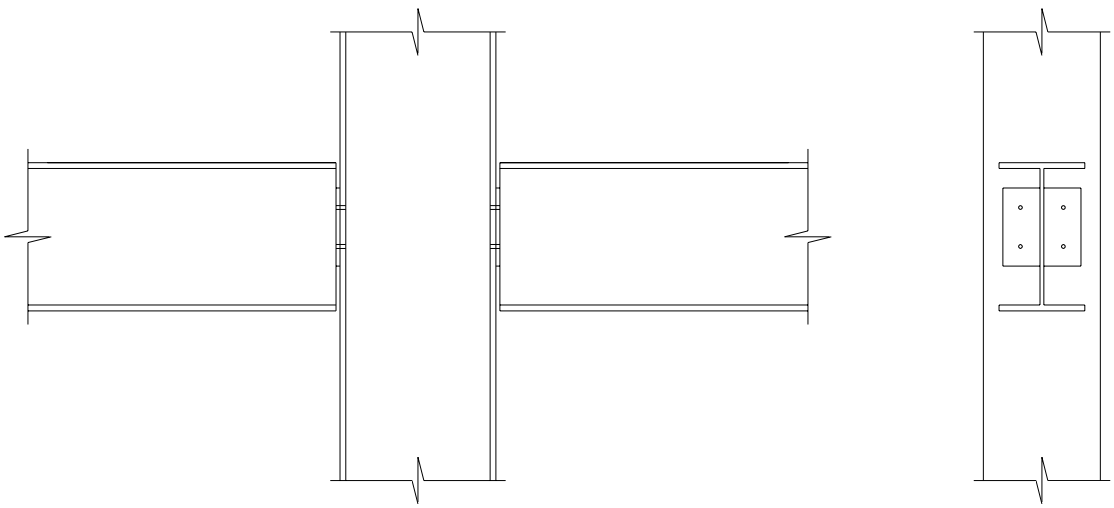

(b) Flexible end plate connection

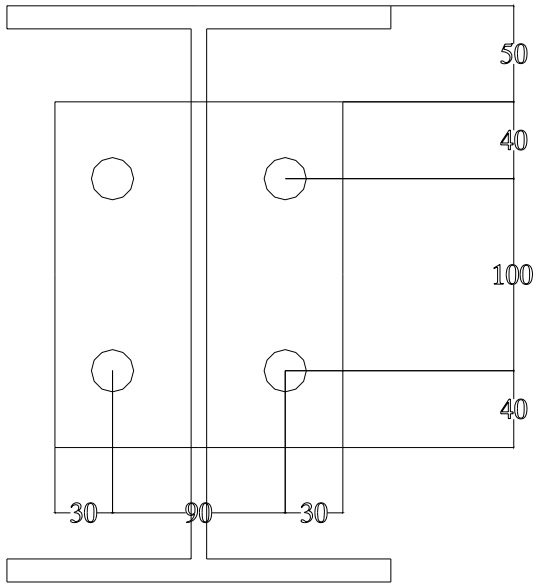

(c) Details of flexible end plate (mm)

Fig. 5.14. Sub-structure used in this study

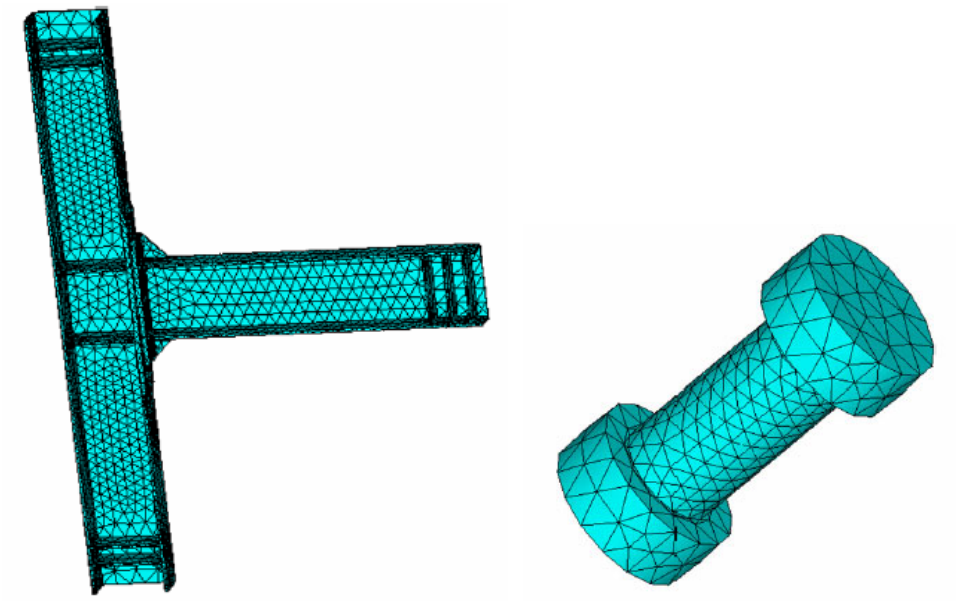

(a) Sub-structure (b) Bolt

Fig. 5.15. Finite element models of sub-structure and bolt by Shi et al. (2008)

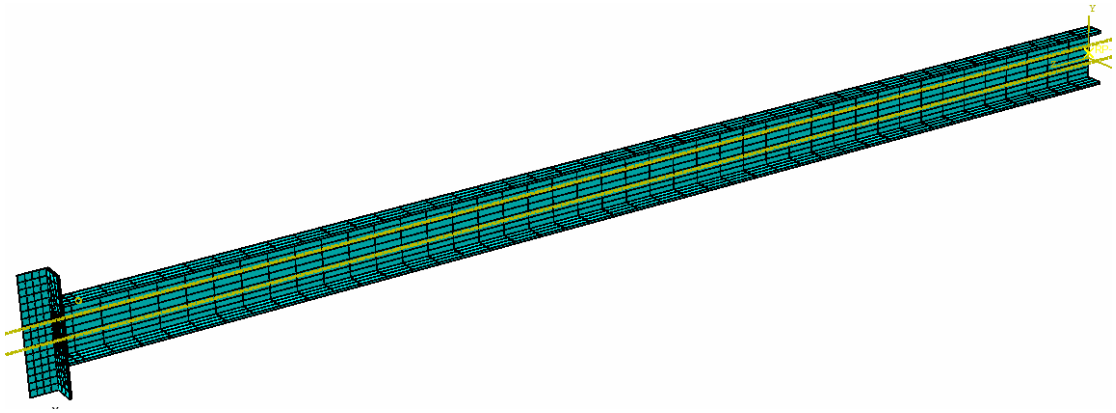

(a) Whole structure with mesh size=0.035m

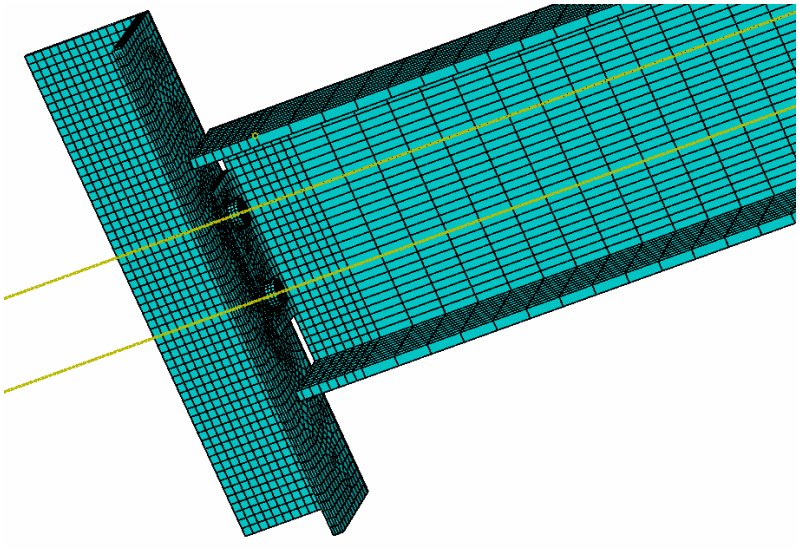

(b) Connection part with mesh size=0.01m

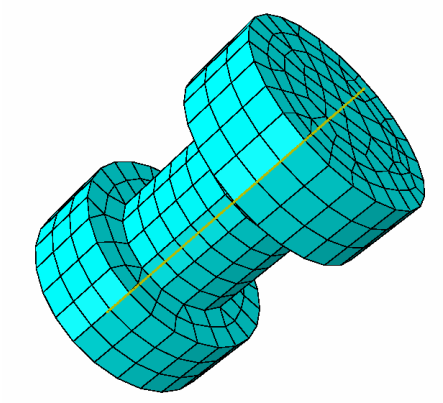

(c) Bolt with mesh size=0.004m

Fig. 5.16. Finite element models of original structure and bolt in this study

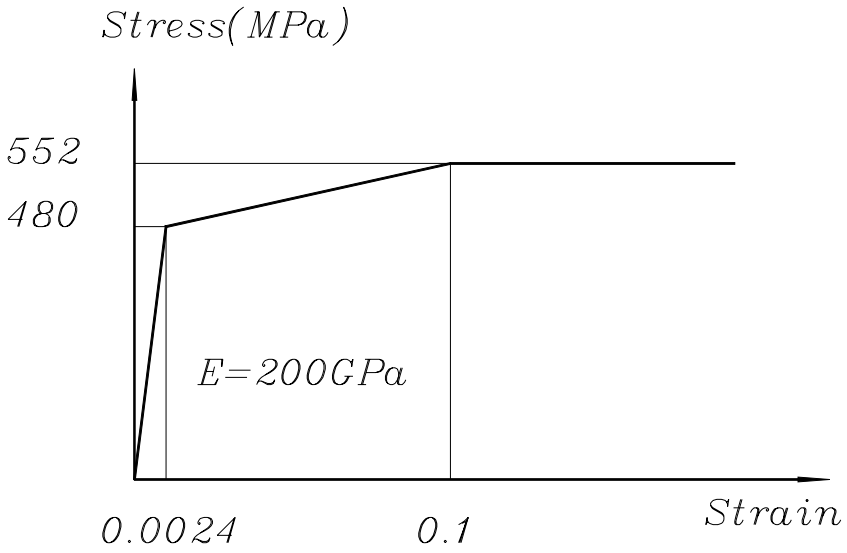

(a) Chao et al. (2006)

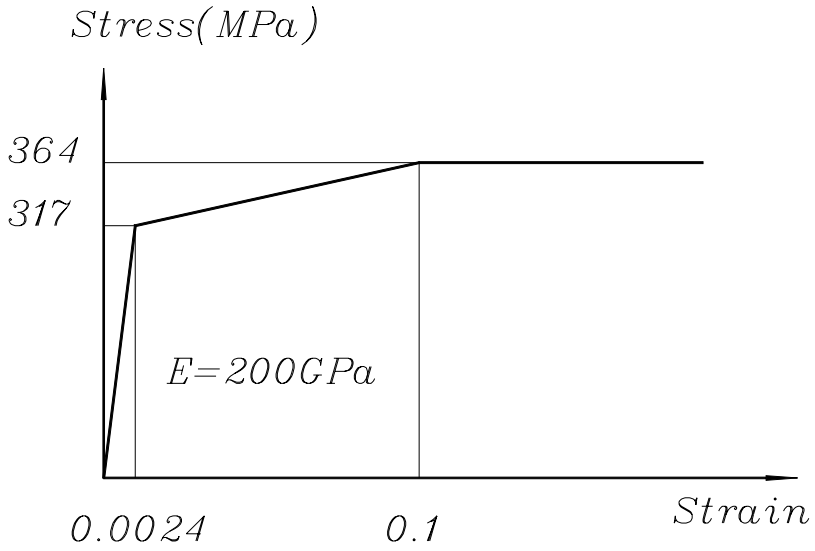

(b) This study

Fig. 5.17. Stress and strain curves for welds

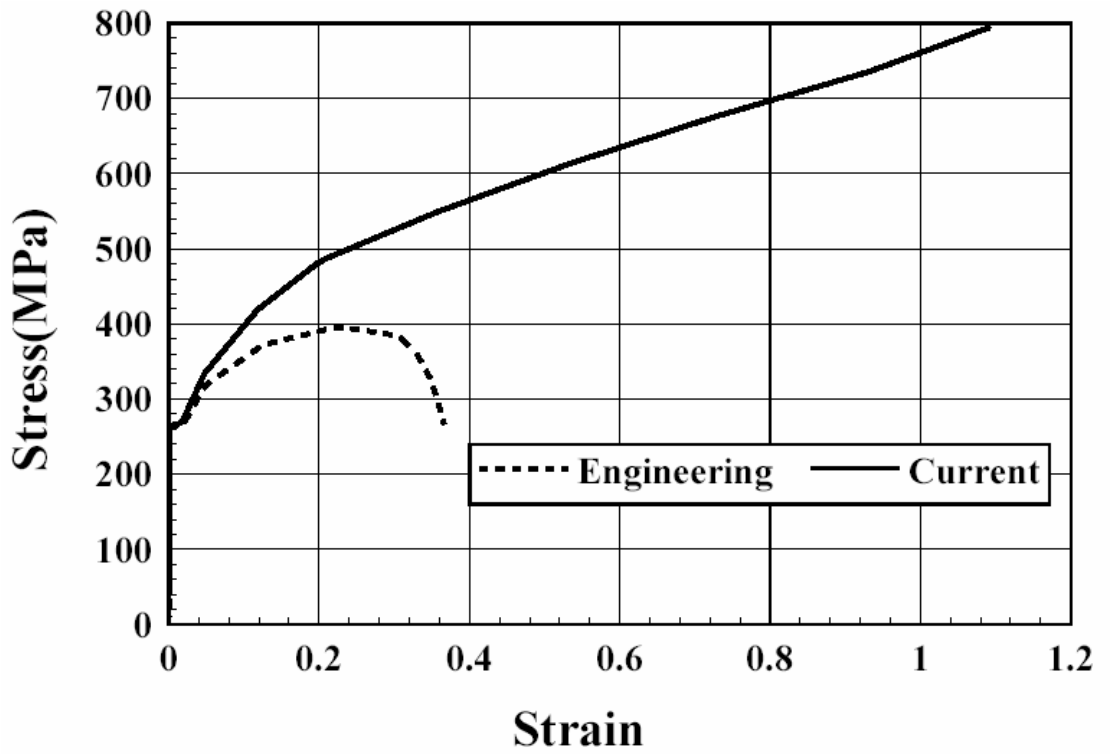

Fig. 5.18. Stress and strain curves for steel plates

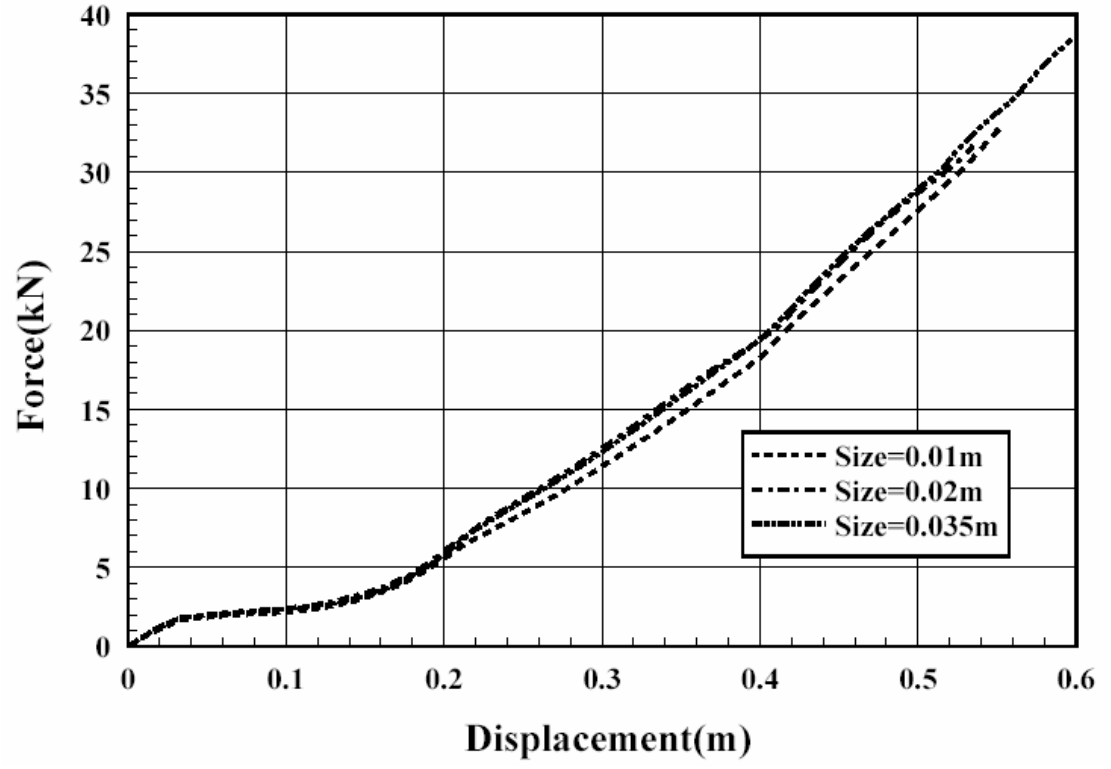

Fig. 5.19. Relationship between vertical reaction force at right end versus vertical displacement at left end for original structure for different mesh sizes

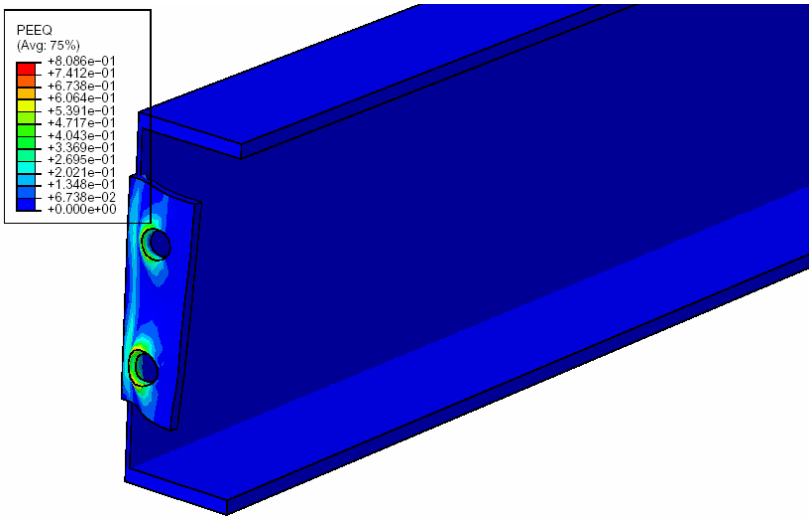

(a) Distribution at flexible end plate when load scaling factor is 0.1235

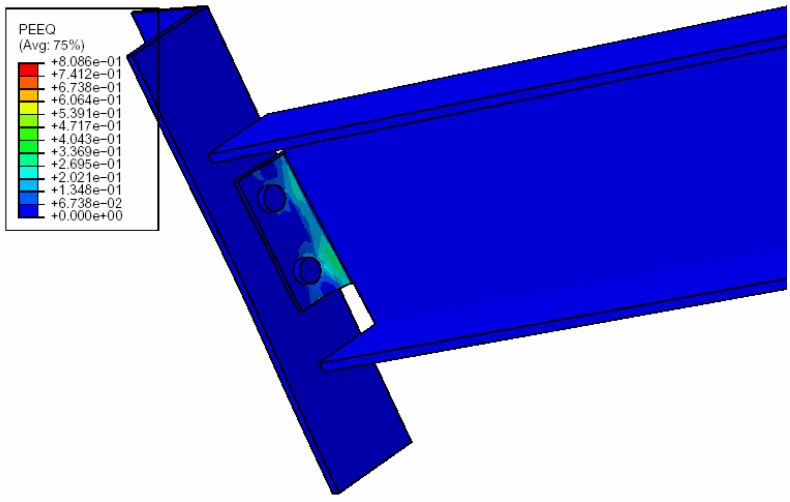

(b) Distribution at connection part when load scaling factor is 0.1235

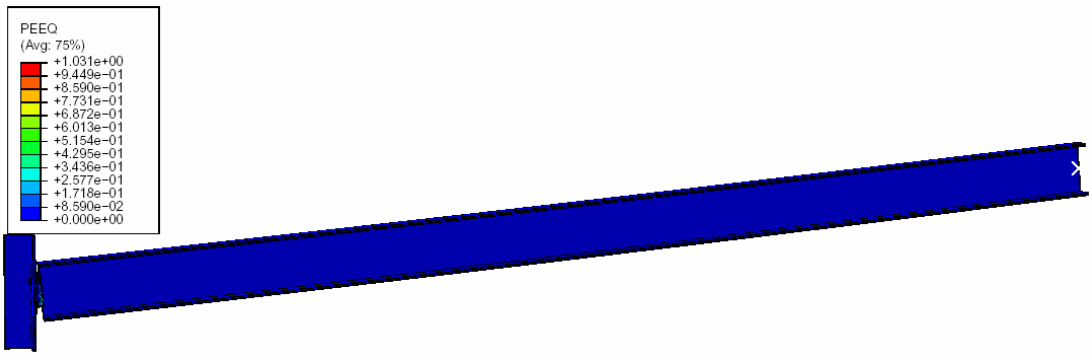

(c) Distribution of whole structure when (load scaling factor is 0.1471

Fig. 5.20. Equivalent plastic strain distributions for original structure

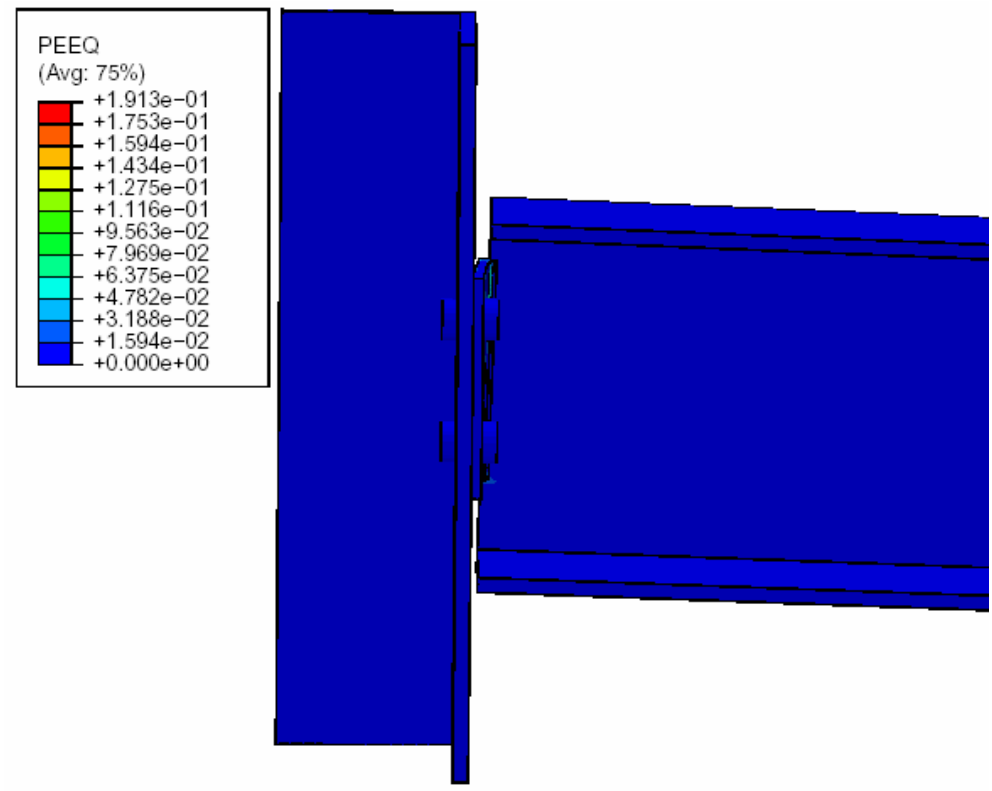

(a) The minimum distance reached when load scaling factor is 0.0403

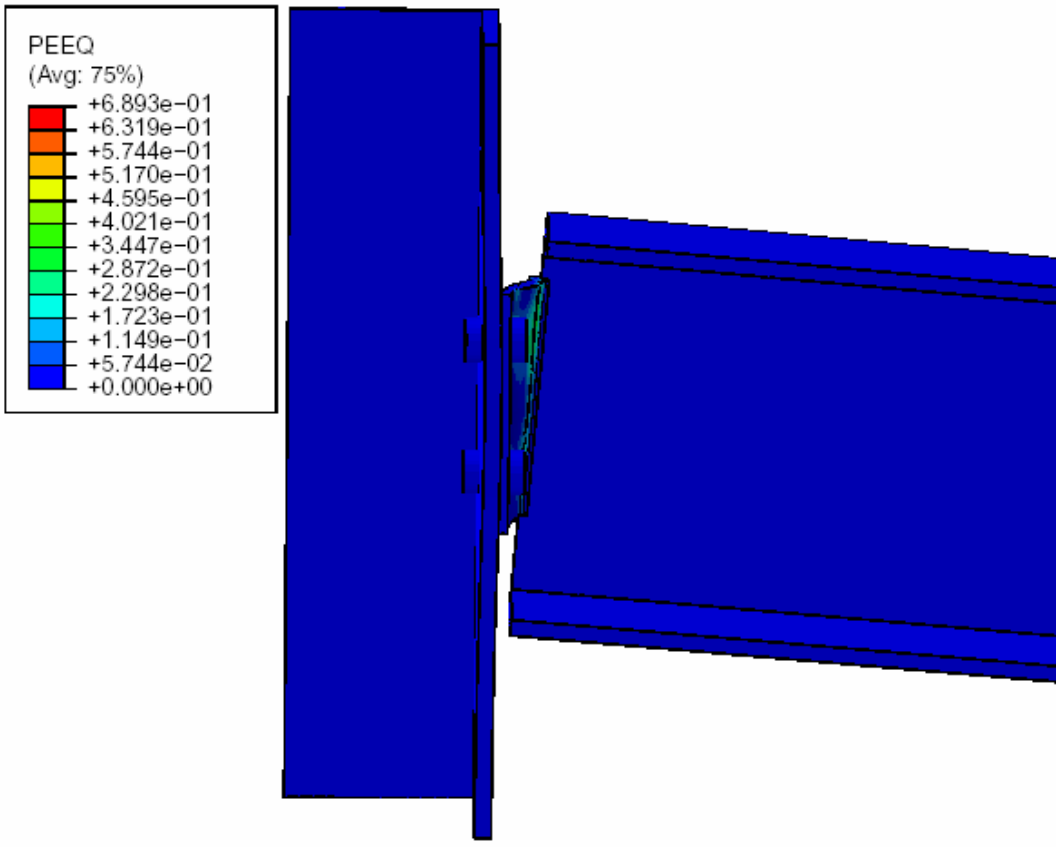

(b) Distance when the load scaling factor is 0.2024.

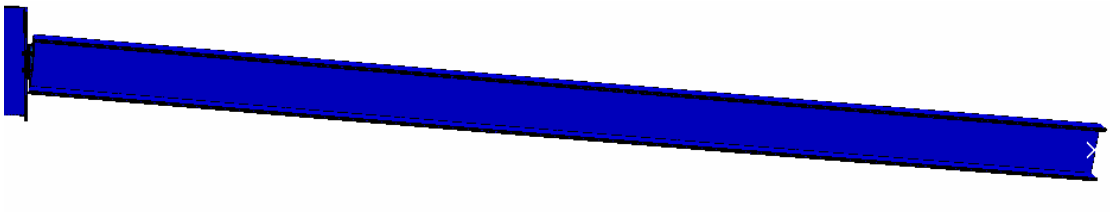

(c) Whole structure when the load scaling factor is 0.2024

Fig. 5.21. Distance between lower beam flange and column flange

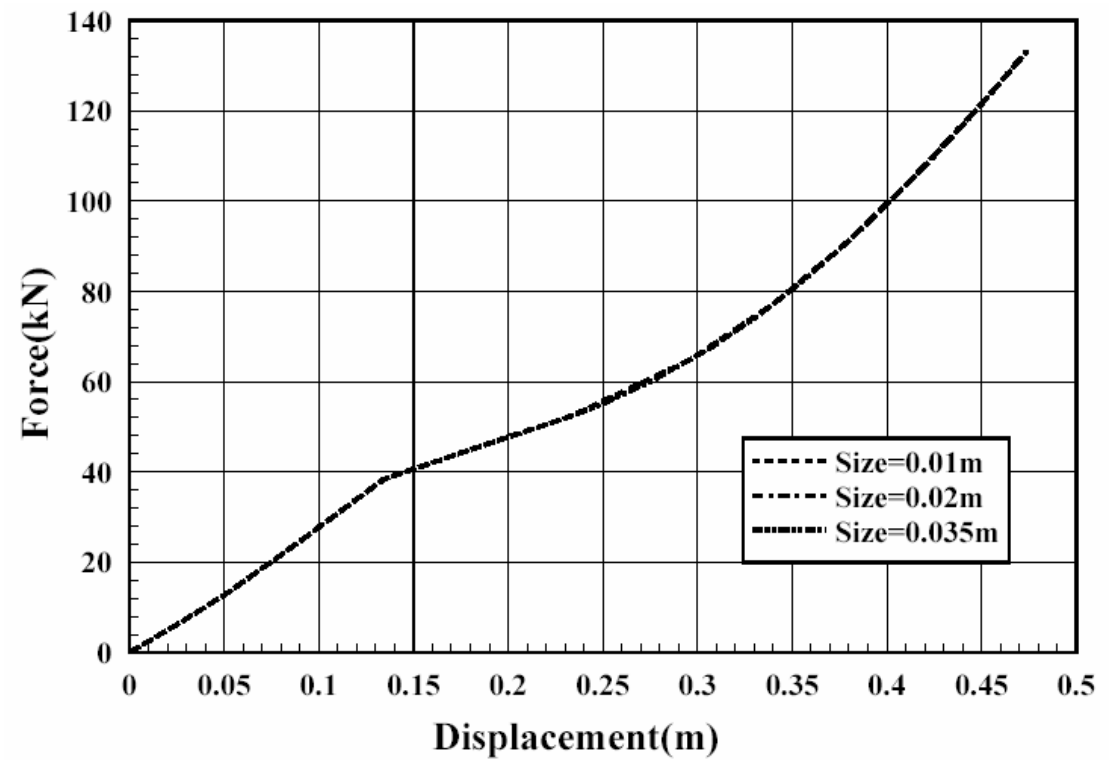

Fig. 5.22. Relationship between vertical reaction force at right end versus vertical displacement at left end for structure retrofitted by flange cover plates for different mesh sizes

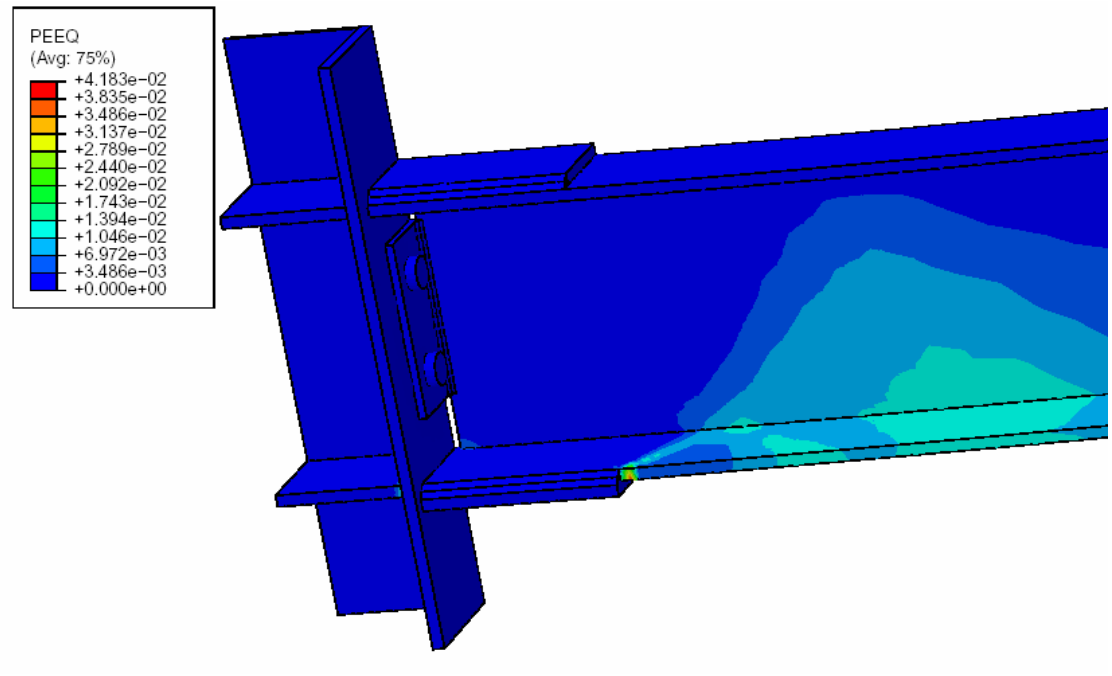

(a) Distribution at connection part

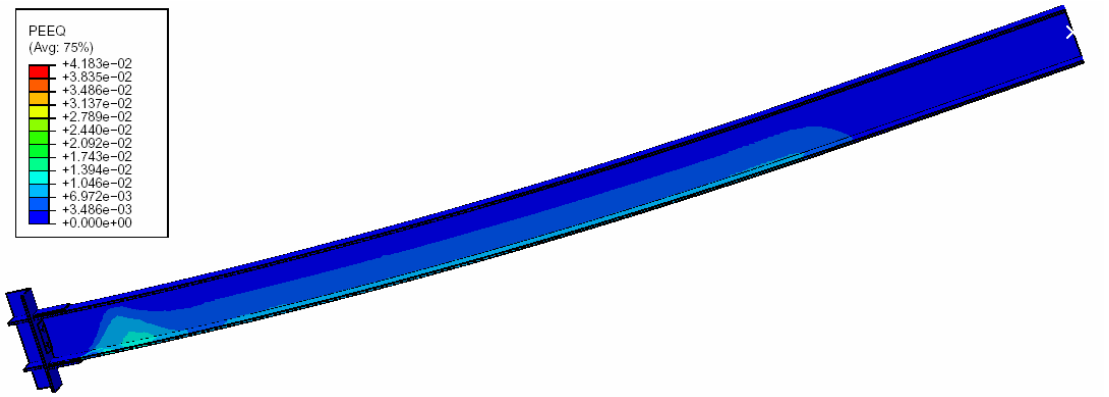

(b) Distribution of whole structure

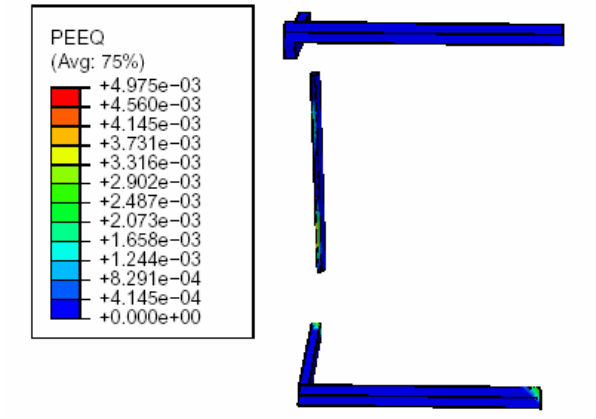

(c) Distribution of welds

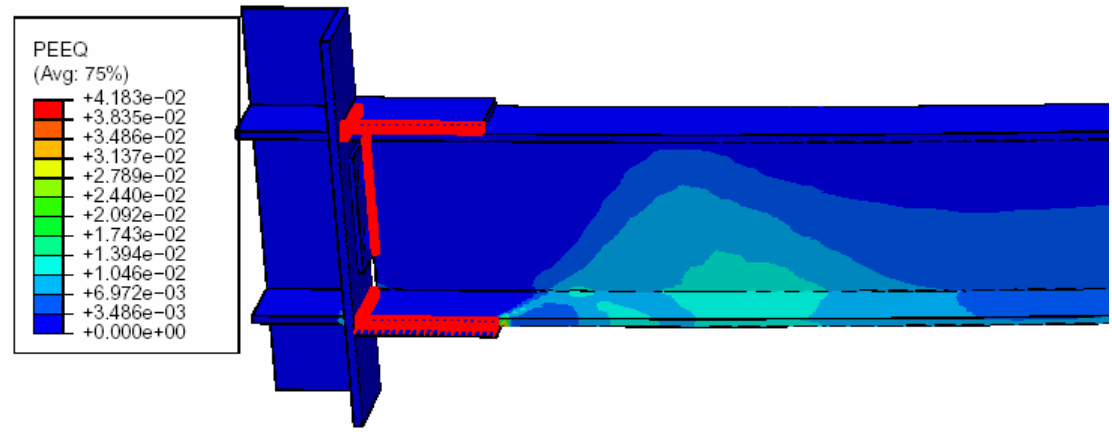

(d) Location of welds at the connection

Fig. 5.23. When load scaling factor is 2, equivalent plastic strain distributions of structure retrofitted by Flange Plate Scheme

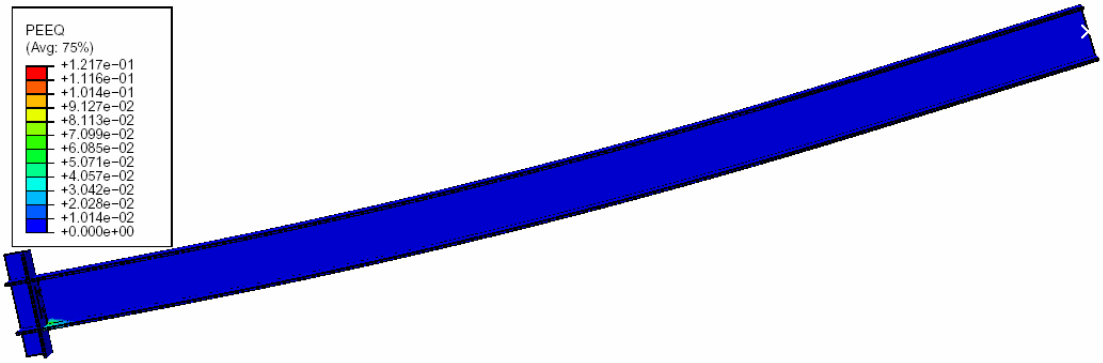

Fig. 5.24. When load scaling factor is 2, equivalent plastic strain distributions of structure retrofitted by Traditional Moment Connection Scheme

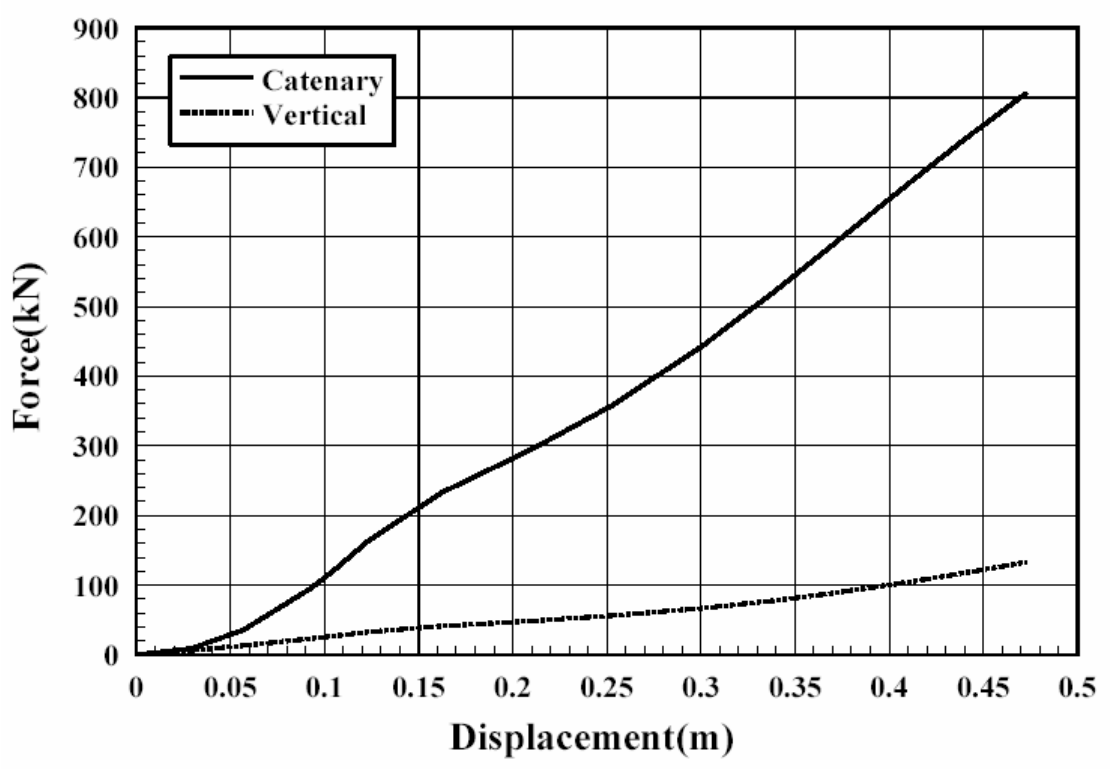

Fig. 5.25. When load scaling factor is 2, relationships between catenary tension at left end and vertical reaction force at right end versus vertical displacement at left end for structure retrofitted by vertical plates

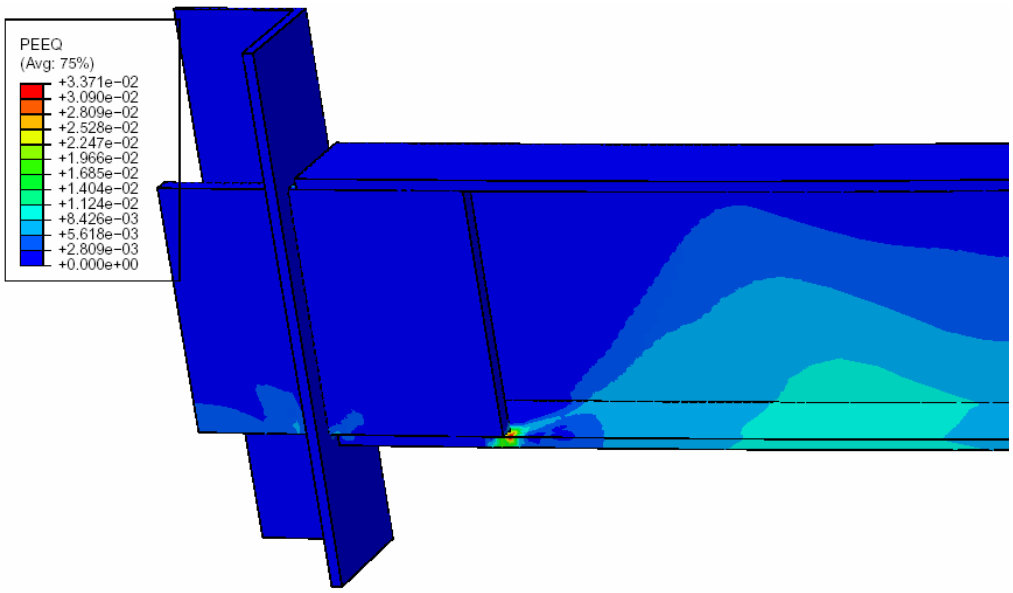

(a) Distribution at connection part with vertical plate

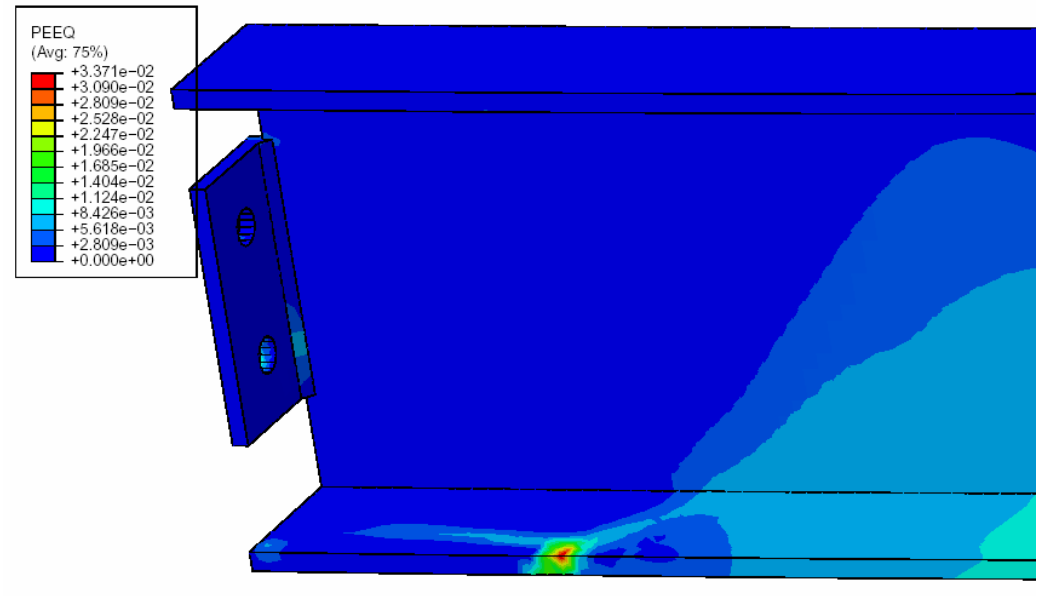

(b) Distribution at connection part without vertical plate

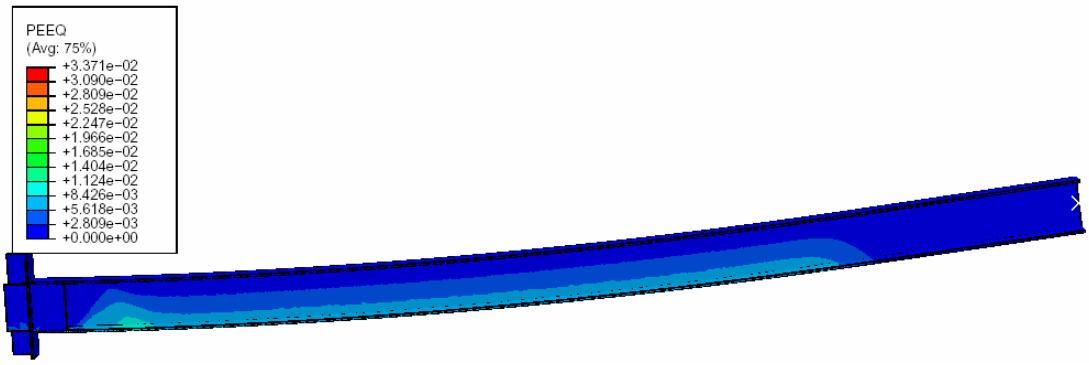

(c) Distribution of whole structure

Fig. 5.26. When load scaling factor is 2, equivalent plastic strain distributions of structure retrofitted by Flange Plate Scheme

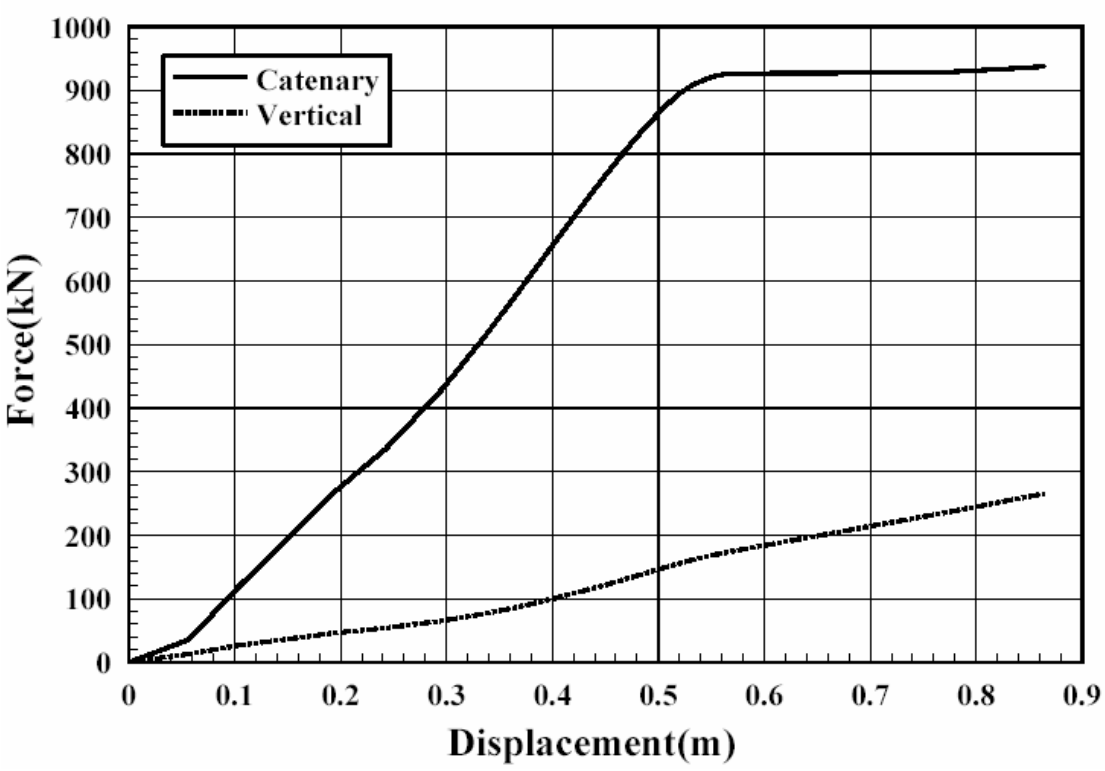

(a) Relationships between catenary tension at left end and vertical reaction force at right end versus vertical displacement at left end

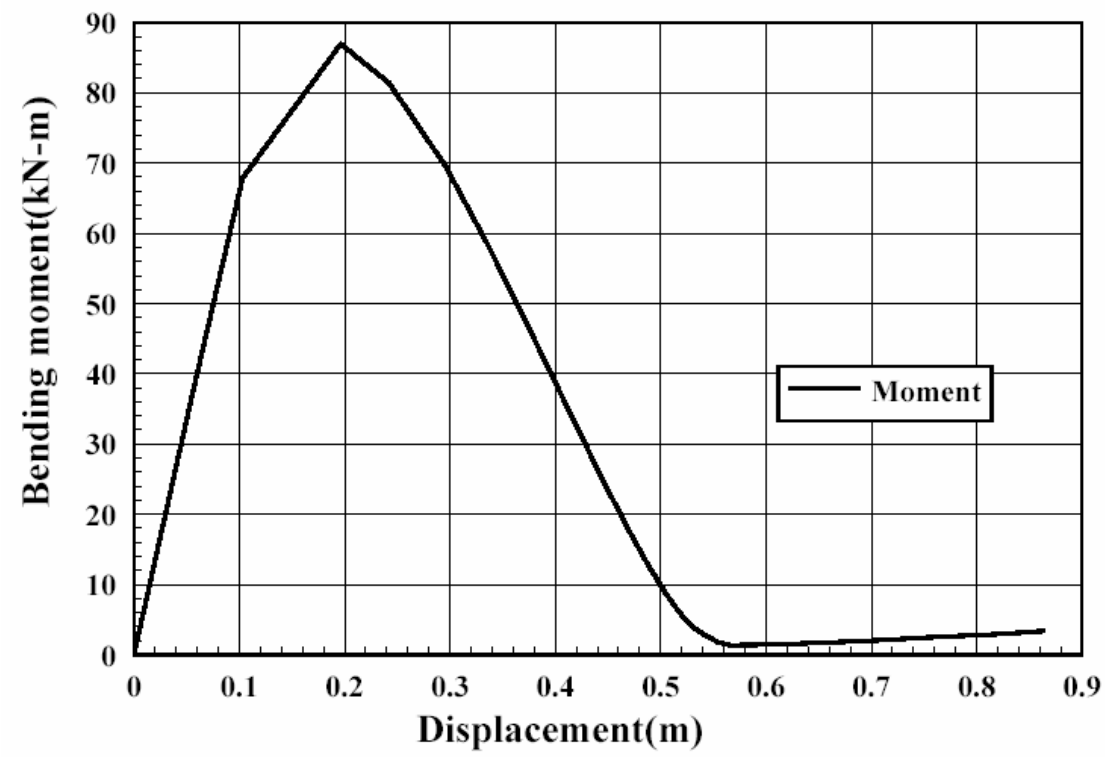

(b) Relationships between bending moment versus vertical displacement at left end

Fig. 5.27. When load scaling factor is 4, relationships between forces versus displacement for structure retrofitted by vertical plates

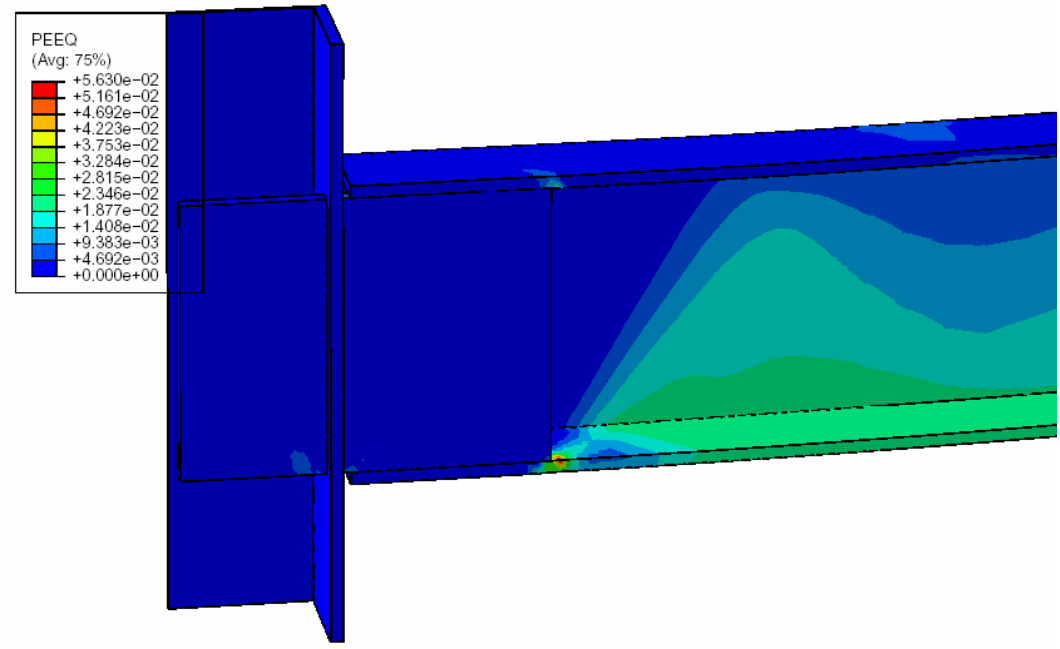

(a) Distribution at connection part

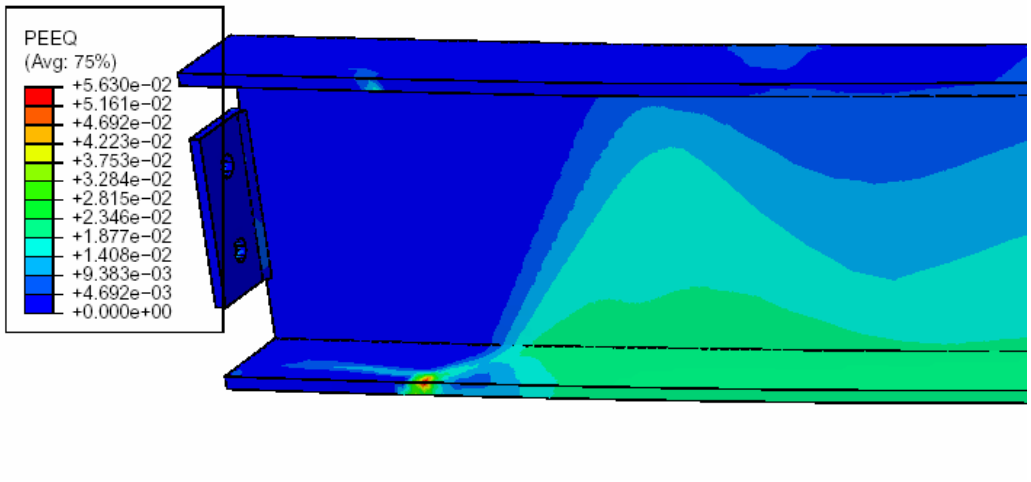

(b) Distribution at connection part without vertical plate

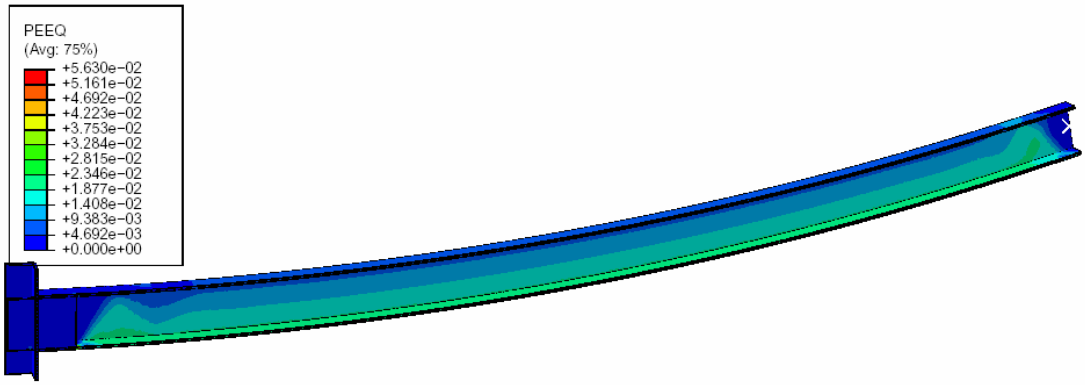

(c) Distribution of whole structure

Fig. 5.28. When load scaling factor is 4, equivalent plastic strain distributions of structure retrofitted by Flange Plate Scheme

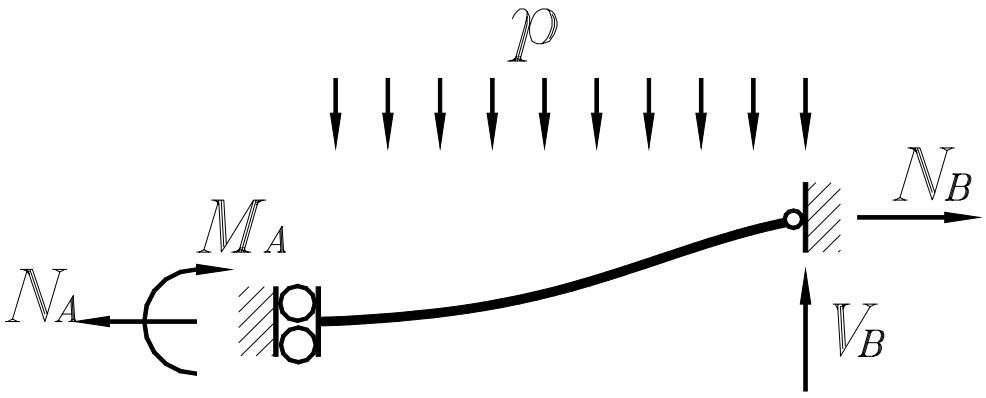

Fig. 5.29. Analysis of catenary tension

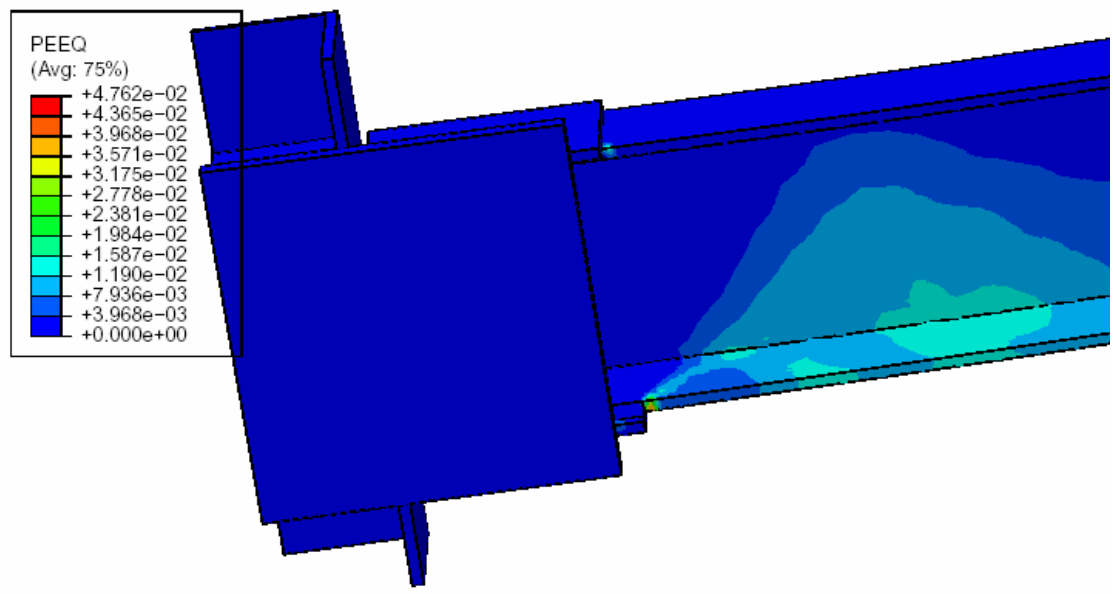

(a) Distribution at connection part

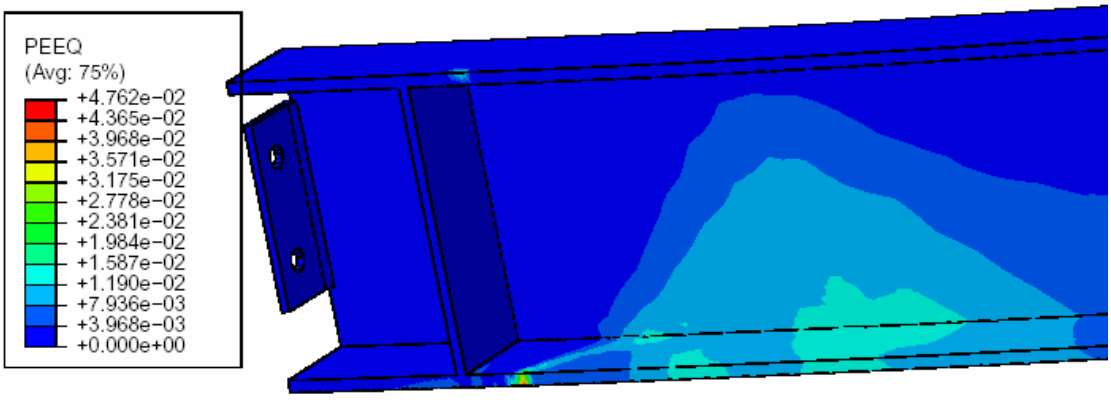

(b) Distribution at connection part behind side plate

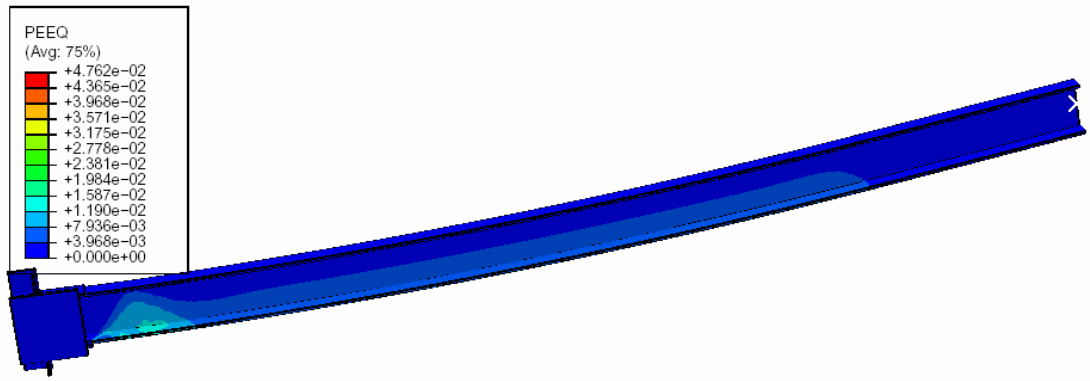

(c) Distribution of whole structure

Fig. 5.30. When load scaling factor is 2, equivalent plastic strain distributions of structure retrofitted by SidePate Scheme

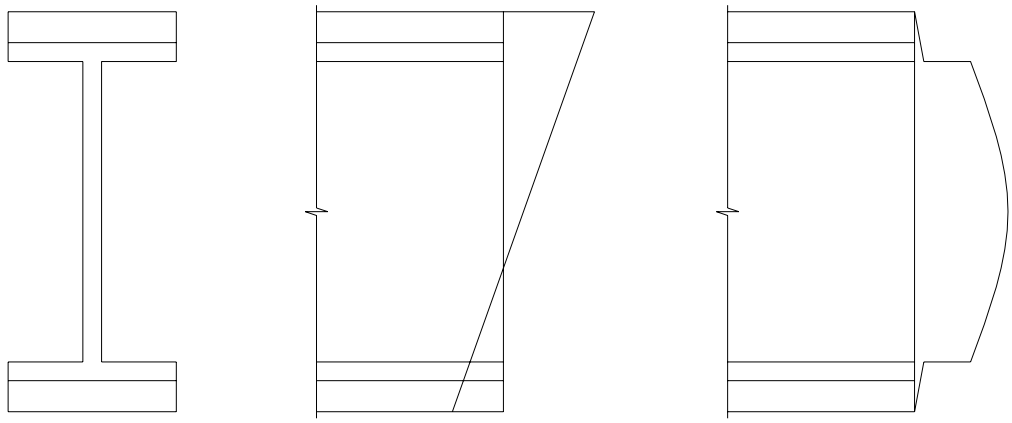

(a) Cross-section, normal stress and shear stress distributions in elastic state

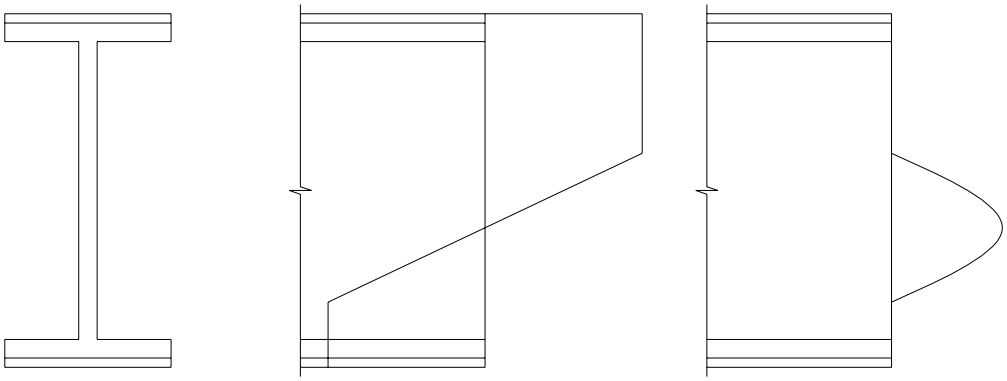

(b) Cross-section, normal stress and shear stress distributions in elasto-plastic state

Fig. 6.1. Variation sequence of stress distributions on cross-section due to reducing thickness of flange cover plates

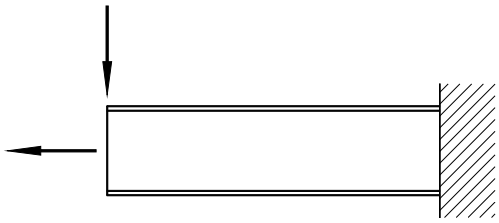

Fig. 6.2. Normal beam before retrofitting in Models 6.1 and 6.2

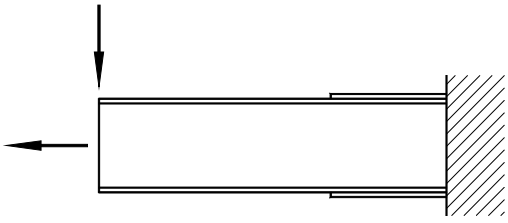

Fig. 6.3. Beam retrofitted by Flange Plate Scheme in Model 6.1

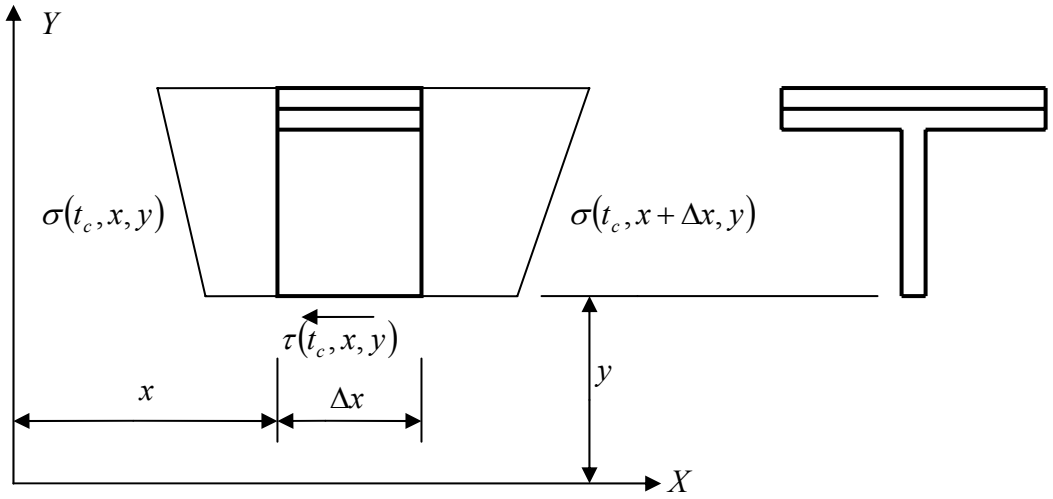

Fig. 6.4. Stress distribution of isolated element

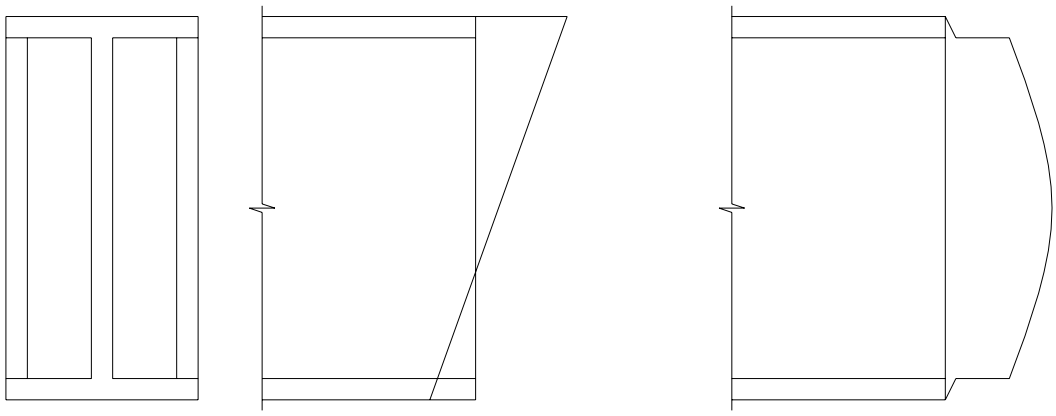

(a) Cross-section, normal stress and shear stress distributions in elastic state

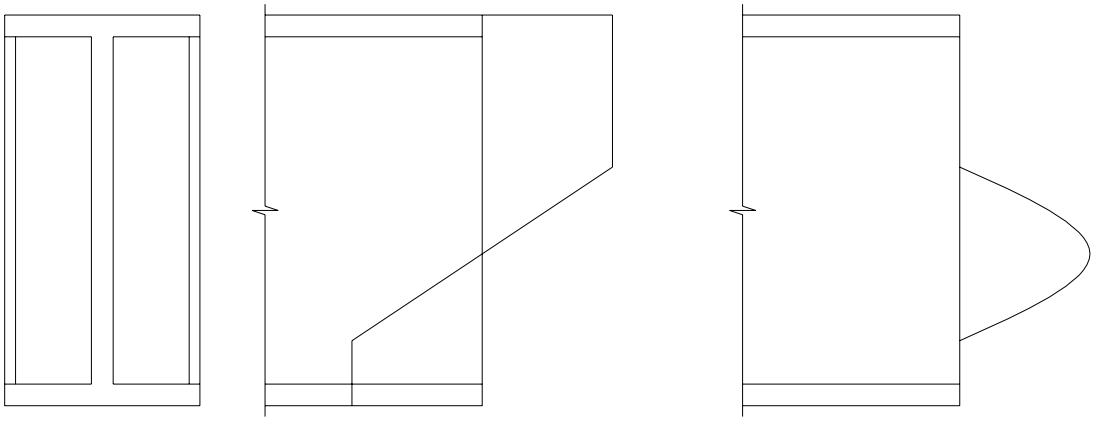

(b) Cross-section, normal stress and shear stress distributions in elasto-plastic state

Fig. 6.5. Variation sequence of stress distributions on cross-section due to reducing thickness of vertical plates

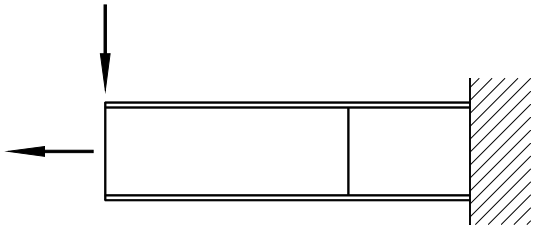

Fig. 6.6. Beam retrofitted by Vertical Plate Scheme in Model 6.2

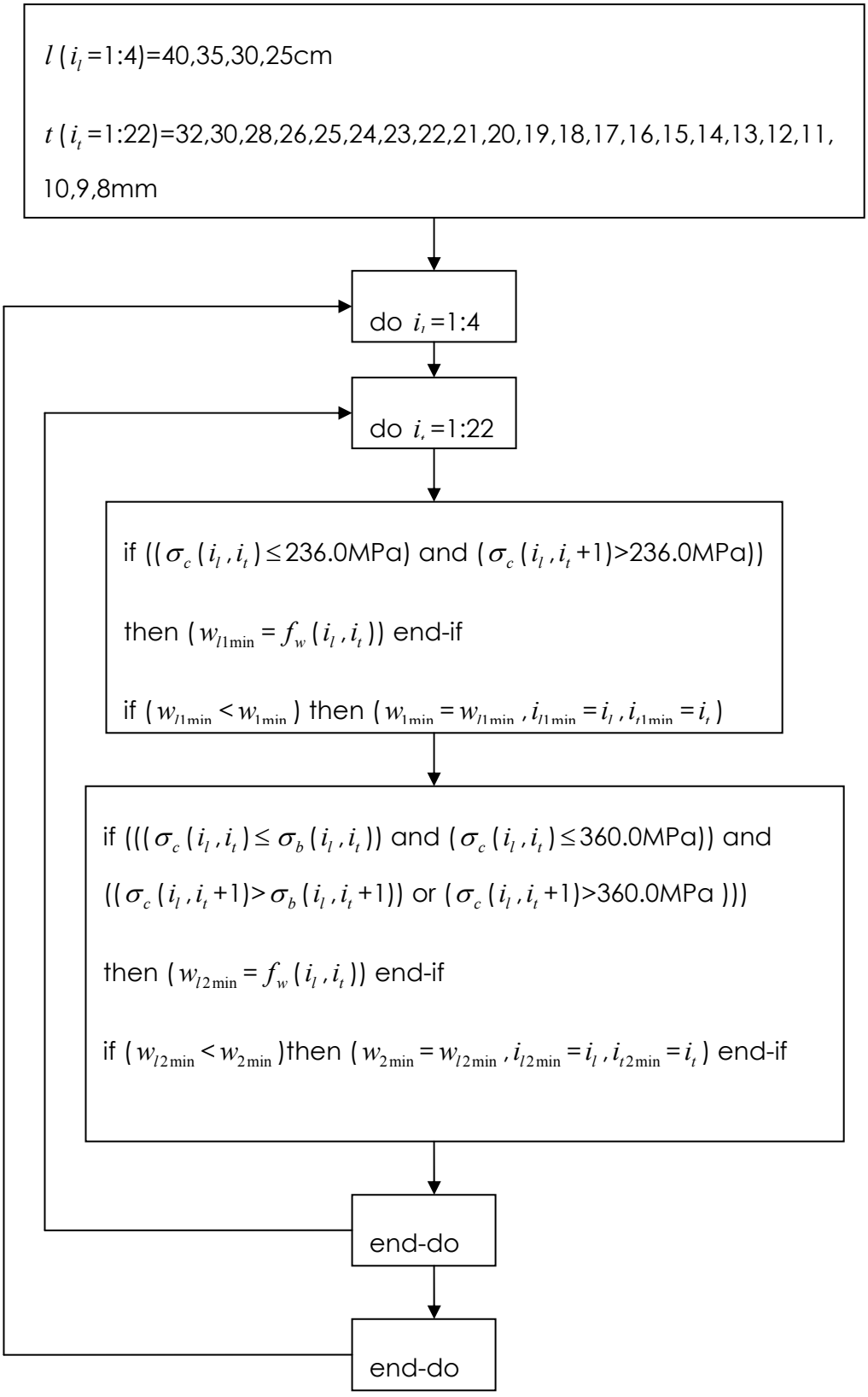

Fig .6.7. Procedure for minimising weight of strengthening plates

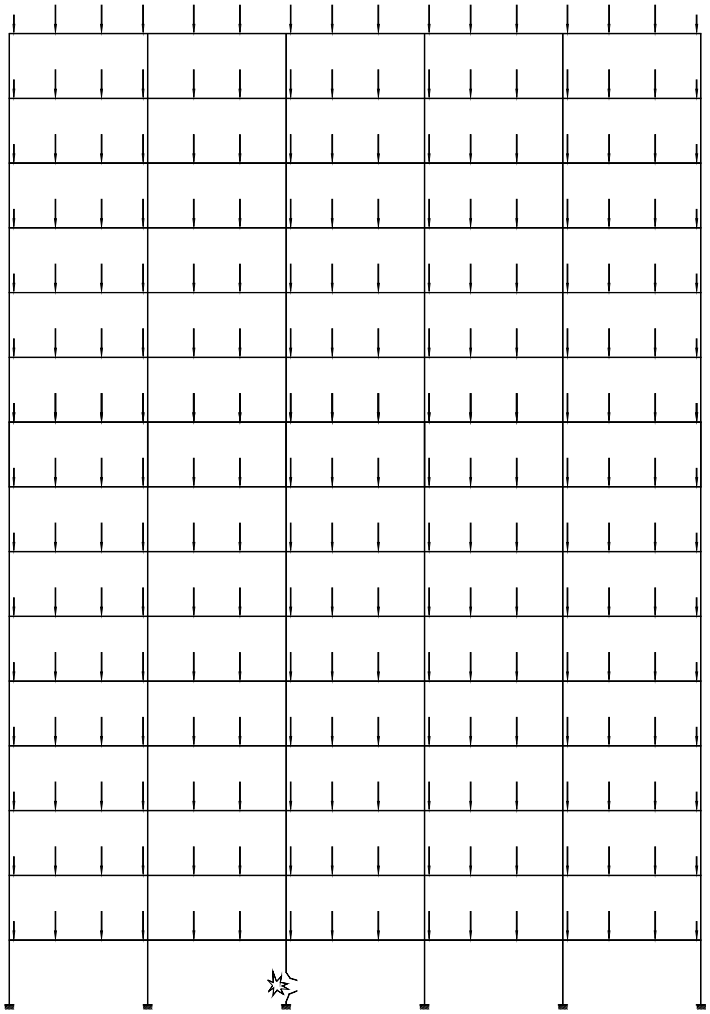

(a) Whole model

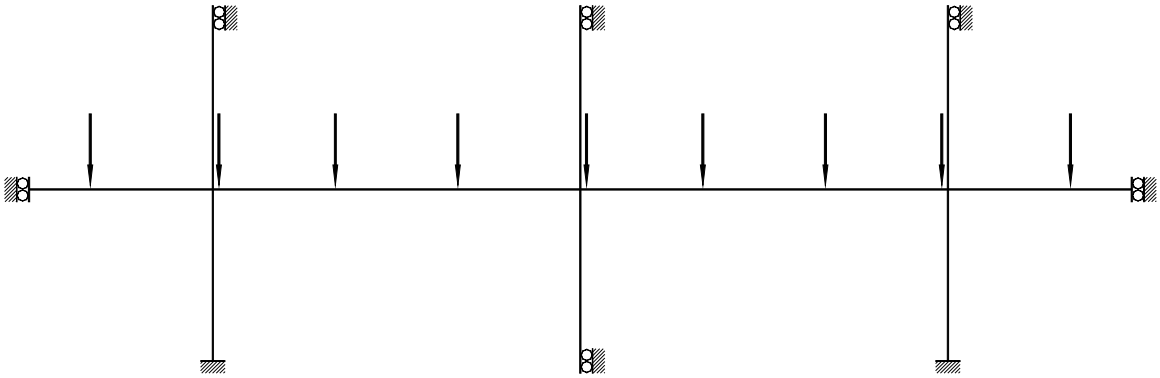

(b) One-storey part model

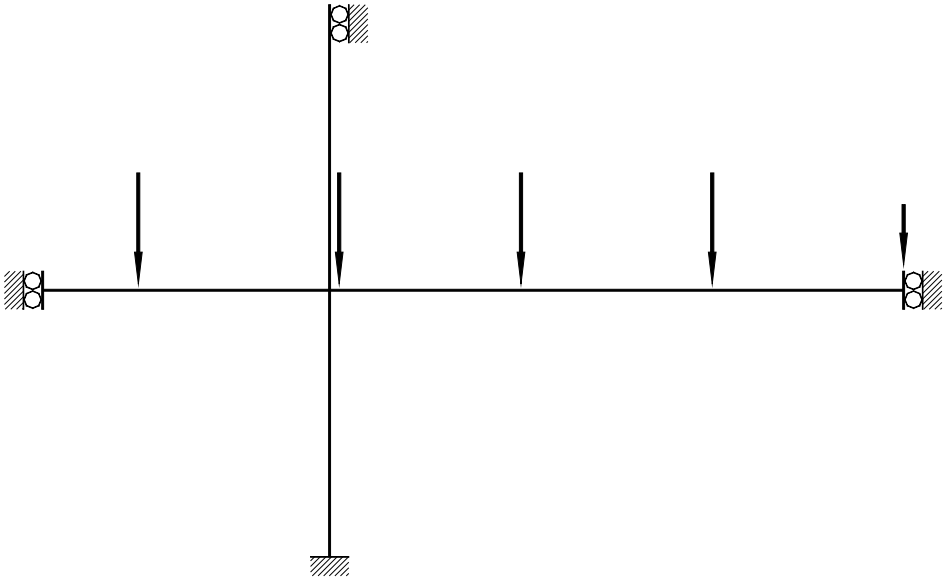

(c) Half Model used in finite element analyses

Fig. 6.8. Structure investigated in Model 6.3

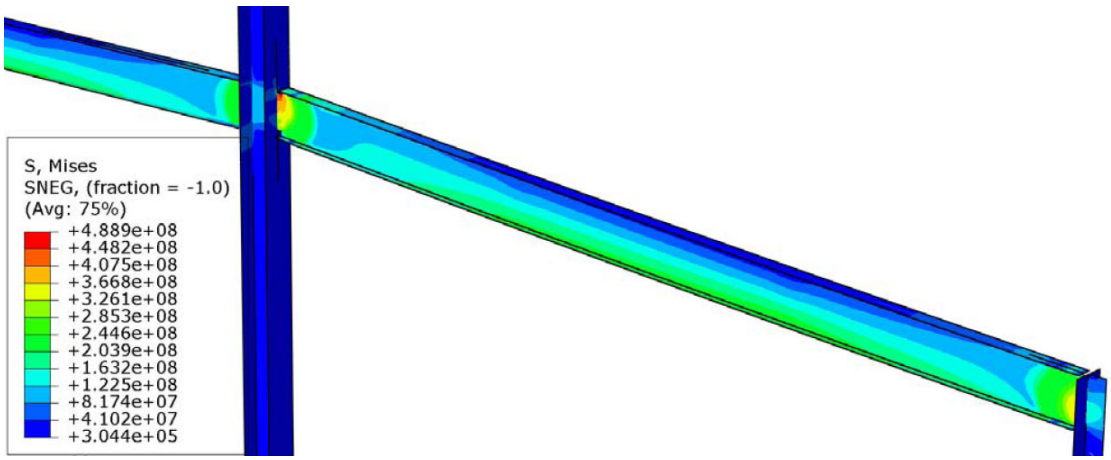

(a) Mises stress distribution

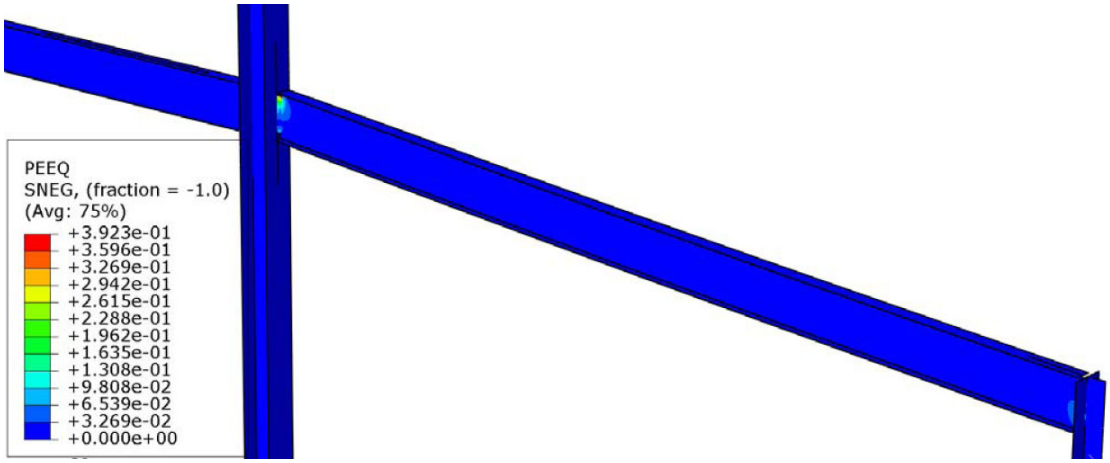

(b) Equivalent plastic strain distribution

Fig. 6.9. Mises stress and equivalent plastic strain distributions of original structure

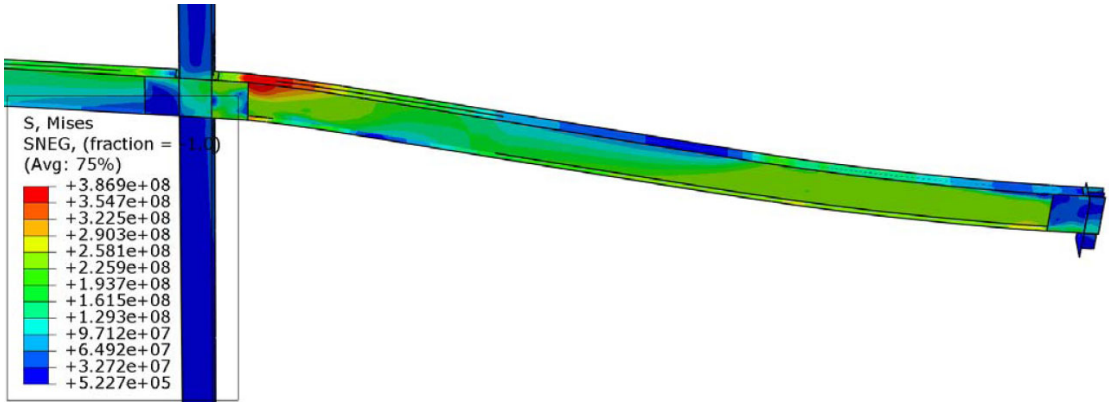

(a) Mises stress(Pa) distribution

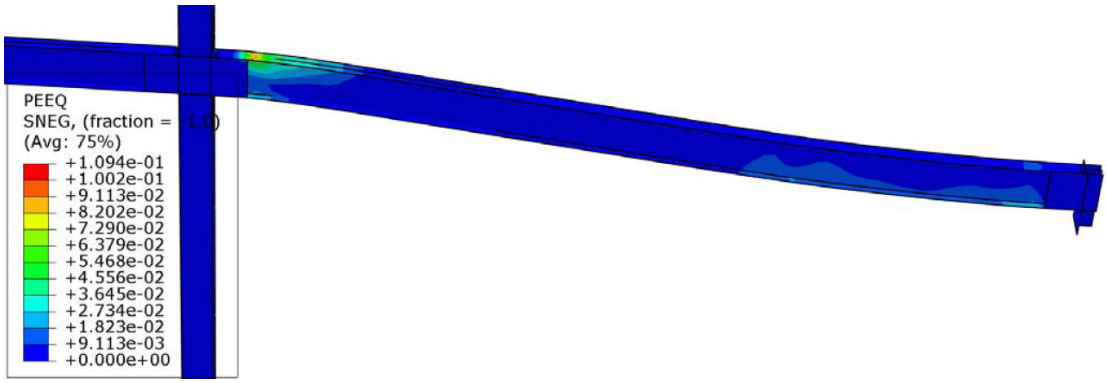

(b) Equivalent plastic strain distribution

Fig. 6.10. Mises stress and equivalent plastic strain distributions of structure retrofitted by vertical plates for first criterion

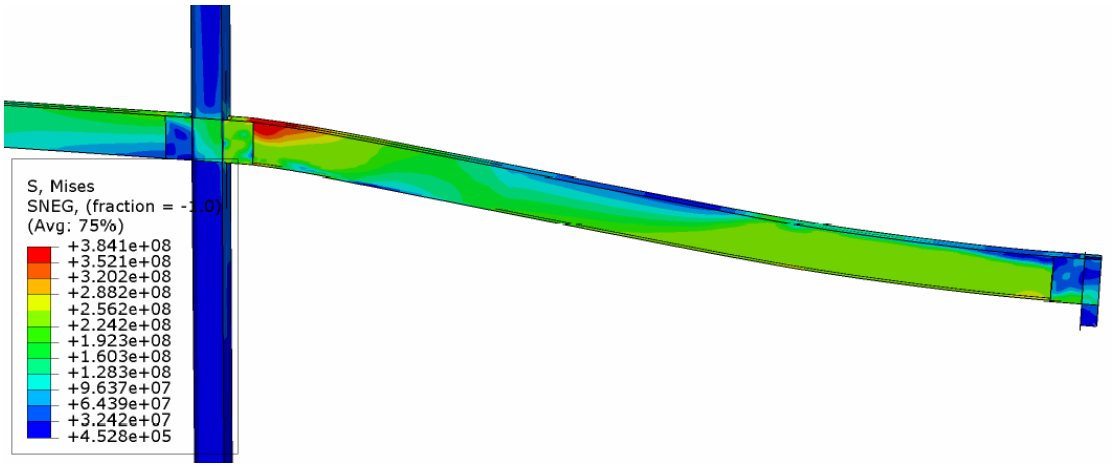

(a) Mises stress (Pa) distribution

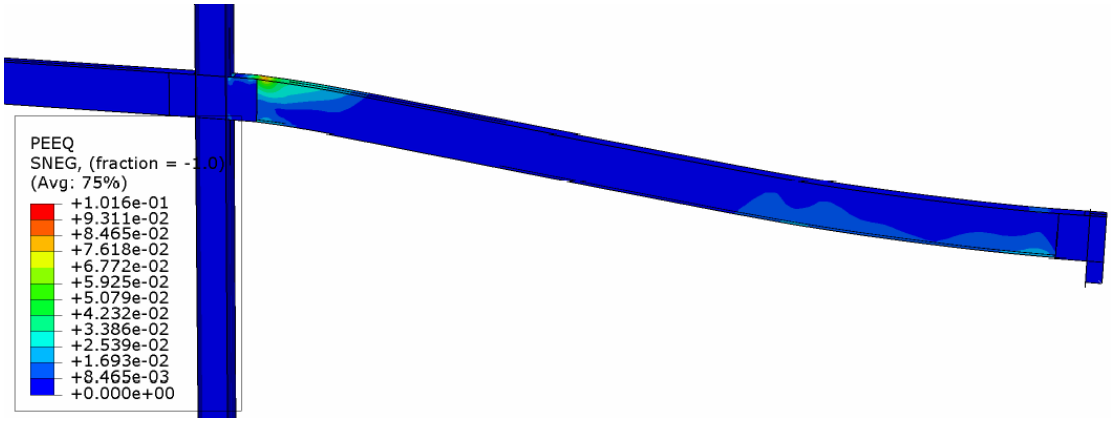

(b) Equivalent plastic strain distribution

Fig. 6.11. Mises stress and equivalent plastic strain distributions of structure retrofitted by vertical plates for second criterion

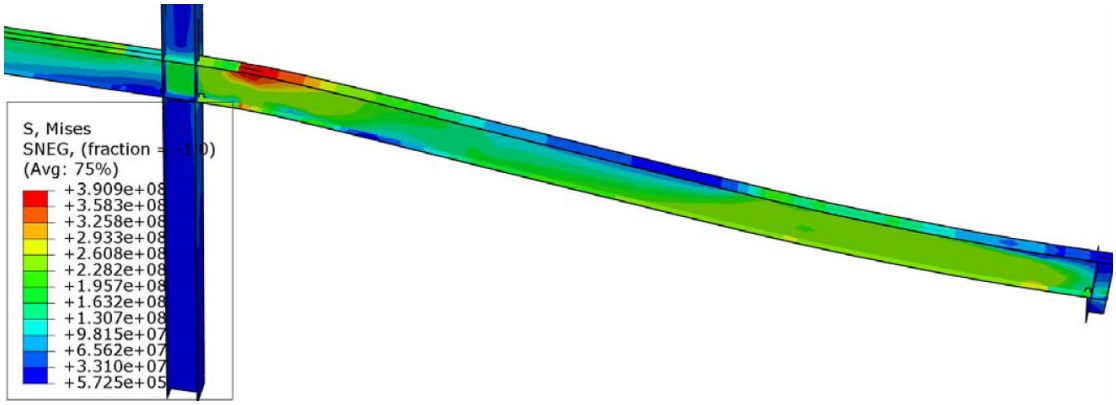

(a) Mises stress (Pa) distribution

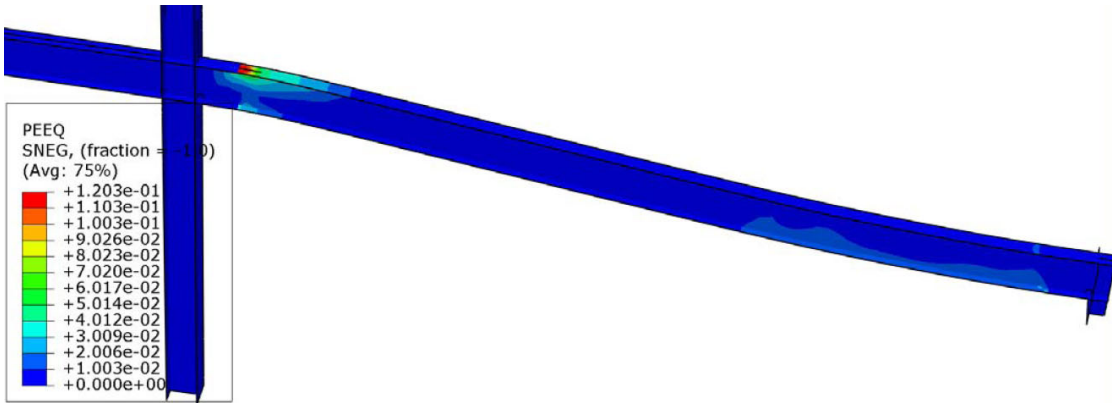

(b) Equivalent plastic strain distribution

Fig. 6.12. Mises stress and equivalent plastic strain distributions of structure retrofitted by flange cover plates for first criterion

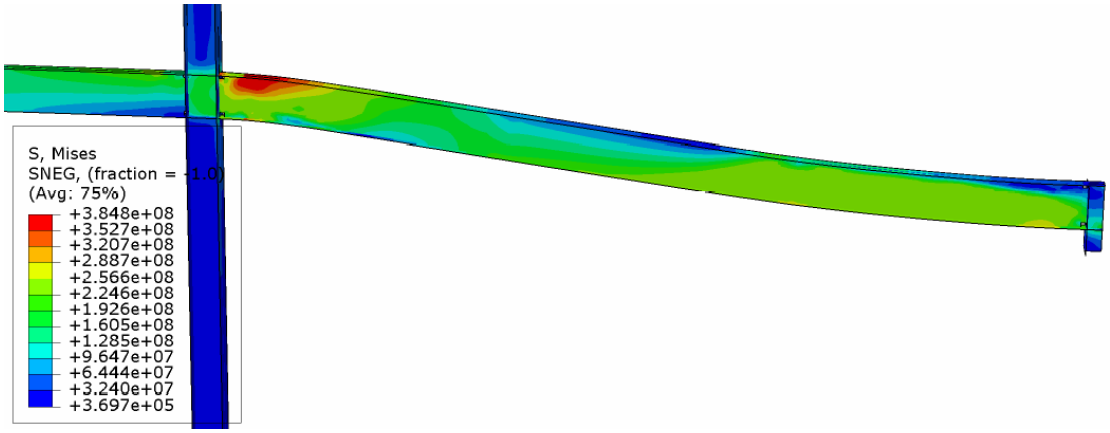

(a) Mises stress (Pa) distribution

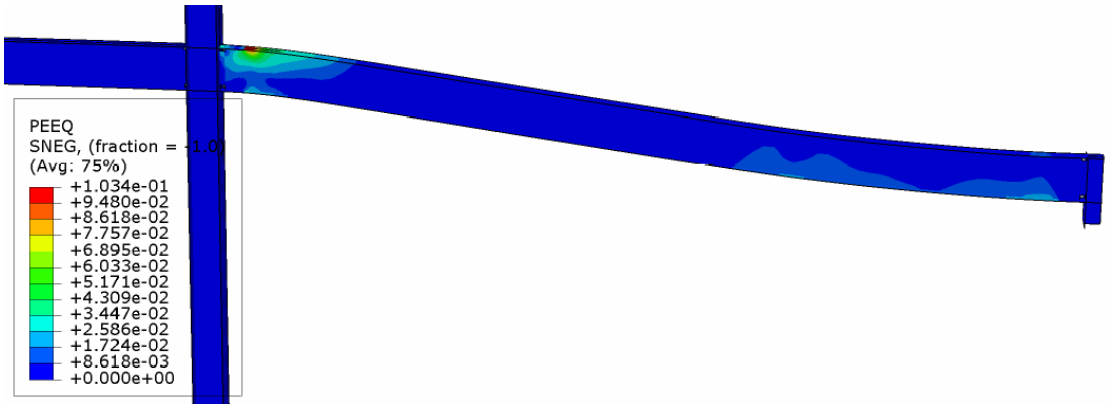

(b) Equivalent plastic strain distribution

Fig. 6.13. Mises stress and equivalent plastic strain distributions of structure retrofitted by flange cover plates for second criterion

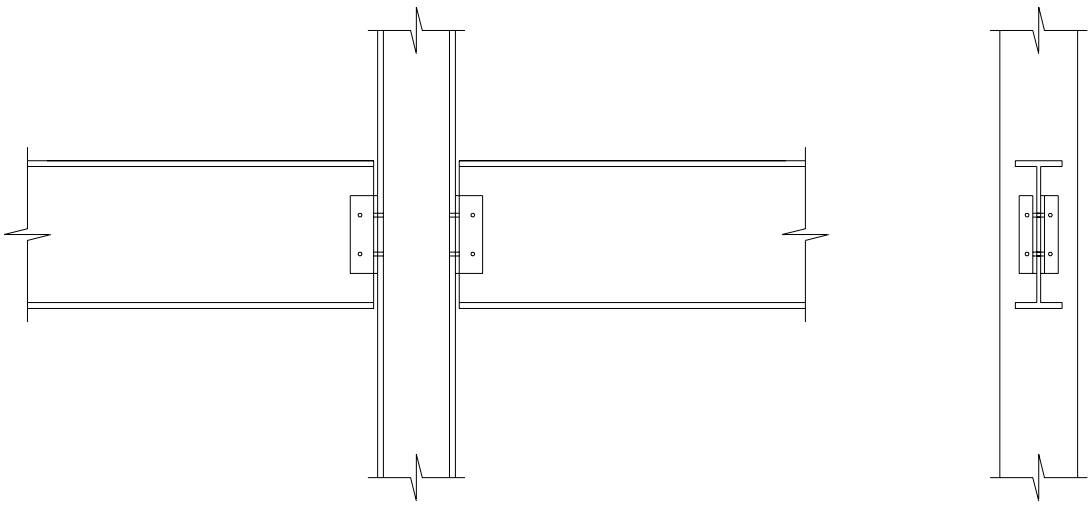

(a) Original double angle web connection

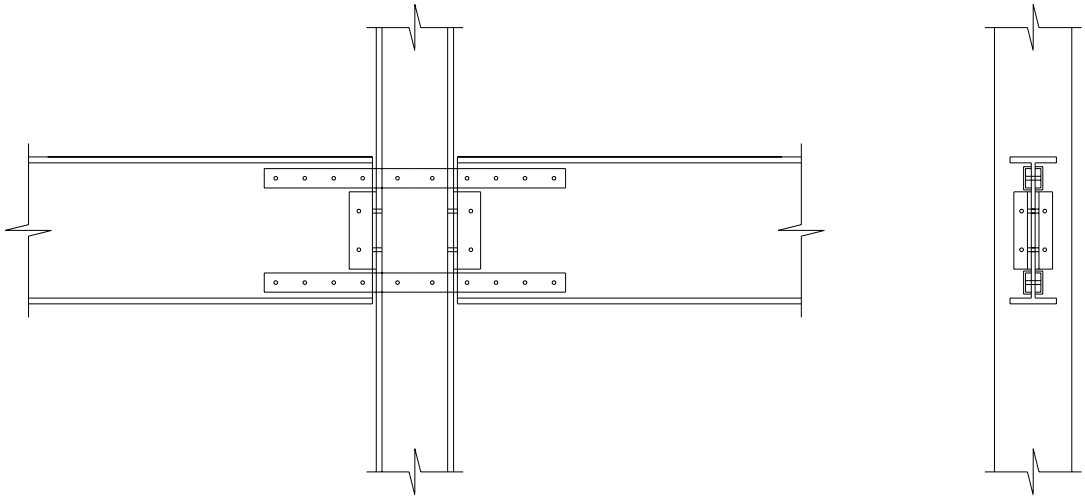

(b) Connection retrofitted by Link Bar Scheme

Fig. 8.1. Beam-to-column connections before and after retrofitted by Link Bar Scheme

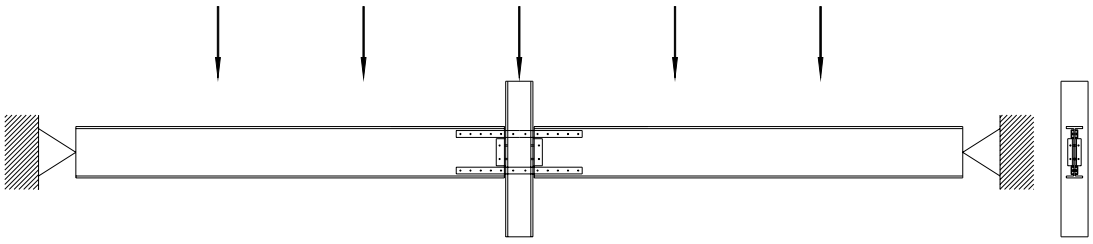

Fig. 8.2. Substructure used for Link Bar Retrofitting Scheme

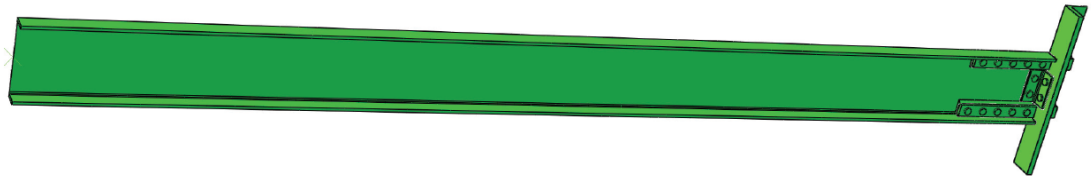

Fig. 8.3. Quart model used in finite element analyses

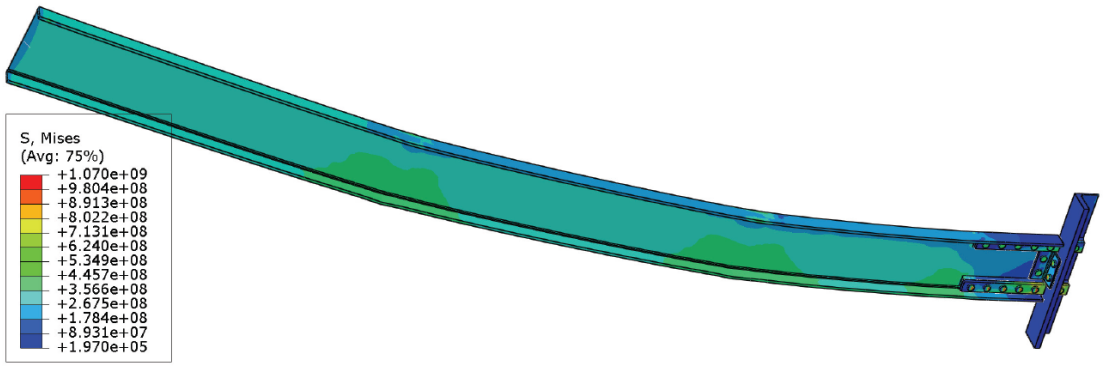

(a) Whole model

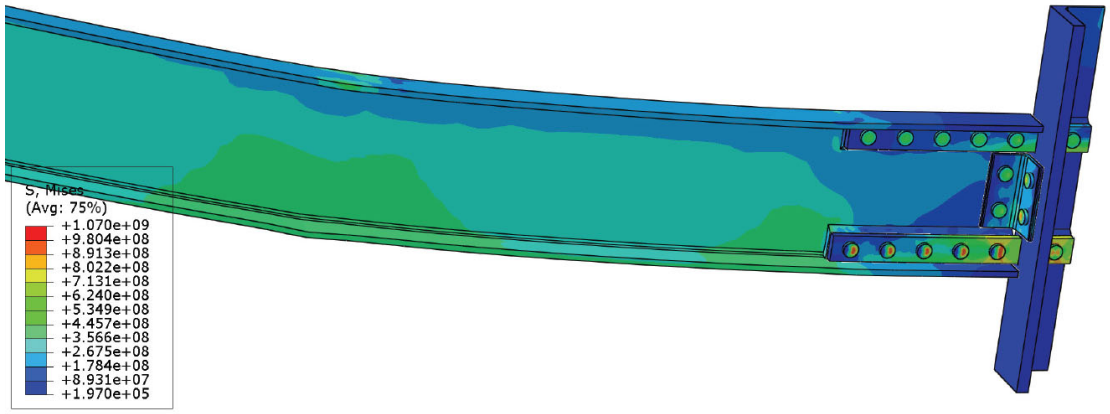

(b) Connection part

Fig. 8.4. Deformation and Mises stress (Pa) distribution after loading